UNIVERSIDADE FEDERAL DO RIO GRANDE DO SUL

INSTITUTO DE CIÊNCIAS BÁSICAS DA SAÚDE

DEPARTAMENTO DE BIOQUÍMICA

O papel das vias de sinalização de PI3K/Akt e NFkappaB na proliferação e viabilidade de glioblastomas multiformes

Rafael Schröder Pereira

Porto Alegre, 2013

UNIVERSIDADE FEDERAL DO RIO GRANDE DO SUL

INSTITUTO DE CIÊNCIAS BÁSICAS DA SAÚDE

DEPARTAMENTO DE BIOQUÍMICA

PROGRAMA DE PÓS-GRADUAÇÃO EM CIÊNCIAS BIOLÓGICAS: BIOQUÍMICA

O papel das vias de sinalização de PI3K/Akt e NFkappaB na proliferação e viabilidade de glioblastomas multiformes

Mestrando: Rafael Schröder Pereira

Orientador: José Cláudio Fonseca Moreira

Dissertação submetida ao Programa de Pós-Graduação em Ciências Biológicas: Bioquímica, como requisito parcial para obtenção do grau de Mestre em Bioquímica.

Porto Alegre, 2013

SUMÁRIO

Parte I

RESUMO

A identificação de novos alvos terapêuticos no tratamento de glioblastomas multiformes (GBMs) se faz necessária devido ao mau prognóstico e ineficiência das terapias associadas a esses tumores. Nesta dissertação, avaliamos o envolvimento do Fator Nuclear kappaB (NFkappaB) e da via da PI3K/Akt no crescimento *in vitro* de glioblastomas, e o potencial uso dos inibidores de NFkappaB e de PI3K/Akt como possíveis agentes antitumorais. Com esta finalidade foram utilizados os inibidores farmacológicos de NFkappaB (partenolide), e de PI3K/Akt (quercetina e Ly294002), e o inibidor misto de NFkappaB/Akt (curcumina). Os inibidores de NFkappaB causaram uma significativa diminuição na viabilidade dos GBMs quando comparado com os inibidores de outras vias de sinalização (MAPK, MEK/ERK1/2, EGFr e JNK1/2), a qual foi tipo dose resposta. Além disso, os inibidores de NFkappaB apresentaram extravasamento de LDH no meio de cultura e perda de integridade da membrana plasmática que foi vista através da técnica do Iodeto de Propideo (PI). Já os inibidores de PI3K/Akt apresentaram um menor efeito do que o apresentado pelos inibidores de NFkappaB, não demonstrando uma curva do tipo dose resposta, ainda assim, diminuíram a viabilidade dos GBMs. Entretanto, não apresentaram extravasamento de LDH no meio de cultura, e não houve incorporação de PI, mostrando que, diferentemente do que ocorre com os inibidores de NFkappaB, a perda de viabilidade vista nas células tratadas com os inibidores de PI3K/Akt está preponderavelmente relacionada com uma diminuição na proliferação, e não com morte celular. Vimos também que os inibidores foram capazes de alterar o imuno-conteúdo de fatores relacionados com morte e sobrevivência celular, tais como caspase 3, LC3 A/B, PARP e Hsp70, assim como o ciclo celular. Portanto, nossos resultados demonstram que a via da PI3K/Akt parece estar preferencialmente

relacionada com a proliferação celular, enquanto a via do NFkappaB preferencialmente com sobrevivência.

ABSTRACT

The identification of new therapeutic targets for treatment of glioblastoma multiforme (GBMs) is necessary due to poor prognosis and ineffective therapies associated with these tumors. In this study we have assessed the role of Nuclear Factor-kappaB (NFkappaB) and the PI3K/Akt pathway in glioblastomas *in vitro* growth, and their inhibitors as potential antitumor agents. For this we used the pharmacological inhibitors of NFkappaB (Parthenolide), and PI3K/Akt (LY294002 and quercetin), and mixed inhibitor of NFkB / Akt (curcumin). NFkappaB inhibitors yielded a significant decrease in viability of GBMs compared to inhibitors of other signaling pathways (MAPK, MEK/ERK1/2, EGFr and JNK1 / 2), which was dose-dependent. Furthermore, inhibitors of NFkappaB showed LDH releasing in culture medium and membrane integrity losing, evaluated through the Propidium Iodide (PI)-based method. The PI3K/Akt inhibitors showed a smaller effect than NFkappaB inhibitors, also decreasing GBMs viability but playing no dose-dependence response. Despite there was not LDH releasing in culture medium and PI incorporation, showing that the loss of viability observed in cells treated with inhibitors of PI3K/Akt is associated with a decrease in the proliferation, unlike what happens with inhibitors of NFkappaB, no cell death was observed. We have also seen that the inhibitors were able to alter the contents of immune-related factors death and cell survival, such as caspase-3, LC3 A / B, PARP and Hsp70, as well as the cell cycle. Therefore, our results demonstrate that the PI3K/Akt pathway seems to be related to cell proliferation, while the NFkappaB pathway to survival.

Lista de Abreviaturas:

3-MA: 3-metiladenina

Akt ou PKB: proteina cinase B

AP-1: ativador da proteina-1 (activator protein-1)

APAF1: fator apoptótico 1 ativador de protease (apoptotic protease activating factor 1)

BAK: antagonista de morte Bcl-2 (Bcl-2 antagonist killer)

BAX: proteína Bcl-2 associada ao X (Bcl-2 associated X protein)

BCL2: proteína 2 de linfoma de células B (B-cell lynphoma protein 2)

Bcl-X_L: proteína de isoforma longa relacionada a Bcl2 (Bcl2 related protein long isoform)

Bid: domínio agonista de morte de interação com BH3 (BH3 interacting domain death agonist)

CREB: nucleotideo ciclico de resposta ao elemento da proteína de ligação (cyclic nucleotide response element binding protein)

DR: receptores de morte (death receptor)

DRAM: gene modulador de autofagia induzido por dano (damage-regulator autophagy modulator)

EGFR: receptor do fator de crescimento endotelial (endothelial growth factor receptor)

ERO: espécies reativas de oxigênio

FADD: domínio de morte associado a Fas (Fas-associated death domain)

Fas: ácido graxo sintetase (fatty acid synthetase)

GBM: glioblastoma multiforme

HSP: proteínas de choque térmico (heat shock protein)

IGF: fator de crescimento semelhante a insulina (insulin growth factor)

IKB: inibidor de NFkappaB (inhibitor of NFkappaB)

IKK: IKB cinase

iRNA: RNA de interferência (interference RNA)

JNK: cinase jun n-terminal (jun n-teminal kinase)

LC3 A/B: formas A e B da cadeia leve 3 das proteínas associadas aos microtúbulos (light chain 3 of microtubule-associated A and B)

MDM2: minuto duplo murino 2 (murine doble minute 2)

MDR1: proteína de resistência a múltiplas drogas (multidrug resistance protein)

MEK: proteína cinase ativada por mitógeno (mitogen-activated protein kinase)

MMP: matrix metaloproteinases

MOMP: permeabilização da membrana mitocondrial externa (mitochondrial outer-membrane permeabilization)

mTOR: proteína alvo da rapamicina de mamíferos (mammalian target of rapamycin)

NFkappaB: Fator Nuclear kappa B (Nuclear Factor Kappa B)

PARP: poli ADP-ribose polimerase (poly ADP ribose polymerase)

PDGF: fator de crescimento derivado de plaquetas (plateled-derived growth factor)

PDK1: proteína cinase 1 dependente de fosfoinositol (phosphoinositide-dependent kinase 1)

PI3K: fosfatidil-inositol 3 cinase

PKA: proteina cinase A

PKC: proteina cinase C

PPI: fosfatidilinositol 3-fosfato (phosphatidylinositol 3-phosphate)

PPI2: fosfatidilinositol 3,4-bifosfato (phosphatidylinositol 3,4-biphosphate)

PPI3: fosfatidilinositol 3,4,5-trifosfato (phosphatidylinosito 3,4,5-triphosphate)

Pten: proteína homóloga fostatase/tensina (phosphatase and tensin homolog)

RPI: serina-treonina cinase (receptor-interacting protein)

siRNA: RNA de interferência (small interference RNA)

SMAC/DIABLO: segundo ativador mitocondrial de caspase

TMZ: temozolamida

TNF: fator de necrose tumoral (tumor necrosis factor)

TRAIL: ligante indutor de apoptose relacionado a TNF (TNF-related apoptosis inducing ligand)

LISTA DE FIGURAS:

LISTA DE TABELA:

1. INTRODUÇÃO

1.1. Glioblastomas

A busca por novos alvos terapêuticos para o tratamento de neoplasias sólidas e hematopoiéticas tem sido objeto de esforços na comunidade científica. Os glioblastomas são tumores sólidos originários de transformações neoplásicas em células da linhagem astrocítica, é classificado como astrocitoma de grau IV pela Organização Mundial de Saúde (OMS), sendo o mais comum entre os tumores cerebrais malignos (Friedman et al., 2000; Louis et al., 2007; Mercer et al., 2009). O GBM é considerado um câncer bastante agressivo, invasivo, e sem muitas alternativas terapêuticas, o que culmina em uma sobrevida média de 1 ano (Stewart et al., 2002; Koukourakis et al., 2009; Sathornsumetee e Reardon, 2009). O tratamento padrão para glioblastomas inclui a remoção cirúrgica do tumor, seguida de radioterapia craniana total, com administração concomitante e adjuvante de quimioterapia alquilante (Stewart et al., 2002; Mercer et al., 2009). A adição da quimioterapia alquilante melhora a sobrevida desses pacientes entre 2 e 5 anos, quando comparada com a radioterapia isolada, em pacientes com diagnóstico precoce. No entanto, pacientes com diagnóstico tardio apresentam uma sobrevida de apenas 14,6 meses (Krakstad et al., 2010). A severidade desse prognóstico provém de diversos fatores que tornam os GBMs um tipo de tumor complexo e de difícil tratamento. Enquanto outros tecidos tumorais podem ter partes removidas sem a perda funcional ou com pequena perda funcional do órgão, o mesmo nem sempre pode ser aplicado aos tumores do sistema nervoso central. Portanto, a necessidade da caracterização de novas vias de sinalização importantes no crescimento de

gliomas pode possibilitar o desenvolvimento de novos agentes farmacológicos, proporcionando, além disso, novas alternativas terapêuticas aos pacientes que não respondem à terapia com os antitumorais clássicos. Recentemente, estudos vêm caracterizando a inibição da proteína cinase B (PKB/Akt) e do fator de transcrição NFkappaB como alvos potenciais para indução de morte celular e sensibilização a quimioterápicos em diversos tipos de células tumorais como, por exemplo, câncer de pulmão, ovário e glioblastomas (Xu et al., 2010; Wu et al., 2008; Koul et al., 2010; Barkett et al., 1999; Rayet et al., 1999; Aggarwal et al., 2004; Kapoor et al., 2004; Sethi et al., 2007; Zanotto-Filho et al., 2010).

1.2. Proteína Cinase B (PKB/Akt)

A proteína cinase B ou Akt (PKB/Akt) é uma proteína cinase de resíduos serina/treonina. Em mamíferos foram encontradas três isoformas de PKB, a PKB α (Akt 1), PKB β (Akt 2) (Jones et al., 1991; Cheng et al., 1992) e PKB γ (Akt 3) (Brodbeck et al., 1999). A ativação da PKB/Akt se dá através de vários estímulos tais como hormônios, fatores de crescimento e componentes da matriz extracelular (Nicholson et al., 2002). A cascata de sinalização inicia com a ativação da PKB / Akt pelas classes 1A e 1B da PI-3K, as quais são ativadas pela tirosina-cinase e pelos receptores acoplados à proteína-G, respectivamente. Seguindo o seu recrutamento para esses receptores na membrana plasmática, PI-3K é ativado e fosforila a fosfatidilinositol-4,5-bifosfato (PPI2) no grupo 3-OH, gerando o segundo mensageiro fosfatidilinositol-3,4,5-trifosfato (PPI3). Os níveis de PPI3 são rigidamente regulados pela ação de fosfatases como a Pten, que remove fosfato a partir da posição 3-OH, e a SHPI, que defosforila na posição 5-OH, inibindo a PPI3, e consequentemente a

via. A PPI3 não ativa PKB/Akt diretamente, mas em vez disso parece recrutar PKB/Akt para a membrana plasmática e alterar a sua conformação para permitir uma subsequente fosforilação pela fosfatidilinositol cinase dependente-1 (PDK-1). Após ser ativada, a PI3K pode promover a ativação de várias proteínas celulares e fatores de transcrição, incluindo BAD, CREB, IKB-cinase (NFkappaB), GSK3 α e β, mTOR, que estão envolvidos em diversos processos, tais como metabolismo, proliferação, diferenciação e estímulos anti-apoptóticos (Nicholson et al., 2002). Particularmente em gliomas, a superativação de via PI3K/Akt tem sido demonstrada em mais de 60% dos tumores, em consequência de mutações que levam a ausência da atividade da proteína Pten, um modulador negativo da PI3K. Devido a esse espectro de modulação anti-apoptótica e proliferativa, a PKB/Akt tem sido considerado um importante fator no desenvolvimento de gliomas (Hill et al., 2002). Portanto, a inibição de PKB/Akt poderia ser um mecanismo de sensibilização de células tumorais por facilitar a ativação da maquinaria apoptótica, sendo um possível alvo na terapia contra o câncer (Hill et al., 2002).

1.3. Fator Nuclear Kappa B (NFkappaB)

Junto com a via de PI3K/Akt, recentemente os estudos apontam o fator de transcrição NFkappaB (Nuclear Factor kappa-B) como um componente importante no processo de crescimento e resistência anti-apoptótica de gliomas, embora os mecanismos envolvidos na ativação deste fator permaneçam por ser elucidados (Barkett et al., 1999; Rayet et al., 1999; Aggarwal et al., 2004; Kapoor et al., 2004; Sethi et al., 2007; Zanotto-Filho et al., 2010). O NFkappaB é um fator de transcrição formado por uma família de proteínas combinadas em homo e heterodímeros

(principalmente heterodímeros entre as proteínas p65 e p50). O complexo p65/p50 é recrutado no citosol sob a forma de um complexo ternário ligado a subunidades inibitórias denominadas IkB. Sob ação de estímulos como, por exemplo, citocinas inflamatórias e espécies reativas de oxigênio, IkB é fosforilada por IKK (IkB cinase) e desliga-se de NFkappaB sendo, então, levada a degradação no proteassoma. Uma vez desligado da subunidade inibitória (IkB), a forma ativa de NFkappaB (p65/p50) migrará para o núcleo, e participará da regulação de diversos genes. Entre os genes modulados por NFkappaB encontram-se principalmente os relacionados às vias de inibição de morte celular como os anti-apoptóticos Bcl-xL, c-FLPI e cIAP1/2 (inibidor de apoptose 1 e 2), e os antioxidantes SOD2 (Superóxido dismutase mitocondrial), invasão (ICAM-1, VCAM-1, MMP2, MMP9), angiogênese (VEGF), proliferação (ciclina D1, MYC) e metástase (CXCR4 e TWIST), os quais são, conjuntamente, relacionados com a inibição da maquinaria apoptótica. Além dos processos já citados o NFkappaB também ativa genes que contribuem para a imunidade adaptativa e a secreção de citocinas pró-inflamatórias. Devido a esse espectro de modulação anti-apoptótica/antioxidante, o NFkappaB tem sido considerado um fator de transcrição diretamente ligado aos eventos de proliferação, metástase e resistência tumoral aos quimioterápicos e ao sistema imune (Barkett et al., 1999; Xie et al., 2010; Zanotto-Filho et al., 2010). Um ponto importante a ser considerado no potencial apoptótico da inibição de NFkappaB é a aumentada expressão e ativação de NFkappaB em células tumorais comparado a células normais, o que, teoricamente, proporcionaria uma seletividade dos inibidores de NFkappaB para as células neoplásicas comparado aos tecidos normais (Pickering et al., 2007; Gill et al., 2002). A seletividade é um fator importante quando consideramos os compostos antitumorais, uma vez que isso preveniria os possíveis efeitos adversos aos tecidos

sadios. Por exemplo, em um painel de linhagens de gliomas foi observada uma aberrante ativação e expressão de NFkappaB, enquanto células não-tumorais não apresentaram aumento deste fator de transcrição. Neste estudo, o tratamento com oligonucleotídeos de interferência (*decoy*) para NFkappaB induziu morte celular em linhagens de glioma, sem efeitos significantes nas células não-tumorais (astrócitos) (Gill et al., 2002). A ativação exacerbada da via de NFkappaB contribui, também, para a proliferação descontrolada e para a resistência aos agentes antitumorais em pacientes refratários aos protocolos de quimioterapia (Piva et al., 2005; Philipp e Ruland 2007; Furman et al., 2000). Tal hiper-ativação de NFkappaB em resposta à quimioterapia tem sido correlacionada com a falha terapêutica associada tanto a drogas clássicas como o taxol, etoposídeo (Morotti et al., 2006), vincristina, vinblastina (Garcia et al., 2005) quanto a fármacos de nova geração como o imatinibe (Cilloni et al., 2006). Neste contexto, os estudos vêm sugerindo que o uso combinado de inibidores de NFkappaB associado a antitumorais clássicos pode potencializar a morte celular ou, até mesmo, quebrar a resistência celular a esses compostos.

1.4. Inibidores de NFkappaB e PI3K/Akt

Existem, atualmente, diversas moléculas inibidoras da via de NFkappaB e de PI3K/Akt, as quais atuam em diferentes pontos da via:

a) Partenolide: lactona sesquiterpênica; inibe IKK-β na Cys179. Além disso, inibe p65 por ligação em resíduos de cisteína no *loop* de ativação (Hehner et al., 1999; Kwok et al., 2001).

b) Curcumina: pigmento extraído da *Curcuma longa*; inibidor de IKKs (Dhandapani et al., 2007).

c) Quercetina: 3,3′,4′,5,7-pentahidroxiflavonoide – é um flavonóide de baixo peso molecular encontrado nos mais variados tipos de frutas e vegetais; inibidor de PI3K (Braganhol et al., 2006).

d) Ly294002: Cloridrato de 2-(4-Morfolinil)-8-Fenil-1(4H)-Benzopiran-4-ona – é um composto químico que foi derivado da quercetina; inibidor de PI3K (Imai et al., 2012).

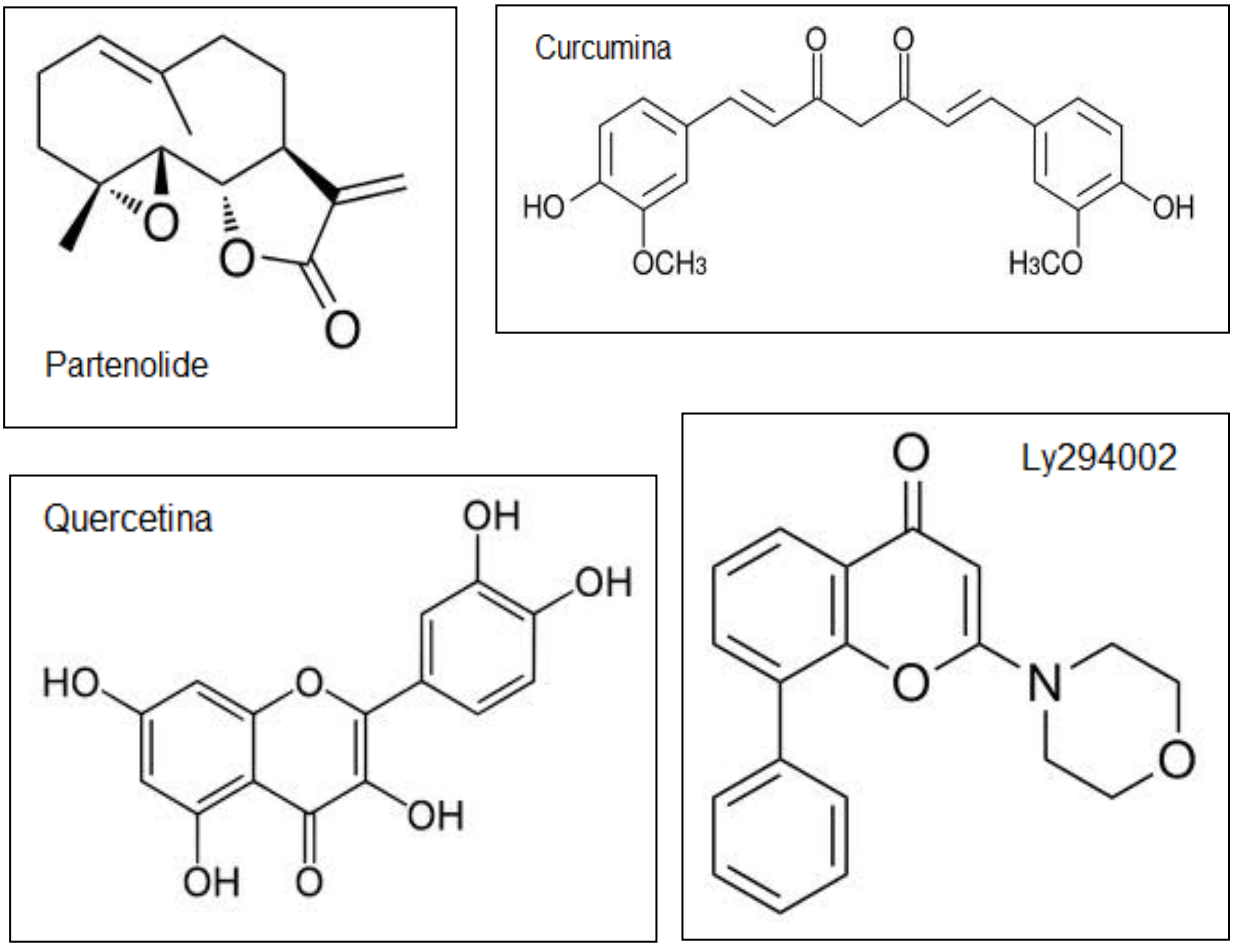

Figura 1: Estruturas moleculares dos inibidores de NFkappaB e de PI3K/Akt. Figuras desenhadas com o software BKChem®.

1.5. Morte Celular

A morte celular pode ser classificada de acordo com o seu aspecto morfológico (que pode ser apoptótica, necrótica, autofágica ou associado com a mitose), critérios enzimáticos (com e sem o envolvimento de nucleases ou de classes diferentes de proteases, tais como as caspases, calpaínas, catepsinas e transglutaminases), aspectos funcionais (programada ou acidental, características fisiológicas ou patológicas) ou imunológica (imunogênicos ou não imunogênica) (Kroemer et al., 2009).

a) Apoptose

A morte celular por apoptose é de grande importância durante o desenvolvimento do organismo, bem como na regulação do sistema imunológico e na defesa contra doenças.

Morfologicamente, a apoptose se caracteriza por alterações nucleares como a condensação e fragmentação da cromatina, assim como a formação de bolhas de membrana, modificações nas organelas e encolhimento de toda a célula. Ocorre a exposição ao lado de fora da célula do fosfolipideo de membrana, a fosfatidilserina, indicando aos macrófagos que aquela célula dever ser fagocitada (Elmore et al., 2007; Ghavami et al., 2009). É importante salientar que esse processo ocorre sem a perda da integridade da membrana plasmática, não havendo a produção de citocinas, e consequentemente impedindo que ocorra um processo inflamatório (Elmore et al., 2007).

Atualmente estão descritos dois mecanismos gerais de indução de apoptose, uma via extrínseca e uma via intrínseca, que divergem na forma de ativação, mas que estão parcialmente interligados, apresentando a mesma finalidade.

A via extrínseca é ativada por sinais externos a célula, através de receptores trasmembrana que irão propagar o sinal para o citoplasma. Estes receptores de morte são chamados DR (*death receptors*) que são membros da superfamília TNFR (*Tumor Necrosis Factors Receptors*). Os membros da superfamília TNFR possuem subdomínios extracelulares ricos em cisteínas, e um domínio citoplasmático de cerca de 80 aminoácidos denominado “domínio de morte” (Ashkenazi e Dixit, 1998; Mahmood, 2010). Este domínio de morte desempenha um papel fundamental na transmissão do sinal de morte à superfície da célula para as vias de sinalização intracelular. Até a data, os principais e melhor caracterizados ligantes e receptores correspondentes de morte incluem FasL/FasR, TNF-α/TNFR1, Apo3L/DR3, Apo2L/DR4 e Apo2L/DR5 (Chicheportiche et al., 1997;. Ashkenazi et al., 1998; Suliman et al., 2001;. Rubio-Moscardo et al., 2005). Após a ativação do receptor, a cascata de caspases é ativada através da dimerização de caspase 8, que cliva e ativa as caspases 3 e 7 para efetivação da apoptose (Mahmood, 2010; Tait, 2010).

A via intrínseca de sinalização não é mediada por receptores, mas sim através da alteração da permeabilidade da mitocôndria. Os estímulos que iniciam a via intrínseca produzem sinais intracelulares que podem atuar tanto de maneira positiva quanto negativa. Sinais negativos envolvem a ausência de determinados fatores de crescimento, hormônios e citocinas, que suprimiriam a morte, desencadeando uma falha na supressão do sinal e consequentemente levando à apoptose. Já os sinais positivos podem ser a radiação, toxinas, hipoxia, hipertermia, infecções virais, e os radicais livres (Elmore, 2007).

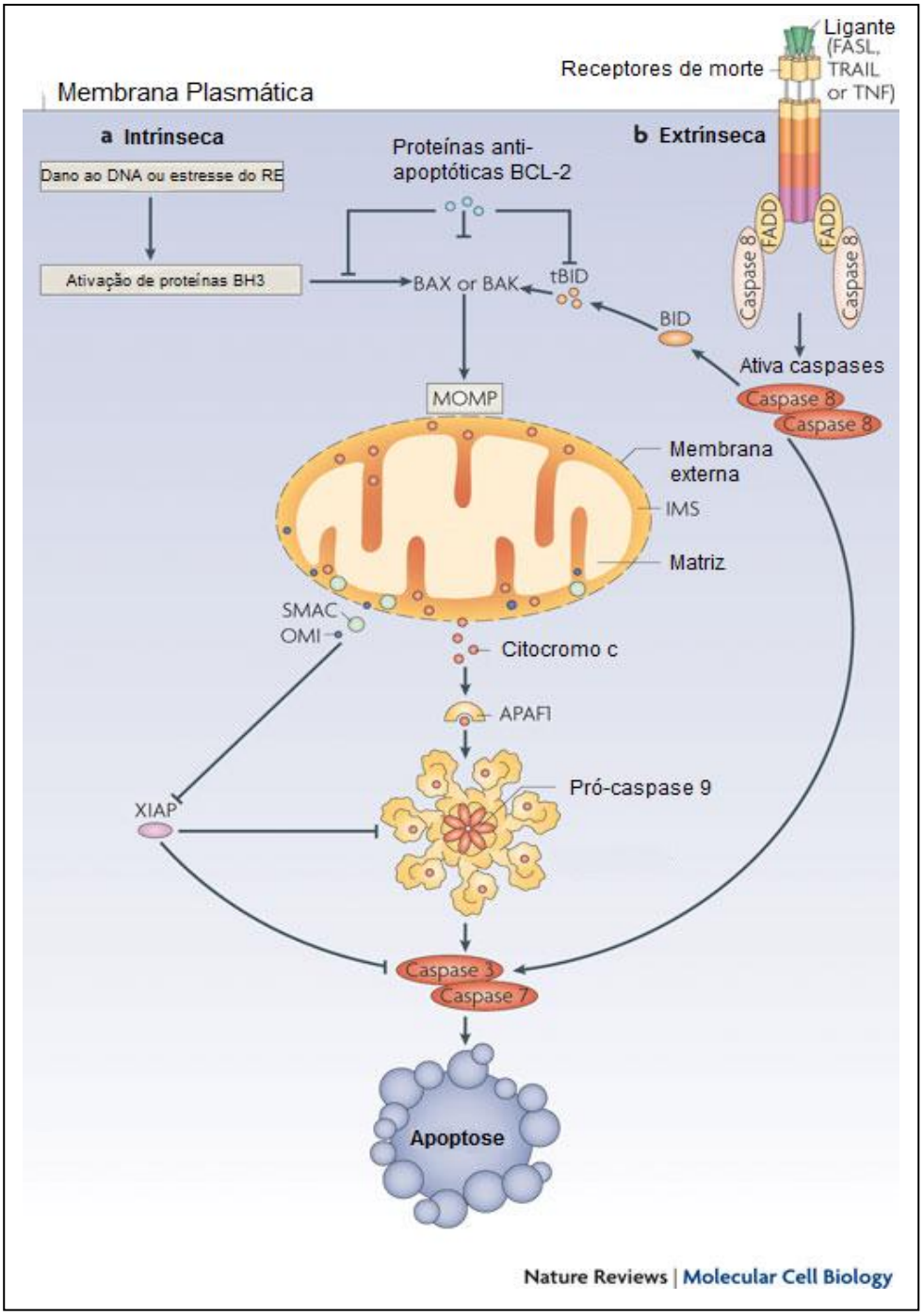

Figura 2: Via intrínseca e extrínseca da apoptose. (a) estímulo apoptótico intrínseco, como o dano ao DNA ou estresse de retículo endoplasmático (RE), ativam BAX e BAK, promovendo a permeabilização da membrana mitocondrial externa (MOMP – *mitochondrial outer membrane permeabilization*). A liberação de proteínas mitocondriais promove a ativação de caspases e resultam em apoptose. (b) a via extrínseca é iniciada pela ativação dos receptores de morte, que levam ao recrutamento de moléculas adaptadoras como FADD e caspase 8, que cliva as caspases efetoras 3 e 7, levando a apoptose. Os fatores que fazem a ligação das duas vias, intrínseca e extrínseca, ocorre através da clivagem da caspase 8 e ativação de BID. Alterado de Tait et al (2010).

Todos estes estímulos provocam alterações na membrana mitocondrial interna, que resulta em uma abertura do poro de permeabilidade transitória (MPT), perda do potencial de membrana mitocondrial e libertação para o citosol do citocromo c, Smac / DIABLO, e da serina protease HtrA2/Omi (Du et al., 2000; Garrido et al., 2005). No citosol o citocromo c se liga e ativa a Apaf-1 (*apoptotic protease activating factor 1*), que irá ativar a caspase-9, formando um apoptossomo, o qual irá promover uma cascata de sinalização, posteriormente ativando as caspases 3 e 7 (Hill et al., 2004; Tait et al., 2010; Galluzzi et al., 2011). O controle e a regulação destes eventos apoptóticos mitocondriais ocorre através de membros da família de proteínas Bcl-2 (Cory e Adams, 2002). A proteína p53 supressora de tumor tem um papel crítico na regulação da Bcl-2, no entanto os mecanismos exatos ainda não foram completamente elucidados (Schuler e Green, 2001). A família de proteínas Bcl-2 regula a permeabilidade da membrana mitocondrial e pode ser tanto pró-apoptótica quanto anti-apoptótica. Até agora, foram identificados um total de 25 genes na família Bcl-2. Algumas das proteínas anti-apoptóticas incluem Bcl-2, Bcl-x, a Bcl-XL, Bcl-XS, Bcl-w, BAG, e pró-apoptóticas Bcl-10, Bax, Bak, Bid, Bad, Bim, Bik, e Blk. Estas proteínas têm um significado especial, já que são elas que determinam se uma célula se compromete a apoptose ou aborta o processo. Acredita-se que o principal mecanismo de ação da Bcl-2, é a regulação da liberação do citocromo c a partir da mitocôndria através da alteração da permeabilidade da membrana mitocondrial. As células tumorais pode adquirir resistência a apoptose através da expressão de proteínas anti-apoptóticas tais como Bcl-2 ou pela sub-regulação, deleção ou mutação de proteínas pró-apoptóticas, tais como Bax. A expressão de ambos Bcl-2 e Bax é regulada pelo gene supressor de tumor p53 (Desbaillets et al., 1999; Demuth e Berens, 2004; de I et al., 2008). Uma das

estratégias terapêuticas em desenvolvimento para os glioblastomas buscam a reestruturação das vias de morte a fim de reduzir ou quebrar a resistência aos quimioterápicos.

b) Necrose

A necrose ocorre quando uma célula perde a capacidade de morrer por apoptose (ex. baixo nível de ATP). As células podem sofrer necrose devido a um estresse extremo com intensidade variável de acordo com o tipo celular. Estresse oxidativo, altas temperaturas, contato com toxinas e choques mecânicos (Syntichaki, 2003). A necrose pode ser melhor definida pela sua morfologia, sendo caracterizada por um inchaço celular, disfunção mitocondrial, ruptura da membrana celular e extravasamento do conteúdo citoplasmático para o espaço extracelular. O extravasamento do citoplasma faz com que a célula libere fatores que podem ativar a resposta do sistema imune inato e adaptativo, levando a um processo inflamatório (Festjens, 2006). Ao contrário da apoptose, a necrose não apresenta condensação, fragmentação e clivagem do DNA, assim como a ativação de caspases (Leist, 2001). A necrose foi, por muito tempo, considerada um processo de morte celular descontrolado, não programado, resultando em alterações dramáticas irreversíveis em parâmetros celulares essenciais para o metabolismo e estrutura celular (Skulachev, 2006). Nos últimos anos, muitos trabalhos vêm demonstrando que a morte celular por necrose pode ser controlada, e já foram descobertos alguns marcadores desse processo. O termo “necrose programada” ou “necroptosis” foi atribuído a um tipo de morte não acidental em que há inibição de caspase e indução de morte não-apoptótica com características necróticas, enfatizando um grau de

regulação e um mecanismo molecular desse processo de morte. A necroptose é especialmente dependente da atividade cinase serina/treonina de RPIK1 (*receptor-interacting protein kinase*), RPIK3, inibidores de caspases, ubiquitinas E3 ligase, enzimas desubiquitinizadoras, PARP-1 [poli(ADP-ribose)polimerase-1], espécies reativas de oxigênio (ERO), reações bioenergéticas, envolvimento de membros da família Bcl-2, hidrolases citosólicas, além da permeabilização da membrana plasmática e lisossomal (Holler et al., 2000; Denecker et al., 2001; Galluzzi et al., 2008; Vandenabeele et al., 2010). O TNF é um importante ativador da necrose, pois induz a formação de ERO mitocondrial e a ativação da PARP-1, levando a uma depleção de ATP (Skulachev, 2006). A formação de ERO induz a danos no DNA e a subsequente ativação da PARP-1, a qual é uma enzima nuclear envolvida na reparação e estabilidade do DNA, assim como na regulação da transcrição (Leist et al., 2001; Los et al., 2002). A ativação da PARP-1 consome grande quantidade de NAD^+ e induz a um consumo maciço de ATP (Jain et al., 2013). O resultado da depleção acelerada de ATP é o favorecimento da necrose, e a consequente inibição da morte celular por apoptose, a qual é dependente de energia (Los et al., 2002).

c) Autofagia

A autofagia é uma via de degradação altamente conservada, o que inclui macroautofagia, microautofagia, e autofagia mediada por chaperonas (Mizushima e Komatsu, 2011). A microautofagia implica no engolfamento do citoplasma por invaginação da membrana lisossomal (Rodriguez-Rocha et al., 2011). Já a autofagia mediada por chaperonas (CMA) envolve o fornecimento seletivo de proteínas citoplasmáticas solúveis pela chaperona hsc70 e co-chaperonas para o lisossomo

para serem degradadas (Majeski et al., 2004). E a macroautofagia (aqui chamada apenas de autofagia, e que será abordada nesse trabalho) que medeia à degradação de componentes intracelulares, incluindo organelas e proteínas de longa duração (Levine et al., 2004). A autofagia está relacionada com diversos processos fisiológicos e patológicos, incluindo a sobrevivência celular, a morte, metabolismo, o desenvolvimento, a infecção, imunidade e envelhecimento (Mehrpour et al., 2010). Esse tipo de morte programada está intimamente envolvida na etiologia de muitas doenças humanas importantes, incluindo câncer, doenças neurodegenerativas e distúrbios metabólicos (Meijer e Codogno, 2009). Ela se caracteriza pela formação de autofagossomos de membrana dupla, que se fusionam com lisossomos para gerar a estrutura funcional, a qual recicla e degrada componentes celulares em um ambiente ácido contendo hidrolases lisossomais (Kroemer, 2005).

A autofagia serve predominantemente como um mecanismo de sobrevivência celular, através de seu papel supressor da morte celular por necrose, tais como necroptose e morte celular mediada por poli (ADP-ribose) polimerase-1 (PARP).

A autofagia é regulada geneticamente por uma família de proteínas chamada Atg (*Autophagy genes)*, que são distinguidas através da sigla e de um número. As Atg5, Atg7, Atg8, Atg10 e a Atg12, são as primeiras a serem recrutadas durante o processo autofágico e são as responsáveis pela formação do autofagossomo.

A Atg8, mais conhecida como LC3 (*Light Chain 3*), existe em duas formas, a LC3-I (localizada no citosol) e a sua forma proteolítica LC3-II (localizada na membrana do autofagossomo) (Kögel et al., 2010). A LC3 é uma proteína do tipo ubiquitina-ligase, que pode ser conjugada com a fosfatidiletanolamina (PE). Inicialmente a LC3 é sintetizada em uma forma não processada, a proLC3, que é

clivada no carbono C-terminal, resultando em LC3-I, para posteriormente ser conjugada a PE, formando a LC3-II. A LC3-II é a única proteína marcadora fielmente associada ao estágio completo do autofagossomo (Klionsky et al., 2008).

Além dessas, temos a Atg6, ou beclina-1, que é um regulador essencial do processo autofágico e um componente de classe III do complexo da PI3K, necessário tanto na formação quanto no transporte dos autofagossomos. A beclina-1 é um gene supressor tumoral, que está deletado em vários tipos de tumores, como os de mama, ovário e de próstata. Em gliomas, constatou-se que os níveis de expressão de beclina-1 são inversamente proporcionais ao grau do tumor. Portanto, pacientes com baixos níveis de beclina-1 apresentam um pior prognóstico, sugerindo que o processo autofágico pode amplificar a resposta à terapia, melhorando o desfecho clínico (Pirtoli et al., 2009).

Normalmente, o receptor de insulina ativa PI3K, e esse estimula a via de Akt. A autofagia pode ser reprimida pela via de PI3K, que pode ser influenciado pela inibição de PTEN na interação de PI3K e Akt. Quando Akt está ativada pode inibir a apoptose e a autofagia através da proteína mTOR. Esta é determinante para iniciar a formação dos autofagossomos pela interação de membros da família Atg (Baehrecke et al., 2005).

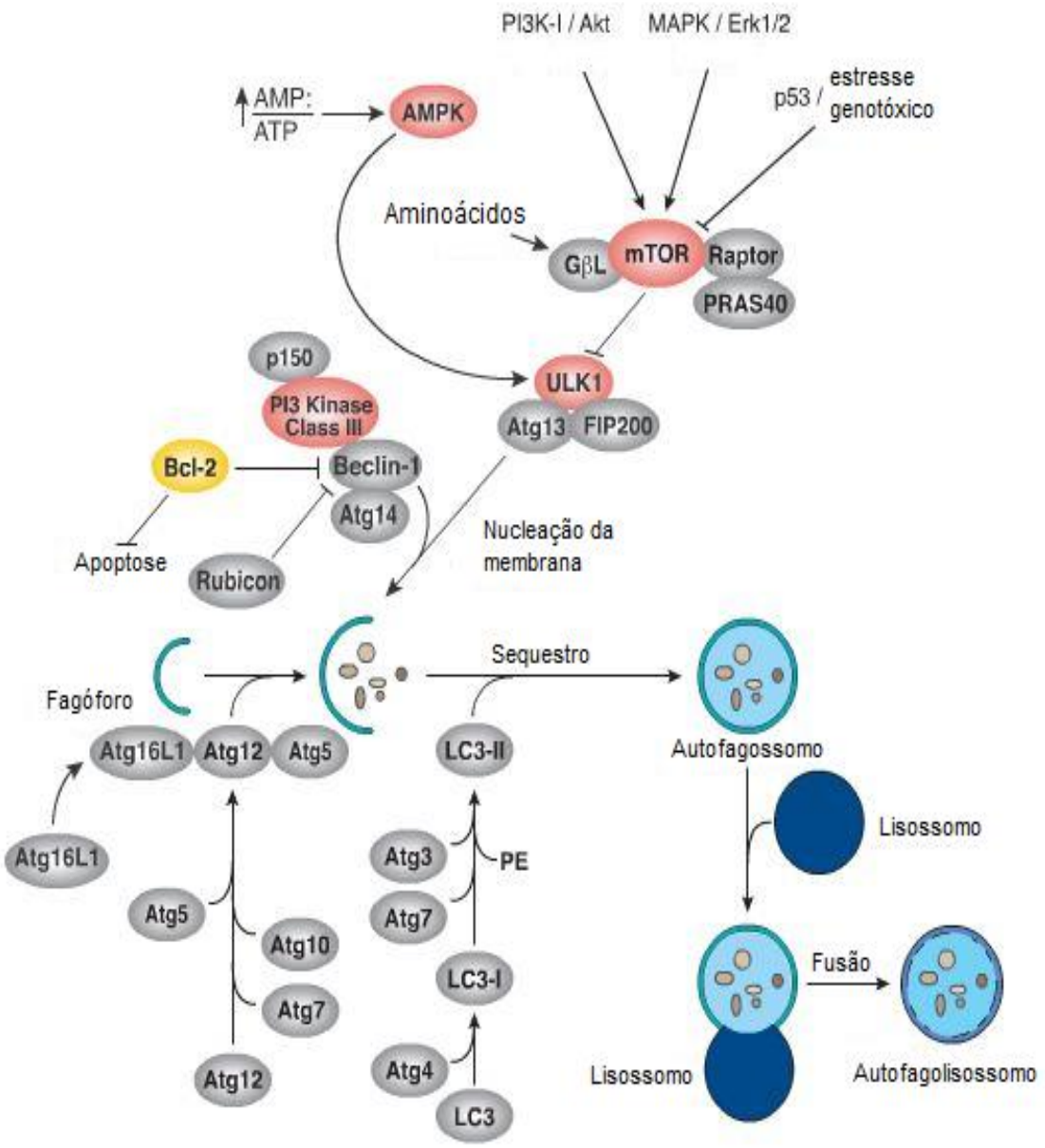

Figura 3: Vias de sinalização autofágica. Visão esquemática das proteínas envolvidas na modulação e execução do processo autofágico, assim como as estruturas formadas. Obtido de: http://www.cellsignal.com/pathways/autophagy-signaling.jsp (acessado em 15/04/2013).

1.6. Justificativa

Uma vez que PI3K e NFkappaB estão super-estimulados em painéis de linhagens de gliomas e pacientes (Koul et al., 2010; Zanotto-Filho et al., 2010), nossa hipótese é que a inibição destas proteínas/vias de sinalização poderia ser uma alternativa para conter o crescimento desses tumores. Um ponto importante a ser considerado no potencial apoptótico da inibição de PI3K/Akt e NFkappaB é a aumentada expressão e ativação destas vias em glioblastomas comparado a células normais, o que, teoricamente, proporcionaria uma seletividade dos seus inibidores para as células neoplásicas comparado aos tecidos normais (Zhang et al., 2010; Koul et al., 2010; Zanotto-Filho et al., 2010). A seletividade é um fator importante quando consideramos os compostos antitumorais, uma vez que isso preveniria os possíveis efeitos adversos aos tecidos sadios. Portanto, essas observações qualificam a inibição da via PI3K/Akt e NFkappaB como um possível alvo na terapia contra os gliomas.

2. OBJETIVOS

2.1. Objetivo Geral

Determinar se a inibição da proteína cinase B (PKB/Akt) e/ou do fator de transcrição NFkappaB pode ser uma estratégia para indução de morte celular em Gliomas, e avaliar alguns mecanismos moleculares envolvidos nesses eventos.

2.2. Objetivos específicos

- Determinar os efeitos do inibidor farmacológico de NFkappaB partenolide, dos inibidores de PI-3K/Akt quercetina e Ly294002, e do inibidor misto curcumina, na viabilidade de culturas de glioblastomas humanos U87MG (PTEN mutada/P53 normal) e U251MG (PTEN mutada/P53 mutada) e em culturas de glioblastomas C6 de ratos;

- Avaliar a ativação de PKB/Akt e NFkappaB em células U87MG,U251MG e C6, através de seu imuno-conteúdo antes e após o tratamento com os inibidores farmacológicos;

- Determinar os mecanismos de morte celular envolvidos, discriminando entre apoptose, necrose ou autofagia, as vias envolvidas, e das caspases na ativação da maquinaria de morte celular, assim como analisar o ciclo celular.

Parte II

3. MATERIAIS E MÉTODOS

3.1. Reagentes e Anticorpos:

Curcumina, Iodeto de Propídeo, Hepes, CHAPS, Ditiotreitol, EDTA, tripsina, MTT (3-(4,5-dimetiil)-2,5-difenil tetrazolio brometo), Nonidet-P40, quercetina [2-(3,4-Diidroxifenil)-3,5,7-triidroxi-4H-1-benzopirano-4; 3, 3′, 4′, 5, 6-Pentaidroxiflavona], Espermina Tetraidrocloreto, RNAse A e os reagentes utilizados na cultura de células foram adquiridos da Sigma Chemical Co (St. Louis, MO, USA). Os anticorpos p-Akt policlonal, p-IKK, PARP, LC3 A/B, HSP70, Caspase 3 e β-actina foram comprados da Cell Signaling Technology. Já para o ensaio de LDH foi utilizado o kit CytoTox 96-NonRadioactive Cytotoxicity Assay da Promega Corporation (Madison, USA). Partenolide e o LY294002 da Biomol International (Plymouth Meeting, PA). Os reagentes usados para Eletroforese/immunoblotting foram adquiridos da Bio-Rad Laboratories (Hercules, CA, USA).

3.2. Cultura de Células:

As linhagens de glioblastomas de rato (C6) e as humanas (U87MG e U251MG) foram obtidas da American Type Culture Collection (Rockville, Maryland, USA). As células foram cultivadas e mantidas em Dulbecco's modified Eagle's medium (DMEM; Gibco BRL, Carlsbad, USA) contendo 0.1% Fungizona, 100U/l de gentamicina e suplementadas com 5% de soro fetal bovino nas células C6 e 10% na U87MG e U373MG. As células foram conservadas em estufa a 37ºC com 5% CO_2 (Zanotto-Filho et al., 2010).

3.3. Ensaios de MTT e de LDH:

A redução do MTT pelas desidrogenases celulares e a liberação da lactato desidrogenase (LDH) no meio de cultura foram utilizados para estimar a viabilidade celular (Dhandapani. et al., 2007; Zanotto-Filho et al., 2009). As células (10^4/por poço) foram semeadas em placas de 96 poços, após atingir a confluência de 60-70% essas células foram tratadas. Após os tratamentos foram realizados os ensaios de MTT e LDH. A liberação de Lactato Desidrogenase (LDH) no meio de cultura das células é um indicativo de perda de integridade de membrana, a qual foi determinada pelo kit de fluorescência (CytoTox 96-NonRadioactive Cytotoxicity Assay, Promega) segundo instruções do fabricante.

3.4. Incorporação de Iodeto de Propídeo e Morfologia Celular:

O iodeto de propídeo (PI) penetra nas células com perda da integridade da membrana plasmática e pode ser analisado por microscopia de fluorescência. Para isso, as células tratadas com os inibidores eram incubadas com 2 µg/mL de PI em meio por 1h em estufa (Braganhol et al., 2006). A fluorescência do PI foi excitada a 515-560 nm usando um microscópio invertido (Nikon Eclipse TE 300) equipado com filtro rodamina. A morfologia das células foi avaliada por microscopia de luz (Nikon Eclipse TE 300) e classificadas como: Normal (células com morfologia inalterada e densidade normal); Baixa densidade (células com morfologia normal e baixa densidade na placa); Células mortas (morfologia celular e nuclear alterada, vacuolização citoplasmática, presença de células soltas). Foram coletadas as microfotografias representativas (até 5 por poço).

3.5. Western Blotting:

As proteínas (50 µg) foram separadas por SDS-PAGE com 10% (w/v) de acrilamida, 0.275% (w/v) de bisacrilamida, e transferidas para uma membrana de nitrocelulose. Essas membranas foram incubadas em TTBS [20 mmol/L Tris–HCl, pH 7.5, 137 mmol/L NaCl, 0.05% (v/v) Tween 20] contendo 5% (w/v) de albumina bovina ou leite desnatado (segundo recomendações do fabricante) por 1h a temperatura ambiente. Após essa primeira incubação, essas membranas foram mantidas durante 12 horas em câmara fria, com o anticorpo primário adequado. Passado esse período, as membranas foram lavadas com TTBS e incubadas com o anticorpo secundário por 2h a temperatura ambiente. As bandas com quimioluminescência foram detectadas por exposição da membrana a um filme, que posteriormente foi analisado por densitometria através do software Image-J® (Zanotto-Filho et al., 2009).

3.6. Ciclo Celular:

Para análise do ciclo celular, as células foram tripsinizadas, centrifugadas e ressuspendidas em tampão de lise (3,5 mmol/L Citrato Trissódico, 0,1% (v/v) Nonidet P-40, 0,5 mmol/L Tris-HCl, 1,2 mg/mL Espermina Tetrahidrocloreto, 5 mg/mL RNAse, 5 mmol/L EDTA, 1 mg/mL de Iodeto de Propídeo, pH 7,6), foram agitadas em vortex e incubadas em gelo durante 10 minutos para completa lise celular. O conteúdo de DNA foi determinado por citometria de fluxo. Foram contados 10.000 eventos por amostra. As análises foram realizadas no software Pro CellQuest (BD Biosciences, CA) (Zanotto-Filho et al., 2010).

3.7. Ensaio de Autofagia:

Para o ensaio de autofagia, as células foram semeadas em placas de 12 poços em uma confluência de 70% e foram tratadas por 48 horas com seus respectivos inibidores. Após 48 horas o meio foi retirado e um novo meio contendo 2µg/mL de acridina foi adicionado as células. Depois de 30 minutos de incubação o meio contendo acridina foi desprezado e as células foram tripsinizadas e ressuspendidas em 400µL de PBS. As células marcadas com acridina foram determinadas por citometria de fluxo. Foram contados 10.000 eventos por amostra. As análises foram realizadas no software Pro CellQuest (BD Biosciences, CA) (Zanotto-Filho et al., 2010).

3.8. Análise Estatística:

Os dados foram expressos como média ± D.P. (desvio padrão) e analisados por ANOVA de uma via, seguido pelo teste post hoc de Tukey. As diferenças foram consideradas significativas quando $p<0,05$.

4. RESULTADOS

4.1. Inibidores de vias de sinalização potencialmente desreguladas em GBMs:

Como teste inicial, as células C6 foram tratadas com inibidores de diferentes vias de sinalização descritas como desreguladas em GBMs (Stewart, 2002; Soni et al., 2005; Yu et al., 2008; Brennan et al., 2009). Inibidores de PI3K/Akt (Ly294002), EGFr (PD158780), MEK/ERK1/2 (UO126), JNK1/2 (SP600129), p38 MAPK (SB203580), e IKK/NFkappaB (BAY117082 e partenolide) foram avaliados em diferentes concentrações. Ao final de 36 horas de incubação, os inibidores de PI3K/Akt e NFkappaB causaram uma diminuição significativa na viabilidade dos GBMs, quando comparado com os inibidores de outras vias. Os inibidores de outras vias de sinalização tais como MAPKs, EGFr, PKC não apresentaram efeitos citotóxicos mesmo em altas concentrações, acima de 60 µM (dado não mostrado) (tabela 1).

Tabela 1: Efeito de inibidores de vias de sinalização celular na viabilidade de Glioblastomas C6 (glioma de rato).

Tratamentos	Viabilidade (MTT)	Morfologia qualitativa
	C6	C6
Não tratadas	100 ± 4	Normal
UO126 (30 µM)	93 ± 15	Normal
SP600129 (30 µM)	103 ± 11	Normal
SB203580 (30 µM)	98 ± 10	Normal
PD158780 (50 µM)	99 ± 4	Normal
Ly294002 (50 µM)	64 ± 17*	Baixa densidade
BAY117082 (30 µM)	15 ± 6*	Células mortas
Partenolide (25 µM)	54 ± 5*	Células mortas

Legenda: Efeito de inibidores de vias de sinalização celular na viabilidade de GBMs. As células C6 foram tratadas por 36 horas com os inibidores das vias, e após esse período foi realizado o teste de MTT e a microscopia qualitativa. Foram realizados três experimentos independentes (n=3) em triplicata, e os resultados expressos como média ± DP para $p<0,05$.

4.2. Ensaio de viabilidade celular:

Para avaliar os efeitos dos inibidores de NFkappaB e PI3K/Akt na proliferação/ viabilidade dos GBMs foram realizados testes de MTT em três linhagens, C6 (glioma de rato), U87MG e U251MG (gliomas humanos). Para isso foram utilizados por 48 horas em diferentes concentrações: o inibidor partenolide (inibidor de IKK/NFkappaB), quercetina e Ly294002 (inibidores de PI3K/Akt) e o inibidor misto curcumina (IKK/NFkappaB e PI3K/Akt). Os inibidores curcumina e partenolide apresentaram uma curva tipo dose resposta na diminuição da viabilidade dos gliomas, enquanto a quercetina e o Ly294002, embora tenham reduzido a viabilidade das culturas, não apresentaram tal efeito de dependência de dose, atingindo um platô de inibição nas diferentes linhagens (figura 4).

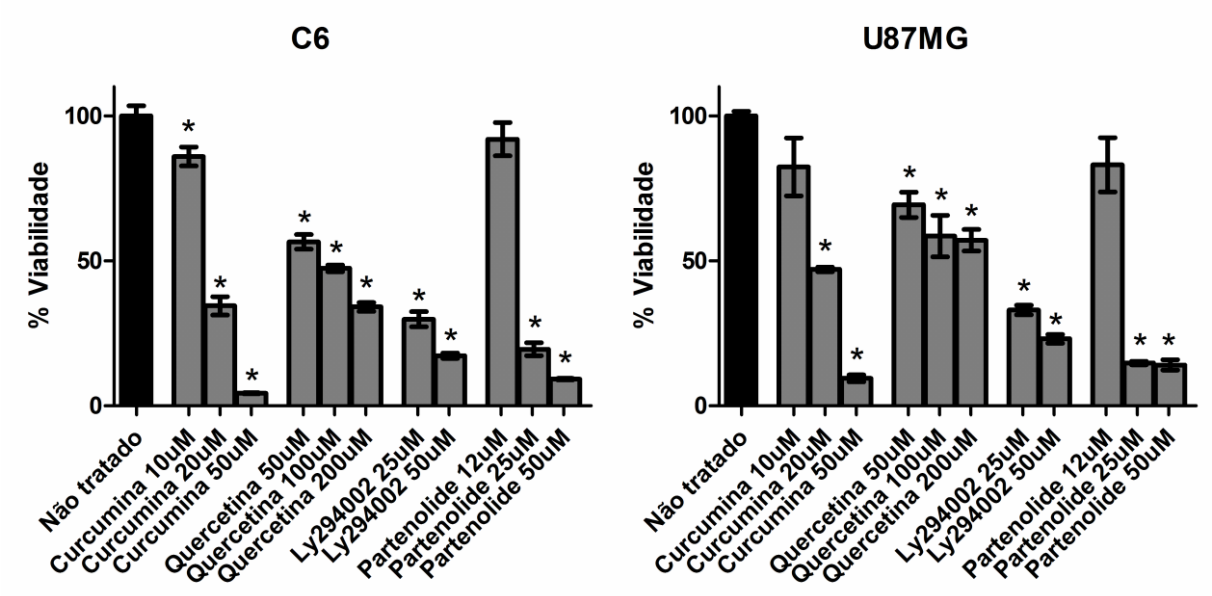

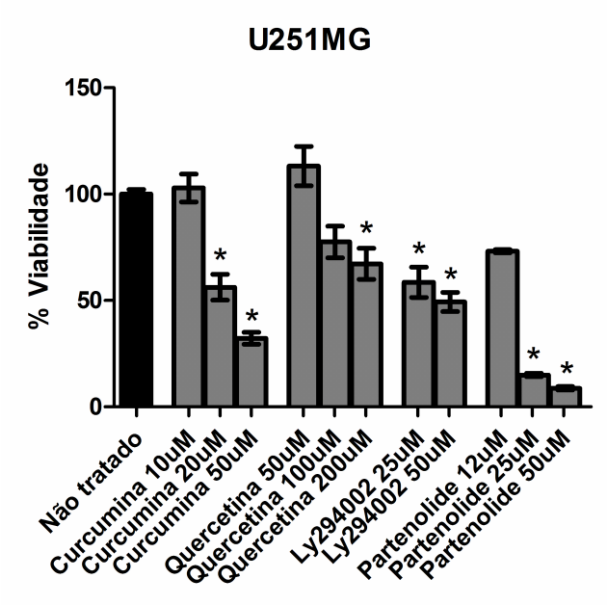

Figura. 4: Os inibidores de NFkappaB e PI3K/Akt induziram diminuição da viabilidade em linhagens de glioblastoma multiforme. MTT realizado nas células C6, U87MG e U251MG. As células foram tratadas por 48 horas com os inibidores em diferentes concentrações, curcumina (10, 20 e 50uM), quercetina (50, 100 e 200uM), Ly294002 (25 e 50uM) e partenolide (12, 25 e 50uM). Foram realizados três experimentos independentes (n=3), em triplicata (gráficos expressos em média ± D.P. $p<0,05$).

4.3. Morfologia Celular e Iodeto de Propídeo:

Para verificar a viabilidade da membrana plasmática e o estado de necrose/apoptose tardia celular, também foi utilizada a técnica de incorporação de Iodeto de Propídeo (PI). As células C6 e U87MG foram tratadas durante 48 horas com os inibidores, após esse período o meio foi trocado e as células foram mantidas por mais 1h com PI. O inibidor de ambas as vias de sinalização, a curcumina, apresentou uma maior citotoxicidade em 30uM para a linhagem U87MG ao passo que inibiu a proliferação em doses menores (15 uM) (figura 5B). Entretanto, na linhagem C6, a curcumina não induziu uma incorporação significativa de PI, apenas uma grande alteração morfológica (figura 5A). Já, em ambas as linhagens, as células tratadas com partenolide apresentaram incorporação de PI, sugerindo perda de integridade da membrana plasmática e morte celular (figura 5A e 5B). As células tratadas com quercetina e Ly294002 não apresentaram incorporação de PI, quando comparadas às células não-tratadas (figura 5A e 5B), confirmando os efeitos antiproliferativos destes inibidores indicados no ensaio de LDH (figura 6).

(A) Linhagem C6:

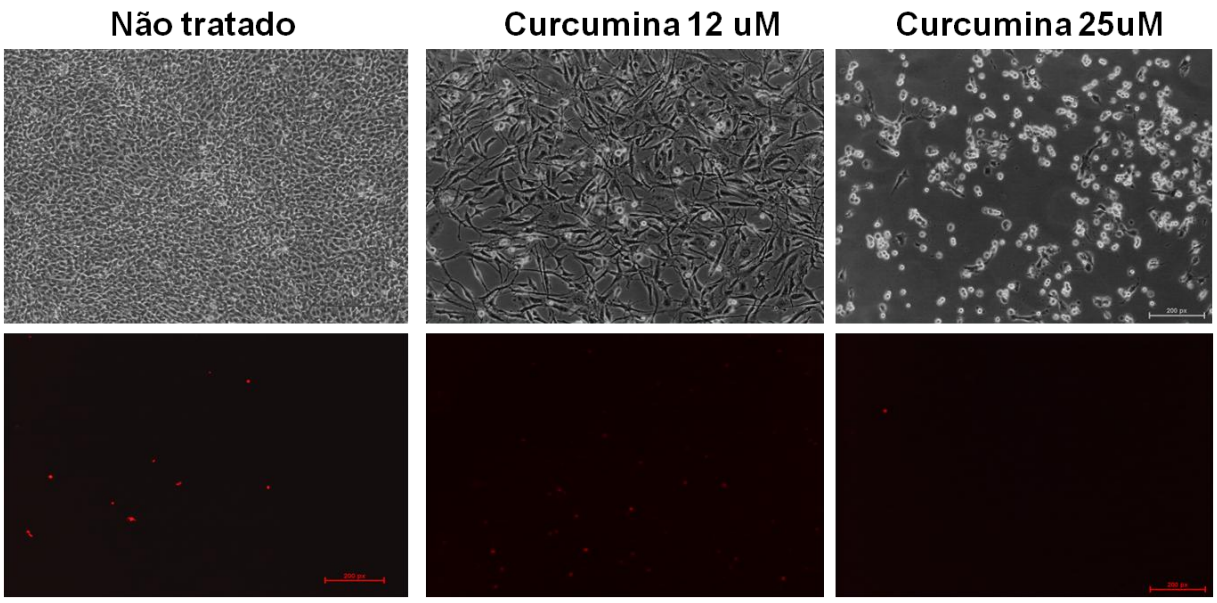

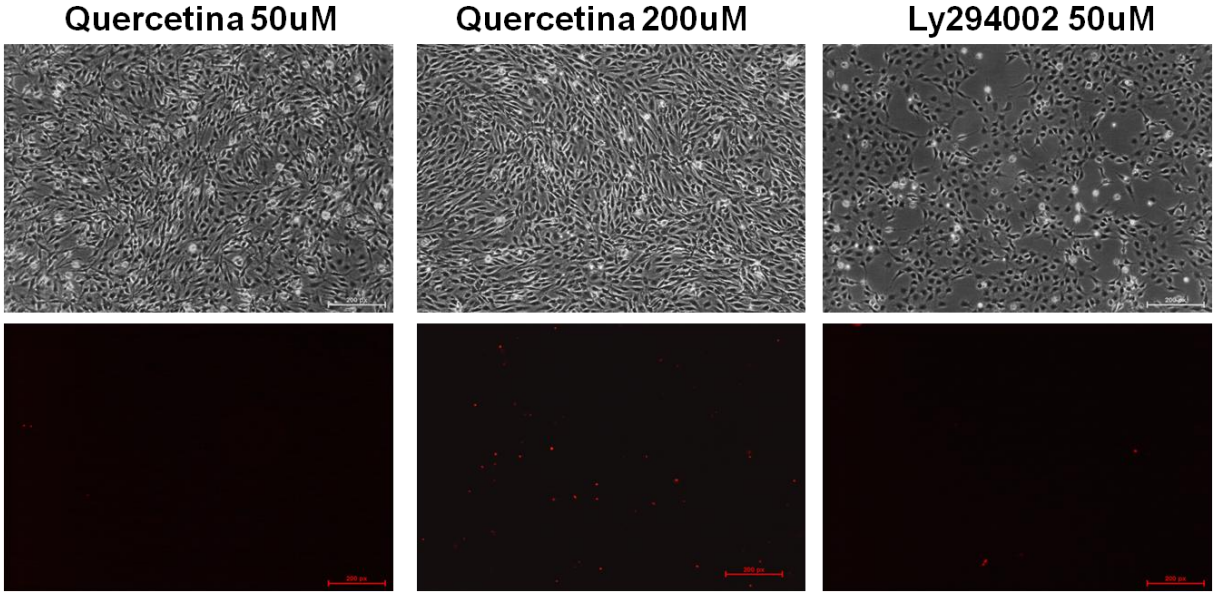

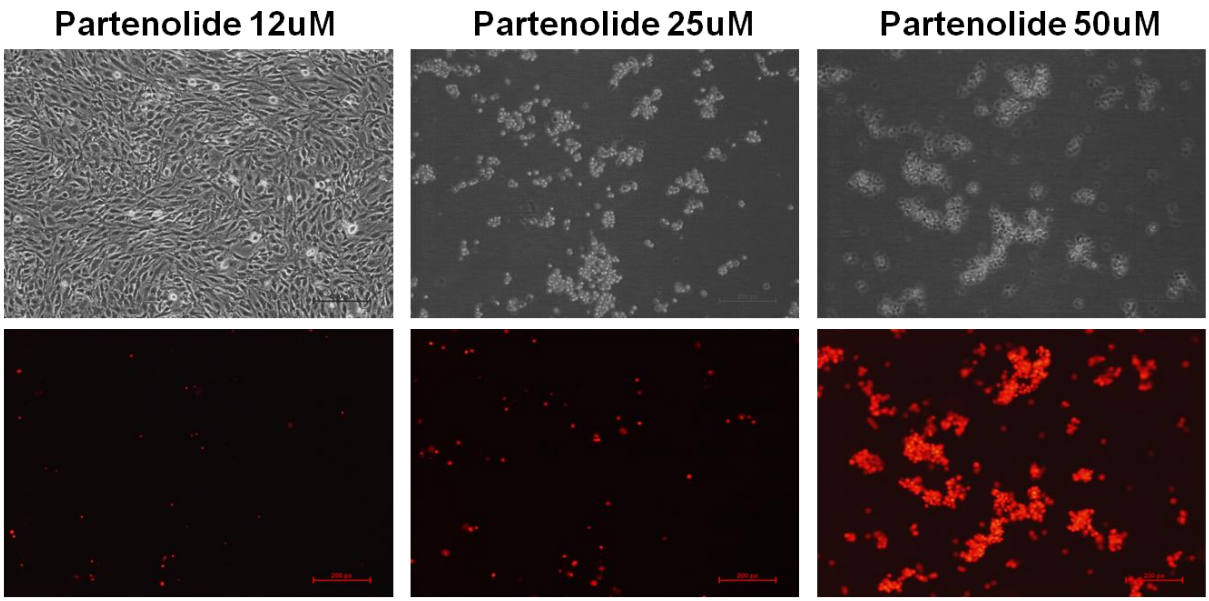

(B) Linhagem U87MG:

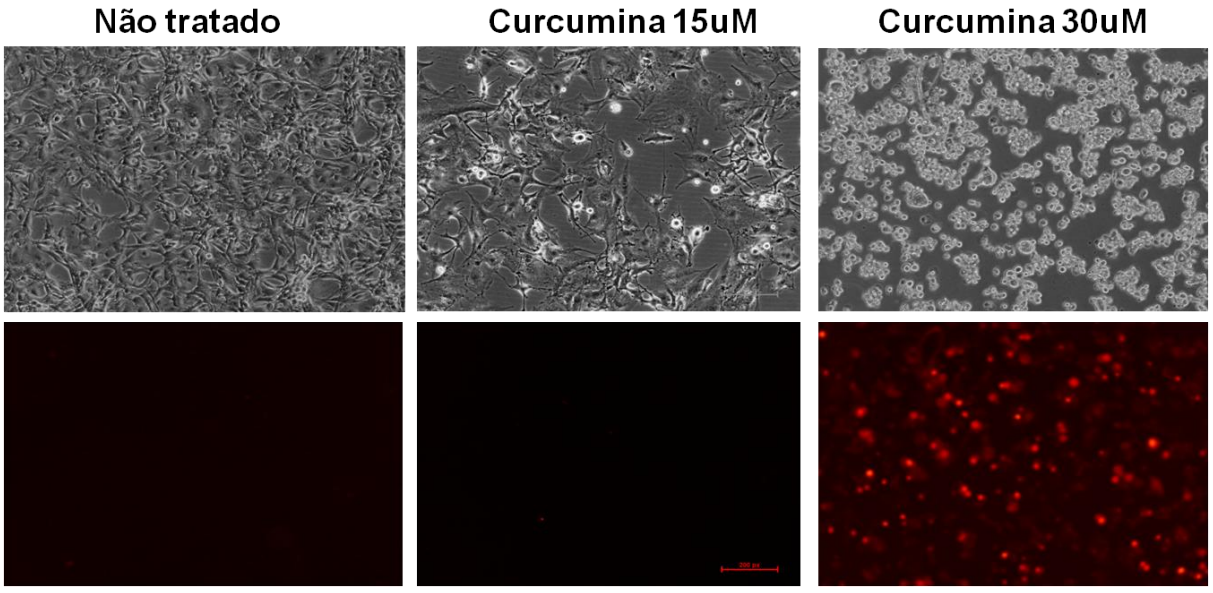

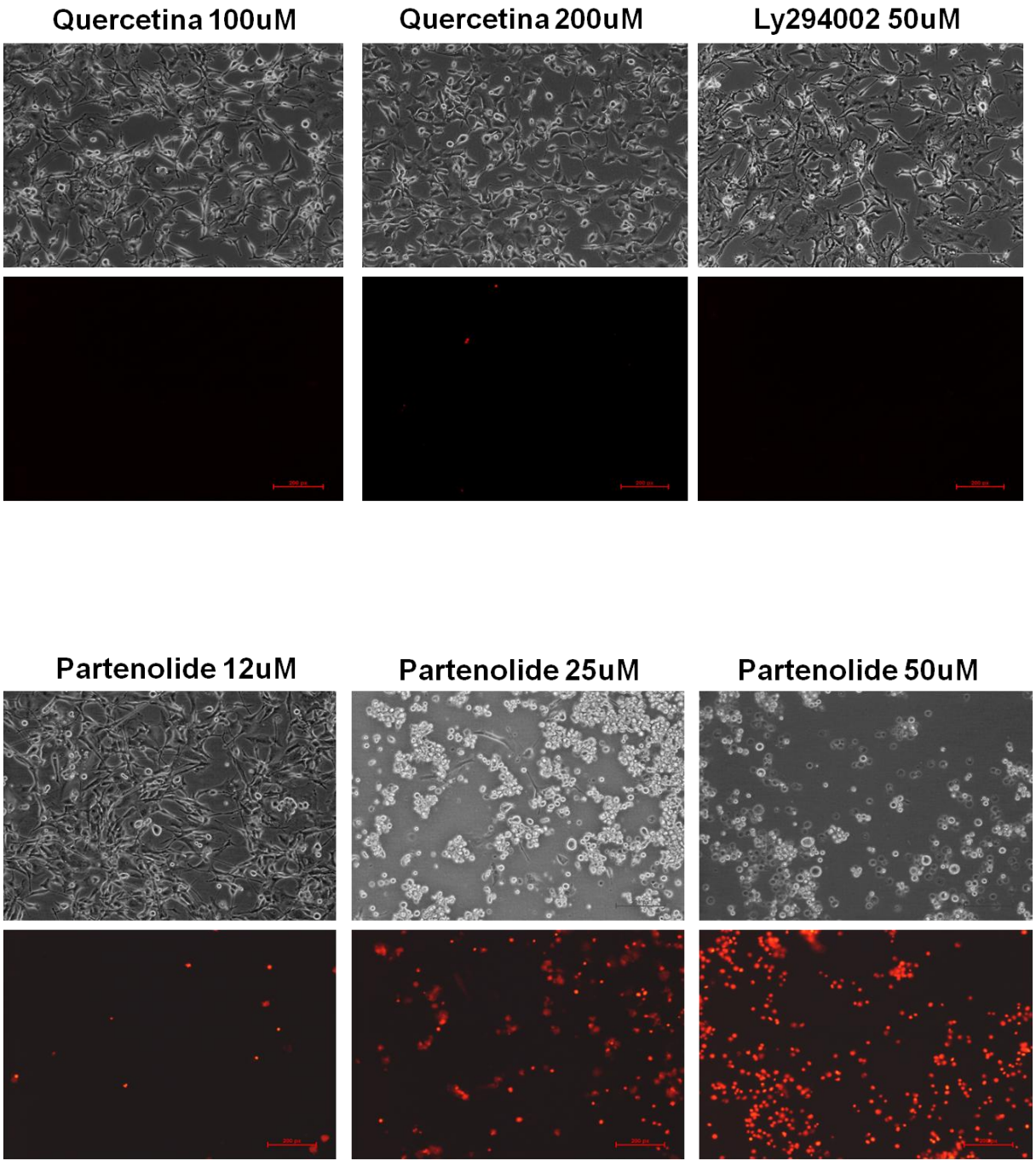

Figura 5: Ambos os inibidores, de NFkappaB e de PI3K/Akt, induziram a alterações morfológicas, mas apenas os de NFkappaB (curcumina e partenolide) induziram a perda de integridade da membrana plasmática após 48 horas de tratamento. Microfotografias representativas (aumento de 40x) do ensaio com Iodeto de Propídeo (PI) e contraste de fase, mostrando a perda de integridade da membrana plasmática e alterações morfológicas nas células tratadas com os inibidores de NFkappaB e PI3K/Akt. **(A)** As células C6 foram tratadas com os inibidores curcumina (12 e 25uM), quercetina (50 e 200uM), Ly294002 (50uM) e partenolide (12, 25 e 50uM) **(B)** As células U87MG foram tratadas com os inibidores curcumina (15 e 30uM), quercetina (100 e 200uM), Ly294002 (50uM) e partenolide (12, 25 e 50uM).

4.4. Quantificação da atividade de LDH liberada nos meios de cultura:

Os dados de morfologia e perfil de inibição nos ensaios de MTT, sugerem que os inibidores de PI3K/Akt (quercetina e Ly294002) causam inibição de proliferação ao passo que a inibição de NFkappaB (com partenolide) parece ser citotóxica. O inibidor de ambas vias de sinalização, a curcumina, apresentou uma maior citotoxicidade em 30 uM para a linhagem U87MG ao passo que inibiu a proliferação em doses menores (15 uM). Para confirmar essa hipótese, realizamos o ensaio de LDH, o qual indica perda de viabilidade da membrana plasmática. Nos ensaios de LDH as células C6 e U87MG foram tratadas por 48 horas com os inibidores curcumina, partenolide, quercetina e Ly294002. Após esse período o meio foi coletado para determinação da atividade de LDH. O Inibidor de NFkappaB (partenolide) apresentou um potente efeito no extravasamento de LDH no meio de cultura, indicando uma perda na viabilidade da membrana plasmática (figura 6). Por outro lado, os inibidores de PI3K/Akt (quercetina e Ly294002) e o inibidor misto (curcumina), não apresentaram diferença significativa do controle, confirmando o efeito antiproliferativo observado para Ly294002 e quercetina, e curcumina em baixas dosagens (figura 6). Por outro lado, as alterações morfológicas causadas pela curcumina em concentrações de 25 uM na linhagem C6 e a não indução de incorporação de PI nesta mesma linhagem, sugerem que as células estão respondendo com um mecanismo programado de perda de integridade, o qual será subsequentemente estudado.

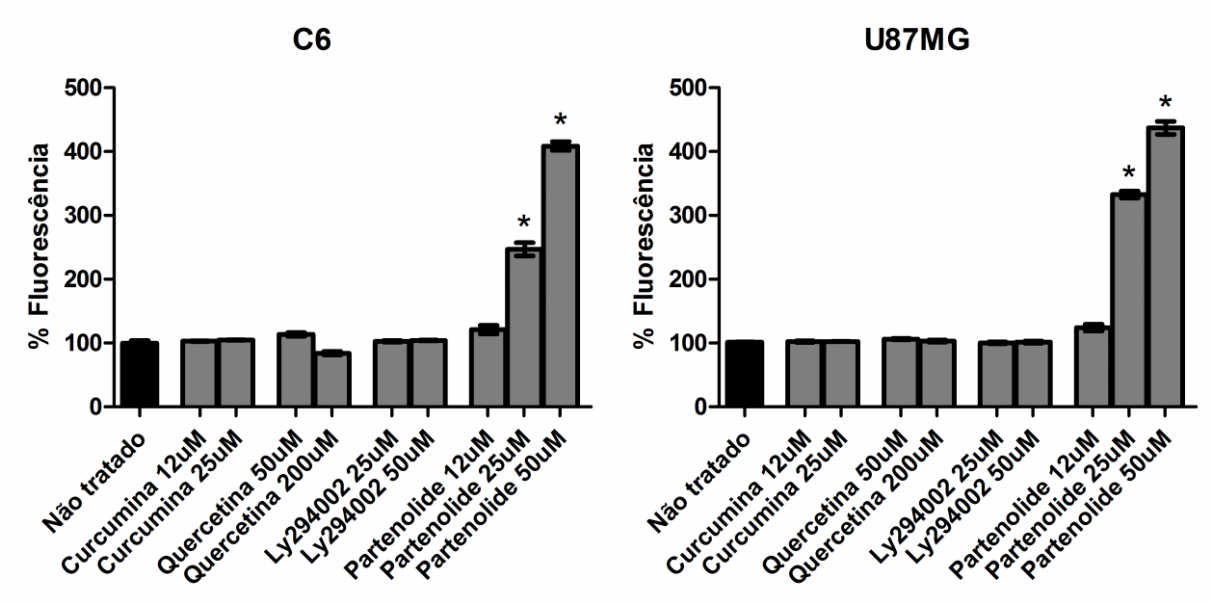

Figura 6: Ensaio de LDH em que o inibidor de NFkappaB, partenolide, apresentou extravasamento de LDH. As células C6 e U87MG foram tratadas por 48 horas com os inibidores curcumina (12 e 25uM), quercetina (50 e 200uM), Ly294002 (25 e 50uM) e partenolide (12, 25 e 50uM). Foram realizados três experimentos independentes (n=3) em triplicata (gráficos expressos em média ± D.P. p<0,05). * Diferente do controle.

4.5. Ciclo Celular:

Considerando que os inibidores em teste diminuíram a densidade celular em cultivo sem um grande efeito citotóxico (exceto para o partenolide), decidimos estudar a possibilidade de os mesmos estarem induzindo paradas no ciclo celular. A análise do ciclo celular nas três linhagens de glioma mostrou que os tratamentos com curcumina, quercetina, Ly294002 e partenolide, durante 48 horas, foram capazes de alterar o perfil do ciclo celular.

Na linhagem C6, que é uma célula com Pten e p53 normais, a curcumina e o partenolide aumentaram o número de células em G2. Além disso, o partenolide teve um pequeno aumento de células hipodiploides (subG1). Já a quercetina e o Ly294002 não afetaram significativamente a proporção de células em cada fase do ciclo, sugerindo que a via de PI3k/Akt é importante na velocidade do ciclo celular, mas sua inibição não está causando *arrest* (figura 7).

Já no caso da linhagem U87MG, mutada apenas em Pten, visualizamos que o tratamento com curcumina e quercetina gerou um grupo de células octaploides (8n), que não foi atribuído a dubletos de células em G2 (controle feito na análise do ciclo celular), sugerindo que as células em G2/M sofreram um ciclo adicional de duplicação de DNA sem passagem pela mitose, o que ocorre com algumas linhagens tumorais que perdem o controle checkpoint da fase G2/M (figura 7). O Ly294002 causou parada na fase G1 (fase diploide) e o partenolide induziu taxas significativas de células em sub-G1(apoptose) (figura 7), em acordo com os dados de citotoxicidade observados no ensaio de LDH e incorporação de PI (figura 6 e 5B).

Na linhagem U251MG, Pten e P53 mutadas, a curcumina causou um grande aumento em G2/M, e um pequeno aumento no número de células em apoptose. Já o

tratamento com partenolide causou um aumento significativo de células em sub-G1 (apoptose). O tratamento com quercetina provocou um pequeno aumento em sub-G1, enquanto que Ly294002 não alterou significativamente o ciclo celular (figura 7).

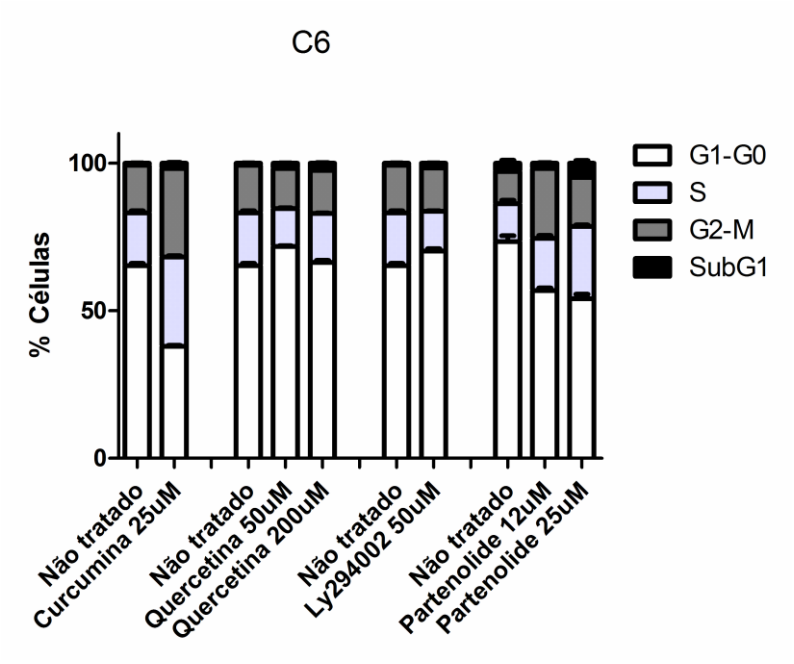

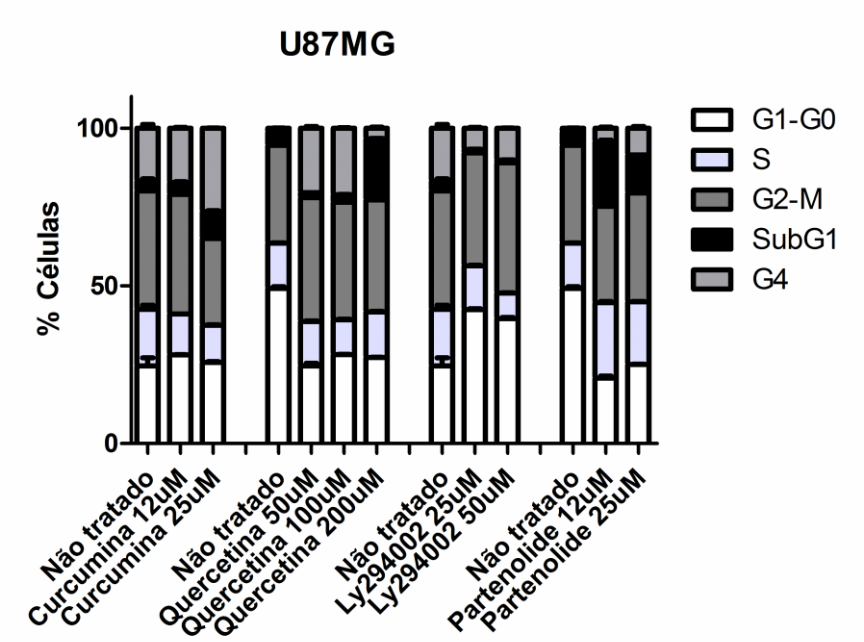

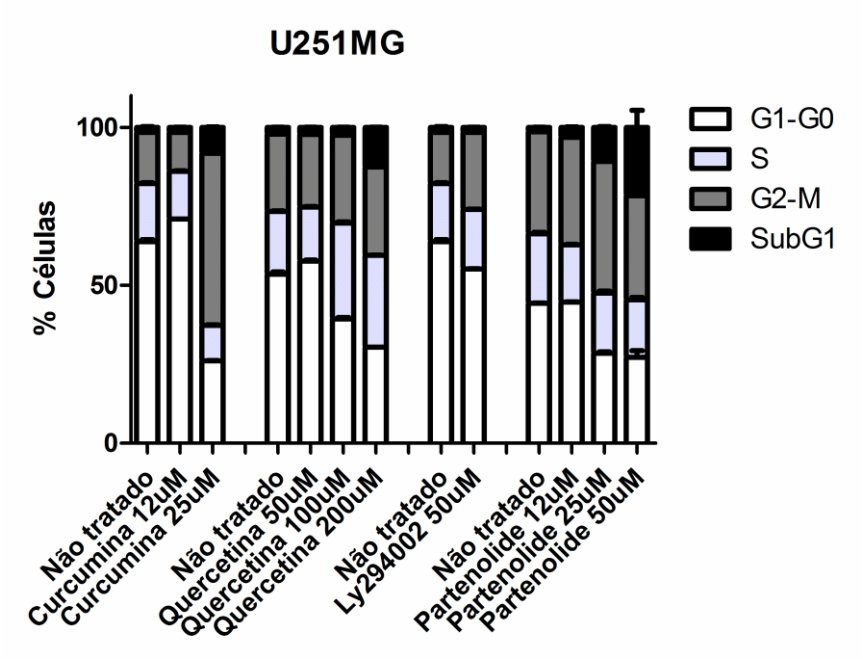

Figura 7: Quantificação da distribuição da população de células nas fases do ciclo celular entre G4, sub-G1, G1/G0, S e G2/M após 48 horas de tratamento nas linhagens C6, U87MG e U251MG com os inibidores de NFkB e de PI3K/Akt. Foram realizados três experimentos independentes (n=3) em triplicata.

4.6. Autofagia:

Considerando que os achados de dimunuição de viabilidade celular observados pelo ensaio de MTT não foram diretamente relacionados a uma significante citotoxicidade observada em ensaios de incorporação de PI e LDH, principalmente nos tratamentos com curcumina, quercetina e Ly294002, decidimos estudar o processo de autofagia, o qual tem sido descrito como um importante mecanismo de resistência celular em gliomas (Jiang et al., 2009).

Para analisar o tipo de morte provocada pelos inibidores, realizamos o teste de incorporação de acridina, que cora os vacúolos autofágicos emitindo uma fluorescência vermelha/alaranjada, um indicativo de morte por autofagia. As células C6 e U87MG foram tratadas por 48 horas com os inibidores, e após esse período o meio foi retirado e adicionado um novo meio contendo o corante de acridina. Nas três linhagens apenas as doses mais altas de curcumina e quercetina foram capazes de aumentar a autofagia. Enquanto que o inibidor Ly294002 aumentou a autofagia nas duas doses utilizadas nas linhagens U87MG e U251MG. Já o inibidor de IKK/NFkappaB, partenolide, aumentou a autofagia nas três linhagens em todas as doses utilizadas, apresentando um efeito tipo dose resposta (figura 8).

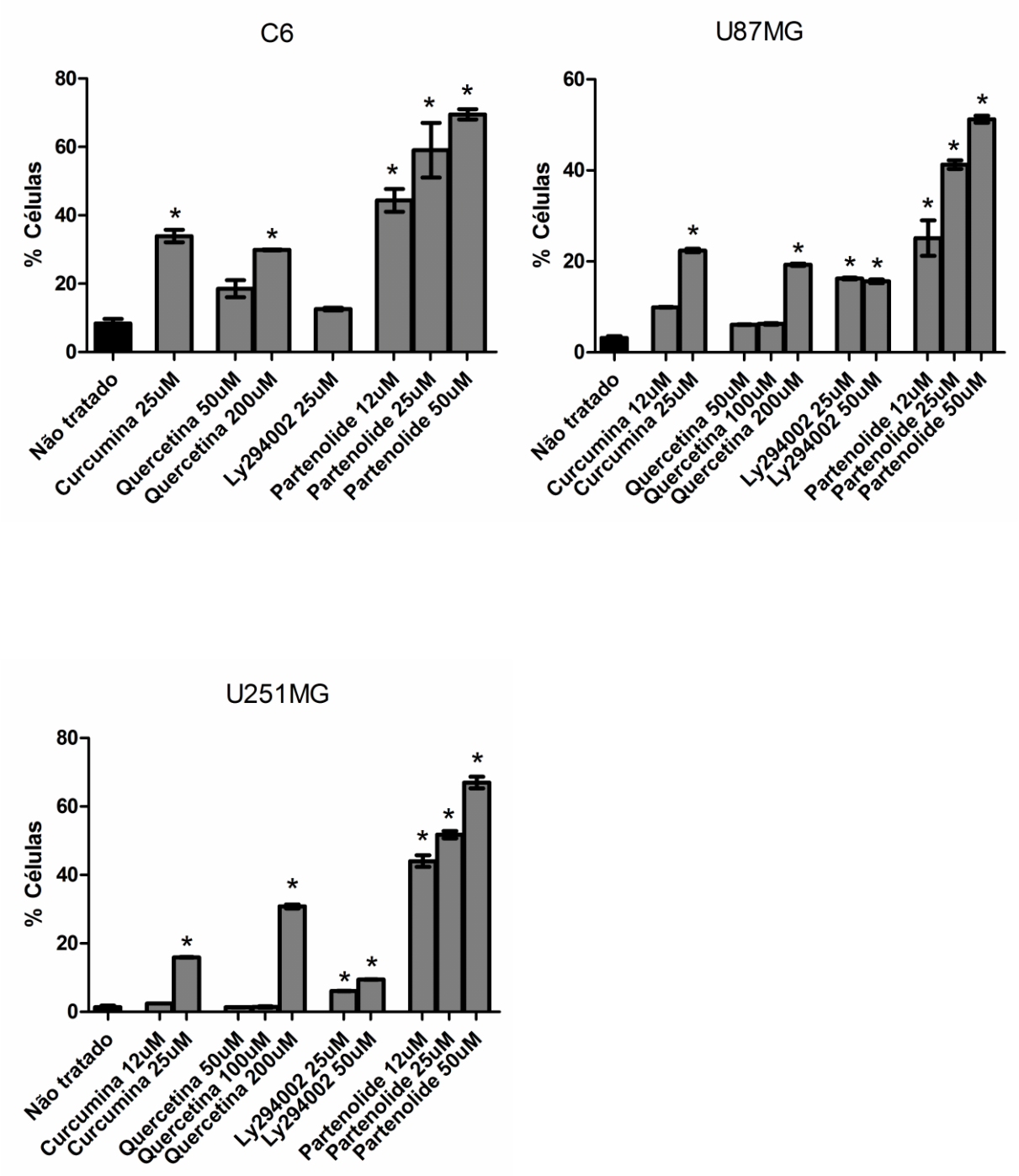

Figura 8: Teste de autofagia ocasionada pelos tratamentos. As células C6, U87MG e U251MG foram tratadas com os inibidores, e a incorporação de acridina foi medida por citometria de fluxo. Foram realizados três experimentos independentes (n=3) em triplicata (gráficos expressos em média ± D.P. $p<0,05$). * Diferente do controle.

4.7. Western Blotting:

Foi realizado o teste de Western Blotting para Akt fosforilada (p-Akt, forma ativa), IKK fosforilada (p-IKK, forma ativa), LC3 A/B (marcador de autofagia), PARP (envolvida no reparo ao DNA), HSP70 (chaperona – estresse celular) e caspase 3 (caspase efetora – apoptose) com a finalidade de analisar os efeitos dos inibidores de PI3K/Akt, quercetina (200µM) e Ly294002 (50µM), e dos inibidores de IKK/NFkB, curcumina (25µM) e partenolide (15µM) sobre os seus alvos farmacológicos e em marcadores de morte e estresse celular. As células das linhagens de glioma de rato C6 e de glioma humano U87MG foram tratadas por 48 horas e os experimentos foram realizados em extratos totais utilizando-se de 50µg de proteína por poço. A β-actina foi utilizada como controle interno do experimento (figura 9). Como mostram os blots, nas duas linhagens C6 e U87MG, todos os inibidores foram capazes de diminuir o imuno-conteúdo de p-IKK, já no caso da p-AKT, apenas os inibidores quercetina e Ly294002 foram capazes de alterar seu imuno-conteúdo. Quando analisamos as vias de sinalização relacionadas aos diferentes tipos de morte, podemos observar um aumento no imuno-conteúdo de LC3 A/B, em ambas as linhagens, exceto no tratamento com o inibidor partenolide na linhagem C6, um importante marcador de autofagia (Figuras 9A e 9B). No caso da PARP não tivemos um aumento do seu imuno-conteúdo em nenhuma das linhagens, indicando que os tratamentos não estão provocando danos ao DNA, podendo também estar relacionado com uma não ocorrência de necrose (Figura 9A e 9B). Já quando estudamos o imuno-conteúdo de caspase 3, a caspase efetora da apoptose, podemos notar na linhagem C6 um aumento significativo nos tratamentos com os inibidores de NFkappaB, curcumina e partenolide, o que não ocorre com os

inibidores de PI3K/Akt, quercetina e Ly294002 (Figura 9A). Em contrapartida, na linhagem U87MG, observamos uma diminuição de caspase 3 em todos os tratamentos (Figura 9B). Nas duas linhagens constatamos uma diminuição do imuno-conteúdo de HSP70, quando tratadas com os inibidores de PI3K/Akt (quercetina e Ly294002) (Figura 9A e 9B), e um aumento do seu imuno-conteúdo na linhagem U87MG, quando tratadas com os inibidores de NFkB (curcumina e partenolide) (Figura 9B). O imuno-conteúdo aumentado de HSP70 é um bom indicativo de que a célula tumoral está perdendo a resistência aos mecanismos de morte, e induzindo uma resposta a proteínas mal formadas (*unfolded protein response*), tipicamente observada em estados de estresse de retículo endoplasmático, os quais estão relacionados com indução de autofagia (Jeco et al., 2010).

A) Linhagem C6:

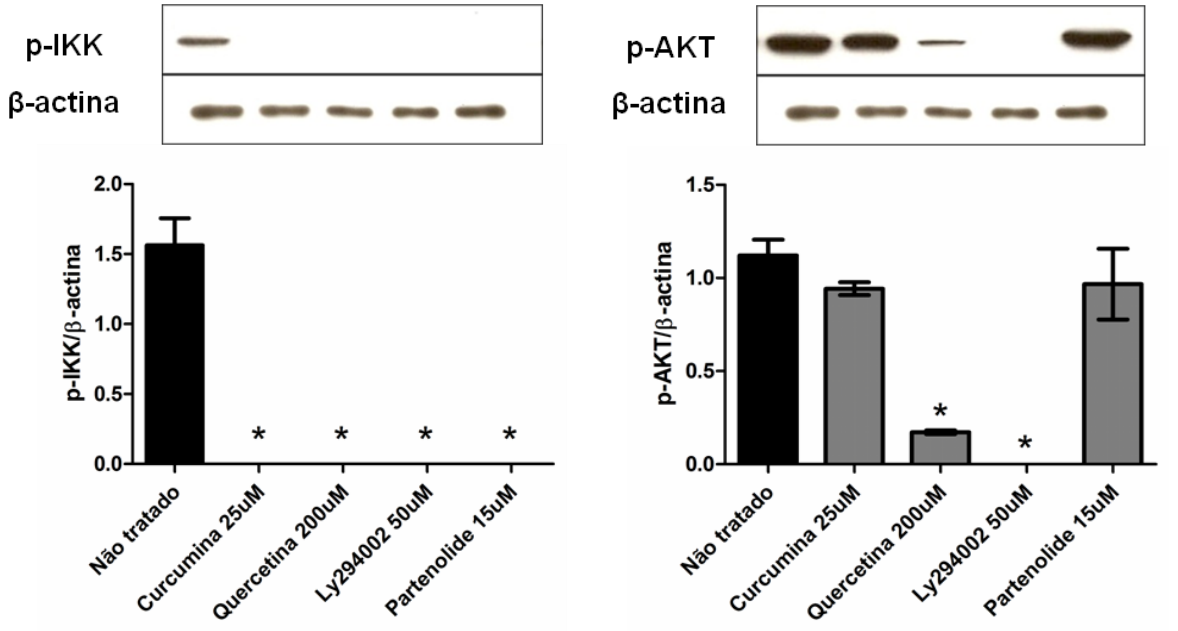

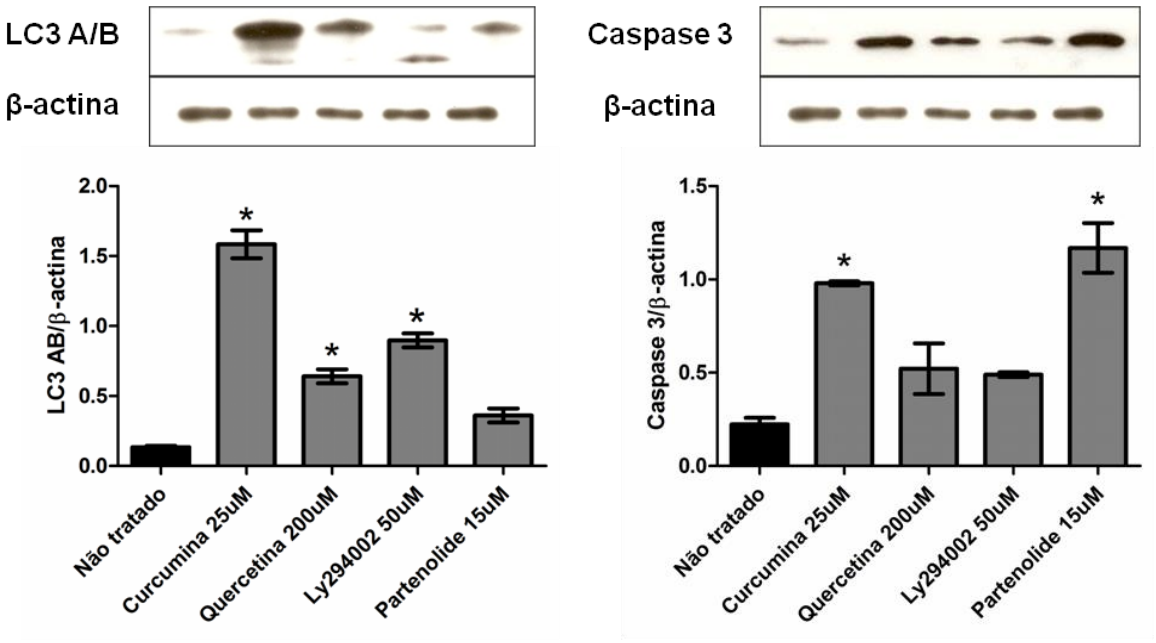
LC3 A/B
β-actina
LC3 AB/β-actina
2.0
1.5
1.0
0.5
0.0
*
*
*
Não tratado
Curcumina 25uM
Quercetina 200uM
Ly294002 50uM
Partenolide 15uM
Caspase 3
β-actina
Caspase 3/β-actina
1.5
1.0
0.5
0.0
*
*
Não tratado
Curcumina 25uM
Quercetina 200uM
Ly294002 50uM
Partenolide 15uM

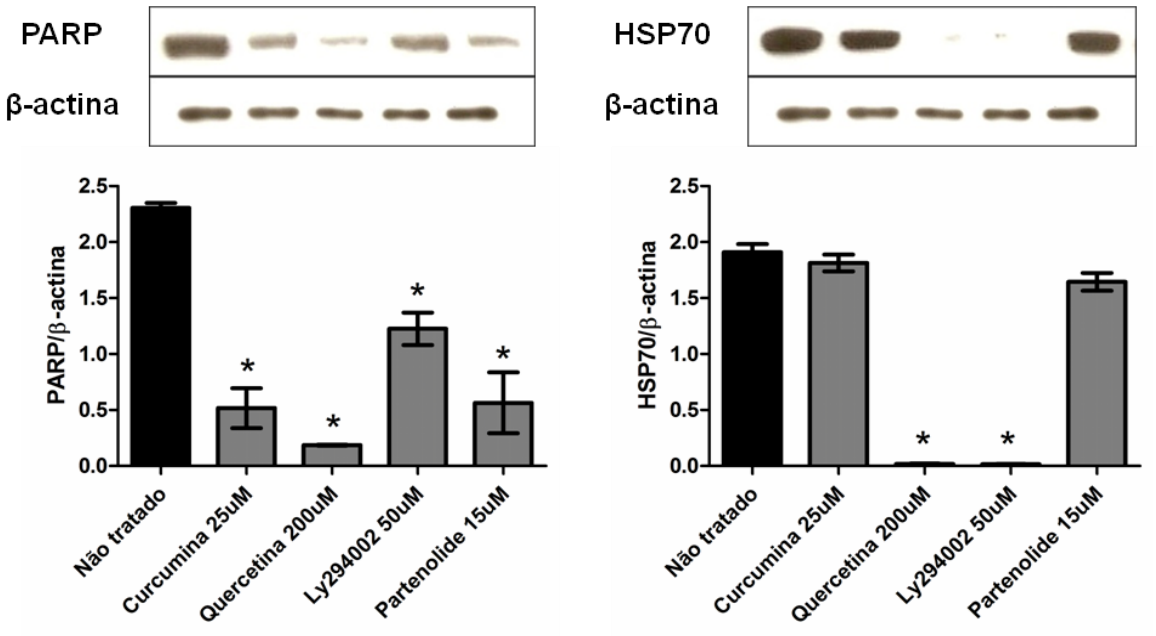
PARP
β-actina
PARP/β-actina
2.5
2.0
1.5
1.0
0.5
0.0
*
*
*
*
Não tratado
Curcumina 25uM
Quercetina 200uM
Ly294002 50uM
Partenolide 15uM
HSP70
β-actina
HSP70/β-actina
2.5
2.0
1.5
1.0
0.5
0.0
*
*
Não tratado
Curcumina 25uM
Quercetina 200uM
Ly294002 50uM
Partenolide 15uM

B) Linhagem U87MG:

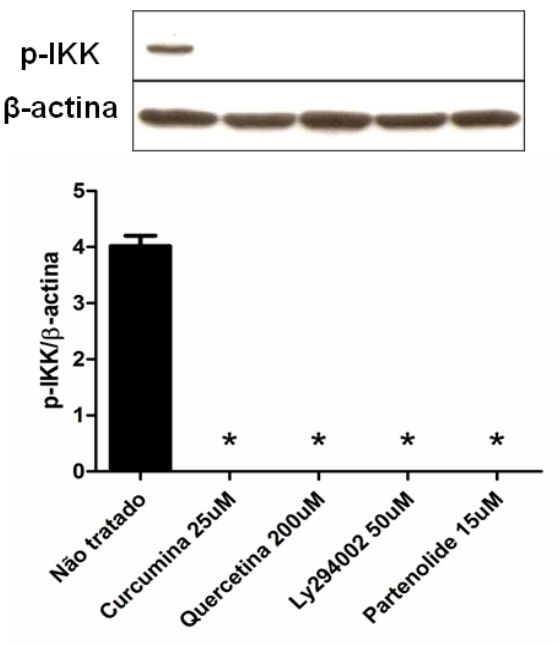

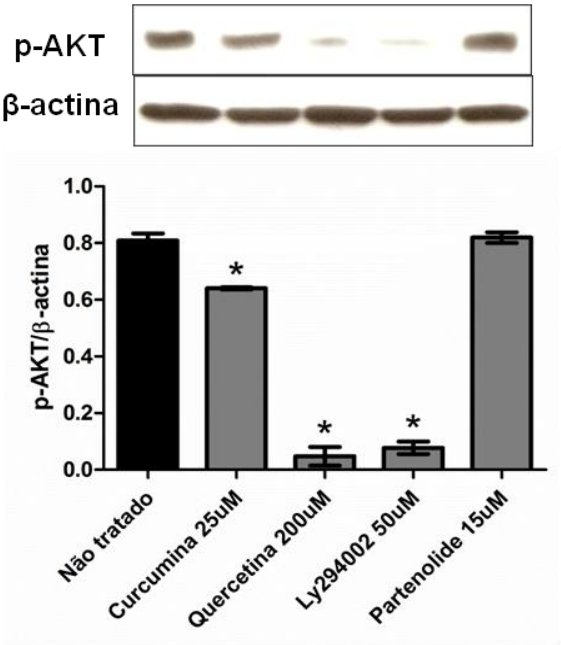

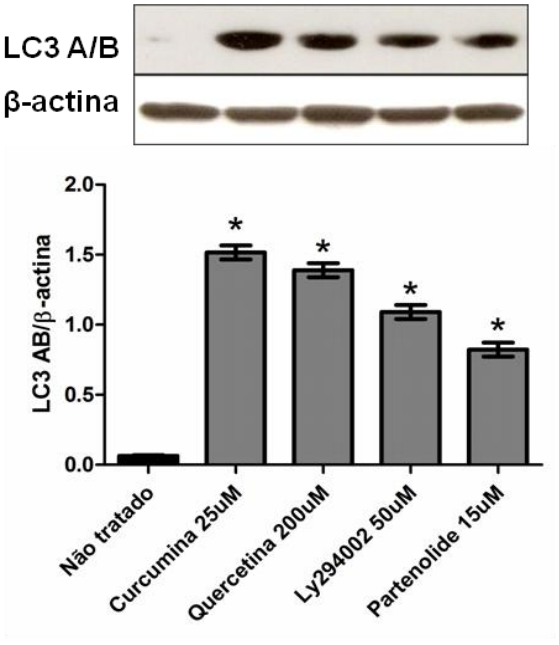

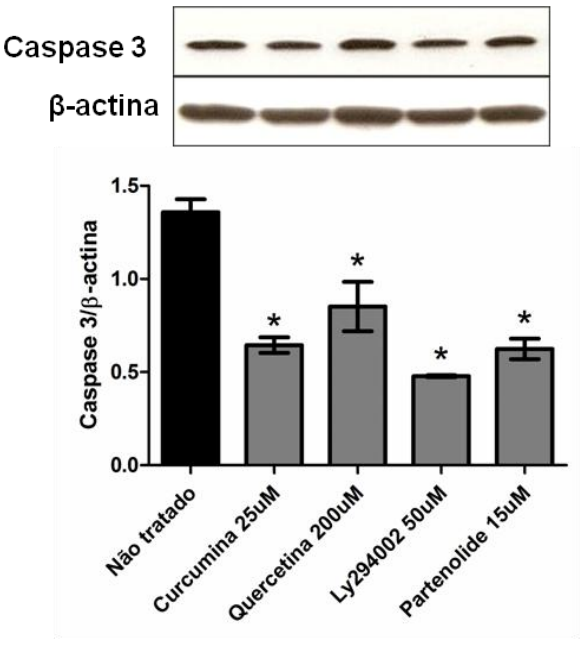

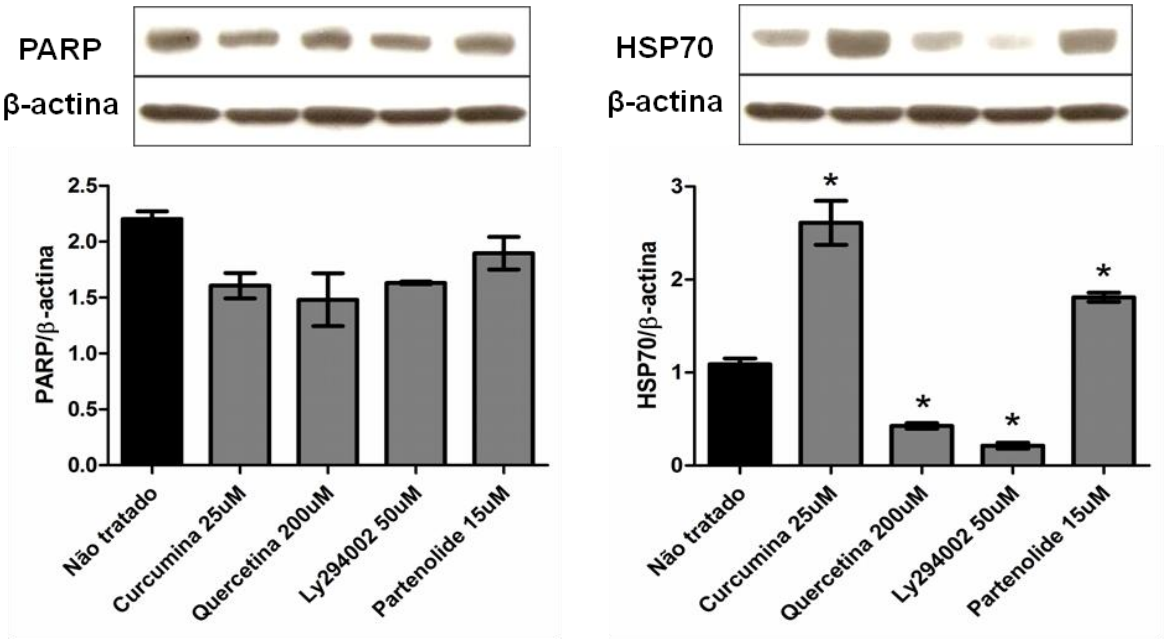

Figura 9: Células foram tratadas por 48 horas com curcumina (25uM), quercetina (200uM), Ly294002 (50uM) e partenolide (15uM), e os extratos celulares foram processados por Western blotting para avaliação dos níveis de p-IKK, p-Akt, LC3 A/B, PARP, HSP70 e Caspase 3. **A)** Linhagem C6 **B)** Linhagem U87MG. Foram realizados três experimentos independentes (n=3) em triplicata (gráficos expressos em média ± D.P. $p<0,05$). * Diferente do controle.

4.8. MTT com 3MA:

A fim de analisarmos a importância da autofagia na diminuição da viabilidade observada nos tratamentos com os inibidores, utilizamos a 3-metiladenina (3-MA) que é usado para inibir e estudar o mecanismo de macroautofagia (auto-degradação mediada por lisossomas) em diversas condições. A 3-MA é conhecida por inibir a autofagia, bloqueando a formação do autofagossomo através da inibição da fosfatidilinositol 3-cinase (PI-3K) do tipo III. Para tanto fizemos um pré-tratamento de 1 hora com 3-MA na concentração de 5mM. Ao término do pré-tratamento, as células foram tratadas com os inibidores curcumina, quercetina, Ly294002 e partenolide por 72 horas, e após esse período realizamos o ensaio de MTT. Foi constatado que na linhagem C6 o pré-tratamento com 3-MA nas células tratadas com curcumina e quercetina foi capaz de diminuir ainda mais a viabilidade, quando comparado apenas com os tratamentos sozinhos (figura 10). Já na linhagem U87MG o pré-tratamento foi capaz de diminuir a viabilidade apenas no tratamento com partenolide (figura 10). Não houve diferenças significativas em nenhum dos tratamentos com a linhagem U251MG (figura 10).

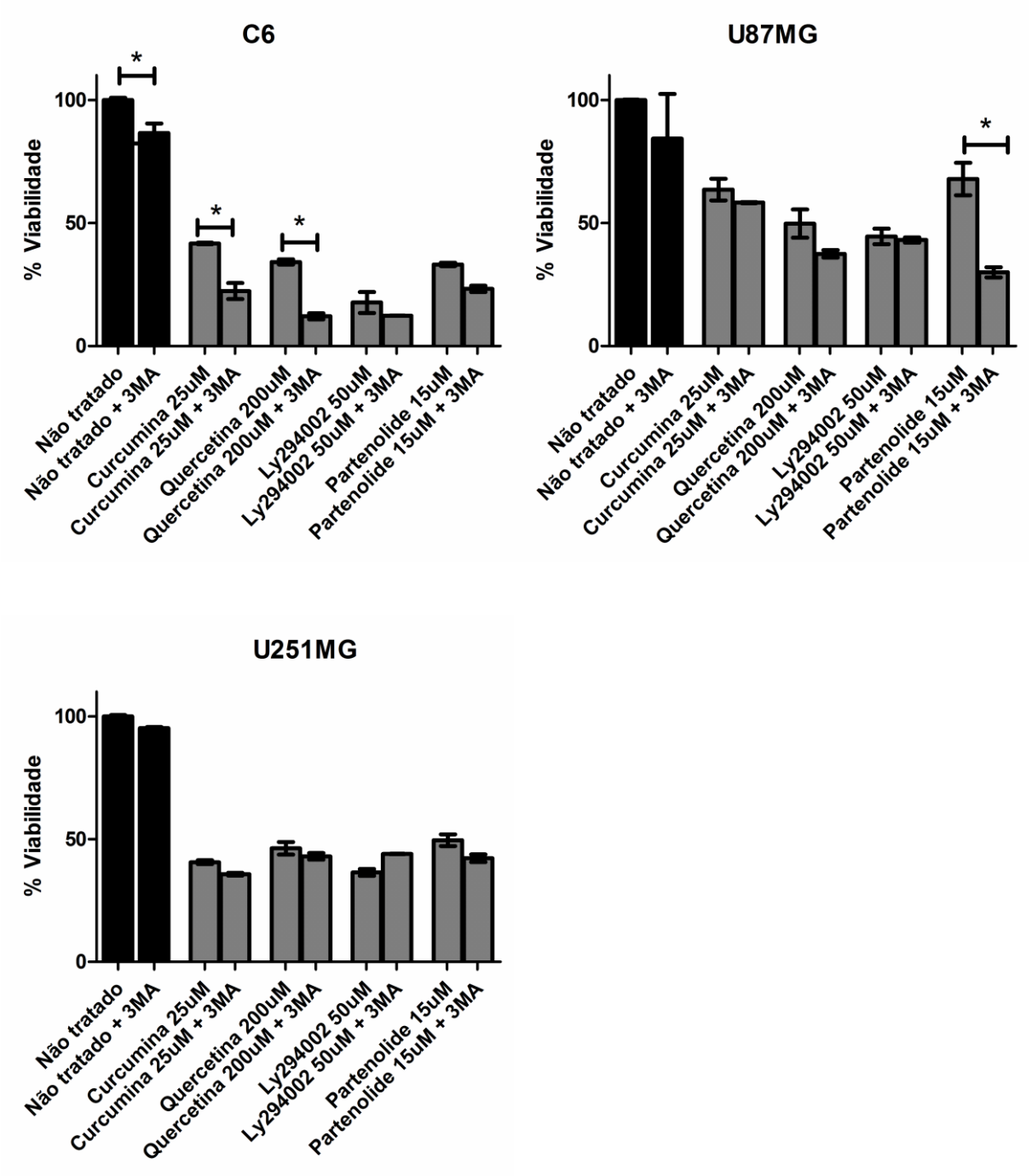

Figura 10: Efeito do pré-tratamento com o inibidor de autofagia 3MA na viabilidade das linhagens de glioblastomas C6, U87MG e U251MG, quando tratadas com curcumina (25uM), quercetina (200uM), Ly294002 (50uM) e partenolide (15uM). Foram realizados três experimentos independentes (n=3) em triplicata (gráficos expressos em média ± D.P. $p<0,05$). * Diferente do controle.

4.9. Incorporação de Iodeto de Propídeo com 3MA:

Também realizamos o ensaio de incorporação de iodeto de propídeo nas células pré-tratadas com o 3-MA com o intuito de analisarmos se a inibição da autofagia seria acompanhada com um aumento na perda da viabilidade da membrana plasmática. Como no ensaio de MTT, as células das linhagens C6 e U87MG foram pré-tratadas por 1h com 3-MA na concentração de 5mM. Ao término desse pré-tratamento, as células foram tratadas por 72 horas com os inibidores curcumina (25uM), quercetina (200uM), Ly294002 (50uM) e partenolide (15uM). Na linhagem C6, nas células controle e nas tratadas com partenolide, o pré-tratamento com 3MA, não alterou sua proliferação, como pode se analisar a partir da densidade das células em cultivo (figura 11A). Já as células tratadas com curcumina, quercetina e Ly294002, que foram pré-tratadas com 3MA, apresentaram uma diminuição significativa na densidade das culturas, sugerindo uma diminuição da proliferação celular (figura 11A). Quando analisamos a incorporação de iodeto de propídeo, podemos observar que o pré-tratamento com 3MA foi capaz de aumentar a perda da integridade da membrana plasmática nas células tratadas com Ly294002 (figura 11A). Em contrapartida, embora tenha diminuído a densidade celular como acima descrito, o pré-tratamento com 3MA nas células tratadas com curcumina e partenolide diminuiu a incorporação de PI, quando comparado com o tratamento sozinho, indicando que a autofagia estava mediando à perda de integridade de membrana das células induzida pela curcumina e partenolide (figura 11A). Nas células tratadas com quercetina, o pré-tratamento com 3MA não alterou a viabilidade da membrana plasmática (figura 11A).

Na linhagem PTEN mutada U87MG, o pré-tratamento com o inibidor de autofagia diminuiu a proliferação e potencializou a perda de viabilidade da membrana plasmática apenas no tratamento com partenolide, não apresentando alterações nos demais tratamentos (Figura 11B), o que sugere que diferentes células tem diferentes perfis de resposta a inibição da autofagia.

A) Linhagem C6:

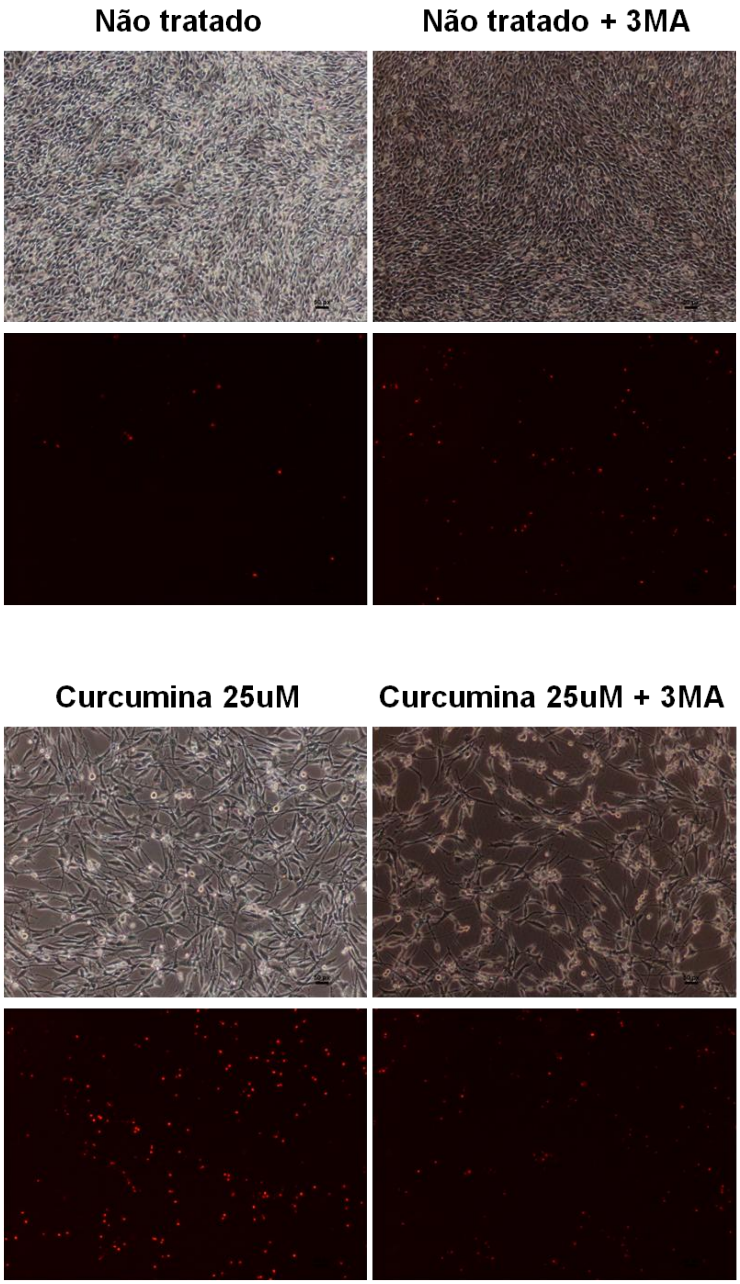

Quercetina 200uM

Quercetina 200uM + 3MA

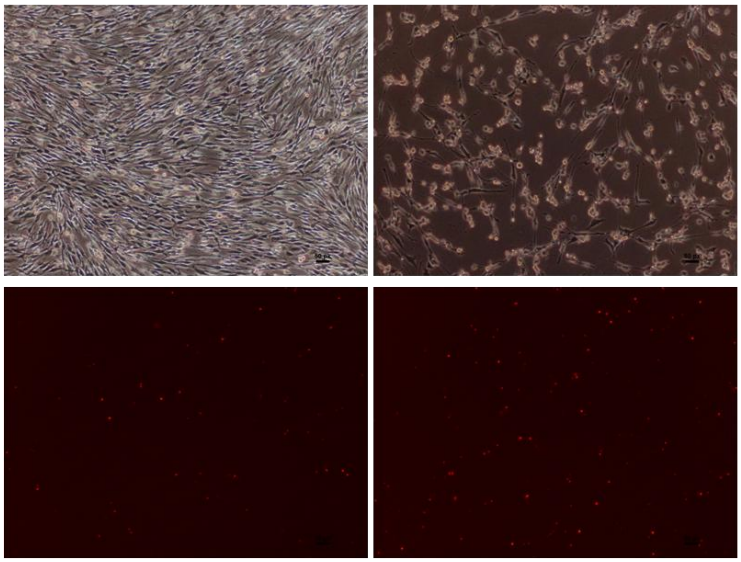

Ly294002 50uM

Ly294002 50uM + 3MA

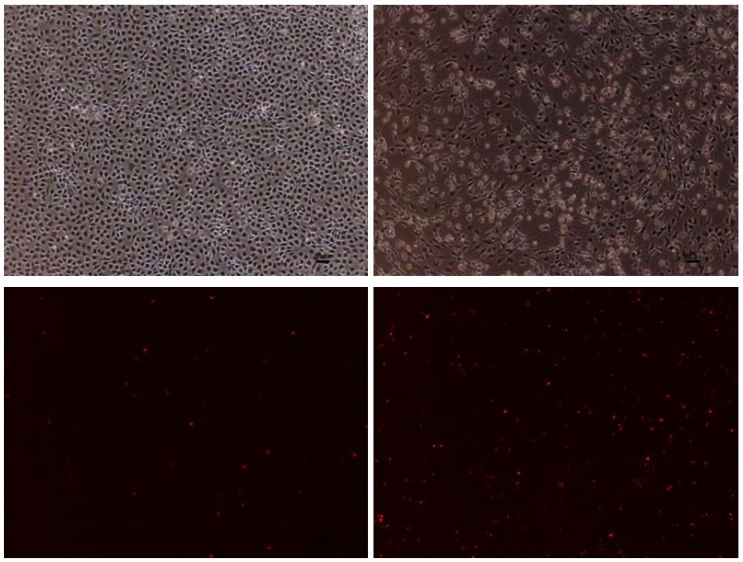

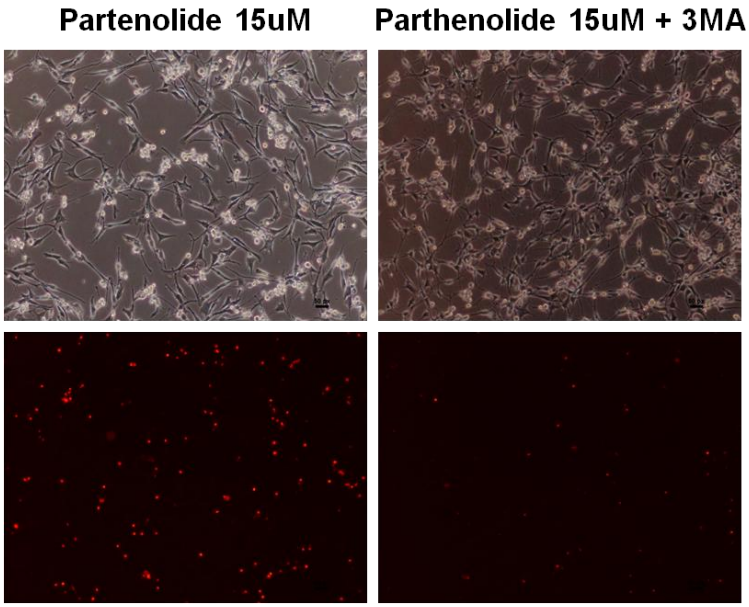

B) Linhagem U87MG:

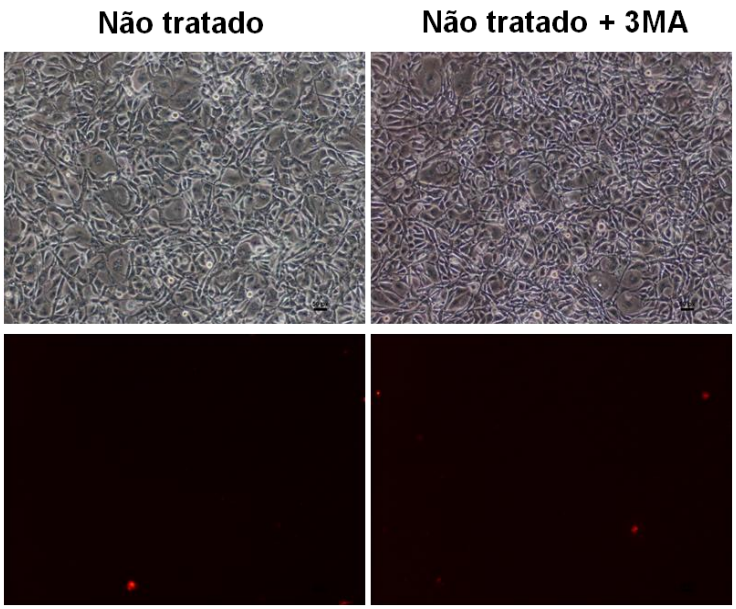

Curcumina 25uM

Curcumina 25uM + 3MA

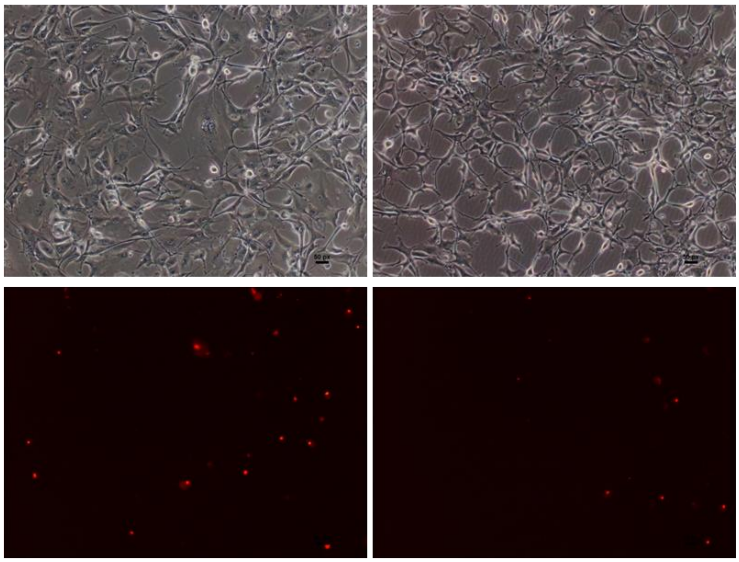

Quercetina 200uM

Quercetina 200uM + 3MA

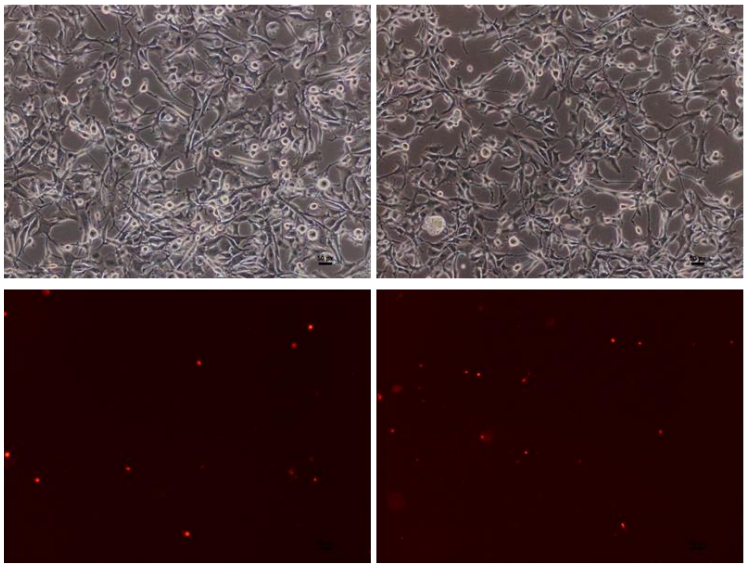

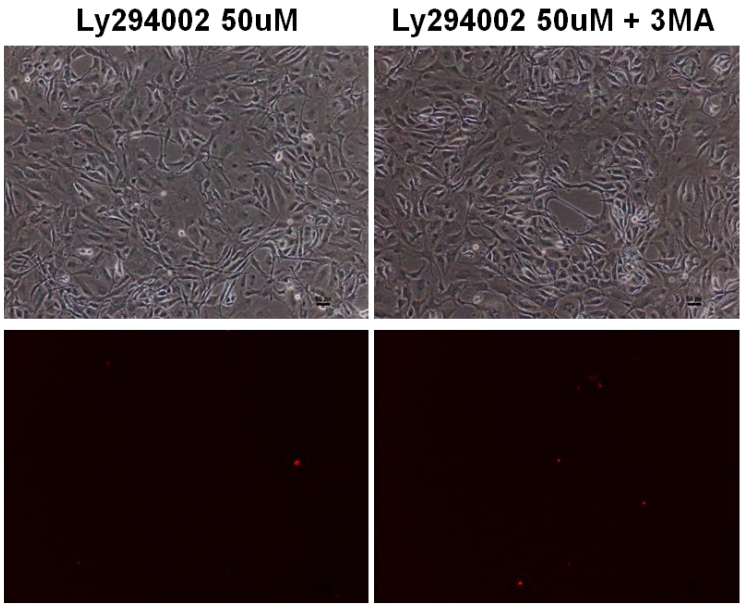

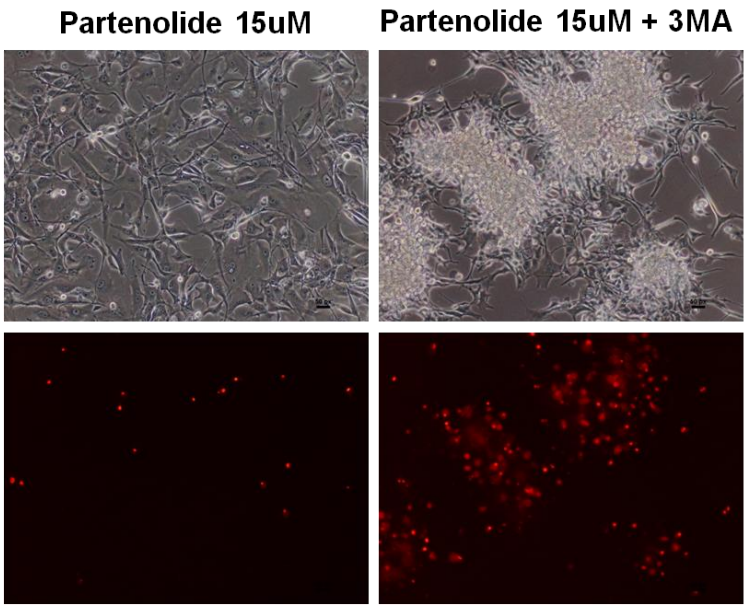

Figura 11: Micrografias representativas do pré-tratamento com o inibidor de autofagia 3-Metiladenina sobre as células tratadas com curcumina (25uM), quercetina (200uM), Ly294002 (50uM) e partenolide (15uM). **A)** Linhagem C6. **B)** Linhagem U87MG.

Parte III

5. DISCUSSÃO

O nosso trabalho se baseou em estudos prévios do nosso grupo (Zanotto-Filho et al., 2011; Zanotto-Filho et al., 2012) que têm demonstrado que o fator de transcrição NFkappaB, assim como a via da PI3K/Akt estão super-estimuladas em glioblastomas multiformes, e essa super-estimulação está associada com o mau prognóstico desses pacientes (Robe et al., 2004; Brown e Law, 2006; Raychaudhuri et al., 2007; Park et al., 2009a, 2009b; Engelman et al., 2009; Karin et al., 2002; Wang et al., 2004). Em um dos mecanismos demonstrados em gliomas, a ativação de Akt se dá por fosforilação e está relacionada com sobrevivência por facilitar a translocação nuclear do NFkappaB (Wang et al., 2004), que ao ser transcrito, ativa genes envolvidos com sobrevivência celular e proliferação como Bcl-xL, VEGF, c-IAP1/2 (Karin et al., 2002). Um estudo em que foi realizado a análise imunohistoquímica de 70 glioblastomas, mostrou que 91,3% deles apresentavam uma alta atividade do NFkappaB, a qual estava correlacionada positivamente com elevados níveis de ativação de Akt (Wang et al., 2004), evidenciando uma ligação entre essas duas rotas. As vias de NFkappaB e PI3K/Akt são vias de sobrevivência bastante importantes em glioblastomas multiformes (GBM) (Wang et al., 2004; Raychaudhuri et al., 2007). Mutações em Pten (*phosphatase and tensin homolog*), um regulador negativo de PI3K, leva a perda da atividade da Pten e, dessa forma, uma ativação constitutiva da via de PI3K/Akt na maioria dos gliomas (Knobbe et al., 2002; Sansal et al., 2004). Por outro lado, a ativação da fosforilação de Akt e consequentemente de NFkappaB, inativa Bad, caspase 9 e os fatores de transcrição Forkhead, que contribuem não somente com a supressão da apoptose, como também com a promoção da sobrevivência celular (Wang et al., 2004).

Em um primeiro experimento de investigação (*screening*) com diversos inibidores de diferentes vias de sinalização (Tabela 1) os inibidores de NFkappaB e PI3K causaram uma diminuição significativa na viabilidade dos GBMs quando comparado com os inibidores de outras vias de sinalização, a qual foi dose dependente, sugerindo que de fato, PI3K/Akt e NFkappaB são duas rotas importantes em gliomas. Dessa forma, nós expandimos nossa investigação utilizando compostos de origem natural com demonstrada atividade sobre essas duas vias (partenolide, quercetina, Ly294002 e curcumina), entretanto com baixa atividade citotóxica em seres humanos (Stalinska et al., 2005). Logo, testamos o efeito de inibidores de NFkappaB (partenolide), os inibidores de PI3K/Akt (Ly294002 e quercetina) e o inibidor misto do eixo/via NFkappaB/Akt (curcumina). A quercetina, a curcumina e o partenolide são compostos produzidos por espécies vegetais, e têm gerado substancial interesse farmacológico em função da atividade antiinflamatória e antioxidante apresentada em estudos *in vitro* e *in vivo*. O partenolide, extraído do *Tanacetum parthenium*, inibe NFkappaB indiretamente através da inibição da IKK-beta e diretamente através da inibição da subunidade p65 do NFkappaB (Kwok et al., 2001; Hehner et al., 1999); o Ly294002 (potente inibidor sintético desenvolvido à partir de modificações químicas na estrutura da quercetina - análogo estrutural da quercetina) e a quercetina (presente em significativas concentrações no vinho tinto, brócolis e maçã) são inibidores da PI3K (Luangdilok et al., 2010); a curcumina é um inibidor de IKKs e PI3K, nas concentrações utilizadas (Kasinski et al., 2008; Santel et al., 2008; Dhandapani et al., 2007). Esperando encontrar um efeito similar em diferentes linhagens de glioma, avaliamos os efeitos e a relação da inibição das vias de PI3K/Akt e NFkappaB com estes diferentes compostos nos parâmetros de morte, proliferação, ciclo celular e autofagia em linhagens de glioma *in vitro* (C6, U87MG e

U251MG). Nossos dados demonstraram que os inibidores de PI3K/Akt (Ly294002 e quercetina) apresentaram um menor efeito quando comparados ao inibidor de NFkappaB (partenolide) na viabilidade dos gliomas, não demonstrando uma dose dependência. A quercetina e o Ly294002 não induziram extravasamento de LDH no meio de cultura, e não houve incorporação de PI, mostrando que, diferentemente do que ocorre com os inibidores de NFkappaB, a perda de viabilidade (quantificada por MTT) nas células tratadas com os inibidores de PI3K/Akt parece estar relacionada com uma diminuição na proliferação, e não com morte celular. Alguns autores já vêm demonstrando que a quercetina e o Ly294002, ao inibirem a via da PI3K/Akt, interferem na viabilidade de alguns tipos de glioblastomas, tais como U138MG, U251MG e LN229 (Braganhol et al., 2007; Han et al., 2010), embora não tenham diferenciado se este efeito foi por citotoxicidade ou inibição da proliferação celular. Em acordo com nossos dados nos tratamentos com partenolide, estudos recentes têm demonstrado que o BAY117082 (Zanotto-Filho et al., 2010), PDTC e helenalina (Dhandapani et al., 2007), compostos com propriedades inibitórias do NFkappaB, diminuem significativamente a viabilidade de diversos tipos de glioblastomas, tais como C6, U87MG, U138MG, U373MG, U251MG e T98G.

Ao analisarmos o ciclo celular, vimos que cada linhagem respondeu de maneira diferente aos tratamentos, muito provavelmente devido às suas particularidades, ou seja, os perfis mutacionais de cada uma. A linhagem C6 apresenta Pten e p53 normais, já a linhagem U87MG é Pten mutada e p53 normal, enquanto que a U251MG é mutada em ambas Pten e p53. Essas mutações são bastante relevantes quando comparamos as respostas dessas células aos mais variados tratamentos, até mesmo quando pensamos nas diferentes respostas de diferentes pacientes a um mesmo quimioterápico, uma vez que tais vias modulam

funções diferentes e importantes dentro da célula tumoral. Por exemplo, em células p53 normal/competente (como a U87MG) a sinalização de p53 pode ser modulada pela via de Pten/PI3K/Akt através da fosforilação de Mdm2, que ao ser fosforilado pela Akt migra do citoplasma ao núcleo, onde é capaz de aumentar a degradação da p53 e reduzir a supressão tumoral/parada no ciclo celular via p53 (Zhou et al., 2001). A p53 induz a transcrição de Pten e essa protege a p53 da degradação através da inibição da forforilação do Mdm2 pela Akt, cooperando em um *feedback* positivo no controle da resposta celular ao estresse, dano ao DNA, e ao câncer (Mayo et al., 2002). Kubiatowski e colaboradores (2001) mostraram que os inibidores de PI3K/Akt, Ly294002 e a wortemanina, diminuíram a invasão de células de glioma *in vitro* e esses efeitos foram acompanhados pela redução na atividade enzimática das matrix metaloproteinases MMP2 e MMP9. A reexpressão da Pten nas linhagens de glioma humano U87MG e U251MG diminuiu consideravelmente os níveis de mRNA e a atividade da MMP2, resultando em uma redução na capacidade de invasividade neste tipo tumoral (Koul et al., 2001). Além disso, a Pten parece ter um importante envolvimento na manutenção da susceptibilidade celular aos estímulos apoptóticos. Já foi demonstrado que células Pten mutadas apresentam a via da Akt superestimuladas, tornando-se resistentes a apoptose, e que a reintrodução do gene PTEN em células de glioma U87MG é capaz de devolver a capacidade de promover a apoptose nesse tipo celular (Tian et al., 1999). A Akt, por sua vez, pode fosforilar diversas proteínas envolvidas com a apoptose, incluindo o fator pró-apoptótico Bad. Quando fosforilado, Bad pode não mais funcionar como uma molécula pró-apoptótica e se desassociar das proteínas Bcl-X_L e Bcl2, aumentando os níveis de proteínas anti-apoptóticas.

O ensaio de Western Blotting nos mostrou que diferentemente do que se pensava, os inibidores de PI3K/Akt, quercetina e Ly294002, foram capazes não somente de diminuir o imuno-conteúdo do seu alvo principal, a p-Akt, mas como também da p-IKK, a cinase responsável por fosforilar a subunidade inibitória do NFkappaB, a IKB. Esse resultado se deve, muito provavelmente, ao fato que, particularmente descrito em gliomas (Dhandapani et al., 2007), PI3K/Akt pode ativar o NFkappaB por fosforilação de IKK (modulando positivamente sua atividade transcricional), dessa forma, estando a Akt inibida isso afetaria diretamente o NFkappaB (Wang et al., 2004). Consequentemente, os resultados apresentados com o tratamento com a quercetina e o Ly294002 podem ser devido a inibição das duas vias PI3K/Akt e NFkappaB e não de apenas uma delas. Já os inibidores curcumina e partenolide inibiram apenas a p-IKK, não tendo tido nenhuma influência na p-Akt.

Quando analisamos a PARP, podemos ver que nenhum dos tratamentos nas duas linhagens foi capaz de aumentar o seu imunoconteúdo ou clivagem (não-mostrado). A PARP aumentada é um indicativo de dano ao DNA, e acaba por levar a célula a uma catástrofe metabólica devido ao seu mecanismo de ação. A PARP-1 é uma enzima nuclear envolvida na reparação e estabilidade do DNA, assim como na regulação da transcrição (Leist et al., 2001; Los et al., 2002). A ativação da PARP-1 consome grande quantidade de NAD^+ e induz a um consumo maciço de ATP (são necessários 4 ATPs para sintetizar 1 NAD^+), o que acaba por bloquear a glicólise (Jain et al., 2013). O resultado da depleção acelerada de ATP é o favorecimento da necrose, e a consequente inibição da morte celular por apoptose, a qual é dependente de energia (Los et al., 2002; Ying et al., 2002; Zeng et al., 2004; Zeng et al., 2007; Erdelyi et al., 2009; Alano et al., 2010). Logo, a clivagem e inativação da

PARP são um dos primeiros eventos mediados pelas caspases ativadas, de modo a garantir o ATP necessário para a apoptose. A morte celular por necrose é considerada potencialmente perigosa, uma vez que é acompanhada pelo extravasamento de material citoplasmático para fora da célula, causando inflamação (Virág et al., 2013).

As células cancerosas, devido as suas necessidades metabólicas mais elevadas, necessitam de uma expressão aumentada de chaperonas. Essa superexpressão em tumores está frequentemente associada com o mau prognóstico e a maior resistência ao tratamento neoplásico (Goloudina et al., 2012). Nos nossos resultados vimos que os tratamentos com quercetina e Ly294002 foram capazes de diminuir o imuno-conteúdo de HSP70, tanto na linhagem C6 quanto na U87MG. Já os tratamentos com curcumina e partenolide não alteraram o imuno-conteúdo de HSP70 na linhagem C6, mas aumentaram na U87MG. Os níveis de HSPs induzíveis, como a HSP70, são extremamente altos em células cancerígenas, levando vários autores a proporem que o conceito de células malignas está intimamente associado a proteínas de estresse, entre elas a HSP70 (Jeco et al., 2010). As células tumorais, por sofrerem constantes estresses, como hipóxia, privação de nutrientes e a própria ação de quimioterápicos, assim como estresses internos tais como a acumulação de proteínas mutantes, além da atividade inadequada e desregulada de diversas vias de sinalização, entre outros fatores, que também ameaçam a sua sobrevivência, as células tumorais acabam sendo bastante dependentes de fatores como a HSP70 (Powers et al., 2010). Estudos em que foram utilizados a abordagem de siRNA para HSP70 promoveram não só a morte de células tumorais, como também sensibilizaram seletivamente as células malignas aos agentes quimioterápicos (Powers et al., 2008; Yang et al., 2012). A HSP70 pode

inibir a apoptose, tanto *upstream* quanto *downstream*, através na inibição da ASK1 (*apoptosis signal regulating kinase 1*) (Park et al., 2002), como de membros da família bcl-2 (Zylicz et al., 2001). Portanto a inibição da HSP70 pode sensibilizar as células tumorais aos agentes quimioterápicos, através do reestabelecimento da sua capacidade de promover a apoptose, e nossos dados apontam a HSP70 como alvo para inibição pelos inibidores de PI3K/Akt.

Nos últimos anos, vários autores tem tentado estabelecer uma ligação entre defeitos/inibição da autofagia e o desenvolvimento do câncer, defendendo a autofagia como uma via supressora de tumor (Levine, 2007; Mathew et al., 2007). Vários genes supressores de tumor estão envolvidos na inibição da sinalização de mTOR, entre eles o PTEN, TSC1 e TSC2, que são capazes de estimular a autofagia, enquanto que a ativação do oncogene mTOR pela PI3K e Akt é capaz de inibir a autofagia. Em células normais, mTOR está ativo apenas quando os nutrientes são abundantes, sendo o maior regulador endógeno da autofagia. Atualmente já existe um grande número de drogas em estudos pré-clínicos e clínicos em que os alvos são o mTOR e o seu ativador a Akt. Foi demonstrado que a droga Rapamicina e os seus análogos (Temsirolimus/CCI-779, Everolimus/RAD001, e AP23573) inibem TORC1 pela ligação com o seu receptor, o FKBP12 (FKBP12/rapamycin-binding) (Faivre et al., 2006). Além disso, foi mostrado que o polifenol curcumina, foi capaz de quebrar o complexo TORC1, pela dissociação de Raptor com mTOR, induzindo autofagia em gliomas (Aoki et al., 2007; Beevers et al., 2009). Outro importante regulador positivo da autofagia é o P53, o gene supressor de tumor mais comumente mutado em tumores humanos (Feng et al., 2005). Essa regulação se dá através da ativação de AMPK do complexo TSC1/TSC2 e a subsequente inibição de mTOR, e pela regulação positiva de DRAM (*damage-regulated autophagy*

modulator), uma proteína lisossomal que pode induzir a autofagia (Feng et al., 2005). Da mesma forma, as proto-oncoproteínas Bcl-2 e Bcl-X_L, superexpressadas em diversos tipos de tumores, incluindo os gliomas, e que são responsáveis por suprimir a permeabilidade da membrana mitocondrial, limitando a apoptose, assim como a autofagia, através da ligação com a proteína autofágica Beclina 1 (Maiuri et al., 2007).

Vários estudos tem demonstrado que a inibição ou mutação em vias associadas à maquinaria autofágica, como as ATGs, entre elas a baixa expressão de Beclina 1, tem sido encontrado em diversos tipos de tumores humanos, comos os de mama, ovário, próstata e cerebrais (Liang et al., 1999; Miracco et al., 2007). Camundongos com mutações em Beclina 1 tiveram uma diminuição na autofagia, e se mostraram mais propensos ao desenvolvimento espontâneo de tumores, incluindo linfomas, câncer de pulmão e hepatocarcinoma, além de lesões pré-tumorais mamárias (Levine et al., 2008).

Entretanto, tem aumentado as evidências que sugerem que as funções supressoras de tumor da autofagia podem ser independentes, apresentando tanto potenciais efeitos de morte quanto de sobrevivência celular (Mathew et al., 2007). White e colaboradores (2008) têm proposto duas hipóteses para explicar como a perda da autofagia, uma via de sobrevivência celular, pode estimular a formação de tumores. Primeiro, quando uma célula não pode morrer por apoptose, após a exposição a um estresse, a autofagia poderia prevenir a morte por necrose, morte essa que pode exacerbar a inflamação local e assim aumentar a taxa de crescimento do tumor (Degenhardt et al., 2006). E em segundo lugar, a deleção do gene ATG pode promover instabilidade genômica em células metabolicamente estressadas, levando à ativação de oncogenes e como consequência a progressão

tumoral (Mathew et al., 2007). Outra possibilidade é que a autofagia desempenhe um papel mais direto no controle do crescimento negativo, talvez degradando especificamente organelas e proteínas essenciais na regulação do crescimento celular. Em apoio a essa teoria, trabalhos tem demonstrado que a expressão aumentada de Beclina 1 em células tumorais diminui sua proliferação, sem afetar a morte celular (Liang et al., 1999; Koneri et al., 2007). Esse achado corrobora com os nossos resultados nas linhagens de gliomas tratados com os inibidores de PI3K/Akt, a quercetina e o Ly294002, em que vimos uma diminuição significativa da proliferação, mas sem alteração na morte celular, entretanto com a presença de autofagia, dependendo da linhagem.

Um grande número de terapias clínicas e experimentais aprovadas atualmente contra o câncer (Temozolomida, Cisplatina, entre outros) induzem a formação de autofagossomos em linhagens de células tumorais *in vitro*, e por muitos anos se pensou que essas terapias matavam as células por autofagia (Knizhnik et al., 2013). No entanto, a inibição específica da autofagia através de siRNAs contra genes ATGs, geralmente acelera, ao invés de impedir a morte celular nesses casos (Maiuri et al., 2007), indicando que a ativação da autofagia representa uma tentativa da célula para lidar com o estresse provocado por agentes citotóxicos. Isso sugere que a inibição da autofagia, ao invés da estimulação, pode ser benéfica no tratamento do câncer. Em um estudo em que camundongos portadores de linfoma foram tratados com a droga Cloroquina, um alcalinizante lisossomal que prejudica a degradação autofágica, aumentou a capacidade da p53 e de um agente alquilante de DNA de induzir a regressão tumoral (Amaravadi et al., 2007), indicando um potencial envolvimento da autofagia na sobrevivência e na pro-tumorogenicidade durante o tratamento do câncer. Em nosso modelo, a curcumina, a quercetina, o

Ly294002 e o partenolide, induziram um significante aumento da autofagia em gliomas e, principalmente nos tratamentos com curcumina, quercetina e partenolide, a inibição da autofagia com o inibidor 3-metil-adenina potencializou a morte celular (como visto nos ensaios de MTT e incorporação de PI), mostrando a autofagia como um mecanismo de proteção contra a morte celular.

De uma maneira geral, a partir de uma análise (*screening*) inicial com vários inibidores, selecionamos as vias de NFkappaB e PI3K/akt como alvos. Testamos várias drogas conhecidas, de baixa citotoxicidade, e estudadas em diferentes modelos de células com os mais diversos efeitos, e o que vimos é que existe uma gama de efeitos que fogem de um padrão uniforme de resposta celular. Algumas linhagens, com alguns perfis de mutações responderam de uma forma, outras de outra. Em algumas células e tratamentos a autofagia teve um papel protetor, em outras foi um fenômeno que não afetou a resistência. O mais importante foi perceber que diferentes mecanismos, ou perfis, podem levar a um mesmo efeito final com estes compostos, a morte celular, paradas no ciclo e diminuição da proliferação.

6. CONCLUSÕES

6.1. Conclusão Geral

Nossos resultados demonstram que a via da PI3K/Akt parece estar relacionada com a proliferação celular, enquanto a via do NFkappaB com sobrevivência. Isso concede a essas vias o *status* de potenciais alvos terapêuticos contra os Glioblastomas, na medida em que elas regulam funções primordiais nesses tipos celulares, tais como proliferação e sobrevivência, além de estarem superexpressas nesses tumores, o conferiria certa seletividade aos inibidores dessas rotas de sinalização.

6.2. Conclusões específicas:

- Nosso estudo mostrou que tanto os inibidores de NFkappaB, quanto os de PI3K/Akt foram eficientes em diminuir a viabilidade dos Glioblastomas. Sendo que os de PI3K/Akt (quercetina e Ly297002) parecem estar relacionados com a proliferação celular, enquanto os de NFkappaB (partenolide e curcumina) com sobrevivência.

- Vimos que as três linhagens (C6, U87MG e U251MG) apresentam imuno-conteúdo aumentado de p-Akt e p-IKK, sendo que os inibidores foram eficientes em diminuir o seu imuno-conteúdo. Além disso, foram capazes de modular o imuno-conteúdo de outras vias relacionadas com morte e sobrevivência celular, tais como caspase 3, LC3 A/B, PARP e Hsp70.

- No tratamento de 48 horas com os inibidores, pudemos constatar a modulação do imuno-conteúdo tanto de caspase 3 (apoptose) quanto de LC3 A/B (autofagia), mas não de PARP (necrose). Isso demonstra que os nossos tratamentos foram capases de ativar a maquinaria apoptótica e autofágica, apesar de não termos conseguido distinguir se em nosso modelo a autofagia está funcionando como um mecanismo de morte ou como uma tentativa de sobrevivência da célula tumoral. Já quando analisamos o ciclo celular, vimos que cada linhagem se comporta de maneira diferente aos tratamentos, muito provavelmente devido as suas diferentes mutações. Mas é importante ressaltar que apesar de suas diferenças, todas as linhagens apresentaram uma modulação do ciclo celular provocada pelos inibidores, seja com paradas no ciclo celular, diminuição da proliferação e até mesmo a morte.

7. PERSPECTIVAS

Como perspectivas do estudo, temos a intenção de avaliar o perfil temporal da indução da autofagia, a apoptose e se houver, a necrose, assim como a senescência e avaliar a relevância da ativação de NFkappaB, e PI3K/Akt assim como as mutações nesses mecanismos de morte e parada celular através de ensaios de siRNA para essas diferentes vias na presença ou ausência dos inibidores, expandindo para inibidores sintéticos. Além disso, testar o uso dos inibidores em outros tipos celulares e posteriormente em modelo *in vivo*, assim como o uso concomitante com drogas antitumorais clássicas (como a Temozolomida) pode ser uma alternativa interessante visando ao tratamento adjuvante.

REFERÊNCIAS

Aggarwal BB. (2004) Nuclear factor-kappaB: the enemy within. Cancer Cell. 6(3):203–8.

Alano CC, Garnier P, Ying W, Higashi Y, Kauppinen TM, Swanson RA (2010). NAD+ depletion is necessary and sufficient for poly(ADP-ribose) polymerase-1-mediated neuronal death. J. Neurosci. doi: 10.1523/JNEUROSCI.5552-09.2010.

Amaravadi RK, Yu D, Lum JJ, Bui T, Christophorou MA, Evan GI, Thomas-Tikhonenko A, Thompson CB (2007). Autophagy inhibition enhances therapy-induced apoptosis in a Myc-induced model of lymphoma. J Clin Invest. 117(2):326-36.

Aoki T, Hashimoto N, Matsutani M (2007) Management of glioblastoma. Expert Opin Pharmacother. 8(18):3133-46.

Ashkenazi A, Dixit VM (1998). Death receptors: signaling and modulation. Science. 281(5381):1305-8.

Baehrecke EH (2005). Autophagy: dual roles in life and death? Nat Rev Mol Cell Biol. 6(6):505-10.

Barkett M, Gilmore TD (1999). Control of apoptosis by Rel/NF-kappaB transcription factors. Oncogene. 18(49):6910-24.

Barkett M., Gilmore TD. (1999) Control of apoptosis by Rel/NFkappaB transcription factors. Oncogene. 18:6910–24.

Beevers CS, Chen L, Liu L, Luo Y, Webster NJ, Huang S (2009). Curcumin disrupts the Mammalian target of rapamycin-raptor complex. Cancer Res. doi: 10.1158/0008-5472.CAN-08-2367.

Braganhol E, Tamajusuku AS, Bernardi A, Wink MR, Battastini AM. (2007) Ecto-5'-nucleotidase/CD73 inhibition by quercetin in the human U138MG glioma cell line. Biochim Biophys Acta. 1770(9):1352-9.

Braganhol E, Zamin LL, Cañedo AD, Horn F, Tamajusuku AS, Wink MR, Salbego C and Battastini AM (2006). Antiproliferative effect of quercetin in the human U138MG glioma cell line. Anticancer Drugs. 17(6): 663-71.

Brennan C, Momota H, Hambardzumyan D, Ozawa T, Tandon A, Pedraza A and Holland E (2009). Glioblastoma subclasses can be defined by activity among signal transduction pathways and associated genomic alterations. PLoS One. 4(11): e7752.

Brodbeck, D., Cron, P., & Hemmings, B. A. (1999). A human protein kinase Bg with regulatory phosphorylation sites in the activation loop and in the C-terminal hydrophobic domain. J Biol Chem. 274, 9133– 9136.

Brown RE, Law A. (2006) Morphoproteomic demonstration of constitutive nuclear factor-kappaB activation in glioblastoma multiforme with genomic correlates and therapeutic implications. Ann Clin Lab Sci. 36(4):421–6.

Cheng, J. Q., Godwin, A. K., Bellacosa, A., Taguchi, T., Franke, T. F.,Hamilton, T. C., Tsichlis, P. N., & Testa, J. R. (1992). AKT2, a putative oncogene encoding a member of a subfamily of protein-serine/threonine kinases, is amplified in human ovarian carcinomas. Proc Natl Acad Sci USA. 89, 9267– 9271.

Chicheportiche Y, Bourdon PR, Xu H, Hsu YM, Scott H, Hession C, Garcia I, Browning JL (1997). TWEAK, a new secreted ligand in the tumor necrosis factor family that weakly induces apoptosis. J Biol Chem. 19;272(51):32401-10.

Cilloni D, Messa F, Arruga F, Defilippi I, Morotti A, Messa E, Carturan S, Giugliano E, Pautasso M, Bracco E, Rosso V, Sen A, Martinelli G, Baccarani M, Saglio G (2006). The NF-kappaB pathway blockade by the IKK inhibitor PS1145 can overcome imatinib resistance. Leukemia. 20(1):61-7.

Cory S, Adams JM (2002). The Bcl2 family: regulators of the cellular life-or-death switch. Nat Rev Cancer. 2(9):647-56.

de la Iglesia N, Konopka G, Lim KL, Nutt CL, Bromberg JF, Frank DA, Mischel PS, Louis DN, Bonni A (2008). Deregulation of a STAT3-interleukin 8 signaling pathway promotes human glioblastoma cell proliferation andinvasiveness. J Neurosci. doi: 10.1523/JNEUROSCI.5385-07.2008.

Degenhardt K, Mathew R, Beaudoin B, Bray K, Anderson D, Chen G, Mukherjee C, Shi Y, Gélinas C, Fan Y, Nelson DA, Jin S, White E (2006). Autophagy promotes tumor cell survival and restricts necrosis, inflammation, and tumorigenesis. Cancer Cell. 10(1):51-64.

Demuth T, Berens ME (2004). Molecular mechanisms of glioma cell migration and invasion. J Neurooncol. 70(2):217-28.

Denecker G, Vercammen D, Declercq W, Vandenabeele P (2001). Apoptotic and necrotic cell death induced by death domain receptors. Cell Mol Life Sci. 58(3):356-70.

Desbaillets I, Diserens AC, de Tribolet N, Hamou MF, Van Meir EG (1999). Regulation of interleukin-8 expression by reduced oxygen pressure in human glioblastoma. Oncogene. 18(7):1447-56.

Dhandapani KM, Mahesh VB and Brann DWJ (2007) Curcumin suppresses growth and chemoresistance of human glioblastoma cells via AP-1 and NFkappaB transcription factors. J. Neurochem.102 (2): 522-38.

Du C, Fang M, Li Y, Li L, Wang X (2000). Smac, a mitochondrial protein that promotes cytochrome c-dependent caspase activation by eliminating IAP inhibition. Cell. 102(1):33-42.

Elmore S (2007). Apoptosis: a review of programmed cell death. Toxicol Pathol. 2007 35(4):495-516.

Engelman JA: (2009) Targeting PI3K signalling in cancer: opportunities, challenges and limitations. Nat Rev Cancer. 9:550-562.

Erdélyi K, Bai P, Kovács I, Szabó E, Mocsár G, Kakuk A, Szabó C, Gergely P, Virág L (2009). Dual role of poly(ADP-ribose) glycohydrolase in the regulation of cell death in oxidatively stressed A549 cells. FASEB J. doi: 10.1096/fj.09-133264.

Faivre S, Djelloul S, Raymond E (2006). New paradigms in anticancer therapy: targeting multiple signaling pathways with kinase inhibitors. Semin Oncol. 33(4):407-20.

Feng, Z., Zhang, H., Levine, A.J., and Jin, S. (2005). The coordinate regulation of the p53 and mTOR pathways in cells. Proc Natl Acad Sci U S A. 102(23):8204-9.

Festjens N, Vanden Berghe T, Vandenabeele P (2006). Necrosis, a well-orchestrated form of cell demise: signalling cascades, important mediators and concomitant immune response. Biochim Biophys Acta. 1757(9-10):1371-87.

Friedman HS, Kerby T, Calvert H (2000). Temozolomide and treatment of malignant glioma. Clin Cancer Res. 6(7):2585-97.

Furman RR, Asgary Z, Mascarenhas JO, Liou HC, Schattner EJ (2000). Modulation of NF-kappa B activity and apoptosis in chronic lymphocytic leukemia B cells. J Immunol. 164(4):2200-6.

Galluzzi L, Kroemer G (2008). Necroptosis: a specialized pathway of programmed necrosis. Cell. doi: 10.1016/j.cell.2008.12.004.

Galluzzi L, Vitale I, Abrams JM, Alnemri ES, Baehrecke EH, Blagosklonny MV, Dawson TM, Dawson VL, El-Deiry WS, Fulda S, Gottlieb E, Green DR, Hengartner MO, Kepp O, Knight RA, Kumar S, Lipton SA, Lu X, Madeo F, Malorni W, Mehlen P, Nuñez G, Peter ME, Piacentini M, Rubinsztein DC, Shi Y, Simon HU, Vandenabeele P, White E, Yuan J, Zhivotovsky B, Melino G, Kroemer G (2012). Molecular definitions of cell death subroutines: recommendations of the Nomenclature Committee on Cell Death 2012. Cell Death Differ. doi: 10.1038/cdd.2011.96.

García MG, Alaniz L, Lopes EC, Blanco G, Hajos SE, Alvarez E (2005). Inhibition of NF-kappaB activity by BAY117082 increases apoptosis in multidrug resistant leukemic T-cell lines. Leuk Res. 29(12):1425-34.

Garrido G, Blanco-Molina M, Sancho R, Macho A, Delgado R, Muñoz E (2005). An aqueous stem bark extract of Mangifera indica (Vimang) inhibits T cell proliferation and TNF-induced activation of nuclear transcription factor NF-kappaB. Phytother Res. 19(3):211-5.

Ghavami S, Hashemi M, Ande SR, Yeganeh B, Xiao W, Eshraghi M, Bus CJ, Kadkhoda K, Wiechec E, Halayko AJ, Los M (2009). Apoptosis and cancer: mutations within caspase genes. J Med Genet. doi: 10.1136/jmg.2009.066944.

Gill JS, Zhu X, Moore MJ, Lu L, Yaszemski MJ, Windebank AJ (2002). Effects of NFkappaB decoy oligonucleotides released from biodegradable polymer microparticles on a glioblastoma cell line. Biomaterials. 23(13):2773-81.

Goloudina AR, Demidov ON, Garrido C (2012). Inhibition of HSP70: a challenging anti-cancer strategy. Cancer Lett. doi: 10.1016/j.canlet.2012.06.003.

Han L, Yang Y, Yue X, Huang K, Liu X, Pu P, Jiang H, Yan W, Jiang T, Kang C. (2010) Inactivation of PI3K/AKT signaling inhibits glioma cell growth through modulation of β-catenin-mediated transcription. Brain Res. doi: 10.1016/j.brainres.2010.09.097.

Hehner SP, Hofmann TG, Droge W, Schmitz ML (1999). The anti inflammatory sesqui- terpene lactone parthenolide inhibits NF-kB by targeting the IkB kinase complex. JImmunol. 163:5617–23.

Hill MM, Adrain C, Duriez PJ, Creagh EM, Martin SJ (2004). Analysis of the composition, assembly kinetics and activity of native Apaf-1 apoptosomes. EMBO J. 23(10):2134-45.

Hill MM, Hemmings BA (2002). Inhibition of protein kinase B/Akt. implications for cancer therapy. Pharmacology and Therapeutics. 93(2-3):243-51.

Holler N, Zaru R, Micheau O, Thome M, Attinger A, Valitutti S, Bodmer JL, Schneider P, Seed B, Tschopp J (2000). Fas triggers an alternative, caspase-8-independent cell death pathway using the kinase RIP as effector molecule. Nat Immunol. 1(6):489-95.

Imai Y, Yamagishi H, Ono Y, Ueda Y (2012). Versatile inhibitory effects of the flavonoid-derived PI3K/Akt inhibitor, LY294002, on ATP-binding cassette transporters that characterize stem cells. Clin Transl Med. doi: 10.1186/2001-1326-1-24.

Jego G, Hazoumé A, Seigneuric R, Garrido C (2013). Targeting heat shock proteins in cancer. Cancer Lett. doi: 10.1016/j.canlet.2010.10.014.

Jiang H, White EJ, Conrad C, Gomez-Manzano C, Fueyo J (2009). Autophagy pathways in glioblastoma. Methods Enzymol. doi: 10.1016/S0076-6879(08)04013-5.

Jones, P. F., Jakubowicz, T., & Hemmings, B. A. (1991). Molecular cloning of a second form of rac protein kinase. Cell Regul. 2, 1001– 1009.

Kapoor GS, Zhan Y, Johnson GR, O'Rourke DM. (2004) Distinct domains in the SHP-2 phosphatase differentially regulate epidermal growth factor receptor/NF- kappaB activation through Gab1 in glioblastoma cells. Mol Cell Biol. 24(2):823–36.

Karin M, Cao Y, Greten FR, Li ZW: (2002) NF-kappaB in cancer: from innocent bystander to major culprit. Nat Rev Cancer. 2:301-310.

Kasinski AL, Du Y, Thomas SL, Zhao J, Sun SY, Khuri FR, et al. (2008) Inhibition of IkappaB kinase–nuclear factor-kappaB signaling pathway by 3,5-bis(2-flur-obenzylidene)piperidin-4-one (EF24), a novel monoketone analog of curcumin. Mol Pharmacol. 74:654–61.

Klionsky DJ, Abdalla FC, Abeliovich H, Abraham RT et al., (2012) Guidelines for the use and interpretation of assays for monitoring autophagy. Autophagy. 8(4):445-544.

Knizhnik AV, Roos WP, Nikolova T, Quiros S, Tomaszowski KH, Christmann M, Kaina B (2013). Survival and death strategies in glioma cells: autophagy, senescence and apoptosis triggered by a single type of temozolomide-induced DNA damage. PLoS One. doi: 10.1371/journal.pone.0055665.

Knobbe CB, Merlo A, Reifenberger G (2002). Pten signaling in gliomas. Neuro Oncol. 4(3):196-211.

Kögel D, Fulda S, Mittelbronn M (2010). Therapeutic exploitation of apoptosis and autophagy for glioblastoma. Anticancer Agents Med Chem. 10(6):438-49.

Koneri K, Goi T, Hirono Y, Katayama K, Yamaguchi A (2007). Beclin 1 gene inhibits tumor growth in colon cancer cell lines. Anticancer Res. 27(3B):1453-7.

Koukourakis GV, Kouloulias V, Zacharias G, Papadimitriou C, Pantelakos P, Maravelis G, Fotineas A, Beli I, Chaldeopoulos D, Kouvaris J (2009). Temozolomide with radiation therapy in high grade brain gliomas: pharmaceuticals considerations and efficacy; a review article. Molecules. doi: 10.3390/molecules14041561.

Koul N, Sharma V, Dixit D, Ghosh S, Sen E (2010). Bicyclic triterpenoid Iripallidal induces apoptosis and inhibits Akt/mTOR pathway in glioma cells. BMC Cancer. 24;10:328.

Krakstad C, Chekenya M (2010). Survival signalling and apoptosis resistance in glioblastomas: opportunities for targeted therapeutics. Molecular Cancer. 9:135.

Kroemer G, El-Deiry WS, Golstein P, Peter ME, Vaux D, Vandenabeele P, Zhivotovsky B, Blagosklonny MV, Malorni W, Knight RA, Piacentini M, Nagata S, Melino G; Nomenclature Committee on Cell Death (2005). Classification of cell death: recommendations of the Nomenclature Committee on Cell Death. Cell Death Differ. Suppl 2:1463-7

Kroemer G, Galluzzi L, Vandenabeele P, Abrams J, Alnemri ES, Baehrecke EH, Blagosklonny MV, El-Deiry WS, Golstein P, Green DR, Hengartner M, Knight RA, Kumar S, Lipton SA, Malorni W, Nuñez G, Peter ME, Tschopp J, Yuan J, Piacentini M, Zhivotovsky B, Melino G; Nomenclature Committee on Cell Death (2009). Classification of cell death: recommendations of the

Nomenclature Committee on Cell Death 2009. Cell Death Differ. doi: 10.1038/cdd.2008.150.

Kubiatowski T, Jang T, Lachyankar MB, Salmonsen R, Nabi RR, Quesenberry PJ, Litofsky NS, Ross AH, Recht LD (2001). Association of increased phosphatidylinositol 3-kinase signaling with increased invasiveness and gelatinase activity in malignant gliomas. J Neurosurg. 95(3):480-8.

Kwok BH, Koh B, Ndubuisi MI, Elofsson M,Crews CM. (2001) The anti-inflammatory natural product parthenolide from the medicinal herb Fever few directly binds to and inhibits IkB kinase. ChemBiol. 8:759–66.

Leist M, Jäättelä M (2001). Triggering of apoptosis by cathepsins. Cell Death Differ. 8(4):324-6.

Levine B (2007). Cell biology: autophagy and cancer. Nature. 12;446(7137):745-7.

Levine B, Klionsky DJ (2004). Development by self-digestion: molecular mechanisms and biological functions of autophagy. Dev Cell. 6(4):463-77.

Levine B, Kroemer G (2008). Autophagy in the pathogenesis of disease. Cell. doi: 10.1016/j.cell.2007.12.018.

Liang BC, Miller L, Weller A (1999). Ethyl-nitrosourea transformed astrocytes exhibit mitochondrial membrane hyperpolarization and constrained apoptosis. Apoptosis. 4(2):89-97.

Los M, Mozoluk M, Ferrari D, Stepczynska A, Stroh C, Renz A, Herceg Z, Wang ZQ, Schulze-Osthoff K (2002). Activation and caspase-mediated inhibition of PARP: a molecular switch between fibroblast necrosis and apoptosis in death receptor signaling. Mol Biol Cell. 13(3):978-88.

louis DO H, Wiestler OD, Cavenee WK: (2007) WHO classification of tumours of the central nervous system. Lyon: IARC.

Luangdilok S, Box C, Harrington K, Rhŷs-Evans P, Eccles S. (2010) MAPK and PI3K signalling differentially regulate angiogenic and lymphangiogenic cytokine secretion in squamous cell carcinoma of the head and neck. Eur J Cancer.

Mahmood Z, Shukla Y (2010). Death receptors: targets for cancer therapy. Exp Cell Res. doi: 10.1016/j.yexcr.2009.12.011.

Maiuri MC, Zalckvar E, Kimchi A, Kroemer G (2007). Self-eating and self-killing: crosstalk between autophagy and apoptosis. Nat Rev Mol Cell Biol. 8(9):741-52.

Majeski AE, Dice JF (2004). Mechanisms of chaperone-mediated autophagy. Int J Biochem Cell Biol. 36(12):2435-44.

Mathew R, Karantza-Wadsworth V, White E (2007). Role of autophagy in cancer. Nat Rev Cancer. 7(12):961-7.

Mayo LD, Dixon JE, Durden DL, Tonks NK, Donner DB (2002). PTEN protects p53 from Mdm2 and sensitizes cancer cells to chemotherapy. J Biol Chem. 15;277(7):5484-9.

Mehrpour M, Esclatine A, Beau I, Codogno P (2010). Overview of macroautophagy regulation in mammalian cells. Cell Res. doi: 10.1038/cr.2010.82.

Meijer AJ, Codogno P (2009). Autophagy: regulation and role in disease. Crit Rev Clin Lab Sci. doi: 10.1080/10408360903044068.

Mercer RW, Tyler MA, Ulasov IV and Lesniak MS. Targeted therapies for malignant glioma: progress and potential. BioDrugs. 23(1): 25-35.

Miracco C, Cosci E, Oliveri G, Luzi P, Pacenti L, Monciatti I, Mannucci S, De Nisi MC, Toscano M, Malagnino V, Falzarano SM, Pirtoli L, Tosi P (2007). Protein and mRNA expression of autophagy gene Beclin 1 in human brain tumours. Int J Oncol. 30(2):429-36.

Mizushima N, Komatsu M (2011). Autophagy: renovation of cells and tissues. Cell. doi: 10.1016/j.cell.2011.10.026.

Morotti A, Cilloni D, Pautasso M, Messa F, Arruga F, Defilippi I, Carturan S, Catalano R, Rosso V, Chiarenza A, Taulli R, Bracco E, Rege-Cambrin G, Gottardi E, Saglio G (2006). NF-kB inhibition as a strategy to enhance etoposide-induced apoptosis in K562 cell line. Am J Hematol. 81(12):938-45.

Nicholson KM, Anderson NG (2002). The protein kinase B/Akt signalling pathway in human malignancy. Cellular Signalling. 14(5):381-95.

Park S, Hatanpaa KJ, Xie Y, Mickey BE, Madden CJ, Raisanen JM, et al. (2009) The receptor interacting protein 1 inhibits p53 induction through NF-kappaB activation and confers a worse prognosis in glioblastoma. Cancer Res. 69(7):2809–16.

Park S, Zhao D, Hatanpaa KJ, Mickey BE, Saha D, Boothman DA, et al. (2009) RIP1 activates PI3K–Akt via a dual mechanism involving NF-kappaB-mediated inhibition of the mTOR–S6K–IRS1 negative feedback loop and down-regulation of PTEN. Cancer Res. 69(10):4107–11

Park SJ, Lee SC, Hong SH, Kim HM (2002). Degradation of IkappaBalpha in activated RAW264.7 cells is blocked by the phosphatidylinositol 3-kinase inhibitor LY294002. Cell Biol Toxicol. 18(2):121-30.

Phillip J, Ruland J (2007). Aberrant NF-kappaB signaling in lymphoma: mechanisms, consequences, and therapeutic implications. Blood. 109(7):2700-7.

Pickering BM, de Mel S, Lee M, Howell M, Habens F, Dallman CL, Neville LA, Potter KN, Mann J, Mann DA, Johnson PW, Stevenson FK, Packham G (2007). Pharmacological inhibitors of NF-kappaB accelerate apoptosis in chronic lymphocytic leukaemia cells. Oncogene. 22;26(8):1166-77.

Pirtoli L, Cevenini G, Tini P, Vannini M, Oliveri G, Marsili S, Mourmouras V, Rubino G, Miracco C (2009). The prognostic role of Beclin 1 protein expression in high-grade gliomas. Autophagy. 5(7):930-6.

Piva R, Gianferretti P, Ciucci A, Taulli R, Belardo G, Santoro MG (2005). 15-Deoxy-delta 12,14-prostaglandin J2 induces apoptosis in human malignant B cells: an effect associated with inhibition of NF-kappa B activity and down-regulation of antiapoptotic proteins. Blood. 105(4):1750-8.

Powers MV, Clarke PA, Workman P (2008). Dual targeting of HSC70 and HSP72 inhibits HSP90 function and induces tumor-specific apoptosis. Cancer Cell. doi: 10.1016/j.ccr.2008.08.002.

Powers MV, Jones K, Barillari C, Westwood I, van Montfort RL, Workman P (2010). Targeting HSP70: the second potentially druggable heat shock protein and molecular chaperone? Cell Cycle. 15;9(8):1542-50.

Raychaudhuri B, Han Y, Lu T, Vogelbaum MA. (2007) Aberrant constitutive activation of nuclear factor kappaB in glioblastoma multiforme drives invasive pheno-type. J Neurooncol. 85(1):39–47.

Rayet B., Gelinas C. (1999) Aberrantrel/NFkappaB genes and activity in human cancer. Oncogene. 18(49):6938–47.

Robe PA, Bentires-Alj M, Bonif M, Rogister B, Deprez M, Haddada H, et al. (2004) In vitro and in vivo activity of the nuclear factor-kappaB inhibitor sulfasalazine in human glioblastomas. Clin Cancer Res. 10(16):5595–603.

Rodriguez-Rocha H, Garcia-Garcia A, Panayiotidis MI, Franco R (2011). DNA damage and autophagy. Mutat Res. doi: 10.1016/j.mrfmmm.2011.03.007.

Sansal I, Sellers WR (2004). The biology and clinical relevance of the PTEN tumor suppressor pathway. J Clin Oncol. 22(14):2954-63.

Santel T, Pflug G, Hemdan NY, Schäfer A, Hollenbach M, Buchold M, et al. (2008) Curcumin inhibits glyoxalase 1: a possible link to its anti-inflammatory and anti-tumor activity. PLoS ONE. 3(10):e3508.

Sathornsumetee S, Reardon DA (2009). Targeting multiple kinases in glioblastoma multiforme. Expert Opin Investig Drugs. doi: 10.1517/13543780802692603 .

Schuler M, Green DR (2001). Mechanisms of p53-dependent apoptosis. Biochem Soc Trans. 29(Pt 6):684-8.

Sethi G, Ahn KS, Chaturvedi MM, Aggarwal BB. (2007) Epidermal growth factor (EGF) activates nuclear factor-kappaB through IkappaBalpha kinase-independent but EGF receptor-kinase dependent tyrosine 42 phosphorylation of Ikappa- Balpha. Oncogene. 26(52):7324–32.

Skulachev VP (2006). Bioenergetic aspects of apoptosis, necrosis and mitoptosis. Apoptosis. 11(4):473-85.

Stalińska K, Guzdek A, Rokicki M, Koj A (2005). Transcription factors as targets of the anti-inflammatory treatment. A cell culture study with extracts from some Mediterranean diet plants. J Physiol Pharmacol. Suppl 1:157-69.

Stewart LA (2002). Chemotherapy in adult high-grade glioma: a systematic review and meta-analysis of individual patient data from 12 randomised trials. Lancet. 359: 1011-18.

Suliman A, Lam A, Datta R, Srivastava RK (2001). Intracellular mechanisms of TRAIL: apoptosis through mitochondrial-dependent and -independent pathways. Oncogene. 20(17):2122-33.

Syntichaki P, Tavernarakis N (2003). The biochemistry of neuronal necrosis: rogue biology? Nat Rev Neurosci. 4(8):672-84.

Tait SW, Green DR (2010). Mitochondria and cell death: outer membrane permeabilization and beyond. Nat Rev Mol Cell Biol. doi: 10.1038/nrm2952.

Tian, X.X., Pang, J.C., To, S.S., and Ng, H.K. (1999) Restoration of wild-type Pten expression leads to apoptosis, induces differentiation, and reduces telomerase activity in human glioma cells. J. Neuropathol. Exp. Neurol. 58, 472-479.

Vandenabeele P, Galluzzi L, Vanden Berghe T, Kroemer G (2010). Molecular mechanisms of necroptosis: an ordered cellular explosion. Nat Rev Mol Cell Biol. doi: 10.1038/nrm2970.

Virág L, Robaszkiewicz A, Vargas JM, Javier Oliver F (2013). Poly(ADP-ribose) signaling in cell death. Mol Aspects Med. doi:pii: S0098-2997(13)00008-3. 10.1016/j.mam.2013.01.007.

Wang H, Wang H, Zhang W, Huang HJ, Liao WS, Fuller GN. (2004) Analysis of the activation status of Akt, NFkappaB, and Stat3 in human diffuse gliomas. Lab Invest. 84(8):941–51.

Wu H, Cao Y, Weng D, Xing H, Song X, Zhou J, Xu G, Lu Y, Wang S, Ma D (2008). Effect of tumor suppressor gene PTEN on the resistance to cisplatin in human ovarian cancer cell lines and related mechanisms. Cancer Letters. 271(2):260-71.

Xie TX, Xia Z, Zhang N, Gong W, Huang S. (2010) Constitutive NF-kappaB activity regulates the expression of VEGF and IL-8 and tumor angiogenesis of human glioblastoma. Oncol Rep. 23(3):725–32.

Xu CX, Jin H, Shin JY, Kim JE, Cho MH (2010). Roles of protein kinase B/Akt in lung cancer. Frontiers in bioscience. 2:1472-84.

Yang X, Wang J, Zhou Y, Wang Y, Wang S, Zhang W (2012). Hsp70 promotes chemoresistance by blocking Bax mitochondrial translocation in ovarian cancer cells. Cancer Lett. doi: 10.1016/j.canlet.2012.01.030.

Ying W, Chen Y, Alano CC, Swanson RA (2002). Tricarboxylic acid cycle substrates prevent PARP-mediated death of neurons and astrocytes. J Cereb Blood Flow Metab. 22(7):774-9.

Zanotto-Filho A, Braganhol E, Edelweiss MI, Behr GA, Zanin R, Schröder R, Simões-Pires A, Battastini AM, Moreira JC (2012). The curry spice curcumin selectively inhibits cancer cells growth in vitro and in preclinical model of glioblastoma. J Nutr Biochem. doi: 10.1016/j.jnutbio.2011.02.015.

Zanotto-Filho A, Braganhol E, Schröder R, de Souza LH, Dalmolin RJ, Pasquali MA, Gelain DP, Battastini AM, Moreira JC (2011). NFκB inhibitors induce cell death in glioblastomas. Biochem Pharmacol. doi: 10.1016/j.bcp.2010.10.014.

Zanotto-Filho A, Delgado-Cañedo A, Schröder R, Becker M, Klamt F, Moreira JC (2010). The pharmacological NFkappaB inhibitors BAY117082 and MG132 induce cell arrest and apoptosis in leukemia cells through ROS-mitochondria pathway activation. Cancer Letters. 288(2):192-203.

Zanotto-Filho A, Gelain DP, Schröder R, Souza LF, Pasquali MA, Klamt F, Moreira JC (2009). The NF kappa B-mediated control of RS and JNK signaling in vitamin A-treated cells: duration of JNK-AP-1 pathway activation may determine cell death or proliferation. Biochemical Pharmacology. 77(7):1291-301.

Zanotto-Filho A, Schröder R, Moreira JC (2008). Xanthine oxidase-dependent ROS production mediates vitamin A pro-oxidant effects in cultured Sertoli cells. Free Radical Research. 42; 593-601.

Zeng, J., Hirai, K., Yang, G.Y., Ying, W., Swanson, R.A., Kelly, M., Mayer, M., James, T.L., Litt, L., (2004). Using 31P NMR spectroscopy at 14.1 Tesla to investigate PARP-1 associated energy failure and metabolic rescue in cerebrocortical slices. J. Bioenerg. Biomembr. 36, 415–419.

Zeng, J., Yang, G.Y., Ying, W., Kelly, M., Hirai, K., James, T.L., Swanson, R.A., Litt, L., (2007). Pyruvate improves recovery after PARP-1-associated energy failure induced by oxidative stress in neonatal rat cerebrocortical slices. J. Cereb. Blood Flow Metab. 27, 304–315.

Zhang J, Han L, Zhang A, Wang Y, Yue X, You Y, Pu P, Kang C (2010). AKT2 expression is associated with glioma malignant progression and required for cell survival and invasion. Oncology Reports. 24(1):65-72.

Zhou, B.P., Liao, Y., Xia, W., Zou, Y., Spohn, B., and Hung, M.C. (2001). HER-2/neu induces p53 ubiquitination via Akt-mediated MDM2 phosphorylation. Nat. Cell Biol. 3, 973-982.

Zylicz M, King FW, Wawrzynow A (2001). Hsp70 interactions with the p53 tumour suppressor protein. EMBO J. 20(17):4634-8.

ANEXOS

Anexo 1: Artigo publicado durante o mestrado relacionado à dissertação: NFκB inhibitors induce cell death in glioblastomas. Zanotto-Filho A, Braganhol E, Schröder R, de Souza LH, Dalmolin RJ, Pasquali MA, Gelain DP, Battastini AM, Moreira JC. Biochemical Pharmacology. 2011 doi: 10.1016/j.bcp.2010.10.014.

Anexo 2: Artigo publicado durante o mestrado relacionado à dissertação: The curry spice curcumin selectively inhibits cancer cells growth in vitro and in preclinical model of glioblastoma. Zanotto-Filho A, Braganhol E, Edelweiss MI, Behr GA, Zanin R, Schröder R, Simões-Pires A, Battastini AM, Moreira JC. The Journal of Nutritional Biochemistry. 2012. doi: 10.1016/j.jnutbio.2011.02.015.

Anexo 3: Artigo publicado durante o mestrado relacionado à dissertação: Curcumin-loaded lipid-core nanocapsules as a strategy to improve pharmacological efficacy of curcumin in glioma treatment. Zanotto-Filho A, Coradini K, Braganhol E, Schröder R, de Oliveira CM, Simões-Pires A, Battastini AM, Pohlmann AR, Guterres SS, Forcelini CM, Beck RC, Moreira JC. European Journal of Pharmaceutics and Biopharmaceutics 2012 doi:pii: S0939-6411(12)00345-1. 10.1016/j.ejpb.2012.10.019.

Biochemical Pharmacology 81 (2011) 412–424

Contents lists available at ScienceDirect

Biochemical Pharmacology

journal homepage: www.elsevier.com/locate/biochempharm

NFκB inhibitors induce cell death in glioblastomas

Alfeu Zanotto-Filho [a,*], Elizandra Braganhol [b], Rafael Schröder [a], Luís Henrique T. de Souza [a], Rodrigo J.S. Dalmolin [a], Matheus A. Bittencourt Pasquali [a], Daniel Pens Gelain [a], Ana Maria Oliveira Battastini [b], José Cláudio Fonseca Moreira [a]

[a] Centro de Estudos em Estresse Oxidativo, Departamento de Bioquímica, Universidade Federal do Rio Grande do Sul (UFRGS), Porto Alegre, Rio Grande do Sul, Brazil
[b] Laboratório de Enzimologia, Departamento de Bioquímica, Universidade Federal do Rio Grande do Sul (UFRGS), Porto Alegre, Rio Grande do Sul, Brazil

ARTICLE INFO

Article history:
Received 14 August 2010
Accepted 21 October 2010

Keywords:
NFκB
Glioblastoma
NFκB inhibitors
Apoptosis
Chemotherapy

ABSTRACT

Identification of novel target pathways in glioblastoma (GBM) remains critical due to poor prognosis, inefficient therapies and recurrence associated with these tumors. In this work, we evaluated the role of nuclear-factor-kappa-B (NFκB) in the growth of GBM cells, and the potential of NFκB inhibitors as antiglioma agents. NFκB pathway was found overstimulated in GBM cell lines and in tumor specimens compared to normal astrocytes and healthy brain tissues, respectively. Treatment of a panel of established GBM cell lines (U138MG, U87, U373 and C6) with pharmacological NFκB inhibitors (BAY117082, parthenolide, MG132, curcumin and arsenic trioxide) and NFκB-p65 siRNA markedly decreased the viability of GBMs as compared to inhibitors of other signaling pathways such as MAPKs (ERK, JNK and p38), PKC, EGFR and PI3K/Akt. In addition, NFκB inhibitors presented a low toxicity to normal astrocytes, indicating selectivity to cancerous cells. In GBMs, mitochondrial dysfunction (membrane depolarization, bcl-xL downregulation and cytochrome c release) and arrest in the G2/M phase were observed at the early steps of NFκB inhibitors treatment. These events preceded sub-G1 detection, apoptotic body formation and caspase-3 activation. Also, NFκB was found overstimulated in cisplatin-resistant C6 cells, and treatment of GBMs with NFκB inhibitors overcame cisplatin resistance besides potentiating the effects of the chemotherapeutics, cisplatin and doxorubicin. These findings support NFκB as a potential target to cell death induction in GBMs, and that the NFκB inhibitors may be considered for in vivo testing on animal models and possibly on GBM therapy.

1. Introduction

Glioblastoma (GBM) is an aggressive, invasive, and difficult to treat primary brain tumor. Standard therapy includes surgical resection, external beam radiation and chemotherapy, with no known curative therapy [1]. A number of dysregulated signaling cascades have been described in GBMs, including the MEK/ERK pathway, PLC/PKC pathway, and the PI3K/Akt pathway. Dysregulation of these pathways is driven by mutation, amplification, or overexpression of multiple genes such as PTEN, EGFR, PDGFR-a, p53, and mTOR [2–4]. Understanding these dysregulated pathways has provideded the basis for designing molecular targeted therapies as monoclonal antibodies against EGF, VEGF and PDGF receptors, as well as new combination therapies and drug delivery systems [4–6]. Despite these new treatment strategies, median survival has remained approximately 1 year for decades [1]. Thus, it is urgent to determine novel molecular targets in GBMs in order to develop more effective therapies and new therapeutic opportunities to patients.

Studies have compelling evidence that the transcription factor NFκB (Nuclear factor κB) plays a role in the control of oncogenesis, tumor progression and chemotherapy resistance of diverse types of malignances as lymphoma, leukemia, breast and ovarian cancers [7–11]. NFκB is formed by homo or heterodimers comprising members of the Rel family of proteins (p50/p105, p52/p100, p65, c-Rel and RelB) which form, upon non-stimulated conditions, a ternary and inactive cytoplasmic complex by interacting with inhibitory proteins of the IκB family. Upon stimulation by cytokines (TNF-alpha and IL1-beta), growth factors (EGF and PDGF), anticancer drugs (cisplatin, doxorubicin and vincristine) and other stressor stimuli, IκBs are phosphorylated by IKK (IκB kinase) proteins thus releasing the active NFκB, which translocates into nucleus and binds to DNA sequences in gene promoters. NFκB binding to DNA modulates the expression of a wide range of genes as that involved in inflammation (IL1-beta, IL-6, COX2, and TNF), apoptosis resistance (bcl-xL, cIAP1/2, XIAP, FLICE and survivin), cell

* Corresponding author at: Depto. Bioquímica (ICBS-UFRGS), Rua Ramiro Barcelos, 2600/Anexo, Porto Alegre CEP 90035-003, Rio Grande do Sul, Brazil. Tel.: +55 51 3308 5578; fax: +55 51 3308 5535.
E-mail address: alfeuzanotto@hotmail.com (A. Zanotto-Filho).

0006-2952/$ – see front matter © 2010 Elsevier Inc. All rights reserved.
doi:10.1016/j.bcp.2010.10.014

invasion (ICAM-1, VCAM-1, MMP2, MMP9), angiogenesis (VEGF), proliferation (cyclin D1, MYC) and metastasis (CXCR4 and TWIST) [7–12]. These groups of genes are directly related to tumor-associated phenomena suggesting NFκB as a potential target to cell death induction and chemosensitization in cancer [9,13–15].

Aberrant NFκB activity has been described in some types of cancer cells upon basal and following anticancer drugs treatments. Besides, constitutive NFκB up-regulation has been found in chemotherapy-resistant cell lines, which correlates with therapy failure [9,13,15–17]. In this context, studies have suggested that molecules with NFκB inhibitory properties are potential anticancer agents [9,15,17,18]. In this intent, researchers have blocking NFκB activity via IKK/NFκB inhibitors (as BAY117082, BAY117085, parthenolide, curcumin, arsenic trioxide and PDTC) or proteasome/NFκB inhibitors (PS-341 and MG132) in order to inhibit the growth of myeloma [10], leukemia [17,19], esophageal [14] and breast cancer cells [20]. Recently, analysis of brain tumor biopsies identified that NFκB and its target genes are overexpressed in GBM and astrocytoma tumors compared to normal brain tissues [21,22]. In addition, a positive correlation between NFκB activation and poor GBM prognosis was reported, suggesting that the known role of NFκB as a survival factor in other cancers could also be considered in GBMs [23]. Taken into account the aforementioned, this study was undertaken in order to determine the role of NFκB in GBM growth, and the selectivity, apoptotic potential and chemosensitizing activity of the NFκB inhibitors BAY117082, parthenolide, curcumin, arsenic trioxide, MG132, and p65 small-interfering RNA in GBM cell lines.

2. Materials and methods

2.1. Reagents and antibodies

BAY117082 ((E)3-[(4-methylphenyl)-sulfonyl]-2-propenenitrile); MG132 (Z-Leu-Leu-Leu-CHO), curcumin, arsenic trioxide, propidium iodide, Hepes, CHAPS, dithiothreitol, EDTA, trypsin, MTT (3-(4,5-dimethyl)-2,5-diphenyl tetrazolium bromide), Nonidet-P40, spermin tetrahydrochloride, RNAse A and culture analytical grade reagents were purchased from Sigma Chemical Co. (St. Louis, MO, USA). Anti-NFκB p65 rabbit polyclonal antibody and anti-Lamin B were from Santa Cruz Biotechnologies; anti-β-actin was from Cell Signaling Technology; SP600129 was from Promega Corporation (Madison, USA). SB203580 were from Merck Biosciences (Darmstadt, Germany). Anti-cytochrome c antibody was from BD PharMingen (San Diego, USA). Parthenolide, LY294002, UO126 and Gö6983 were from Biomol International (Plymouth Meeting, PA). PD158780 was from Tocris Bioscience (MO, USA). Electrophoresis/immunoblotting reagents were from Bio-Rad Laboratories (Hercules, CA, USA).

2.2. Cell cultures

The rat (C6) and human (U138MG, U87 and U373) malignant GBM cell lines were obtained from American Type Culture Collection (Rockville, MD, USA). Cells were grown and maintained in low glucose Dulbecco's modified Eagle's medium (DMEM; Gibco BRL, Carlsbad, USA), containing 0.1% Fungizone, 100 U/l gentamicin and supplemented with 10% fetal bovine serum. Cells were kept at 37 °C in a humidified atmosphere with 5% CO_2. Primary astrocyte cultures were prepared as previously described [24]. Briefly, cortex of newborn Wistar rats (1–2 days old) was removed and mechanically dissociated in a Ca^{2+} and Mg^{2+} free balanced salt solution (137 mmol/L NaCl, 5.36 mmol/L KCl, 0.27 mmol/L Na_2HPO_4, 1.1 mmol/L KH_2PO_4, 6.1 mmol/L glucose; pH 7.4). After centrifugation at 1000 rpm (5 min), the pellet was resuspended in DMEM supplemented with 10% FBS. The cells (2×10^5) were plated in 48 multi-well plates pretreated with poly-L-lysine. After 4 h platting, plates were gently shaken, cells were washed with PBS, and medium was changed to remove neuron and microglia contaminants. Cultures were allowed to grow by 20–25 days (100% confluence). Medium was replaced every 4 days.

2.3. MTT and LDH assays

Dehydrogenase-dependent MTT reduction (MTT assay) and lactate dehydrogenase release into culture medium from cells with losses in membrane integrity (LDH assay) were used as an estimative of cell viability [15,17]. Cells were plated in 96-well plates (10^4/well) and treated after to reach 60–70% confluence as detailed in Section 3. At the end of incubation, MTT and LDH assays were performed. Lactate dehydrogenase (LDH) release into culture medium was determined by fluorescent assay kit (CytoTox 96-NonRadioactive Cytotoxicity Assay, Promega) as recommended by the manufacturer. Qualitative morphology of the cell cultures was also evaluated by light microscopy (Nikon Eclipse TE 300), and the cell cultures were classified as: normal (cells with unaltered morphology and normal density); low-density (cell with normal morphology and low-density/lower number in plates); and dead cells (altered cellular/nuclear morphology, cytoplasm vacuolization, and presence of detached cells).

2.4. Propidium iodide incorporation and staining of chromatin

For the determination of propidium iodide (PI) uptake in cells with losses in membrane integrity, treated cells were incubated with 2 μg/mL PI in complete medium for 1 h. PI fluorescence was excited at 515–560 nm using an inverted microscope (Nikon Eclipse TE 300) fitted with a standard rhodamine filter. Representative microphotographs (at least 5/well) were collected [25]. For the detection of the morphological alterations in chromatin (condensation and fragmentation) and apoptotic body formation, cells were fixed in methanol/acetone (1:1) for 5 min and washed with PBS (3 times). Then, chromatin was stained with PI (0.5 μg/mL, 10 min) followed by fluorescent microscopy (Nikon Eclipse TE 300).

2.5. Cell cycle analysis

For cell cycle analysis, cells were trypsinized, centrifuged and resuspended in a lysis buffer (3.5 mmol/L trisodium citrate, 0.1% (v/v) Nonidet P-40, 0.5 mmol/L Tris–HCl, 1.2 mg/mL spermine tetrahydrochloride, 5 μg/mL RNAse, 5 mmol/L EDTA, 1 μg/mL propidium iodide, pH 7.6), vortexed and incubated for at least 10 min on ice for cell lysis. DNA content was determined by flow cytometry. Ten thousand events were counted per sample. FACS analyses were performed in the CellQuest Pro software (BD Biosciences, CA) [17].

2.6. Caspase-3 activity

Caspase-3 activity was assessed in agreement with CASP3F Fluorimetric kit (Sigma, St. Louis/MI). Treated cells were harvested and incubated in a lysis buffer (50 mmol/L Hepes, 5 mmol/L CHAPS and 5 mmol/L dithiothreitol, pH 7.4) for 20 min in ice. Later, extracts were clarified by centrifugation at 13,000 × *g* (15 min, 4 °C). Supernatants were collected and proteins were measured by Bradford method. For assays, 150 μg proteins were mixed with 200 μL of the assay buffer (20 mmol/L Hepes, 0.1% CHAPS, 5 mmol/L dithiothreitol, 2 mmol/L EDTA, pH 7.4) plus 20 μM Ac-DEVD-AMC (Acetyl-Asp-Glu-Val-Asp-7-amido-4-methylcoumarin), a caspase-3 specific substrate. Caspase-3-mediated substrate cleavage was monitored for 1 h (37 °C) in a fluorimetric reader (excitation 360 nm/emission 460 nm) [17].

2.7. Cellular fractionation

For nuclear extracts preparation, cells (~5×10^6, 70–80% confluence) were washed with cold phosphate-buffered saline (PBS) and suspended in 0.4 mL hypotonic lysis buffer (10 mmol/L HEPES (pH 7.9), 1.5 mmol/L $MgCl_2$, 10 mmol/L KCl, 0.5 mmol/L phenylmethylsulfonyl fluoride, 0.5 mmol/L dithiothreitol plus protease inhibitor cocktail (Roche)) for 15 min. Cells were then lysed with 12.5 μL 10% Nonidet P-40. The homogenate was centrifuged (13,000 × *g*, 30 s), and supernatants containing the cytoplasmic extracts (fraction 1) were stored at −80 °C. The nuclear pellet was resuspended in 100 μL ice-cold hypertonic extraction buffer (10 mmol/L HEPES (pH 7.9), 0.42 M NaCl, 1.5 mmol/L $MgCl_2$, 10 mmol/L KCl, 0.5 mmol/L phenylmethylsulfonyl fluoride, 1 mmol/L dithiothreitol plus protease inhibitors). After 40 min of intermittent mixing, extracts were centrifuged (13,000 × *g*, 10 min, 4 °C), and supernatants containing nuclear proteins were secured. To detect cytochrome c release from mitochondria, mitochondria-free cytoplasmic extracts were obtained from centrifugation of the cytoplasmic extracts (fraction 1) at 14,000 × *g*, 20 min, 4 °C. The resultant supernatant (mitochondria-free cytosolic proteins) and mitochondrial pellets were stored at −80 °C. The protein content was measured by the Bradford method [17,26].

2.8. NFκB-p65 ELISA assay for the determination of NFκB activity

A total of 10 μg of nuclear extracts was used to determine NFκB activation (NFκB p65 ELISA kit, Stressgen/Assays designs) as per the manufacturer protocols. This ELISA-based chemiluminescent detection method rapidly detects activated NFκB complex binding (p65 detection) to a plate-adhered NFκB consensus oligonucleotide sequence. Kit-provided nuclear extracts prepared from TNF-stimulated Hela cells were used as a positive control for NFκB activation. To demonstrate assay specificity, a 50-fold excess of an NFκB consensus oligonucleotide was used as competitor to block NFκB binding. In addition, a mutated consensus NFκB oligonucleotide (which do not binds NFκB) is provided for the determination of binding reactions' specificity [15].

2.9. siRNA knockdown of the NFκB protein p65

The Silencer® Select Validated NFκB-p65 siRNA (siRNA ID# s11914; Ambion® Inc.) was transfected using the siPORT™ NeoFX™ Transfection Agent (Ambion®, Applied Biosystems Inc.) in agreement with manufacturer's protocol. U138MG cells were transfected with 50–100 nM of NFκB-p65 siRNA by reverse transfection and then incubated for 72 h in Opti-MEM to allow knockdown of the p65 protein, which was confirmed by Western blotting. Silencer® Select Negative Control#1 siRNA containing scrambled sequences was used as negative control.

2.10. Immunocytochemistry for NFκB p65 localization

For the determination of subcellular distribution of NFκB, cells were cultured up to 60–70% confluence in 12-well plates. After a brief washing with PBS, cells were fixed in 4% (v/v) formaldehyde in PBS for 20 min at room temperature. Fixed cells were rinsed three times with PBS and then permeabilized with 0.5% Triton X-100 in PBS for 15 min at room temperature. After that, cells were washed with PBS and blocked with 5% BSA for 1 h. At the end of incubation, cells were incubated with rabbit anti-p65 polyclonal antibody (1:500; overnight at 4 °C), and then incubated with a goat anti-rabbit IgG Alexa 594-conjugated antibody (1:500) for 2 h at room temperature. Cells were visualized in a fluorescence microscope (Nikon Eclipse TE 300) [27].

2.11. Western blotting

Proteins (20 μg) were separated by SDS-PAGE on 10% (w/v) acrylamide, 0.275% (w/v) bisacrylamide gels, and electrotransfered onto nitrocellulose membranes. Membranes were incubated in TBS-T (20 mmol/L Tris–HCl, pH 7.5, 137 mmol/L NaCl, 0.05% (v/v) Tween 20) containing 1% (w/v) non-fat milk powder for 1 h at room temperature. Subsequently, the membranes were incubated for 12 h with the appropriate primary antibody (dilution range 1:500–1:1000), rinsed with TBS-T, and exposed to horseradish peroxidase-linked anti-IgG antibodies for 2 h at room temperature. Chemiluminescent bands were detected using X-ray films, and densitometry analyses were performed using Image-J® software.

2.12. Mitochondria membrane potential (JC-1 assay)

For the determination of the mitochondrial membrane potential (MMP), treated cells (5×10^5) were incubated for 30 min at 37 °C with the lipophilic cationic probe JC-1 (5,5′,6,6′-tetrachloro-1,1′,3,3′ tetraethylbenzimidazolcarbocyanine iodide, 2 μg/mL). After that, JC-1-loaded cells were centrifuged and washed once with PBS. Cells were transferred to a 96-well plate and assayed in a fluorescence plate reader with the following settings: excitation at 485 nm, emission at 540 and 590 nm, and cutoff at 530 nm (SpectraMax M2, Molecular Devices, USA). $\Delta\Psi_m$ was calculated using the ratio of 590 nm (J-aggregates)/540 nm (monomeric form) [28].

2.13. Clonogenic potential

Exponentially growing cells (1×10^6) were plated in Petri plates overnight, and then incubated for 36 h with either vehicle or NFκB inhibitors. After treatments, the medium containing NFκB inhibitors was replaced by a new medium without the tested compounds, and remaining cells were maintained for additional 24 h to growth. Survival cells were gently washed and trypsinized, and viability was assessed by Trypan Blue staining. Viable cells (10^4 cells) were re-plated in 6-well plates and maintained for additional 6 days in complete culture medium. Cell growth was estimated by colony counting followed by MTT assay [15,29]. The percentage of colony forming efficiency was calculated in relation to values of untreated cells.

2.14. Soft agar colony assay

Cells (1×10^5) were resuspended in 2 mL DMEM supplemented with 15% FBS and mixed with 1 mL of 1.6% agarose (final conditions: 0.53% agarose and 10% FBS) at 37 °C. Cell suspensions were placed on top of a base layer comprising 2 mL of DMEM with 10% FBS and 0.8% agarose in each well of a six-well plate. Cells were then covered with 2 mL of complete media and, after 3 days, a new medium containing NFκB inhibitors was added. Media containing treatments or vehicle were replaced every 72 h. At the end of 9 days, MTT (1 mg/mL) was added to the cultures and the number of colonies was scored using a microscope [15].

2.15. NFκB gene/protein-association network and landscape analysis of gene expression

The NFκB gene/protein interaction network was constructed by associating 46 NFκB-induced and cancer-related human genes involved in antiapoptotic defenses (14 genes), proliferation (8 genes), inflammation (10 genes) and invasion/metastasis/angiogenesis (9 genes), besides the NFκB subunits (5 genes). Genes were selected based on current literature [7,11,30,31]. Briefly, the network is generated using STRING database [32] with input

options 'databases', 'experiments', 'textmining' and 0.700 confidence level. STRING integrates different curate and public databases containing information on direct and indirect functional protein–protein associations/interactions. Each protein is identified according to both HUGO Gene Symbol [33] and Ensembl Peptide ID [34]. The selected gene list is applied in the STRING database and the links (interaction strength) between two different genes are saved in data files, which were handled in the Medusa software [35].

After being constructed, the NFκB gene network was analyzed by the ViaComplex software, which was previously developed and validated in our laboratory [36]. ViaComplex plots the gene expression activity over the Medusa network topology. To do this, ViaComplex overlaps functional information (micro-array expression data) with interaction information (the NFκB network) and distributes the microarray signal according to the coordinates of the network objects (i.e. nodes and links) thus constructing 3D landscape modules. Microarray expression data were collected from the international repository Gene Expression Omnibus (GEO-accession number: GSE12657; Platform: GPL8300, Affymetrix), and were composed of 20 human gliomas – 7 GBM; 7 oligodendroglioma (ODG); 6 pilocytic astrocytoma (PA) – which were compared to 5 healthy brain (HB) control biopsies. For each gene, means of each gene expression in each glioma type was plotted over the expression of the same gene in healthy brains (HB), and landscapes were constructed. Gene expression in GBM, ODG and PA versus HB tissues was statistically analyzed by *t*-test, and *p*-values were calculated.

2.16. Statistical analysis

Data are expressed as means ± SD and were analyzed by one-way ANOVA followed by Duncan's post hoc test. Differences were considered significant at $p < 0.05$.

3. Results

3.1. NFκB as potential target to cell death induction in GBMs

Initially, we treated U138MG and C6 cells with inhibitors of some signaling pathways which are described as dysregulated in GBMs and other cancers [2–4]. Inhibitors of PI3K/Akt (LY294002, wortmannin), EGFR (PD158780), MEK/ERK1/2 (UO126), JNK1/2 (SP600129), p38 MAPK (SB203580), PKC (Gö6983), proteasome/NFκB (MG132) and IKK/NFκB (BAY117082) were tested at different concentrations (1–60 μM) based on the literature range and manufacturer instructions, which describe IC_{50} values < 20 μM for all the tested drugs. At the end of 36 h incubation, only the compounds with NFκB inhibitory activity (BAY11082 and MG132) promoted significant decreases in GBM viability compared to inhibitors of other tested signaling pathways (Table 1). NFκB inhibitors reduced viability as assessed by MTT assays, increased LDH release in culture medium and altered cell

Table 1
Effect of cell signaling pathway inhibitors on viability of GBMs.

Treatments	Viability (MTT assay)		LDH	Qualitative morphology
	C6	U138MG	U138MG	U138MG
Untreated	100 ± 4	100 ± 6	100 ± 11	Normal
UO126 (30 μM)	93 ± 15	96 ± 7	92 ± 10	Normal
SP600129 (30 μM)	103 ± 11	101 ± 4	109 ± 6	Normal
SB203580 (30 μM)	98 ± 10	95 ± 6	101 ± 5	Normal
LY294002 (50 μM)	64 ± 17*	74 ± 4*	108 ± 9	Low-density
Wortmannin (10 μM)	85 ± 5*	75 ± 9*	102 ± 4	Low-density
Gö6983 (30 μM)	96 ± 9	95 ± 7	111 ± 7	Normal
PD158780 (50 μM)	99 ± 4	96 ± 5	112 ± 6	Normal
MG132 (5 μM)	21 ± 14*	23 ± 17*	223 ± 38*	Dead cells
BAY117082 (30 μM)	15 ± 6*	36 ± 9*	554 ± 39*	Dead cells

C6 and U138MG cells were treated for 36 h with well-established pathway inhibitors and MTT, LDH and qualitative microscopy assays were performed. Experiments were repeated three times ($n = 3$) in triplicate, and data were expressed in mean ± SD.
* Different from untreated cells in each type of assay.

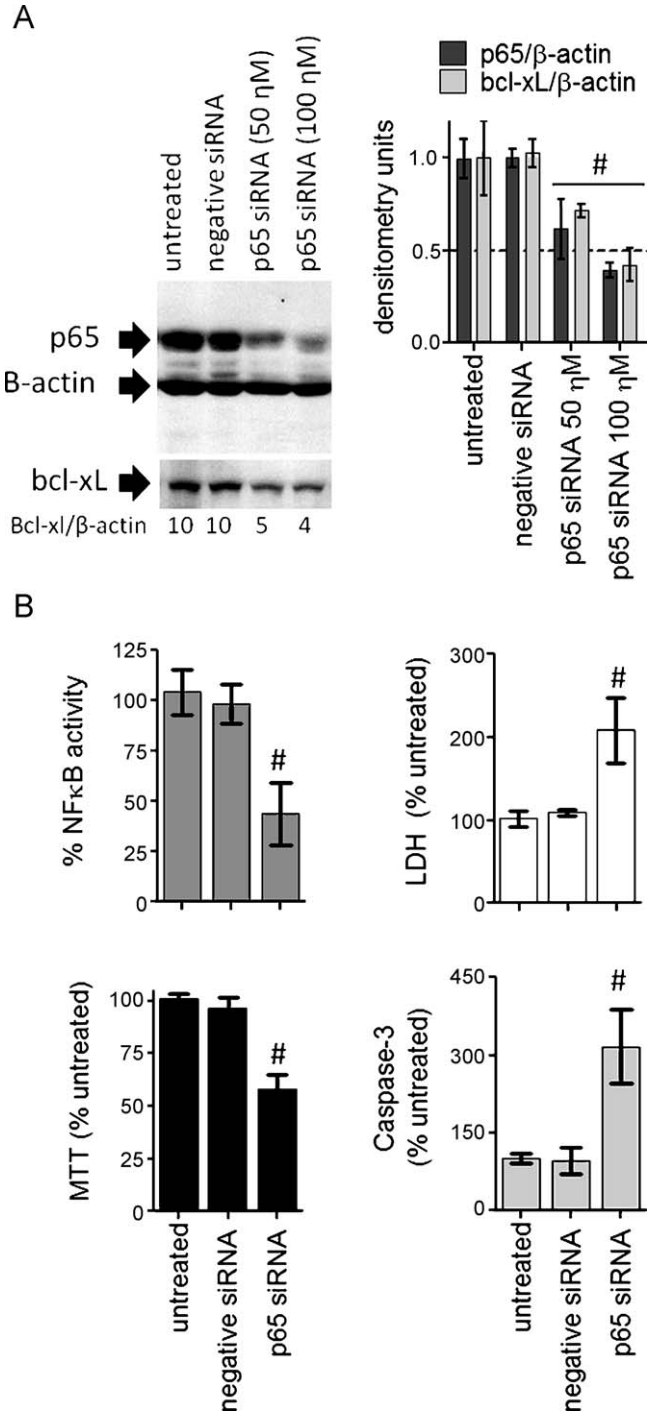

Fig. 1. NFκB-p65 knockdown induces apoptotic cell death in U138MG cells. (A) Representative immunoblotting and densitometry for the determination of p65 knockdown efficiency and bcl-xL levels. U138MG cells were incubated for 72 h with 50 or 100 nM p65 siRNA and cellular extracts were collected. (B) MTT, LDH, caspase-3 activity and NFκB ELISA assays in p65-downregulated U138MG cells. For these experiments, cells were incubated for 72 h with 100 nM p65 siRNA. All experiments were performed in triplicate. Graphs were expressed in mean ± SD. #Different from untreated cells from its respective assay.

morphology as indicative of cell death (Table 1 and Fig. 3A). Although the PI3K/Akt inhibitors LY294002 and wortmannin decreased MTT values, the absence of both LDH release and alterations in cell morphology, besides the observed decreases in cell density, suggests that PI3K/Akt inhibition affected GBM cell proliferation, but not induced cell death (Table 1). Thus, we decided to perform our further experiments with NFκB inhibitors. MAPKs (JNK, p38 and ERK1/2), EGFR, PKC inhibitors did not present cytotoxic effects up to 60 μM (data not shown). As control, we also performed Western blotting for the detection of the basal levels of phosphorylated forms of MAPKs (JNK, p38 and ERK1/2), Akt and PKC substrates; ELISA assay was performed to detect NFκB activity. Of the tested pathways, only PI3K/Akt and NFκB were detected at basal/non-stimulated conditions (data not shown).

3.2. NFκB-p65 member knockdown induces apoptosis in GBM cells

To assess the specific role of NFκB in GBM cells survival, we performed siRNA experiments to knockdown the NFκB p65 member in human U138MG cells. Immunoblotting confirmed the p65 siRNA protocol efficiency to down p65 protein after 72 h incubation with siRNAs (Fig. 1A). p65 knockdown was accompanied by the inhibition of NFκB DNA-binding activity (Fig 1B, upper left panel) and by decreases in bcl-xL protein levels (Fig. 1A), a classical antiapoptotic NFκB target gene product [7,11,13], thus confirming the effect of p65 knockdown upon NFκB signaling. As a consequence of NFκB downregulation, cell viability decreased by 45–55% as assessed by MTT. Detection of increased LDH release into culture medium and caspase-3 activation confirmed cell death induction in p65-silenced cells (Fig. 1B).

3.3. NFκB is up-regulated in GBMs compared to non-tumor astrocytes

NFκB overstimulation has been observed in several cancer cell lines as a consequence of cytokine overproduction, mutations, cell cycle dysregulation and apoptosis resistance [8,15,19]. In C6 and U138MG, we found a 5–10-fold increase in the basal activity of NFκB compared to primary astrocytes as assessed by NFκB p65 ELISA (Fig. 2A). LPS-treated cells (0.5 μg/mL, 3 h) were used as positive control for NFκB activation. Assay specificity was assessed by the incubation of nuclear extracts with a 50-fold excess of an unlabeled oligonucleotide containing the NFκB consensus sequence, which completely inhibited the constitutive NFκB binding (C6 + 50X lane). In addition, mutated NFκB oligonucleotides did not alter the constitutive NFκB activity confirming the specificity of binding reactions (C6 + mut lane, Fig. 2A). Determination of total and nuclear p65 immunocontent confirmed that a significant fraction of p65 is found in nuclear compartment of GBM cells whereas astrocytes expressed predominantly cytoplasmic/latent p65 (Fig. 2B). In C6 cells, nuclear accumulation of p65 was more accentuated. Detection of Lamin B and absence of Adenine Nucleotide Translocator (ANT) were assessed to confirm the purity of nuclear extracts (Fig. 2B). Immunocytochemistry to p65 confirmed the accumulation of p65 in nuclear compartment of C6 cells, corroborating with the Western blotting data shown in Fig. 2C.

3.4. Landscape analysis of NFκB target genes expression in human gliomas

Besides in vitro detection of NFκB in GBM cell lines (Fig. 2), we decided to test whether the cancer-related NFκB target genes are

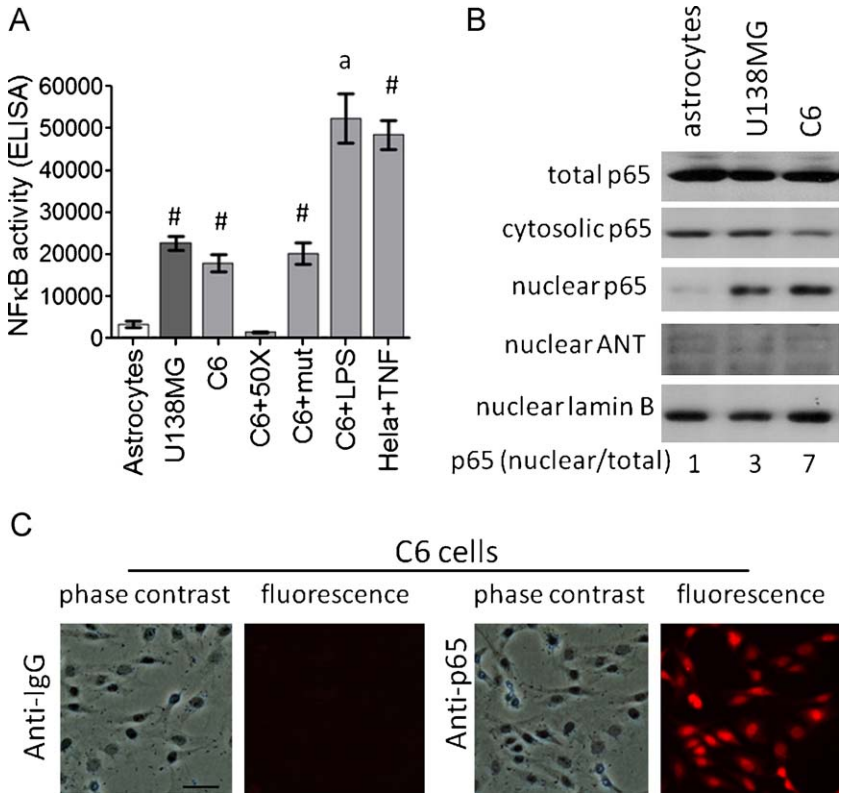

Fig. 2. NFκB is up-regulated in GBMs compared to primary astrocytes. (A) Basal NFκB activation in nuclear extracts isolated from C6, U138MG and astrocytes as assessed by ELISA. (B) Representative Western blotting showing p65 protein compartmentalization in C6, U138MG and astrocytes. (C) Representative immunocytochemistry for p65 in C6 cells (20× magnification). In these experiments, cells were maintained in basal conditions (complete culture medium for 48 h) and nuclear and cytoplasmic extracts were isolated to detect NFκB activity, p65 immunocontent, or fixed for immunocytochemistry. Lamin B and ANT levels in nuclear extracts were used as controls of nuclear extract purity. [#]Different from astrocytes; [a]different from its respective untreated cell line ($p < 0.05$, ANOVA, $n = 3$).

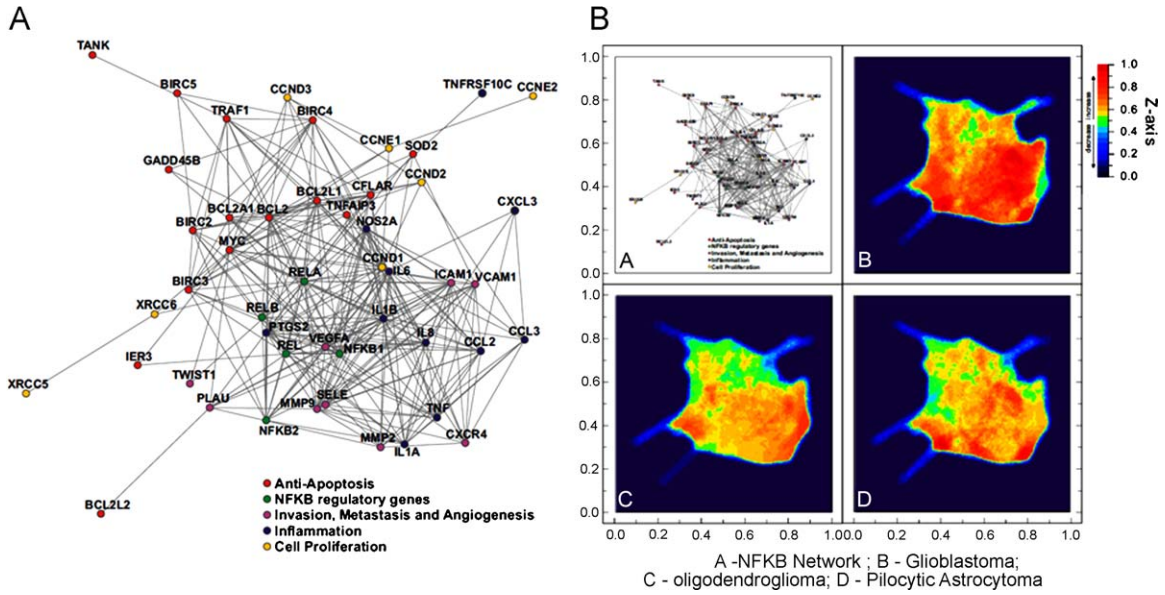

Fig. 3. Landscape analysis of NFκB gene/protein interaction networks in gliomas. (A) NFκB-target gene interaction network. Network was generated using STRING database. Gene symbol was collected from HUGO, and interactions were handled in Medusa software for network construction. (B) Landscape analysis of NFκB network gene expression in clinical specimens of glioblastoma (B panel), oligodendroglioma (C panel) and pilocytic astrocytoma (D panel). Gene expression in different types of glioma was plotted against gene expression in healthy brain tissues, and *Z*-axis for relative gene expression was constructed using the ViaComplex software.

modulated in human GBM biopsies. We collected microarray experiments containing the gene expression pattern for different glioma grades [pilocytic astrocytoma (PA), oligodendroglioma (ODG) and glioblastoma multiforme (GBM)], besides health brain (HB) biopsies. First, we constructed an NFκB gene/protein interactions network (Fig. 3A), which was subsequently analyzed by ViaComplex software as described in Section 2. ViaComplex landscapes were constructed by plotting gene expression values of each different glioma types over HB gene expression. ViaComplex-constructed *Z*-axis gives the relative gene expression in gliomas over gene expression in healthy brains. Fig. 3B shows that NFκB gene interaction network was up-regulated in the 3 grades of

Table 2
Normalized expression of NFκB-target genes in healthy brains (HB), glioblastoma (GBM), oligodendroglioma (ODG) and pilocytic astrocytoma (PA) specimens.

Gene function	Invasion/angiogenesis/metastasis								Antiapoptosis				Inflammation	
	MMP9	MMP2	CXCR4	ICAM1	PLAU	VCAM1	VCAM2	VEGFA	SOD2	MYC	A20	IER3	CCL2	IL8
HB1	102	130	304	106	102	148	136	92	70	118	177	112	320	97
HB2	109	114	61	107	73	38	89	88	10	107	121	65	30	139
HB6	99	72	44	98	44	117	91	98	251	60	71	112	20	95
HB7	95	93	63	93	54	136	91	113	394	71	67	81	27	85
HB11	94	91	28	96	226	61	93	108	102	143	67	131	100	85
GBM1	256	149	1525	3512	882	5629	2755	2320	1400	506	1077	372	825	103
GBM4	383	221	277	92	4776	305	144	1176	22	1051	140	8	12	124
GBM6	98	301	448	1866	2702	9004	5019	180	841	257	232	92	777	76
GBM7	11,212	214	2392	23,316	5237	6452	4164	19,305	2078	1235	2619	1334	2800	74,989
GBM10	2951	129	2805	2531	190	6931	3034	6413	916	175	960	315	297	965
GBM12	4490	256	911	141	484	363	312	7849	111	180	282	261	1219	434
GBM13	36,827	296	1021	17,323	11,240	4757	2020	3791	921	490	1331	916	2858	59,217
p-Value	0.017	0.005	0.005	0.048	0.005	0.003	0.006	0.016	0.049	0.040	0.010	0.035	0.073	0.103
ODG1	102	129	577	80	46	324	425	543	81	1081	177	452	174	120
ODG3	107	225	647	110	73	1213	656	43	87	2559	121	542	554	149
ODG4	222	163	50	115	91	91	104	162	9	189	71	95	153	185
ODG5	117	149	27	121	74	62	224	223	99	3196	67	371	194	1761
ODG6	109	247	226	118	101	425	298	150	9	1269	67	221	201	146
ODG7	104	144	257	120	124	2069	2062	88	34	419	97	509	783	128
ODG8	77	112	252	76	48	270	255	207	224	181	105	49	45	60
p-Value	0.190	0.020	0.340	0.270	0.930	0.073	0.0092	0.220	0.270	0.0025	0.930	0.036	0.073	0.310
PA1	88	220	1278	112	1556	215	78	156	14	298	805	619	333	97
PA2	88	139	1492	472	183	715	375	126	135	143	729	292	243	90
PA3	126	123	2938	1011	4179	65	93	376	106	875	1016	479	276	90
PA5	100	137	453	3318	14345	59	137	174	92	899	150	459	179	82
PA6	93	132	1049	5745	4805	81	75	228	43	181	781	421	342	63
PA12	86	342	1153	85	372	62	75	249	12	257	835	98	159	68
p-Value	0.25	0.069	0.007	0.082	0.0087	0.790	0.850	0.017	0.530	0.010	0.135	0.006	0.033	0.123

Mean of expression of each gene in HB was plotted as 100% (±SD) and the respective gene expression in glioma (GBM, ODG or PA) specimens was compared to these values and percentage was calculated. Percentage and *p*-values were expressed. Other details are provided in Section 2.

glioma, although GBM samples presented the higher levels of gene expression for the NFκB-regulated genes as evidenced by the red colors in *Z*-axis plots. Grouping NFκB genes by biological functions, we found that 8/9 (89%) of the selected NFκB-regulated genes described as involved in angiogenesis, invasiveness and metastasis (VEGFA, MMP2, MMP9, ICAM1, VCAM1, VCAM2, CXCR4 and PLAU) and in antiapoptotic defenses (MYC, SOD2, A20/TNFAIP3 and IER3) were markedly up-regulated in GBM patients (up to 64-fold increases, $p < 0.05$) compared to HB tissues (Table 2). Increases in the inflammatory IL8 and CCL2 mRNAs ($p < 0.1$) also were observed in GBM patients. Gene expression for NFκB subunits (RELA, REL, NFKB2 and RELB, except NFKB1) was comparable to HB, suggesting that NFκB is regulated at the activation level, not at subunit expression (data not shown). Besides increasing in GBMs, MYC, CCL2 and IER3 genes also were increased in the lower grades of glioma (ODG and PA; Table 2).

Table 3
IC_{50} levels of NFκB inhibitors in a panel of GBMs and in primary astrocytes.

Treatments	IC_{50} (μM)				
	U138MG	C6	U87	U373	Astrocytes
BAY117082	17 ± 5*	15 ± 6*	9.5 ± 7*	15 ± 4*	75 ± 8
Parthenolide	22 ± 5*	29 ± 6*	17 ± 4*	13 ± 5*	186 ± 10
MG132	2.5 ± 0.8*	3.9 ± 0.7*	5 ± 1*	2.7 ± 1*	35 ± 5
Curcumin	23 ± 5*	25 ± 4*	20 ± 6*	21 ± 3*	135 ± 12
Arsenic trioxide	4.6 ± 2*	4.2 ± 1.5*	3.6 ± 2*	5 ± 1*	18 ± 2

Cells (U138MG, U87, C6, U373 and astrocytes) were treated for 36 h with different concentrations of NFκB signaling inhibitors (BAY117082, curcumin, parthenolide, MG132 and arsenic trioxide; 1–200 μM) and cell viability was determined by MTT assay. Experiments were repeated three times ($n = 3$) in triplicate, and data were expressed in mean ± SD.

* Different from untreated cells, and from its respective astrocytic IC_{50} value ($p < 0.05$).

3.5. Pharmacological inhibitors of NFκB selectively induce cell death in GBMs

Data from Table 1, and Figs. 2 and 3, indicate that NFκB could be a potential target pathway to cell death induction in GBMs. Thus, we decided to test the cytotoxic effect of some NFκB pathway inhibitors such as BAY117082, parthenolide, arsenic trioxide, MG132 and curcumin in a panel of GBM cell lines. In parallel, primary astrocyte cultures were treated in order to evaluate the drug selectivity to cancer cells. GBMs and astrocytes were incubated with different concentrations of NFκB inhibitors for 36 h, and MTT assays were performed. Results show that astrocytes were less sensitive to NFκB inhibitors than GBM cell lines, indicating selectivity of NFκB inhibitors to tumor cells (Table 3). For BAY117082, parthenolide, MG132, curcumin and arsenic trioxide, the IC_{50} values in MTT assay were, respectively, at least 4.4, 6.4, 7, 4 and 3.6-fold lower in the GBM cell lines compared to astrocytes as shown in Table 3. Thus, for further experiments, we used ~IC_{50} concentrations for NFκB inhibitors (17 μM BAY117082; 25 μM curcumin; 3 μM MG132; 4 μM arsenic trioxide; 25 μM parthenolide) and C6/U138MG cell lines. To determine whether the effects of pharmacological NFκB inhibitors are directly NFκB related, indirectly related to NFκB inhibition, or have nothing to do with NFκB, we evaluated different concentrations of the compounds on NFκB activity and on cell viability as shown in Table 4. Correlations between NFκB inhibition and decreases in cell viability were calculated (Table 4). Data showed that pharmacological agent-induced NFκB inhibition significantly correlated with decreases in cell viability of both C6 and U138MG cells. As control, we also determined that inhibitors of the signaling pathways which were previously tested in Table 1 did not affect NFκB activity (Table 5). Taken together, data from Tables 1, 4 and 5 suggest that the antiglioma effects of the tested compounds were directly related to their NFκB inhibitory activity.

3.6. NFκB inhibitors induce anchorage-independent cell death and reduce the clonogenic potential in GBMs

Results from clonogenic survival assay showed that 36 h treatment with NFκB inhibitors followed by 6-day washout significantly decreased the clonogenic proliferation in GBMs, suggesting that the antiglioma effects of NFκB inhibition were long-term thus remaining after drug withdrawal (Fig. 4B). In addition, data from soft agar experiments showed that NFκB

Table 4
NFκB inhibition is correlated with decreases in cell viability in GBMs.

Treatments	Concentration (μM)	NFκB activity (%, mean ± SD)		% cell viability (MTT assay)		Correlation (r^2) Viability × NFκB	
		C6	U138MG	C6	U138MG	C6	U138MG
Untreated	0	100 ± 11	100 ± 12	100 ± 7	100 ± 6		
BAY117082	5	85 ± 14	87 ± 15	86 ± 6	95 ± 7	0.931#	0.952#
	25	47 ± 15*	35 ± 10*	17 ± 9*	37 ± 12*		
	50	13 ± 9*	17 ± 5*	5 ± 3*	15 ± 4*		
Parthenolide	5	92 ± 13	88 ± 12	80 ± 12	91 ± 5	0.846#	0.971#
	25	24 ± 11*	34 ± 21*	54 ± 5*	48 ± 7*		
	50	15 ± 14*	20 ± 9*	15 ± 6*	19 ± 4*		
MG132	1	72 ± 9*	79 ± 6*	66 ± 11*	71 ± 6*	0.974#	0.981#
	5	37 ± 13*	21 ± 17*	26 ± 5*	23 ± 7*		
	10	12 ± 6*	14 ± 8*	15 ± 7*	11 ± 5*		
Curcumin	5	93 ± 8	99 ± 10	94 ± 5	89 ± 4	0.978#	0.962#
	25	47 ± 12*	49 ± 22*	46 ± 7*	40 ± 9*		
	50	24 ± 13*	11 ± 7*	9 ± 8*	21 ± 11*		
Arsenic	1	82 ± 7*	91 ± 12	95 ± 9	92 ± 7	0.954#	0.975#
	5	25 ± 13*	29 ± 18*	41 ± 7*	45 ± 4*		
	10	18 ± 6*	24 ± 9*	17 ± 11*	27 ± 9*		

C6 and U138MG cells were treated with different concentrations of BAY117082, curcumin, parthenolide, MG132 or arsenic trioxide. MTT was performed after 36 h treatment; ELISA assays for NFκB-p65 DNA-binding activity were performed in nuclear extracts isolated from 6 h-treated GBMs. Cell viability and NFκB inhibition were expressed as percentage compared to untreated cells. *R* squared (R^2) was calculated using GraphPad Prism software®. Experiments were repeated three times ($n = 3$) in duplicate; data were expressed as mean ± SD.

* Different from untreated cells.

\# Positive correlation.

inhibitor-induced cell death was independent of cell anchorage since NFκB inhibitors decreased cell colony formation in soft agar (Fig. 4C). At the end of 36 h treatment with NFκB inhibitors, we also observed significant alterations in cell morphology, which were accompanied by PI uptake, cell detachment and LDH release as indicative of cell death (Fig. 4A). PI uptake did not occur in all cells with morphological changes, suggesting that morphological alterations preceded the losses in cell membrane integrity. These effects suggest a programmed mechanism of cell death induction by NFκB inhibitors thus stimulating us to evaluate apoptotic markers (Fig. 4A).

3.7. NFκB inhibitors cell cycle arrest and apoptosis in GBMs

PI staining of chromatin showed that NFκB inhibitors induced chromatin condensation and apoptotic body formation in U138MG cells (Fig. 5A). The results were similar in C6 cells (data not shown). Determination of caspase-3 activity showed that all the tested NFκB inhibitors promoted caspase-3 activation in C6 whereas only MG132 and arsenic trioxide increased caspase-3 activity in the p53/PTEN mutant U138MG, suggesting that apoptosis can be caspase-3 dependent or independent depending on cell type and on NFκB inhibitor (Fig. 5B). Analysis of cell cycle distribution evidenced that, after 18 h treatment, NFκB inhibitors caused accumulation of cells in the G2/M phase of the cell cycle followed by the formation of sub-G1 apoptotic cells at 36 h, suggesting that arrest in G2/M phase preceded apoptosis (Fig. 5C).

3.8. Mitochondrial dysfunction precedes apoptosis in NFκB inhibitor-treated cells

We also evaluated the mitochondrial function in NFκB inhibitor-treated GBMs. In time-effect experiments, we determined that NFκB inhibitors promoted an early decrease in MMP (JC-1 assay) which was observed between 8 and 16 h treatment whereas cell membrane integrity (PI uptake assay) only decreased at later time points (24 h treatment) (Fig. 6A). It suggests that mitochondrial dysfunction occurred at the early steps of NFκB inhibitor-induced

Table 5
Effect of MAPKs, EGFR, PKC and PI3K/Akt inhibitors on NFκB activity.

Treatments	Concentration (μM)	NFκB activity (%, mean ± SD)
Untreated	0	100 ± 8
UO126	10	110 ± 11
	30	112 ± 22
SP600129	10	106 ± 12
	30	114 ± 7
SB203508	10	88 ± 22
	30	95 ± 16
PD158780	10	90 ± 8
	30	106 ± 14
LY294002	10	88 ± 11
	30	86 ± 21
Gö6983	10	112 ± 13
	30	93 ± 9
Wortmannin	1	89 ± 15
	10	93 ± 11
BAY117082	30	39 ± 12*

C6 cells were treated with different concentrations of pharmacological inhibitors of MEK/ERK (UO126), JNK1/2 (SP600129), p38 (SB203508), EGFR (PD158780), PI3K/Akt (LY294002 and wortmannin) and PKC (Gö6983). BAY117082 was used as control for NFκB inhibition. ELISA assays for NFκB-p65 DNA-binding activity were performed in nuclear extracts isolated from 6 h-treated cells. NFκB activity was expressed as percentage compared to untreated cells (mean ± SD). Experiments were performed in triplicate.
* Different from untreated cells ($p < 0.05$).

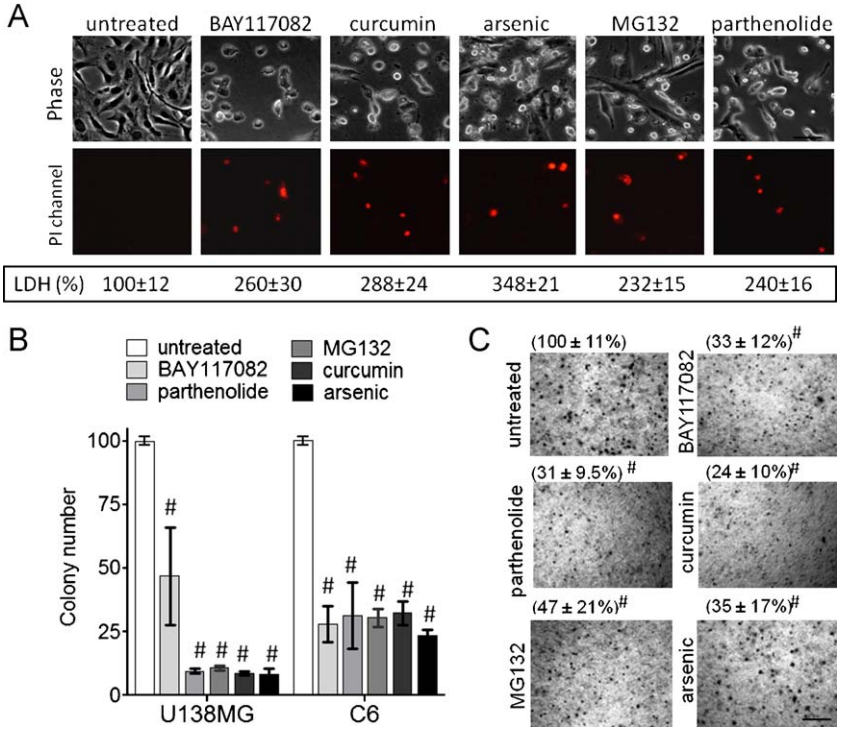

Fig. 4. NFκB inhibitors induce anchorage-independent cell death and reduce clonogenic potential of GBMs. (A) Representative microphotographs (20× magnification) showing cell morphology and PI uptake in U138MG cells after 36 h treatment with NFκB inhibitors. Below microphotographs are presented as means ± SD of the LDH activity detected in the culture medium of GBMs. (B) Clonogenic survival in U138MG cells after treatment with NFκB inhibitors. (C) Representative microphotographs and quantification of colonies in soft agar growing C6 cells (see details in Section 2). In these experiments were used IC_{50} concentrations of NFκB inhibitors. #Different from untreated cells ($n = 3$).

cell death. Like observed in p65 knockdown experiments (Fig. 1), pharmacological inhibitors also decreased the levels of the NFκB-regulated mitochondrial cytoprotective protein bcl-xL [7,10,11] (Fig. 6B). Mitochondrial dysfunction also was accompanied by the release of the pro-apoptotic factor cytochrome c from mitochondrial to cytoplasmic fraction as assessed after 16 h treatment with NFκB inhibitors (Fig. 6B).

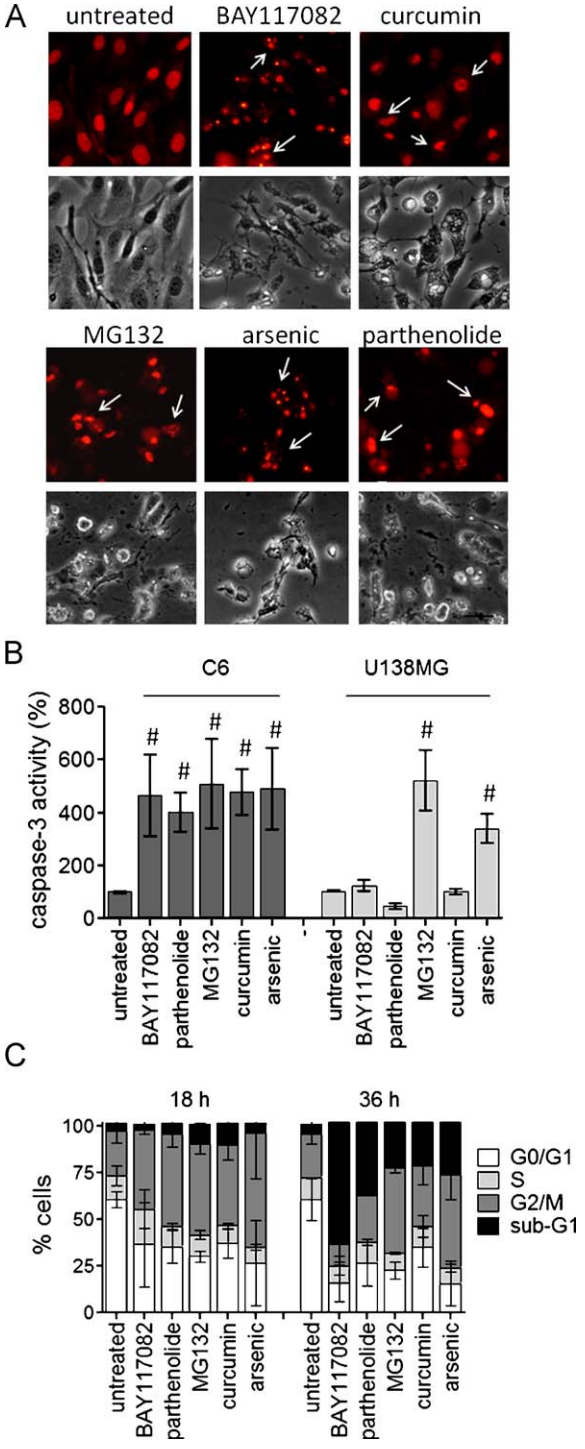

Fig. 5. NFκB inhibitors induce apoptosis in GBMs. (A) Representative fluorescent and phase contrast microphotographs (20×) showing chromatin condensation and apoptotic body formation after 36 h incubation with NFκB inhibitors. U138MG cells were fixed, and chromatin was stained with propidium iodide. (B) Caspase-3 protease activity after 36 h treatment with pharmacological inhibitors in C6 and U138MG cell lines. (C) Quantification of cell population distribution between sub-G1, G1/G0, S and G2/M phases of the cell cycle after 18 or 36 h treatment of U138MG cells with NFκB inhibitors. In Fig. 7 experiments, NFκB inhibitors were incubated using IC_{50} concentrations. #Different from untreated cells ($n = 3$, $p < 0.05$, ANOVA).

3.9. NFκB inhibitors synergize with the anticancer drugs cisplatin and doxorubicin

An interesting field in the NFκB research is the possibility of combination of NFκB inhibitors with classical chemotherapy in order to decrease chemotherapy doses and adverse cytotoxicity to normal tissues [9]. In synergism/antagonism experiments, we established two protocols: (1) 6 h pre-treatment with apoptotic levels of NFκB inhibitors, washout, and 48 h mono-treatment with doxorubicin or cisplatin; (2) 6 h pre-treatment with sub-apoptotic concentrations of NFκB inhibitors followed by 48 h co-incubation with doxorubicin or cisplatin. At the end of the treatments, MTT assays were performed. Results showed that NFκB inhibitors synergized with doxorubicin and cisplatin in both apoptotic and sub-apoptotic concentrations potentiating the anticancer effects of these drugs in C6 and U138MG lines (Table 6).

3.10. NFκB inhibitors overcame cisplatin resistance in GBM

In other approach, we selected cisplatin-resistant cells by incubating C6 cells with 50 μM cisplatin for 48 h followed by a 20–

Table 6
NFκB inhibitors synergize with cisplatin and doxorubicin to induce GBM cell death.

Treatments	Viability (mean ± SD)	
	C6	U138MG
Untreated	100 ± 6	100 ± 7
Cisplatin 5 μM	73 ± 3*	84 ± 8*
Cisplatin + BAY 7.5 μM	55 ± 12#	64 ± 8#
Cisplatin + BAY 25 μM	19 ± 5#	34 ± 16#
Cisplatin + Part 10 μM	56 ± 4#	74 ± 6
Cisplatin + Part 25 μM	38 ± 11#	22 ± 4#
Cisplatin + MG132 1 μM	60 ± 14	68 ± 4#
Cisplatin + MG132 5 μM	33 ± 10#	23 ± 1#
Cisplatin + curcumin 10 μM	46 ± 6#	47 ± 13#
Cisplatin + curcumin 25 μM	36 ± 5#	28 ± 2#
Cisplatin + arsenic 0.5 μM	51 ± 10#	56 ± 1#
Cisplatin + arsenic 15 μM	29 ± 9#	25 ± 3#
Doxorubicin 2.5 μM	70 ± 8*	75 ± 7*
Doxorubicin + BAY 7.5 μM	24 ± 12#	61 ± 6.5
Doxorubicin + BAY 25 μM	21 ± 12#	29 ± 10#
Doxorubicin + Part 10 μM	46 ± 11#	23 ± 5#
Doxorubicin + Part 25 μM	23 ± 2#	19 ± 1#
Doxorubicin + MG132 1 μM	32 ± 7#	22 ± 18#
Doxorubicin + MG132 5 μM	7 ± 1#	2 ± 3#
Doxorubicin + curcumin 10 μM	67 ± 5	59 ± 2#
Doxorubicin + curcumin 25 μM	46 ± 5#	39 ± 3#
Doxorubicin + arsenic 0.5 μM	61 ± 6	25 ± 2#
Doxorubicin + arsenic 15 μM	30 ± 5#	25 ± 1#
BAY 7.5 μM	102 ± 13	103 ± 10
BAY 25 μM	37 ± 5*	53 ± 12*
Part 10 μM	92 ± 9	90 ± 7
Part 25 μM	58 ± 13*	45 ± 13*
MG132 1 μM	114 ± 8	82 ± 10*
MG132 5 μM	77 ± 11*	28 ± 4*
Curcumin 10 μM	94 ± 7	74 ± 12*
Curcumin 25 μM	75 ± 17*	53 ± 11*
Arsenic 0.5 μM	110 ± 18	90 ± 12
Arsenic 15 μM	58 ± 11*	49 ± 10*

Wild-type U138MG and C6 glioma cell lines were treated with different concentrations of NFκB inhibitors as described in Section 3, followed by exposure to 5 μM cisplatin or 2.5 μM doxorubicin (approximately IC_{25} levels) for 48 h. After that, MTT assays were performed. Data were expressed as percentage compared to untreated cells (mean ± SD). Experiments were repeated three times ($n = 3$) in quadruplicate. BAY (BAY117082); Part (Parthenolide).

* Different from untreated cells.

Different from untreated and from cisplatin or doxorubicin-treated cells ($p < 0.05$).

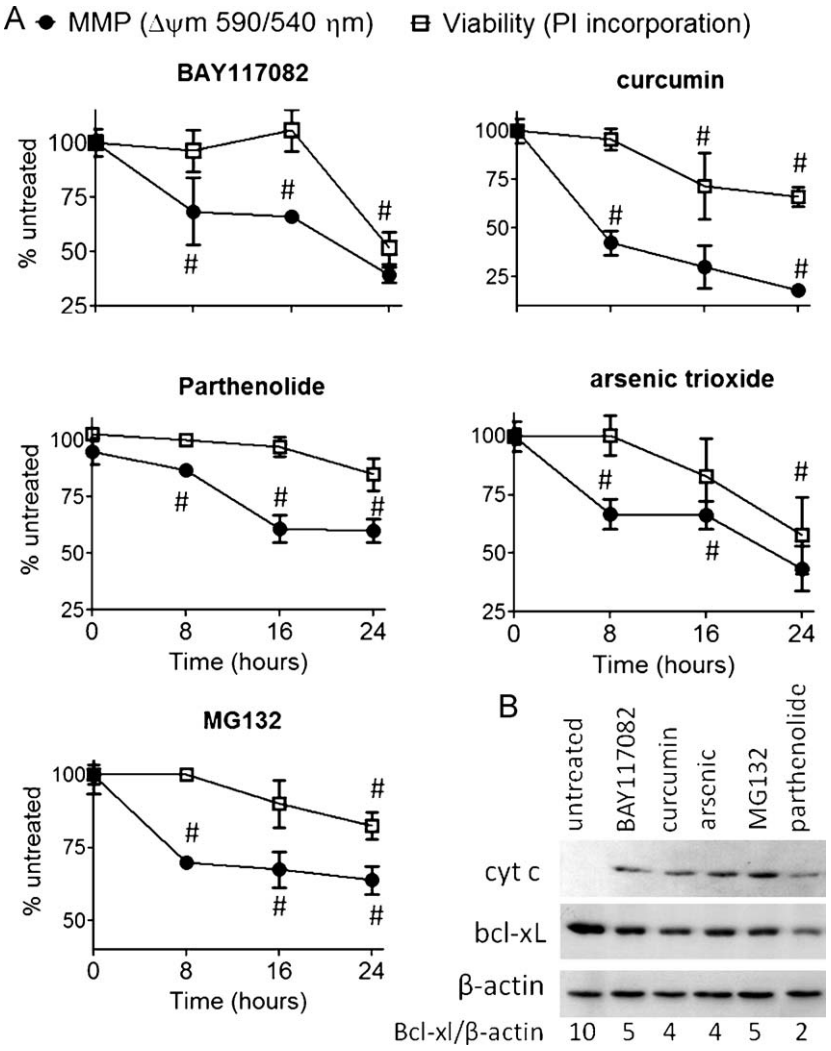

Fig. 6. Mitochondrial dysfunction precedes apoptosis in NFκB inhibitor-treated cells. (A) Time course effect of NFκB inhibitors on MMP was co-evaluated with PI incorporation for the determination of cell membrane integrity. U138MG was treated for different times and, at the end of treatments, cells were trypsinized and different aliquots were assayed by JC-1 or PI incorporation. (B) Western blotting detection of cytochrome c in the cytosolic fraction, and total bcl-xL protein levels in U138MG cells after 16 h treatment with NFκB inhibitors. Experiments were performed in triplicate, and graphs were expressed in mean ± SD. #Different from untreated cells.

25 day washout for the recovery of survival clones. After that, cells were tested for cisplatin resistance. IC_{50} values increased by almost 8-fold (from 20 to 155 μM) confirming the resistance to the alkylating agent (Fig. 7A). Interestingly, NFκB was found over-stimulated in cisplatin-resistant cells compared to wild-type C6 (Fig. 7B). The antiglioma potential of NFκB inhibitors was independent of cisplatin resistance, since drugs were effective to induce cell death in the cisplatin-resistant C6 cell line. Interestingly, co-treatment of cisplatin (IC_{25} concentration = 75 μM) plus NFκB inhibitors overcame cisplatin resistance, finally inducing high rates of cell death after 48 h treatment when compared to mono-treatments of NFκB inhibitors or cisplatin (Fig. 7C). Altogether, data showed that increased NFκB correlated with cisplatin resistance, and NFκB inhibitors efficiently induced cell death in resistant cells besides overcoming cisplatin resistance. Importantly, cell resistance to cisplatin was transitory and decreased after 3–4 passages.

4. Discussion

GBMs are associated with a poor prognosis due to intrinsic malignance and drug/radiation resistance, besides limited therapeutic opportunities such as neurosurgery and temozolomide/radiotherapy regimens [1,15,25]. Studies reported that NFκB activation correlates with therapeutic implications and worse prognosis in human gliomas [21–23,37–39]. Aberrant NFκB activity was found critical for focal necrosis formation, invasive phenotype establishment [22] and resistance to O^6 alkylating agents in GBMs [40]. In vitro, the expression of an IκB super-repressor protein decreased C6 cell viability [21]. Also, the literature indicates that most of the factors that mediate proliferation, invasion, angiogenesis and apoptotic resistance in cancer, including GBMs, such as EGF/EGFR, VEGF, PDGF, MCP-1, MMPs, VCAM, bcl-xL and FLICE are activators of or products of NFκB-regulated genes, conferring to NFκB a potential role on GBM growth and thus a potential target pathway [7,8,11,41,42]. In this way, some experimental drugs possessing antiglioma activities showed mechanisms involving NFκB inhibition [43–46].

In this work, knockdown of the NFκB member p65 and pharmacological inhibition of NFκB caused significant decreases in GBM cell viability whereas inhibitors of other signaling pathways such as MEK/ERK, JNK, p38, EGFR and PKC had no significant effects, except for a cytostatic activity following PI3K/Akt inhibition. Corroborating, Carapancea et al. showed that inhibitors of PDGF, EGFR, PI3K and MEK1/2 (AG1433, AG1024, LY294002 and PD98059, respectively) failed to induce cell death in MO59J and

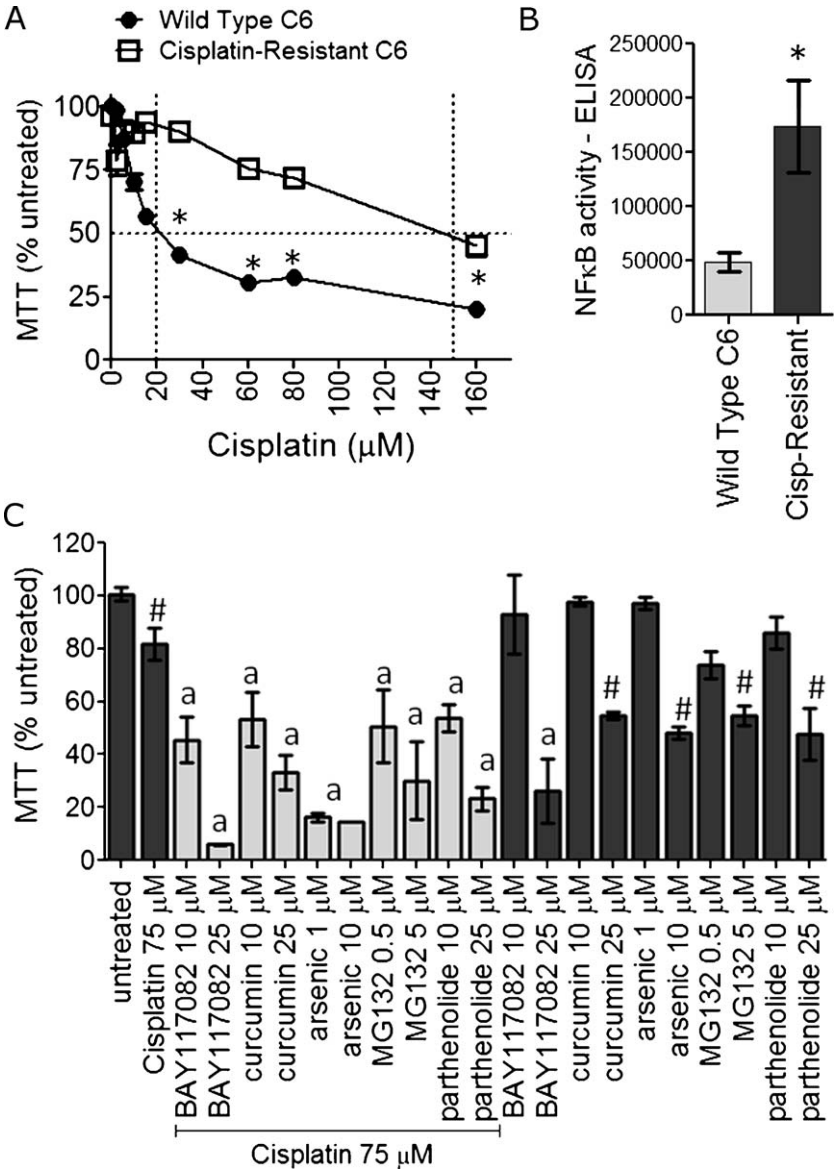

Fig. 7. NFκB inhibitors overcame cisplatin resistance GBM cells. (A) Representative MTT assay showing the validation of cisplatin resistance in C6 cells. (B) NFκB ELISA assay showing that NFκB DNA-binding activity is increased in cisplatin-resistant compared to that of wild-type C6 cells. (C) NFκB inhibition abolishes cisplatin resistance in cisplatin-resistant cells. Cells were treated with IC_{25} concentrations of cisplatin in the presence or absence of NFκB inhibitors (IC_{50} levels) for 48 h, and viability was determined by MTT. Resistance induction was performed twice, and experiments were performed in triplicate. *Different from C6-wild type cells; #different from untreated cells; [a]different from cisplatin and from its respective NFκB inhibitor alone treatment.

MO59K cell lines, and in primary cultures derived from GBM patients [47]. NFκB inhibitors induced cell death in liquid and soft agar growing cells regardless of the p53 or PTEN mutational status since cytotoxicity was similar for C6 (p53 and PTEN normal), U87 (PTEN mutant), U373 (p53 and PTEN mutant) and U138MG (p53 and PTEN mutant) cell lines. NFκB was found overstimulated in GBMs, and its inhibitors were selective to cell death induction in tumor cells as compared to astrocytes. The antiglioma potential of the pharmacological agents correlated with NFκB inhibition as demonstrated in Tables 4 and 5. Tumor-specific targeting represents an improvement over classical chemotherapeutics, which adversely affect both diseased and normal brain in a non-specific manner [6,9,13]. Nuclear p65 was found in GBMs whereas latent/cytosolic p65 was detected in astrocytes. Total p65 protein was similar between GBM and astrocytes suggesting that NFκB was modulated at the level of activation. Nonetheless, landscapes analysis for NFκB gene interaction network revealed that NFκB target genes were up-regulated in the three tumor grades (GBM, oligodendroglioma and astrocytoma) compared to healthy brain tissues. Landscapes evidenced a high expression of NFκB target genes in the most aggressive form of glioma, GBM; marked increases were observed in VEGFA, MMP2, MMP9, PLAU, VCAM1, ICAM1, IER3, SOD2, MYC, CCL2 and IL8 gene expression. In agreement with these results, Xie et al. showed that constitutive NFκB regulates the expression of VEGF and IL-8 and tumor angiogenesis in human GBM [12]. This exacerbated activation of NFκB has been pivotal to explain the selective toxicity of NFκB inhibitors to cancer cells [10,13,17,19].

Previous works showed that downregulation of NFκB leads to mitochondrial dysfunction due to decreases in the expression of mitochondrial cytoprotective genes such as bcl-xL and SOD2, which result in cytotoxicity [11,15,17,26]. Jiang et al. reported that selective bcl-xL knockdown rendered U87 and NS008 GBM cells to apoptosis [48]. In our model, NFκB inhibitors caused bcl-xL protein downregulation, mitochondrial depolarization and release of the apoptotic factor cytochrome c, which preceded the losses in cell

membrane integrity and apoptosis, thus implying that mitochondrial dysfunction is an early step of NFκB inhibitor-induced cell death [7,11,15,48]. In previous studies, arsenic trioxide induced G2/M arrest in the U87 and T98G [49], and mitochondrial aggregation and cytochrome c release in A172 GBMs [50]. Here, all NFκB inhibitors elicited cell arrest in the G2/M phase of the cell cycle before sub-G1 induction, apoptotic body formation and caspase-3 activation. The herein reported impairment on mitochondrial function and induction of G2/M arrest were previously demonstrated by our group and others during curcumin [51], parthenolide [52], BAY117082 and MG132 [17] treatment in other types of cancer cells, but not in gliomas.

In GBMs, defects in caspase-mediated apoptotic signaling due to p53 mutations limit the effectiveness of chemotherapy thus promoting chemoresistance and poor clinical outcome [53–56]. Induction of caspase-independent mechanisms of cell death could be useful for circumventing GBM resistance. In our model, all tested NFκB inhibitors activated caspase-3 in C6 whereas only MG132, arsenic trioxide and p65 siRNA stimulated caspase-3 in the p53-mutant U138MG; curcumin, BAY117082 and parthenolide exerted caspase-independent cell death in U138MG. Besides the distinct genetic aberrations between C6 and U138MG cell lines, differences in the action mechanisms of the tested NFκB inhibitors and possible off-target effects could explain their differential effects upon caspase-3. BAY117082 is a specific IKK-beta inhibitor ($IC_{50} \sim 10\ \mu M$) [57]; parthenolide inhibits NF-κB both indirectly by blocking IKK-beta at cys179 and directly by inhibiting p65 at the cysteine residue in its activation loop ($IC_{50} \sim 10\ \mu M$) [58,59]; MG132 inhibits proteasome ($IC_{50} \sim 0.1\ \mu M$) and proteasome-dependent IκB-alpha degradation ($IC_{50} \sim 3\ \mu M$) thus blocking the nuclear activity of NFκB; arsenic trioxide inhibits degradation and up-regulates expression of IκB-alpha [60]; curcumin inhibits IKKs ($IC_{50} \sim 13\ \mu M$), although unspecific effects upon activator protein-1 and glyoxalase I activity, for example, were described [15,61,62]. In U138MG, the IKK inhibitors did not increase caspase-3 in contrast to inhibitors of IκB degradation such as MG132 and arsenic. In T98G and U87 GBMs, curcumin induces caspase- and calpain-independent cell death irrespective of the p53 status of the cells [15]. Thus, elucidation of these mechanistic differences requires further investigation.

Besides their apoptotic activity per se, NFκB inhibitors presented adjuvant activity by potentiating the anticancer effect of cisplatin and doxorubicin in both C6 and U138MG cells, besides overcoming cisplatin resistance in cisplatin-resistant C6. Several lines of evidence suggest NFκB as a key mediator of cancer cells resistance to chemotherapy and anticancer therapy failure in vivo [9,18,40]. Bredel et al. reported that NFκB mediates GBM resistance to the alkylating agents, temozolomide and BCNU, in primary GBM cultures [40]. In addition, Weaver et al. demonstrated that chemotherapy-induced DNA damage may activate NFκB, and inhibition of NFκB by mutant IκB-alpha enhances BCNU, carboplatin and TNF-induced cell death in U87 and U251 cells [63]. In our model, NFκB activity was up-regulated in cisplatin-resistant C6 cells compared to that in wild-type C6. Cisplatin-resistant cells remained sensitive to NFκB inhibitors, and combination of cisplatin plus NFκB inhibitors overcame cisplatin resistance, suggesting that alkylation resistance involved NFκB pathway. In agreement, previous studies reported that the proteasome inhibitors LLnL and MG132, which are known by acting through NFκB inhibition, sensitized GBMs to TRAIL-induced apoptosis [18]. Clinically, the adjuvant potential of NFκB inhibitors could be used for therapeutic advantage in order to potentiate the efficacy of classical anticancer drugs in chemotherapy-resistant patients thus decreasing the anticancer agents' doses and the frequently observed collateral effects to healthy tissues [9,15].

As above cited, some previous studies exploited the antiglioma effects of some of the herein used compounds as arsenic trioxide [49,50,64], curcumin [15,65–67], parthenolide [68] and proteasome/NFκB inhibitors [3,18,63,69,70] in GBMs. Here, we suggest that a mechanism by which they induce GBM cells death is mediated by their NFκB inhibitory activity. We add information by evaluating inhibitors of different signaling pathways, NFκB pathway activation in cell lines and in clinical specimens, and effect of different NFκB inhibitors in a panel of GBM cell lines; p65 knockdown also was evaluated. Importantly, selectivity to cancer cells, mitochondrial dysfunction, adjuvant potential and ability of NFκB inhibitors to abolish chemoresistance were examined. The results were positive and support a rationale for further testing inhibition of NFκB pathway in animal models of GBMs, and possibly other cancers.

Disclosure statement

The authors report no conflicts of interest. The authors alone are responsible for the content and writing of the paper.

Acknowledgements

We acknowledge the Brazilian funds CAPES, FINEP/IBNNet (01060842-00) and CNPq for financial support, and Dr Rafael Roesler (Hospital de Clinicas de Porto Alegre, HCPA) for kindly providing U87 and U373 cell lines.

References

[1] Stewart LA. Chemotherapy in adult high-grade glioma: a systematic review and meta-analysis of individual patient data from 12 randomised trials. Lancet 2002;359:1011–8.
[2] Soni D, King JA, Kaye AH, Hovens CM. Genetics of glioblastoma multiforme: mitogenic signaling and cell cycle pathways converge. J Clin Neurosci 2005;12:1–5.
[3] Yu C, Friday BB, Yang L, Atadja P, Wigle D, Sarkaria J, et al. Mitochondrial Bax translocation partially mediates synergistic cytotoxicity between histone deacetylase inhibitors and proteasome inhibitors in glioma cells. Neuro Oncol 2008;10(3):309–19.
[4] Brennan C, Momota H, Hambardzumyan D, Ozawa T, Tandon A, Pedraza A, et al. Glioblastoma subclasses can be defined by activity among signal transduction pathways and associated genomic alterations. PLoS ONE 2009; 4(11):e7752.
[5] Gerstner ER, Sorensen AG, Jain RK, Batchelor TT. Anti-vascular endothelial growth factor therapy for malignant glioma. Curr Neurol Neurosci Rep 2009;9(3):254–62.
[6] Mercer RW, Tyler MA, Ulasov IV, Lesniak MS. Targeted therapies for malignant glioma: progress and potential. BioDrugs 2009;23(1):25–35.
[7] Barkett M, Gilmore TD. Control of apoptosis by Rel/NFkB transcription factors. Oncogene 1999;18:6910–24.
[8] Rayet B, Gélinas C. Aberrant rel/NFκB genes and activity in human cancer. Oncogene 1999;18(49):6938–47.
[9] Nakanishi C, Toi M. Nuclear factor-kappaB inhibitors as sensitizers to anticancer drugs. Nat Rev Cancer 2005;5(4):297–309.
[10] Baud V, Karin M. Is NF-kB a good target for cancer therapy? Hopes and pitfalls. Nat Rev Drug Discov 2009;8:33–40.
[11] Aggarwal BB. Nuclear factor-kappaB: the enemy within. Cancer Cell 2004;6(3):203–8.
[12] Xie TX, Xia Z, Zhang N, Gong W, Huang S. Constitutive NF-kappaB activity regulates the expression of VEGF and IL-8 and tumor angiogenesis of human glioblastoma. Oncol Rep 2010;23(3):725–32.
[13] Orlowski RZ, Baldwin Jr AS. NF-kappa B as a therapeutic target in cancer. Trends Mol Med 2002;8:385–9.
[14] Li B, Li YY, Tsao SW, Cheung AL. Targeting NF-kappaB signaling pathway suppresses tumor growth, angiogenesis, and metastasis of human esophageal cancer. Mol Cancer Ther 2009;8(9):2635–44.
[15] Dhandapani KM, Mahesh VB, Brann DWJ. Curcumin suppresses growth and chemoresistance of human glioblastoma cells via AP-1 and NFkappaB transcription factors. J Neurochem 2007;102(2):522–38.
[16] Xie TX, Aldape KD, Gong W, Kanzawa T, Suki D, Kondo S, et al. NF-kappaB activity is critical in focal necrosis formation of human glioblastoma by regulation of the expression of tissue factor. Int J Oncol 2008;33(1):5–15.
[17] Zanotto-Filho A, Delgado-Cañedo A, Schröder R, Becker M, Klamt F, Moreira JC. The pharmacological NFkappaB inhibitors BAY117082 and MG132 induce cell arrest and apoptosis in leukemia cells through ROS–mitochondria pathway activation. Cancer Lett 2010;288(2):192–3.

[18] Kasuga C, Ebata T, Kayagaki N, Yagita H, Hishii M, Arai H, et al. Sensitization of human glioblastomas to tumor necrosis factor-related apoptosis-inducing ligand (TRAIL) by NF-kappaB inhibitors. Cancer Sci 2004;95(10):840–4.
[19] Pickering BM, de Mel S, Lee M, Howell M, Habens F, Dallman CL, et al. Pharmacological inhibitors of NF-kB accelerate apoptosis in chronic lymphocytic leukemia cells. Oncogene 2007;26:1166–77.
[20] Domingo-Domènech J, Pippa R, Tápia M, Gascón P, Bachs O, Bosch M. Inactivation of NF-kappaB by proteasome inhibition contributes to increased apoptosis induced by histone deacetylase inhibitors in human breast cancer cells. Breast Cancer Res Treat 2008;112(1):53–62.
[21] Robe PA, Bentires-Alj M, Bonif M, Rogister B, Deprez M, Haddada H, et al. In vitro and in vivo activity of the nuclear factor-kappaB inhibitor sulfasalazine in human glioblastomas. Clin Cancer Res 2004;10(16):5595–603.
[22] Raychaudhuri B, Han Y, Lu T, Vogelbaum MA. Aberrant constitutive activation of nuclear factor kappaB in glioblastoma multiforme drives invasive phenotype. J Neurooncol 2007;85(1):39–47.
[23] Brown RE, Law A. Morphoproteomic demonstration of constitutive nuclear factor-kappaB activation in glioblastoma multiforme with genomic correlates and therapeutic implications. Ann Clin Lab Sci 2006;36(4):421–6.
[24] da Frota Jr ML, Braganhol E, Canedo AD, Klamt F, Apel MA, Mothes B, et al. Brazilian marine sponge Polymastia janeirensis induces apoptotic cell death in human U138MG glioma cell line, but not in a normal cell culture. Invest New Drugs 2009;27(1):13–20.
[25] Braganhol E, Zamin LL, Cañedo AD, Horn F, Tamajusuku AS, Wink MR, et al. Antiproliferative effect of quercetin in the human U138MG glioma cell line. Anticancer Drugs 2006;17(6):663–71.
[26] Zanotto-Filho A, Gelain DP, Schröder R, Souza LF, Pasquali MA, Klamt F, et al. The NFkappaB-mediated control of RS and JNK signaling in vitamin A-treated cells: duration of JNK–AP-1 pathway activation may determine cell death or proliferation. Biochem Pharmacol 2009;77:1291–301.
[27] Bharti AC, Donato N, Singh S, Aggarwal BB. Curcumin (diferuloylmethane) down-regulates the constitutive activation of nuclear factor-kappa B and IkappaBalpha kinase in human multiple myeloma cells, leading to suppression of proliferation and induction of apoptosis. Blood 2003;101(3):1053–62.
[28] Klamt F, Shacter E. Taurine chloramine, an oxidant derived from neutrophils, induces apoptosis in human B lymphoma cells through mitochondrial damage. J Biol Chem 2005;280:21346–52.
[29] Hirose Y, Berger MS, Pieper RO. p53 affects both the duration of G2/M arrest and the fate of temozolomide-treated human glioblastoma cells. Cancer Res 2001;61:1957–63.
[30] Kucharczak J, Simmons MJ, Fan Y, Gélinas C. To be, or not to be: NF-kappaB is the answer: role of Rel/NF-kappaB in the regulation of apoptosis. Oncogene 2003;22(56):8961–82.
[31] Kim HJ, Hawke N, Baldwin AS. NF-kappaB and IKK as therapeutic targets in cancer. Cell Death Differ 2006;13(5):738–47.
[32] von Mering C, Jensen LJ, Snel B, Hooper SD, Krupp M, Foglierini M, et al. STRING: known and predicted protein–protein associations, integrated and transferred across organisms. Nucleic Acids Res 2005;33:433–7.
[33] Wain HM, Lush MJ, Ducluzeau F, Khodiyar VK, Povey S. Genew: the Human Gene Nomenclature Database, 2004 updates. Nucleic Acids Res 2004;32:255–7.
[34] Birney E, Andrews D, Caccamo M, Chen Y, Clarke L, Coates G, et al. Ensembl 2006. Nucleic Acids Res 2006;34:556–61.
[35] Hooper SD, Bork P. Medusa: a simple tool for interaction graph analysis. Bioinformatics 2005;21:4432–3.
[36] Castro MAA, Rybarczyk Filho JL, Dalmolin RJS, Sinigaglia M, Moreira JCF, Mombach JCM, et al. ViaComplex: software for landscape analysis of gene expression networks in genomic context. Bioinformatics 2009;25(11):1468–9.
[37] Park S, Hatanpaa KJ, Xie Y, Mickey BE, Madden CJ, Raisanen JM, et al. The receptor interacting protein 1 inhibits p53 induction through NF-kappaB activation and confers a worse prognosis in glioblastoma. Cancer Res 2009;69(7):2809–16.
[38] Park S, Zhao D, Hatanpaa KJ, Mickey BE, Saha D, Boothman DA, et al. RIP1 activates PI3K–Akt via a dual mechanism involving NF-kappaB-mediated inhibition of the mTOR–S6K–IRS1 negative feedback loop and down-regulation of PTEN. Cancer Res 2009;69(10):4107–11.
[39] Wang H, Wang H, Zhang W, Huang HJ, Liao WS, Fuller GN. Analysis of the activation status of Akt, NFkappaB, and Stat3 in human diffuse gliomas. Lab Invest 2004;84(8):941–51.
[40] Bredel M, Bredel C, Juric D, Duran GE, Yu RX, Harsh GR, et al. Tumor necrosis factor-alpha-induced protein 3 as a putative regulator of nuclear factor-kappaB-mediated resistance to O^6-alkylating agents in human glioblastomas. J Clin Oncol 2006;24(2):274–87.
[41] Kapoor GS, Zhan Y, Johnson GR, O'Rourke DM. Distinct domains in the SHP-2 phosphatase differentially regulate epidermal growth factor receptor/NF-kappaB activation through Gab1 in glioblastoma cells. Mol Cell Biol 2004;24(2):823–36.
[42] Sethi G, Ahn KS, Chaturvedi MM, Aggarwal BB. Epidermal growth factor (EGF) activates nuclear factor-kappaB through IkappaBalpha kinase-independent but EGF receptor-kinase dependent tyrosine 42 phosphorylation of Ikappa-Balpha. Oncogene 2007;26(52):7324–32.
[43] Gao X, Deeb D, Jiang H, Liu Y, Dulchavsky SA, Gautam SC. Synthetic triterpenoids inhibit growth and induce apoptosis in human glioblastoma and neuroblastoma cells through inhibition of prosurvival Akt, NF-kappaB and Notch1 signaling. J Neurooncol 2007;84(2):147–57.
[44] Kotliarova S, Pastorino S, Kovell LC, Kotliarov Y, Song H, Zhang W, et al. Glycogen synthase kinase-3 inhibition induces glioma cell death through c-MYC, nuclear factor-kappaB, and glucose regulation. Cancer Res 2008;68(16):6643–51.
[45] Sharma V, Tewari R, Sk UH, Joseph C, Sen E. Ebselen sensitizes glioblastoma cells to Tumor Necrosis Factor (TNFalpha)-induced apoptosis through two distinct pathways involving NF-kappaB downregulation and Fas-mediated formation of death inducing signaling complex. Int J Cancer 2008;123(9):2204–12.
[46] Kuwayama K, Matsuzaki K, Mizobuchi Y, Mure H, Kitazato KT, Kageji T, et al. Promyelocytic leukemia protein induces apoptosis due to caspase-8 activation via the repression of NFkappaB activation in glioblastoma. Neuro Oncol 2009;11(2):132–41.
[47] Carapancea M, Alexandru O, Fetea AS, Dragutescu L, Castro J, Georgescu A, et al. Growth factor receptors signaling in glioblastoma cells: therapeutic implications. Neurooncology 2009;92(2):137–47.
[48] Jiang Z, Zheng X, Rich KM. Down-regulation of Bcl-2 and Bcl-xL expression with bispecific antisense treatment in glioblastoma cell lines induce cell death. J Neurochem 2003;84:273–81.
[49] Zhao S, Tsuchida T, Kawakami K, Shi C, Kawamoto K. Effect of As_2O_3 on cell cycle progression and cyclins D1 and B1 expression in two glioblastoma cell lines differing in p53 status. Int J Oncol 2002;21(1):49–55.
[50] Haga N, Fujita N, Tsuruo T. Involvement of mitochondrial aggregation in arsenic trioxide (As_2O_3)-induced apoptosis in human glioblastoma cells. Cancer Sci 2005;96(11):825–33.
[51] Chiu TL, Su CC. Curcumin inhibits proliferation and migration by increasing the Bax to Bcl-2 ratio and decreasing NF-kappaB p65 expression in breast cancer MDA-MB-231 cells. Int J Mol Med 2009;23(4):469–75.
[52] Hayashi S, Sakurai H, Hayashi A, Tanaka Y, Hatashita M, Shioura H. Inhibition of NF-kappaB by combination therapy with parthenolide and hyperthermia and kinetics of apoptosis induction and cell cycle arrest in human lung adenocarcinoma cells. Int J Mol Med 2010;25(1):81–7.
[53] Sidransky D, Mikkelsen T, Schwechheimer K, Rosenblum ML, Cavanee W, Vogelstein B. Clonal expansion of p53 mutant cells is associated with brain tumour progression. Nature 1992;355:846–7.
[54] Lowe SW, Bodis S, McClatchey A, Remington L, Ruley HE, Fisher DE, et al. p53 status and the efficacy of cancer therapy in vivo. Science 1994;266:807–10.
[55] Lowe SW, Ruley HE, Jacks T, Housman DE. p53-dependent apoptosis modulates the cytotoxicity of anticancer agents. Cell 1993;74:957–67.
[56] Igney FH, Krammer PH. Death and anti-death: tumour resistance to apoptosis. Nat Rev Cancer 2002;2:277–88.
[57] Pierce JW, Schoenleber R, Jesmok G, Best J, Moore SA, Collins T, et al. Novel inhibitors of cytokine-induced IκBα phosphorylation and endothelial cell adhesion molecule expression show anti-inflammatory effects in vivo. J Biol Chem 1997;272:21096–103.
[58] Kwok BH, Koh B, Ndubuisi MI, Elofsson M, Crews CM. The anti-inflammatory natural product parthenolide from the medicinal herb Feverfew directly binds to and inhibits IκB kinase. Chem Biol 2001;8:759–66.
[59] Hehner SP, Hofmann TG, Droge W, Schmitz ML. The antiinflammatory sesquiterpene lactone parthenolide inhibits NF-κB by targeting the IκB kinase complex. J Immunol 1999;163:5617–23.
[60] Han SS, Kim K, Hahm ER, Park CH, Kimler BF, Lee SJ, et al. Arsenic trioxide represses constitutive activation of NF-kappaB and COX-2 expression in human acute myeloid leukemia, HL-60. J Cell Biochem 2005;94:695–7.
[61] Kasinski AL, Du Y, Thomas SL, Zhao J, Sun SY, Khuri FR, et al. Inhibition of IkappaB kinase–nuclear factor-kappaB signaling pathway by 3,5-bis(2-flurobenzylidene)piperidin-4-one (EF24), a novel monoketone analog of curcumin. Mol Pharmacol 2008;74:654–61.
[62] Santel T, Pflug G, Hemdan NY, Schäfer A, Hollenbach M, Buchold M, et al. Curcumin inhibits glyoxalase 1: a possible link to its anti-inflammatory and anti-tumor activity. PLoS ONE 2008;3(10):e3508.
[63] Weaver KD, Yeyeodu S, Cusack Jr JC, Baldwin Jr AS, Ewend MG. Potentiation of chemotherapeutic agents following antagonism of nuclear factor kappa B in human gliomas. J Neurooncol 2003;61:187–96.
[64] Pucer A, Castino R, Mirković B, Falnoga I, Slejkovec Z, Isidoro C, et al. Differential role of cathepsins B and L in autophagy-associated cell death induced by arsenic trioxide in U87 human glioblastoma cells. Biol Chem 2010;391(5):519–31.
[65] Perry MC, Demeule M, Régina A, Moumdjian R, Béliveau R. Curcumin inhibits tumor growth and angiogenesis in glioblastoma xenografts. Mol Nutr Food Res 2010;54(8):1192–201.
[66] Karmakar S, Banik NL, Ray SK. Curcumin suppressed anti-apoptotic signals and activated cysteine proteases for apoptosis in human malignant glioblastoma U87MG cells. Neurochem Res 2007;32(12):2103–13.
[67] Liu E, Wu J, Cao W, Zhang J, Liu W, Jiang X, et al. Curcumin induces G2/M cell cycle arrest in a p53-dependent manner and upregulates ING4 expression in human glioma. J Neurooncol 2007;85(3):263–70.
[68] Anderson KN, Bejcek BE. Parthenolide induces apoptosis in glioblastomas without affecting NF-kappaB. J Pharmacol Sci 2008;106(2):318–20.
[69] Wagenknecht B, Hermisson M, Groscurth P, Liston P, Krammer PH, Weller M. Proteasome inhibitor-induced apoptosis of glioma cells involves the processing of multiple caspases and cytochrome c release. J Neurochem 2000;75(6):2288–97.
[70] Wagenknecht B, Hermisson M, Eitel K, Weller M. Proteasome inhibitors induce p53/p21-independent apoptosis in human glioma cells. Cell Physiol Biochem 1999;9(3):117–25.

Available online at www.sciencedirect.com

SciVerse ScienceDirect

Journal of Nutritional Biochemistry 23 (2012) 591–601

Journal of Nutritional Biochemistry

The curry spice curcumin selectively inhibits cancer cells growth *in vitro* and in preclinical model of glioblastoma☆

Alfeu Zanotto-Filho[a,*], Elizandra Braganhol[b], Maria Isabel Edelweiss[c], Guilherme A. Behr[a], Rafael Zanin[b], Rafael Schröder[a], André Simões-Pires[a], Ana Maria Oliveira Battastini[b], José Cláudio Fonseca Moreira[a]

[a]*Centro de Estudos em Estresse Oxidativo, Departamento de Bioquímica, Universidade Federal do Rio Grande do Sul (UFRGS), Porto Alegre, Rio Grande do Sul, Brasil*
[b]*Laboratório de Enzimologia, Departamento de Bioquímica, Universidade Federal do Rio Grande do Sul (UFRGS), Porto Alegre, Rio Grande do Sul, Brasil*
[c]*Laboratório de Patologia, Hospital de Clínicas de Porto Alegre (HCPA), Porto Alegre, Rio Grande do Sul, Brasil*

Received 14 December 2010; received in revised form 30 January 2011; accepted 24 February 2011

Abstract

Previous studies suggested that curcumin is a potential agent against glioblastomas (GBMs). However, the *in vivo* efficacy of curcumin in gliomas remains not established. In this work, we examined the mechanisms underlying apoptosis, selectivity, efficacy and safety of curcumin from *in vitro* (U138MG, U87, U373 and C6 cell lines) and *in vivo* (C6 implants) models of GBM. *In vitro*, curcumin markedly inhibited proliferation and migration and induced cell death in liquid and soft agar models of GBM growth. Curcumin effects occurred irrespective of the p53 and PTEN mutational status of the cells. Interestingly, curcumin did not affect viability of primary astrocytes, suggesting that curcumin selectivity targeted transformed cells. In U138MG and C6 cells, curcumin decreased the constitutive activation of PI3K/Akt and NFkappaB survival pathways, down-regulated the antiapoptotic NFkappaB-regulated protein bcl-xl and induced mitochondrial dysfunction as a prelude to apoptosis. Cells developed an early G2/M cell cycle arrest followed by sub-G1 apoptosis and apoptotic bodies formation. Caspase-3 activation occurred in the p53-normal cell type C6, but not in the p53-mutant U138MG. Besides its apoptotic effect, curcumin also synergized with the chemotherapeutics cisplatin and doxorubicin to enhance GBM cells death. In C6-implanted rats, intraperitoneal curcumin (50 mg kg^{-1} d^{-1}) decreased brain tumors in 9/11 (81.8%) animals against 0/11 (0%) in the vehicle-treated group. Importantly, no evidence of tissue (transaminases, creatinine and alkaline phosphatase), metabolic (cholesterol and glucose), oxidative or hematological toxicity was observed. In summary, data presented here suggest curcumin as a potential agent for therapy of GBMs.

Keywords: Curcumin; Glioblastoma; Apoptosis; *In vitro*; Preclinical

1. Introduction

Glioblastoma (GBM) is an aggressive, invasive and difficult to treat primary brain tumor. Standard therapy includes surgical resection, external beam radiation and chemotherapy, with no known curative therapy [1,2]. A number of deregulated signaling cascades have been described in GBMs, including the nuclear factor kappa-B (NFkappaB), the phosphoinositide-3-kinase (PI3K/Akt) pathway and the Ras/MEK/ERK mitogen-activated protein kinase pathway. Deregulation of these pathways is driven by mutation, amplification or overexpression of multiple genes such as PTEN, EGFr, PDGFR-a, p53 and mTOR [3–5]. Understanding these deregulated pathways has provided the basis for designing molecular targeted therapies as well as new combination therapies and drug delivery systems [6–8]. Despite the aforementioned findings, median survival in GBM has remained approximately 1 year for decades [1,2]. Therefore, validation of new antiglioma drugs may offer new therapeutic opportunities to patients.

Curcumin (diferuloylmethane), a naturally occurring polyphenol derived from the root of the rhizome *Curcuma longa*, possesses anti-inflammatory, antioxidant and anticancer properties by inhibition of signaling pathways such as NFkappaB, PI3K/Akt and activator protein-1 (AP-1) [9]. Recently, curcumin entered into phase I clinical trials for the treatment of some high-risk cancers [10]. In GBMs, an emerging *in-vitro*-based literature [11–16] suggests that curcumin exerts antiglioma effects through enhancement of TRAIL-induced apoptosis [11], inhibition of metalloproteinase-9 expression [12,14] and induction of apoptosis in T98G and U87MG cell lines [13,15,16]. However, the apoptotic mechanisms, selectivity to transformed cells and principally the *in vivo* efficacy of curcumin in GBMs remain to be better studied. In this work, we examined the mechanisms underlying curcumin anti-GBM effects based on *in vitro* (C6, U138MG, U87 and U373 cell lines) and *in vivo* (C6 implants in rat brain) models of the disease. *In vitro*, we evaluated curcumin effects on proliferation, apoptosis and migration as well as antagonism with classical GBM survival pathways (PI3K/Akt and NFkappaB), selectivity to cancer

☆ Conflict of interest statement: The authors report that there are no conflicts of interest.

* Corresponding author. Depto. Bioquímica (ICBS-UFRGS), Rua Ramiro Barcelos, 2600/Anexo, CEP 90035-003, Porto Alegre, Rio Grande do Sul, Brazil. Tel.: +55 51 3308 5578; fax: +55 51 3308 5535.

E-mail address: alfeuzanotto@hotmail.com (A. Zanotto-Filho).

0955-2863/$ - see front matter © 2012 Elsevier Inc. All rights reserved.
doi:10.1016/j.jnutbio.2011.02.015

cells and adjuvant potential. *In vivo*, we tested the hypothesis that curcumin may decrease glioma growth without inducing toxicity to healthy tissues.

2. Materials and methods

2.1. Reagents

Curcumin, propidium iodide (PI), Hepes, CHAPS, dithiothreitol, EDTA, trypsin, 3-(4,5-dimethyl)-2,5-diphenyl tetrazolium bromide (MTT), Nonidet-P40, spermin tetrahydrochloride, RNAse A and culture analytical-grade reagents were purchased from Sigma Chemical Co. (St. Louis, MO, USA). Anti-lamin B (C-20) and anti-p65 NFkappaB antibodies were from Santa Cruz Biotechnologies; anti-β-actin, anti-phospho-Akt(ser^{473}) , anti-Akt and anti-bcl-xl were from Cell Signaling Technology. Parthenolide (PTL) and LY294002 were from Biomol International (Plymouth Meeting, PA, USA). Electrophoresis and immunoblotting reagents were from Bio-Rad Laboratories (Hercules, CA, USA). Kits for biochemical analysis were acquired from Labtest Diagnostica (MG, Brazil).

2.2. Cell cultures

The rat (C6) and human (U138MG, U87 and U373) malignant GBM cell lines were obtained from American Type Culture Collection (Rockville, MD, USA). The cells were grown and maintained in low-glucose Dulbecco's modified Eagle's medium (DMEM; Gibco BRL, Carlsbad, CA, USA) containing 0.1% Fungizone and 100 U/L gentamicin and supplemented with 10% fetal bovine serum (FBS). Cells were kept at 37°C in a humidified atmosphere with 5% CO_2. Primary astrocyte cultures were prepared as previously described [17]. Briefly, cortex of newborn Wistar rats (1–2 days old) were removed and dissociated mechanically in a Ca^{+2} and Mg^{+2} free balanced salt solution, pH 7.4, (137 mmol/L NaCl, 5.36 mmol/L KCl, 0.27 mmol/L Na_2HPO4, 1.1 mmol/L KH_2PO4, 6.1 mmol/L glucose). After centrifugation at 1000 rpm for 5 min, the pellet was resuspended in DMEM supplemented with 10% FBS. The cells (2×10^5) were plated in poly-L-lysine-coated 48-well plates. After 4-h plating, plates were gently shaken and phosphate-buffered saline (PBS)-washed, and medium was changed to remove neuron and microglia contaminants. Cultures were allowed to grow to confluence by 20–25 days. Medium was replaced every 4 days.

2.3. MTT and lactate dehydrogenase assays

Dehydrogenases-dependent MTT reduction (MTT assay) and lactate dehydrogenase release into culture medium [lactate dehydrogenase (LDH) assay] were used as an estimative of cell viability [18]. Cells were plated in 96-well plates (10^4/well) and treated at 60%–70% confluence. At the end of incubations, MTT and LDH assays were performed. Lactate dehydrogenase activity in the culture medium was determined in agreement with manufacturer instructions (CytoTox 96-NonRadioactive Cytotoxicity Assay, Promega). Cell morphology was evaluated by light microscopy (Nikon Eclipse TE 300).

2.4. PI incorporation and staining of chromatin

For determination of PI uptake in cells with losses in membrane integrity, treated cells were incubated with 2 μg/ml PI in complete medium for 1 h. Propidium iodide fluorescence was excited at 515–560 nm using an inverted microscope (Nikon Eclipse TE 300) fitted with a standard rhodamine filter. Representative microphotographs (at least five per well) were collected [19]. For detection of the morphological alterations in chromatin (condensation and fragmentation) and apoptotic bodies formation, cells were fixed in methanol/acetone (1:1) for 5 min and washed with PBS (three times). Afterward, chromatin was stained with PI (0.5 μg/ml, 10 min) followed by fluorescent microscopy (Nikon Eclipse TE 300).

2.5. Cell cycle analysis

For cell cycle analysis, cells were trypsinized, centrifuged and resuspended in a lysis buffer containing 3.5 mmol/L trisodium citrate, 0.1% vol/vol Nonidet P-40, 0.5 mmol/L Tris-HCl, 1.2 mg/ml spermine tetrahydrochloride, 5 μg/ml RNAse, 5 mmol/L EDTA and 1 μg/ml PI, pH 7.6. Afterward, cells were incubated for at least 10 min on ice for cell lysis. DNA content was determined by flow cytometry. Ten thousand events were counted per sample. FACS analyses were performed in the CellQuest Pro Software (BD Biosciences, CA, USA) [18].

2.6. Caspase-3 activity

Caspase-3 activity was assessed in agreement with CASP3F Fluorometric kit (Sigma, Saint Louis, MI, USA). Treated cells were harvested and incubated in a lysis buffer (50 mmol/L Hepes, 5 mmol/L CHAPS and 5 mmol/L dithiothreitol, pH 7.4) for 20 min in ice. Afterward, extracts were clarified by centrifugation at 13,000*g* (15 min, 4°C). Supernatants were collected, and proteins were measured by Bradford method. For assays, 150 μg proteins were mixed with 200 μl of the assay buffer (20 mmol/L Hepes, 0.1% CHAPS, 5 mmol/L dithiothreitol, 2 mmol/L EDTA, pH 7.4) plus 20 μM Ac-DEVD-AMC (Acetyl-Asp-Glu-Val-Asp-7-amido-4-methylcoumarin), a caspase-3-specific substrate. Caspase-3-mediated substrate cleavage was monitored during 1 h (37°C) in a fluorometric reader (excitation 360 nm/emission 460 nm) [18].

2.7. Cellular fractionation

For nuclear extracts preparation, cells (~5×10^6, 70%–80% confluence) were washed with cold PBS and suspended in 0.4-ml hypotonic lysis buffer [10 mmol/L HEPES (pH 7.9), 1.5 mmol/L $MgCl_2$, 10 mmol/L KCl, 0.5 mmol/L phenylmethylsulfonyl fluoride, 0.5 mmol/L dithiothreitol plus protease inhibitor cocktail (Roche)] for 15 min. Cells were then lysed with 12.5 μl 10% Nonidet P-40. The homogenate was centrifuged (13,000*g*, 30 s), and supernatants containing the cytoplasmic extracts were stored at −80°C. The nuclear pellet was resuspended in 100-μl ice-cold hypertonic extraction buffer [10 mmol/L HEPES (pH 7.9), 0.42 M NaCl, 1.5 mmol/L $MgCl_2$, 10 mmol/L KCl, 0.5 mmol/L phenylmethylsulfonyl fluoride, 1 mmol/L dithiothreitol plus protease inhibitors]. After 40 min of intermittent mixing, extracts were centrifuged (13,000*g*, 10 min, 4°C), and supernatants containing nuclear proteins were secured. The protein content was measured by the Bradford method [18–20].

2.8. NFκB-p65 enzyme-linked immunosorbent assay for determination of NFκB activity

A total of 10 μg of nuclear extracts was used to determine the NFκB DNA-binding activity [NFκB p65 enzyme-linked immunosorbent assay (ELISA) kit, Stressgen/Assays designs] per manufacturer's protocols. This ELISA-based chemiluminescent detection method rapidly detects activated NFκB complex binding (p65 detection) to a plate-adhered NFκB consensus oligonucleotide sequence. Kit-provided nuclear extracts prepared from TNF-stimulated Hela cells were used as a positive control for NFκB activation. To demonstrate assay specificity, a 50-fold excess of an NFκB consensus oligonucleotide was used as competitor to block NFκB binding. In addition, a mutated consensus NFκB oligonucleotide (which does not bind NFκB) is provided for determination of binding reactions' specificity [21].

2.9. Western blotting

Proteins (20 μg) were separated by sodium dodecyl sulfate polyacrylamide gel electrophoresis on 10% (wt/vol) acrylamide and 0.275% (wt/vol) bisacrylamide gels and electrotransferred onto nitrocellulose membranes. Membranes were incubated in TBS-T [20 mmol/L Tris–HCl, pH 7.5, 137 mmol/L NaCl, 0.05% (vol/vol) Tween 20] containing 1% (wt/vol) nonfat milk powder for 1 h at room temperature. Subsequently, the membranes were incubated for 12 h with the appropriate primary antibody (dilution range 1:500–1:1000), rinsed with TBS-T and exposed to horseradish-peroxidase-linked anti-IgG antibodies for 2 h at room temperature. Chemiluminescent bands were detected using X-ray films, and densitometry analyses were performed using Image-J software.

2.10. Mitochondria membrane potential (JC-1 assay)

For determination of the mitochondrial membrane potential (MMP), treated cells (5×10^5) were incubated for 30 min at 37°C with the lipophilic cationic probe JC-1 (5,5′,6,6′-tetrachloro-1,1′,3,3′ tetraethylbenzimidazolcarbocyanine iodide, 2 μg/ml). Afterward, JC-1-loaded cells were centrifuged and washed once with PBS. Cells were transferred to a 96-well plate and assayed in a fluorescence plate reader with the following settings: excitation at 485 nm, emission at 540 and 590 nm and cutoff at 530 nm (SpectraMax M2, Molecular Devices, USA). $\Delta\Psi m$ was calculated using the ratio of 590 nm (J-aggregates)/540 nm (monomeric form) [22].

2.11. Clonogenic potential

Exponentially growing cells (1×10^6) were plated in petri plates overnight and then incubated for 36 h with either vehicle or curcumin. After treatments, the medium containing curcumin was replaced by a curcumin-free medium, and remaining cells were maintained for additional 24 h to growth. Survival cells were gently washed and

Table 1
IC_{50} levels of curcumin in a panel of GBMs and astrocytes

Cell lines	Curcumin IC_{50} (μM)
U138MG	29±5[a]
C6	25±4[a]
U87	19±7[a]
U373	21±3[a]
Astrocytes	135±12

Legend: Cells (U138MG, U87, C6, U373 and astrocytes) were treated for 36 h with different concentrations of curcumin (1–150 μM), and cell viability was determined by MTT assay. Experiments were repeated three times (n=3) in triplicate, and data were expressed in mean±S.D.

[a] Different from astrocytic IC_{50} value (P<.05, t test).

Table 2
LDH release and cellular viability in curcumin-treated C6 and astrocytes

Curcumin (μM)	C6 cells		Astrocytes	
	Viability (MTT, %)	LDH (%)	Viability (MTT, %)	LDH (%)
0	100±3	100±14	100±9	100±11
7.5	90±2[a]	113±21	101±3	102±13
15	78±5[b]	120±36	103±4	98±19
25	67±2[b]	276±92[a]	102±17	89±9
50	28±3[b]	907±105[b]	108±13	121±13
100	10±5[b]	1251±57[b]	110±15	115±33
120	3±1[b]	1290±154[a]	81±9[a]	169±14[a]

Legend: Cells were treated with curcumin for 36 h; medium was collected for LDH activity determination, and cells were used for viability estimation by MTT assay. Experiments were repeated three times (n=3) in triplicate, and data were expressed in mean±S.D.
[a] Different from untreated cells.
[b] Different from untreated cells and from the immediately lower curcumin concentration (P<.05, ANOVA).

trypsinized, and viability was assessed by trypan blue staining. Viable cells (10^4 cells) were replated in six-well plates and maintained for additional 6 days in complete culture medium. Cell growth was estimated by colony counting followed by MTT assay [21]. The percentage of colony forming efficiency was calculated in relation to values of untreated cells.

2.12. Soft agar colony assay

Cells (1×10^5) were resuspended in 2 ml DMEM supplemented with 15% FBS and mixed with 1 ml of 1.6% agarose (final conditions: 0.53% agarose and 10% FBS) at 37°C. Cell suspensions were placed on top of a base layer comprised of 2 ml of DMEM with 10% FBS and 0.8% agarose in each well of a six-well plate. Cells were then covered with 2 ml of complete media, and after 3 days, a new medium containing curcumin was added. Medium containing treatments or vehicle was replaced every 72 h. At the end of 9 days, MTT (1 mg/ml) was added to the cultures, and the number of colonies was scored using a microscope [21].

2.13. Migration assay

The monolayer of confluent C6 and U138MG cells was pretreated for 12 h with curcumin and subsequently scratched with a 200 μl pipette tip to create a wound. Cells were washed twice with PBS to remove floating cells and then incubated in DMEM with 2% FBS plus treatments. Cells were incubated for additional 16–18 h, and the rate of wound closure was investigated through photographs (100×) taken at final time points. Migration of treated cells was compared to untreated cells and expressed as percentage [23].

2.14. Proliferation assay

For proliferation assay, 24-well-plated cells were treated at 50%–60% confluence during 72 h (chronic exposure) with curcumin inhibitors. After treatments, cells were fixed in ethanol:acetone (1:1) for 5 min followed by PBS washing (three times). Fixed cells were stained with trypan blue 0.4% (Sigma, CA, USA) for 30 min and washed three times with PBS. Trypan-stained cells were lysed with 1 N NaOH for 5 min. Afterward, equal volume of distillated water was added, and trypan blue color was estimated in spectrophotometer at 595 nm [24]. Sample absorbance was compared to controls and expressed as percentage of untreated cells.

2.15. Preclinical study: glioma in vivo experiments

2.15.1. Implantation

In vivo model of rat C6 glioma was carried out as previously described by Takano et al. [25] and validated in our laboratory [26,27]. Exponentially growing C6 cells were trypsinized, washed once in DMEM, spun down and resuspended at 10^6 cells/3 μl DMEM. Cells were injected using a 5-μl Hamilton microsyringe coupled in the infusion pump (1 μl/min) at a depth of 6.0 mm into the right striatum (coordinates with regard to bregma: 0.5 mm posterior and 3.0 mm lateral) of adult male Wistar rats (8 weeks old, 220–260 g) previously anesthetized by intraperitoneal (ip) administration of

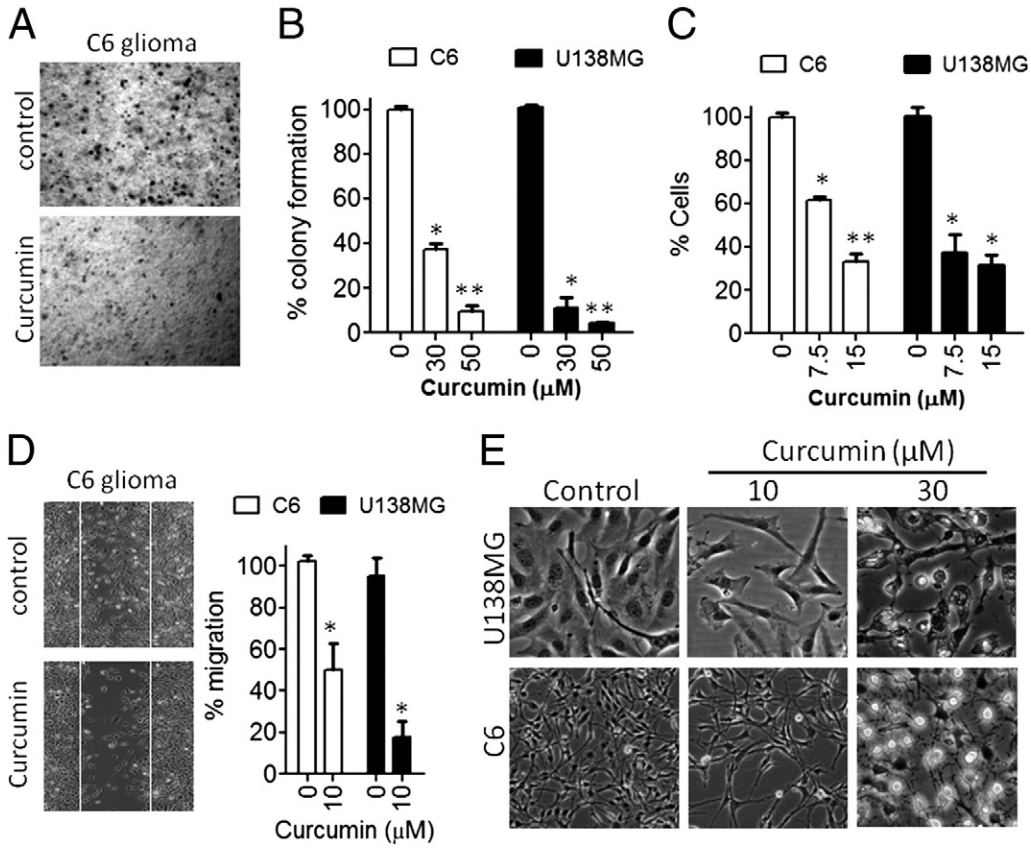

Fig. 1. Curcumin inhibits GBM cells growth. (A) Curcumin 30 μM inhibits the growth of C6 cells in soft agar. (B) Short-term incubation with curcumin reduces clonogenic potential of C6 and U138MG cells. (C) Effect of subtoxic concentrations of curcumin on proliferation of C6 and U138MG cell lines. Cells were treated for 72 h with 7.5 or 15 μM curcumin, fixed and stained with trypan blue for estimation of cell density. Cell morphology was monitored by light microscopy. *Different from untreated cells; **different from the immediately lower curcumin concentration, P<.05, ANOVA. (D) Subtoxic concentrations of curcumin (10 μM) decrease U138MG and C6 cells migration. *Different from untreated cells, P<.05, t test. (E) Representative microphotographs (20×) showing the effect of cytotoxic (30 μM) and subapoptotic (10 μM) concentrations of curcumin on morphology of U138MG and C6 cells. All experiments were repeated at least four times (n=4).

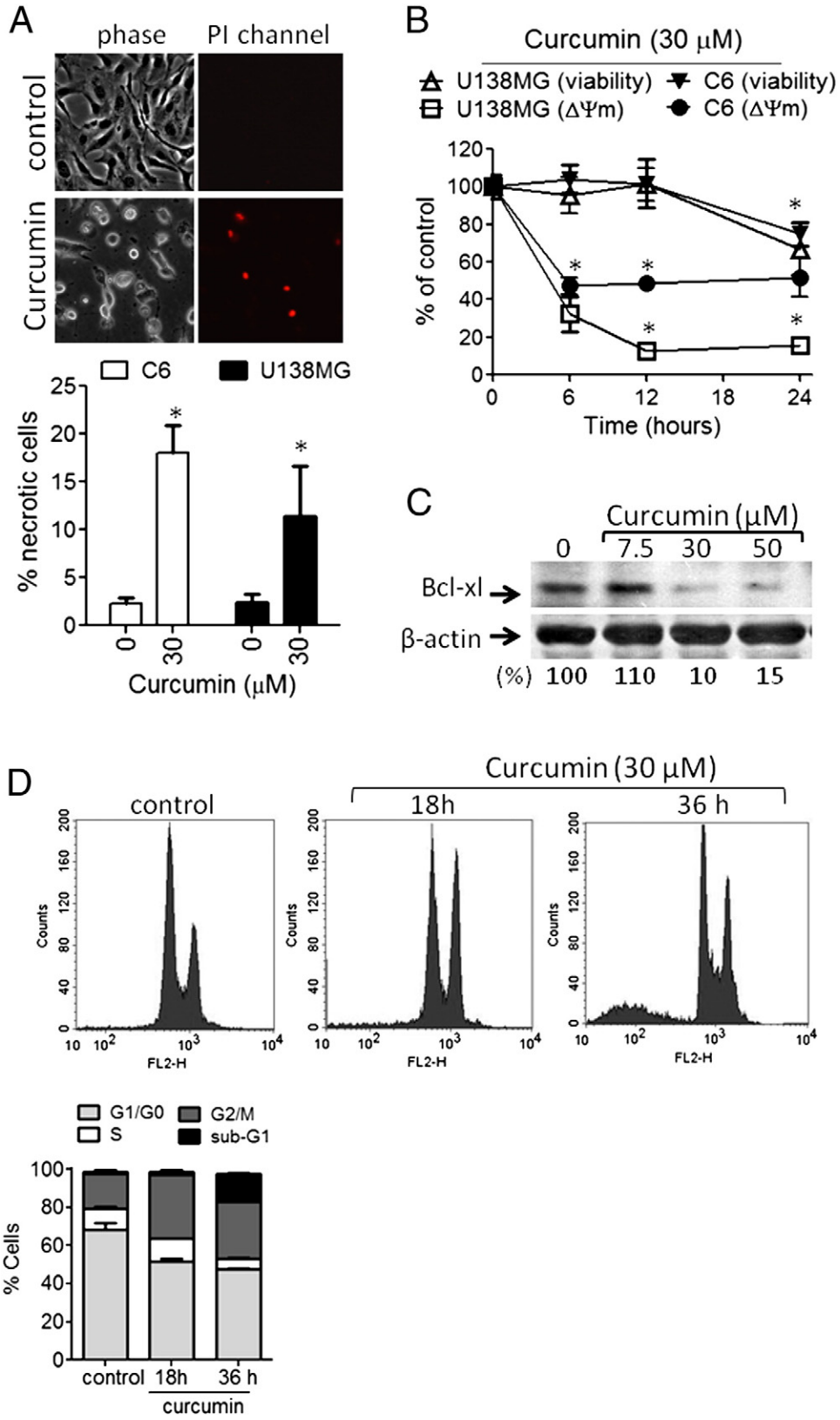

Fig. 2. Curcumin induces mitochondrial dysfunction and programmed cell death in GBMs. (A) Propidium iodide incorporation in U138MG cells. After 36-h treatment with 30 μM curcumin, cells were incubated with PI diluted in culture medium. Fluorescence and phase contrast microphotographs were taken (20×). The percentage of PI-stained cells was quantified. *Different from untreated cells, $P<.05$, t test. (B) Time course effect of curcumin on MMP was co-evaluated with PI incorporation for determination of cell membrane integrity. U138MG cells were treated for different times and trypsinized, and different aliquots were collected for JC-1 or PI incorporation assays. *Different from untreated cells, $P<.05$, t test. (C) Curcumin decreases bcl-xL protein immunocontent as assessed by Western blotting in total cell extracts of 12-h-treated U138MG cells. (D) Flow cytometry for determination of cell cycle distribution (sub-G1, G1/G0, S and G2/M) in untreated and 30 μM curcumin-treated (18–36 h) U138MG cells. All experiments were repeated at least three times ($n=3$).

ketamine/xylazine. The number of animals for 95% confidence was statistically calculated in agreement with our previously determined standard deviations (S) and means (μ) of tumor size for the *in vivo* model of glioma [26]. Data/legends: A=DMSO-treated rats (control); B=alkylation-agent-treated rats (control for antiglioma activity); statistical parameters: μ_A=73 mm^3; μ_B=27 mm^3; S_A=13 mm^3; S_B=37 mm^3; α=0.05, power=1−β=0.9; β=0.1; t_α=2.101; u_β=1,734; n_0=10. Formula: $n=((S_A)^2+(S_b)^2)/(\mu_A-\mu_b)^2\times(t_\alpha+u_\beta)^2$; n=11 rats/group. All procedures used in the present study followed the "Principles of Laboratory Animal Care" of the National Institutes of Health and were approved by the Ethical Committee of the Hospital de Clinicas de Porto Alegre.

2.15.2. Treatments

Ten days after glioma implantation, animals were divided into two groups (n=11 per group) as follows: (a) DMSO/vehicle-treated group and (b) curcumin-treated group (50 mg/kg/day curcumin solubilized in sterile DMSO). The formulations were administered ip for 10 consecutive days.

2.15.3. Analysis

After 20 days (10 days for glioma implantation+10 days for treatments), rats were anesthetized and decapitated. The brain was removed, sectioned and fixed with 10% paraformaldehyde. Cerebellum, liver and kidney were also removed and frozen at −80°C for biochemical analysis. Blood samples were collected for determination of glucose, total cholesterol, creatinine, alkaline phosphatase, alanine aminotransferase (ALT) and aspartate aminotransferase (AST) activity in serum, which were used as markers of metabolic and tissue toxicity. These experiments were performed in a LabMax 240 analyzer (Labtest Diagnostica, Brazil). Hematological parameters were evaluated in a Sysmex KX-21-N hematologic analyzer (Sysmex, Lille, France). The oxidative stress parameters TBARS (lipoperoxidation), protein sulfhydryl and carbonyl groups, catalase, superoxide dismutase and glutathione *S*-transferase (GST) activity were evaluated in cerebellum, liver and kidney in agreement with our previously described protocols [28].

For tumor volume quantification, three hematoxylin and eosin (H&E) coronal sections (2–3 μm thick, paraffin embedded) from each animal were analyzed. Images were captured using a digital camera connected to a microscope (Nikon Eclipse TE300), and the tumor area (mm^2) was determined using Image Tool Software. The total volume (mm^3) of the tumor was computed by the multiplication of the slice sections and by summing the segmented areas [26,27]. In animals with detectable tumor mass, histopathological parameters were evaluated by two expert pathologists.

2.16. Statistical analysis

The statistical significance among three or more groups was assessed by one-way analysis of variance (ANOVA) followed by Tukey's test. The statistical significance between DMSO-treated and curcumin-treated groups and other two-group analyses were carried out by means of unpaired Student's t test (Prism GraphPad Software, San Diego, CA, USA). For qualitative data (Table 4 experiments), Z-test for two proportions and Fisher's Exact Test were chosen. Significant differences among groups were calculated at P<.05.

3. Results

3.1. Curcumin inhibits proliferation and induces cell death in GBMs but not in astrocytes

First, we examined the effect of curcumin on viability of GBMs by treating a panel of GBM cell lines (C6, U138MG, U87, U373) with different concentrations of curcumin for 36 h. At the end of incubation, MTT assays were carried out. In parallel, primary astrocytes cultures were used as a nontransformed model of glial cells in order to test the selectivity of curcumin. Curcumin markedly decreased the viability of the four GBM cells lines (IC_{50} range=19–28 μM), whereas astrocytes were much less sensitive to curcumin treatment (IC_{50}=135 μM) as assessed by MTT (Table 1). Curcumin also caused a dose-dependent release of LDH into culture medium of GBMs, indicating losses in cell membrane integrity. Curcumin-induced LDH release was associated with decreases in cell viability as assessed by MTT (Table 2). In astrocytes, toxicity only was observed at high curcumin concentrations (120 μM). Taken together, these data suggest that the cytotoxic effects of curcumin selectively targeted GBMs (Table 2). For further experiments, we used ~IC_{50} concentrations of curcumin, and the C6 and U138MG cell lines since (a) they have different patterns of p53 mutations, (b) curcumin mechanisms were not determined in these cell lines and (c) C6 cells were used in *in vivo* experiments.

Curcumin-induced growth inhibition was independent on cell anchorage to extracellular matrix as evaluated by soft agar growth experiments (Fig. 1A). In addition, results from clonogenic survival assays showed that curcumin treatment (24 h) followed by 6-day washout significantly decreased the clonogenic proliferation in GBMs, suggesting that curcumin effects were prolonged and persisted after drug withdrawal (Fig. 1B). Significant morphological alterations and cell detachment were observed in 30 μM curcumin-treated cells (Fig. 1E). At low concentrations (≤15 μM), curcumin caused decreases in cell viability and cell density (Table 2 and Fig.

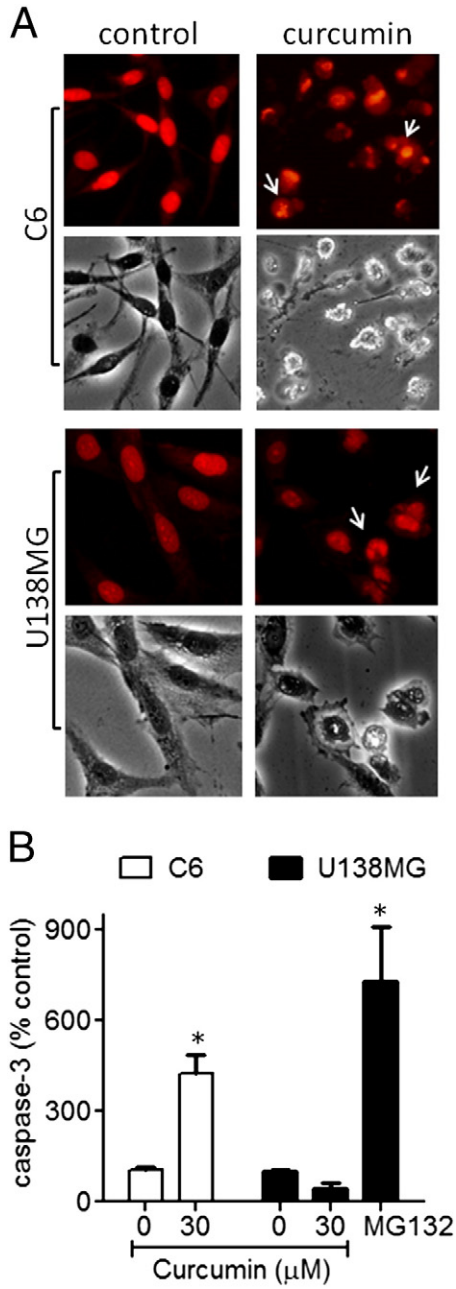

Fig. 3. Curcumin promotes chromatin condensation and modulates caspase-3 in GBMs. (A) Representative fluorescence and phase contrast microphotographs (40×) showing the effect of 30 μM curcumin (36-h treatment) on condensation of chromatin and formation of apoptotic bodies in C6 and U138MG cells. (B) Caspase-3 activity after 36-h treatment with 30 μM curcumin in C6 and U138MG. *Different from untreated cells, P<.05, t test, n=4.

1E), but induced neither LDH release nor alterations in cell morphology (Fig. 1E), indicating a cytostatic/antiproliferative effect of curcumin at noncytotoxic concentrations. Therefore, we decided to test whether a long-term exposure to subtoxic curcumin could decrease cell proliferation. Curcumin (7.5 and 15 μM) decreased cell proliferation by up to 73%±12% after 72-h exposure when compared

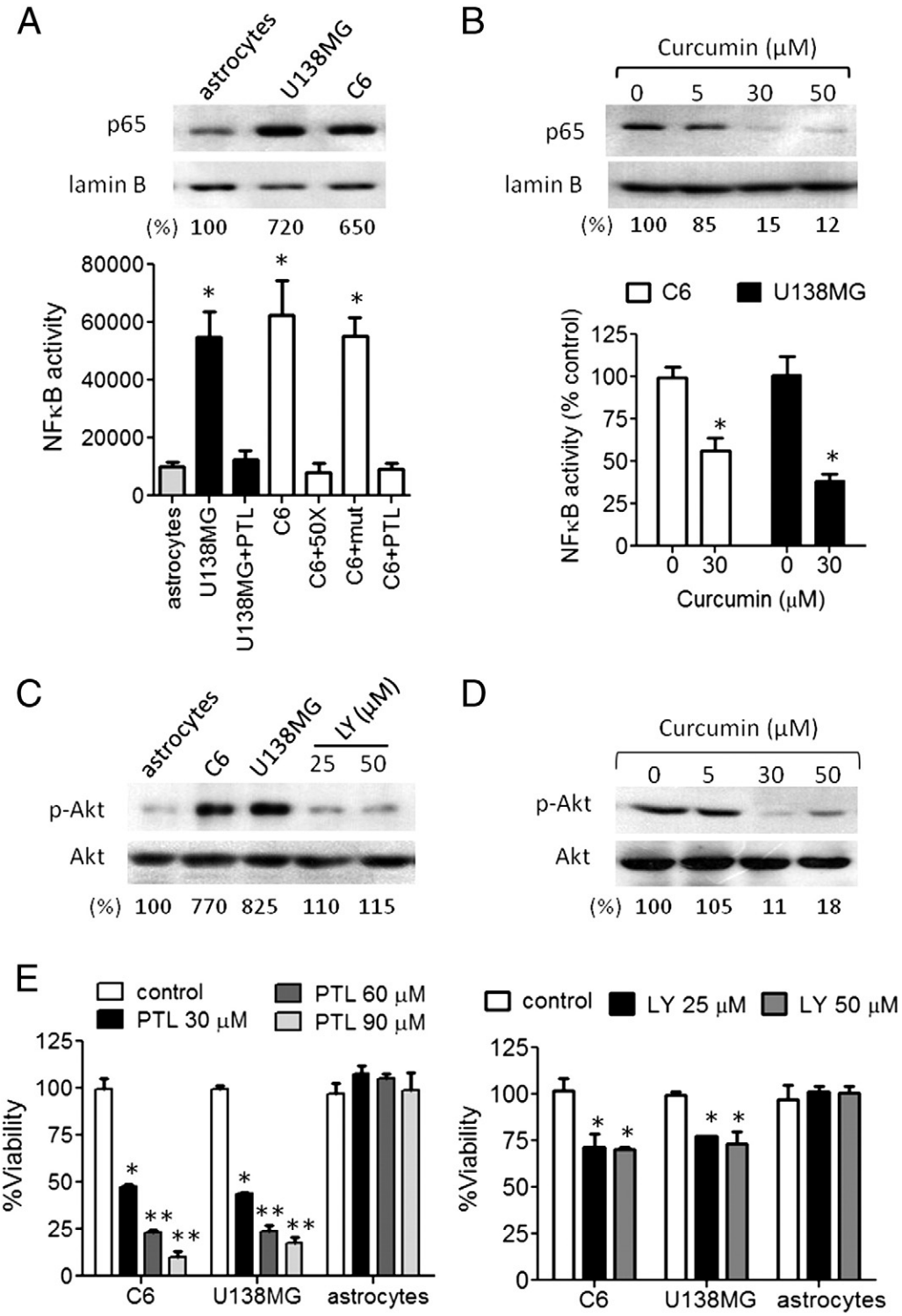

Fig. 4. Curcumin suppresses activation of NFkappaB and PI3K/Akt in GBMs. (A) Constitutive NFkappaB activation and nuclear levels of p65 in C6, U138MG and astrocytes. Cells were maintained in equal basal conditions (complete culture medium for 48 h), and nuclear extracts were isolated for detection of NFkappaB activity (ELISA kit) and p65 immunocontent (Western blotting). Lamin B was used as loading control for nuclear extracts. *Different from astrocytes, $P<.05$, ANOVA. (B) Curcumin inhibits NFkappaB DNA-binding activity and p65 translocation in GBM. The ELISA assays and Western blots were carried out in nuclear extracts isolated from 6-h-treated U138MG cells. [a]Different from untreated cells, $P<.05$, t test. (C) Constitutive PI3K/Akt pathway activation in C6, U138MG and astrocytes. Cells were maintained in basal conditions (above cited), and Western blotting for p-Akt and total-Akt forms was performed in total extracts. Beta-actin was used as loading control (not shown). (D) Curcumin inhibits Akt phosphorylation. U138MG cells were treated for 6 h with 5 to 60 μM curcumin followed by Western blotting for p-Akt protein detection. (E) The MTT assays showing the effect of different concentrations of PTL or LY294002 (LY) on viability of GBM cell lines and astrocytes. *Different from untreated cells; **different from untreated and from the immediately lower concentration of PTL or LY, $P<.05$, ANOVA, $n=3$.

Table 3
Curcumin synergizes with classical chemotherapy

Treatments	Viability (MTT, %)	
	U138MG	C6
Untreated	100±5.7	100±2.1
Cisplatin	63±6.0[a]	42±3.3[a]
Cisplatin+curcumin 10 μM	46±5.9[b]	29±2.4[b]
Cisplatin+curcumin 25 μM	30±3.2[b]	10±4.2[b]
Doxorubicin	66±2.0[a]	73±4.2[a]
Doxorubicin+curcumin 10 μM	48±3.3[b]	61±3.0[b]
Doxorubicin+curcumin 25 μM	36±4.6[b]	46±5.4[b]
Curcumin 10 μM	76±1.2[a]	88±5.1[a]
Curcumin 25 μM	55±5.0[a]	75±7.3[a]

Legend: U138MG and C6 cells lines were treated with different concentrations of curcumin, followed by exposure to cisplatin or doxorubicin for 48 h. Data were collected from three independent experiments (n=3) performed in triplicate.
[a] Different from untreated cells.
[b] Different from its respective cisplatin or doxorubicin monotreatment, P<.05, ANOVA.

to untreated cells (Fig. 1B). In addition, subtoxic curcumin (10 μM) also inhibited the migration of both C6 and U138MG cells as assessed by scratching assay (Fig. 1C).

3.2. Curcumin induces mitochondrial dysfunction, cell cycle arrest and apoptosis in GBMs

At the end of 36-h incubation, we observed significant morphological alterations in curcumin-treated cells, which were accompanied by PI uptake (Fig. 2A). However, PI uptake did not occur in all cells with changes in morphology, suggesting that morphological alterations preceded the losses in cell membrane permeability (Fig. 2A). These events suggest a programmed mechanism of cell death. Curcumin caused an early collapse in the MMP ($\Delta\Psi$m, Fig. 2B) and decreased the immunocontent of the cytoprotective mitochondrial protein bcl-xL (Fig. 2C). These events preceded curcumin-induced losses in plasmatic membrane integrity (PI incorporation assays, Fig. 2B). Curcumin-induced decreases in MMP and bcl-xl protein were clearly observed at 12-h treatment, whereas PI uptake only increased at later time points (24 h). By flow cytometry, we determined that curcumin caused cell arrest in the G2/M phase of the cell cycle at 18-h treatment, which cumulated in formation of a significant population of hypodiploid (sub-G1) cells at 36 h, indicating that G2/M arrest preceded apoptosis in curcumin-treated cells (Fig. 2D). Staining of chromatin with PI showed that curcumin induced chromatin condensation and formation of apoptotic bodies in GBMs after 36-h incubation (Fig. 3A). Activation of the executor caspase-3 was detectable in C6 cells but not in the p53-mutant U138MG (Fig. 3B). The proteasome inhibitor MG132 was used as a positive control for caspase-3 activation in order to confirm the noneffect of curcumin on caspase-3 in U138MG.

3.3. Curcumin inhibits PI3K/Akt and NFkappaB survival pathways in GBMs

NFkappaB and PI3K/Akt are considered as two important GBMs survival pathways [29,30]. NFkappaB was found up-regulated in the GBM cell lines (six- to sevenfold) compared to astrocytes as detected by ELISA assays for NFkappaB activity and Western blotting for nuclear p65 protein (Fig. 4A). Treatment with curcumin for 6 h decreased both NFkappaB activity and nuclear accumulation of p65 (Fig. 4B). Taking into account that curcumin also decreased the NFkappaB-regulated protein bcl-xl (Fig. 3B), these results indicate that curcumin inhibits NFkappaB signaling in GBMs. The ELISA assay specificity was confirmed by incubation of nuclear extracts with kit-provided 50× unlabeled oligonucleotides, which inhibited completely NFkappaB basal binding (C6+50× lane). In addition, mutant oligonucleotides did not alter NFkappaB activity, confirming the specificity of the binding reactions (C6+mut lane). The pharmacological NFkappaB inhibitor PTL was used as a control for NFkappaB inhibition (Fig. 4A); LPS was used as a control for NFkappaB activation (not shown).

PI3K/Akt pathway also was found up-regulated (seven- to eightfold increase) in C6 and U138MG cell lines compared to astrocytes (Fig. 4C). Curcumin inhibited about 80% the constitutive activation of the PI3K/Akt pathway as detected from levels of the phosphorylated forms of Akt, a surrogate to evaluate PI3K/Akt pathway activation in GBMs. Total forms of Akt were not altered, indicating that the protein was modulated in the posttranslational level (Fig. 4D). Controls for specific PI3K/Akt inhibition were performed by incubating cells with LY294002 (see Fig. 4C, LY lanes).

To evaluate/confirm whether NFkappaB and PI3K/Akt pathways, which were blocked by curcumin, play a role in survival of GBMs, we treated C6, U138MG and astrocytes with inhibitors of NFkappaB (PTL) and PI3K/Akt (LY294002) for 36 h; MTT assays were performed. NFkappaB and PI3K inhibitors decreased the cellular viability in GBM cell lines but exerted no effects on astrocytic viability (Fig. 4E).

3.4. Curcumin synergizes with clinically utilized anticancer drugs

Adjuvant therapy has the therapeutic advantage of potentiating the effect of classical anticancer drugs, thereby decreasing the frequently observed systemic side effects and damage to healthy tissues [31]. To explore the potential of curcumin as a chemotherapeutic adjuvant, we pretreated U138MG and C6 cells with subapoptotic (12-h pretreatment followed by 48-h coincubation) or apoptotic (12-h curcumin pretreatment, washout and subsequent 48-h incubation with anticancer drugs alone) concentrations of curcumin either alone or in combination with the alkylation agent cisplatin (5 μM) or the topoisomerase inhibitor doxorubicin (2.5 μM). The MTT assays showed that curcumin synergized with the anticancer drugs in both apoptotic and subapoptotic concentrations, potentiating the effects of the cisplatin and doxorubicin in the two tested cell lines (Table 3).

3.5. Curcumin inhibits GBM growth in vivo

In order to determine whether curcumin antiglioma potential *in vitro* could be achieved *in vivo*, we treated C6-implanted Wistar rats with 50 mg/kg/day curcumin, ip, from the 10th to the 20th day after glioma implantation. This *in vivo* model is one of the most useful tools to evaluate the pharmacologic potential of a drug in the growth of gliomas since tumor cells are induced to grow in the brain of immune-competent animals, thus simulating much of the *in vivo* conditions of GBMs [25–27]. Of the curcumin-treated rats, only 7/11 (63%) developed detectable tumors vs. 11/11 (100%) in the DMSO-treated

Table 4
Histological analysis of H&E-stained brain sections of glioma-implanted rats

Histology	DMSO	Curcumin	Z-value/confidence
Rats with tumor development	11/11 (100%)	7/11 (64%)	1.66[a]/96%[a]
Coagulative necrosis	10/11 (91%)	5/7 (71%)	0.43/67%
Intratumoral hemorrhage	9/11 (82%)	3/7 (43%)	1.2/88%
Lymphocytic infiltration	9/11 (82%)	4/7 (57%)	0.6/72%
Peritumoral edema	9/11 (82%)	5/7 (71%)	−0.065/47%
Peripheral pseudopalisading	6/11 (54%)	5/7 (71%)	−0.065/47%

Legend: The proportion of animals that developed a defined tumor mass as evaluated by H&E analysis. The histological variables (coagulative necrosis, intratumoral hemorrhage, lymphocytic infiltration, peritumoral edema, peripheric pseudopalisading) were regarded as present or absent.
[a] Different from DMSO-treated rats at α>95 % confidence level (DMSO vs. curcumin , Z-test).

group (Table 4) as evaluated by histochemistry. Quantification of tumor volume was carried out exclusively in animals presenting a body mass that could be quantified. In the curcumin-treated rats with detectable tumors (seven rats), we observed decreases in tumor volume in five of seven (71%) animals, whereas all DMSO-treated rats (11/11) presented marked tumor masses (Fig. 5A). Results showed

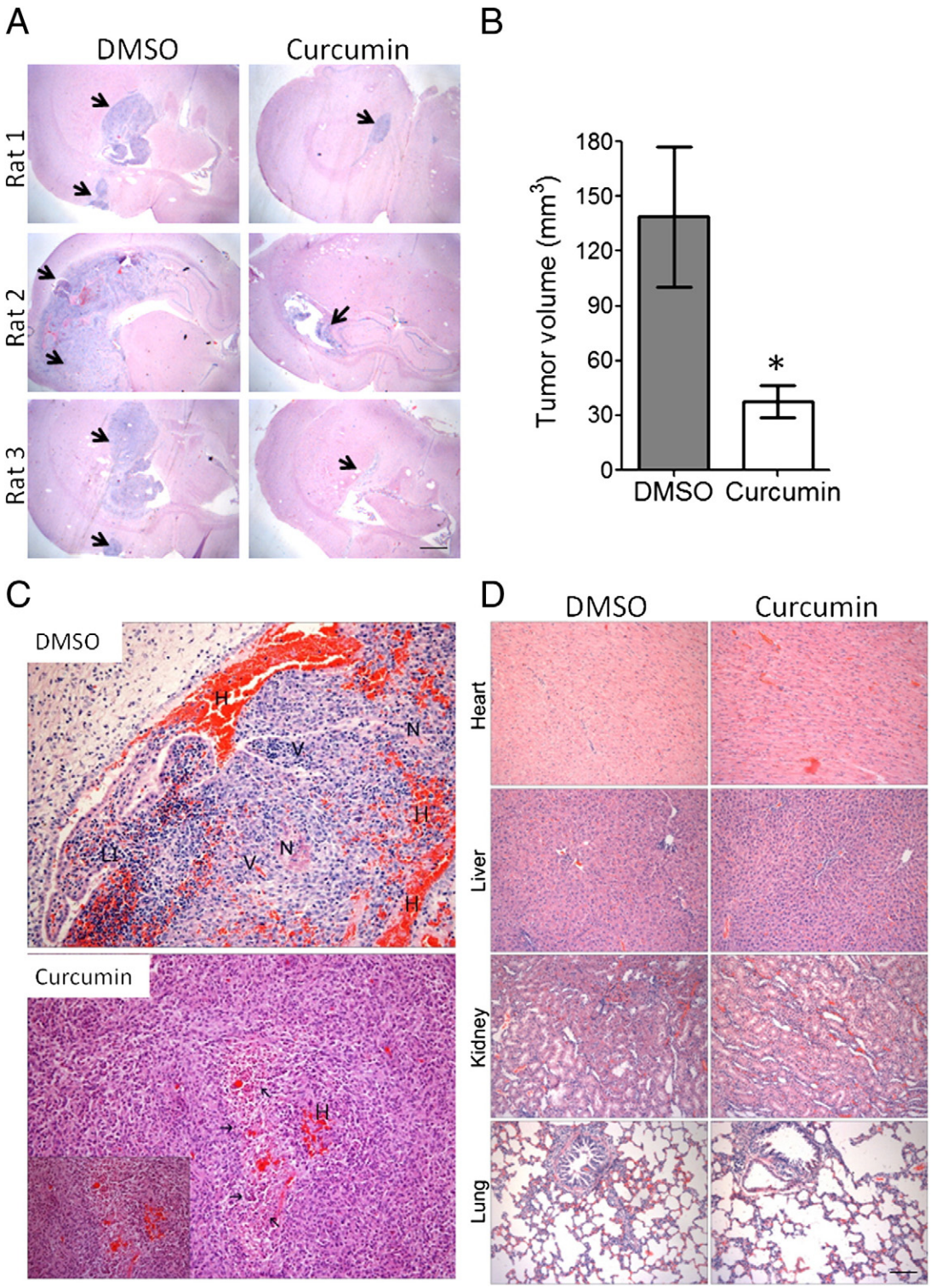

Fig. 5. Curcumin inhibits GBM growth *in vivo*. Animals were treated, and samples were analyzed as described in Materials and Methods. (A) Representative H&E-stained brain coronal sections of C6 tumors (arrows) of three representative animals of the control group (DMSO treated) and of the curcumin-treated group. Scale bars=1 mm. (B) Tumor volume (mm^3) quantification of implanted gliomas. *Different from DMSO-treated controls, $P<.05$, DMSO vs. curcumin , *t* test, mean±S.D. (C) Histopathology of C6 tumors. Legends: DMSO-treated group: (N) necrosis, (H) hemorrhages, (V) vascular proliferation, (LI) lymphocytic infiltration; curcumin-treated group: pathological characteristics of tumor in involution; arrows: apoptotic cells; (H) hemorrhages. Magnification 20×; insert 40×. (D) Representative microphotographs showing H&E-stained sections of liver, lung, kidney and heart of DMSO-treated and curcumin-treated glioma-implanted rats; magnification 10×.

Table 5
Hematological parameters and tissue damage serum markers in curcumin- and DMSO-treated C6 implanted rats

	DMSO	Curcumin
White blood cells ($\times 10^3$/mm^3)	4.8±1.2	4.92±1.6
Red blood cells ($\times 10^6$/mm^3)	7.38±0.7	7.37±0.6
Hematocrit (%)	40±4	41±3
Platelets ($\times$103/mm^3)	872±67	850±140
RDW (%)	14±0.4	15.1±0.5
Lymphocytes (%)	74.3±2.5	75.2±5.5
Granulocytes (%)	15.3±3.2	15.7±3.6
Monocytes (%)	10.3±2.4	9.1±2.1
AST (U/L)	186±30	194±35
ALT (U/L)	82±9	71±5
Alkaline phosphatase (U/L)	240±61	166±78
Creatinine (mg/dl)	0.5±0.05	0.49±0.1
Glucose (mg/dl)	161±33	143±35
Total cholesterol (mg/dl)	41±3	44±8

that the animals treated with curcumin displayed a significant reduction in tumor size (mean±S.D.: 37±9 mm^3, n=7) compared to the DMSO-treated (mean±S.D.=138±37 mm^3, n=11) group (Fig. 5B). Representative H&E-stained tumor sections are shown in Fig. 5A (arrows indicate tumor areas). It is important to cite that, of the 11 tumor-implanted animals in the DMSO group, two animals presented losses in body weight and motor impairment and died between the 18th and 19th day of experiment due to glioma complications.

Besides reducing tumors size, curcumin increased the number of apoptotic cells in tumors as detected by microscopic analysis of H&E-stained brain sections (Fig. 5C, arrows show apoptotic areas). On the other hand, although the percentage/proportion of animals with intratumoral hemorrhage (curcumin: 3/7 vs. DMSO: 9/11) and lymphocytic infiltration (curcumin: 4/7 vs. DMSO: 9/11) appeared to be lower in curcumin-treated rats, the proportions, which were based on qualitative analysis of "presence or absence" of the alterations, were not statistically different from DMSO-treated rats (Table 4). However, the hemorrhagic areas in curcumin-treated rats were clearly reduced when compared to DMSO-treated rats (Fig. 5C, red regions indicate intratumoral hemorrhage, H).

Importantly, curcumin neither altered hematological parameters (leukogram and hemogram) nor exerted tissue or metabolic toxicity as evaluated from determination of ALT, AST (liver damage marker), creatinine (kidney damage marker), alkaline phosphatase (pancreas, liver and bone unspecific damage markers), glucose and total cholesterol (Table 5). Means in curcumin-treated group did not differ from means in DMSO-treated rats (t test; P>.05). In addition, curcumin did not alter oxidative stress parameters in cerebellum, liver and kidney as evaluated from quantification of TBARS, protein carbonyl, sulfhydryl and antioxidant enzymes activity (Table 6). Microscopic investigation of liver, kidney, lungs and hearts by H&E analysis also demonstrated absence of tissue toxicity in curcumin-treated rats. Representative histologies of liver, kidney, lungs and heart tissues in curcumin- and DMSO-treated rats are shown in Fig. 5D.

4. Discussion

The present study showed a potent and selective cytotoxic effect of the dietary compound curcumin in a panel of GBM cell lines and in glioma implants. Curcumin effect occurred in both adhered and agar-growing GBMs, evidencing an anchorage-independent mechanism. In addition, the antiglioma activity of curcumin was prolonged and persisted for several days after drug withdrawal as assessed by clonogenic assays. Besides cell death induction at cytotoxic levels, low concentrations of curcumin decreased proliferation and migration and synergized with classical anticancer drugs, suggesting that subtoxic concentrations of curcumin also could be taken for therapeutic advantage.

Curcumin appeared to act irrespective of the p53 or PTEN mutational status of the cells, since U138MG, U373 (PTEN mutated/p53 mutated), U87 (PTEN mutates/p53 wild-type) and C6 (PTEN wild-type/p53 wild-type), which possess different mutations, were sensitive to curcumin. Defects in apoptotic signaling pathways as p53 mutations and caspases down-regulation promote chemoresistance and limit the effectiveness of chemotherapeutics [32–37]. Curcumin stimulated effector caspase-3 in C6 but not in the p53-mutant U138MG, indicating that curcumin can activate either caspase-dependent or caspase-independent cell death pathways depending on the cell line. In agreement, prior studies reported that curcumin exerts caspases, calpains and p53-independent cell death via inhibition of NFkappaB in the p53-mutated T98G cell line [21]. Thus, curcumin's ability to induce caspase/p53-independent cell death circumvents two frequent aberrations that contribute to GBM resistance.

Curcumin suppressed NFkappaB and PI3K/Akt, which are two pivotal survival pathways in GBMs [38–44]. Mutations in the tensin homolog PTEN, a negative regulator of PI3K, leads to losses in PTEN activity and to constitutive activation of the PI3K/Akt pathway in most of gliomas [40,45]. On the other hand, NFkappaB up-regulation has been attributed to cytokine overproduction, deregulation of PI3K/Akt [40], RIP-1 [41] and EGFR pathways [42]. Aberrant activation of NFkappaB has been reported in GBM biopsies, and focal necrosis formation, invasive phenotypes [43] and resistance to O^6 alkylating agents [39] paralleled the activity of this pathway in these tumors. In high-grade astrocytoma and GBM, a positive correlation between phospho-Akt, NFκB activation and glioma progression was observed [43]. Therefore, PI3K/Akt and NFkappaB pathways become important therapeutic targets for these tumors. We found a constitutive activation of PI3K/Akt and NFkappaB in GBM cell lines but not in astrocytes. Inhibition of NFkappaB and PI3K/Akt with the pharmacological inhibitors LY294002 and PTL selectively decreased cellular viability in GBMs, confirming the role of these pathways in GBM cells survival. Taking into account the aforementioned, the mechanisms whereby curcumin is protective in normal cells, yet death inducing in tumor cells, could be explained by its ability to block survival pathways that are constitutively active in cancer but not in healthy cells, such as PI3K/Akt and NFkappaB [31,43,44]. Although markedly

Table 6
Oxidative stress markers in liver, kidney and cerebellum of C6 implanted rats after 10 days of DMSO or curcumin treatment

	DMSO	Curcumin
Liver		
TBARS (nmol/mg protein)	0.092±0.031	0.078±0.026
Sulfhydryl (μmol/mg protein)	76.1±3.9	78.6±1.0
Carbonyl (nmol/mg protein)	1.1±0.3	0.77±0.35
Catalase (U/mg protein)	113±14.5	107±9.1
SOD (U/mg protein)	48.4±2.2	48.9±1.9
GST (U/mg protein)	2.70±0.12	2.68±0.11
Kidney		
TBARS (nmol/mg protein)	0.64±0.05	0.59±0.04
Sulfhydryl (μmol/mg protein)	73.8±1.2	71.5±2.0
Carbonyl (nmol/mg protein)	1.47±0.6	1.15±0.25
Catalase (U/mg protein)	29.9±1.7	27.6±0.8
SOD (U/mg protein)	62.8±1.8	63.1±1.4
GST (U/mg protein)	1.1±0.02	1.2±0.08
Cerebellum		
TBARS (nmol/mg protein)	0.50±0.04	0.47±0.03
Sulfhydryl (μmol/mg protein)	79.6±3.4	78±1.8
Carbonyl (nmol/mg protein)	1.2±0.31	0.95±0.4
Catalase (U/mg protein)	2.25±0.11	2.32±0.12
SOD (U/mg protein)	35.5±0.84	33.7±0.63
GST (U/mg protein)	2.08±0.13	2.23±0.12

cytotoxic to GBMs, curcumin spared nontransformed cells, except for a minor reduction in astrocytic viability after 100 μM, which may be restricted to proliferating astrocytes in culture; a property not shared *in vivo* [21]. The arrest in the G2/M phase as an early step of the apoptotic mechanism also could contribute to curcumin selectivity, since cancer cells are in constant cell cycle progression through S to G2/M phase, in contrast to nonproliferative cells. Previous studies showed that curcumin seems unlikely to affect normal brain function and, in fact, is neuroprotective in animal models of ischemic stroke and Alzheimer's disease [46–49].

Despite aggressive neurosurgery and chemotherapy, GBMs frequently exhibit chemoresistance [39,48–51]. Identifying novel strategies to overcome drug resistance may aid in the development of improved therapeutics. In C6 and U138MG, curcumin decreased the nuclear activity of NFkappaB, causing reduction of the bcl-xl protein immunocontent, which is a classical NFkappaB-regulated mitochondrial antiapoptotic protein. Moreover, curcumin synergized with the chemotherapeutics doxorubicin and cisplatin to cause toxicity in GBMs. This implies that curcumin may be a potential adjuvant by decreasing the antiapoptotic threshold, leading to sensitization to anticancer drugs' apoptotic stimuli. Previous studies have shown that curcumin decreases the expression of NFkappaB-regulated genes as bcl-xL, XIAP, cIAPs and survivin in T98G cells, which contribute to chemoresistance [21,52,53]. We previously reported that down-regulation of NFkappaB by BAY117082 and MG132 leads to mitochondrial dysfunction due to decreases in bcl-xL and SOD2 in leukemic cell lines [18]. Selective bcl-xL knockdown rendered U87 and NS008 GBM cells apoptosis [53], suggesting that bcl-xL down-regulation may induce mitochondrial dysfunction that ultimately results in cytotoxicity. Here, curcumin decreased bcl-xL and caused mitochondrial depolarization, which preceded the losses in cell membrane integrity, suggesting the mitochondrial dysfunction as an early step of curcumin-induced cell death. These findings corroborate with the reported caspase-9 activation in curcumin-treated T98G cells [16].

Despite the promising results in cell culture models of cancer at concentrations as low as 10 μM, curcumin blood levels are unlikely to reach these concentrations via dietary consumption in humans due to limited mucosal absorption [54]. Oral administration of 8 g/day produced peak blood levels around 2 μM of curcumin in patients [54]. These findings show a gap between the basic and clinical applications of curcumin. On the other hand, studies have found anticancer activities associated with oral, ip and intravenous administration of curcumin in xenografts [55–58]. In our model, we used ip curcumin in order to circumvent the problems associated with its oral absorption. Moreover, ip curcumin may cross the brain blood barrier [57,58]; 50 mg/kg/day was chosen based on the reported literature range (10–120 mg/kg/day) [55–58]. In our model, curcumin significantly reduced the size of brain tumors in C6-implanted rats. Interestingly, curcumin treatment did not induce toxicity to health tissues as evaluated from quantification of serum biomarkers of tissue damage, oxidative stress, hematological parameters and tissue histochemistry. Corroborating with *in vitro* data, these findings suggest a selective toxicity of curcumin against cancer cells *in vivo*. Recently, Perry et al. reported that ip curcumin (60 and 120 mg/kg/day) decreased the subcutaneous growth of U87 tumors in xenografts [58]. In that study, 120 mg/kg/day of curcumin also increased the survival rate in nude mice bearing brain-implanted U87 tumors, although the size of the tumors was not quantified [58]. In brain-implanted B16F10 melanoma cells, tail vein and intracerebral injection of curcumin blocked tumor formation in C57BL6 mice [57]. Therefore, application of injectable formulations of curcumin or direct delivery into the surgical resection cavity could be useful to circumvent the poor oral absorption into a safe therapeutic strategy for treating brain tumors.

This work is the second report of an *in vivo* antiglioma effect of curcumin, but the first using immune-competent rats. The C6 model maintains the immunological and inflammatory surveillances founded *in vivo*, which are critical for gliomas growth and resistance to apoptosis [59]. Perry et al. used immune-compromised mice to implant U87 human cells, and the results also were positive [58]. Given the documented safety of curcumin in humans [54], data presented here and data from Perry et al. provide a provocative foundation for further studies testing and improving the ability of curcumin to limit human brain tumors.

Acknowledgments

We acknowledge the Brazilian funds CAPES, CNPq and FINEP/IBNNet (01060842-00) for financial support.

References

[1] Singh SK, Hawkins C, Clarke ID, Squire JA, Bayani J, Hide T, et al. Identification of human brain tumour initiating cells. Nature 2004;432:396–401.
[2] Legler JM, Ries LA, Smith MA, Warren JL, Heineman EF, Kaplan RS, et al. Cancer surveillance series [corrected]: brain and other central nervous system cancers: recent trends in incidence and mortality. J Natl Cancer Inst 1999; 91:1382–90.
[3] Soni D, King JA, Kaye AH, Hovens CM. Genetics of glioblastoma multiforme: mitogenic signaling and cell cycle pathways converge. J Clin Neurosci 2005;12: 1–5.
[4] Yu C, Friday BB, Yang L, Atadja P, Wigle D, Sarkaria J, et al. Mitochondrial Bax translocation partially mediates synergistic cytotoxicity between histone deacetylase inhibitors and proteasome inhibitors in glioma cells. Neuro Oncol 2008;10(3):309–19.
[5] Brennan C, Momota H, Hambardzumyan D, Ozawa T, Tandon A, Pedraza A, et al. Glioblastoma subclasses can be defined by activity among signal transduction pathways and associated genomic alterations. PLoS One 2009;4(11):e7752.
[6] Roesler R, Brunetto AT, Abujamra AL, de Farias CB, Brunetto AL, Schwartsmann G. Current and emerging molecular targets in glioma. Expert Rev Anticancer Ther 2010;10(11):1735–51.
[7] Gerstner ER, Sorensen AG, Jain RK, Batchelor TT. Anti-vascular endothelial growth factor therapy for malignant glioma. Curr Neurol Neurosci Rep 2009; 9(3):254–62.
[8] Mercer RW, Tyler MA, Ulasov IV, Lesniak MS. Targeted therapies for malignant glioma: progress and potential. BioDrugs 23(1), 25–35.
[9] Singh S, Khar A. Biological effects of curcumin and its role in cancer chemoprevention and therapy. Anticancer Agents Med Chem 2006;6(3):259–70 [Review].
[10] Cheng AL, Hsu CH, Lin JK, Hsu MM, Ho YF, Shen TS, et al. Clinical trial of curcumin, a chemopreventive agent, in patients with high-risk or pre-malignant lesions. Anticancer Res 2001;21:2895–900.
[11] Gao X, Deeb D, Jiang H, Liu YB, Dulchavsky AS, Gautam SC. Curcumin differentially sensitizes malignant glioma cells to TRAIL/Apo2L-mediated apoptosis through activation of procaspases and release of cytochrome c from mitochondria. J Exp Ther Oncol 2005;5:39–48.
[12] Kim SY, Jung SH, Kim HS. Curcumin is a potent broad spectrum inhibitor of matrix metalloproteinase gene expression in human astroglioma cells. Biochem Biophys Res Commun 2005;337:510–6.
[13] Nagai S, Kurimoto M, Washiyama K, Hirashima Y, Kumanishi Y, Endo S. Inhibition of cellular proliferation and induction of apoptosis by curcumin in human malignant astrocytoma cell lines. J Neurooncol 2005;74:105–11.
[14] Woo MS, Jung SH, Kim SY, Hyun JW, Ko KH, Kim WK, et al. Curcumin suppresses phorbol ester-induced matrix metalloproteinase-9 expression by inhibiting the PKC to MAPK signaling pathways in human astroglioma cells. Biochem Biophys Res Commun 2005;335:1017–25.
[15] Belkaid A, Copland IB, Massillon D, Annabi B. Silencing of the human microsomal glucose-6-phosphate translocase induces glioma cell death: potential new anticancer target for curcumin. FEBS Lett 2006;580:3746–52.
[16] Karmakar S, Banik NL, Patel SJ, Ray SK. Curcumin activated both receptor-mediated and mitochondria-mediated proteolytic pathways for apoptosis in human glioblastoma T98G cells. Neurosci Lett 2006;407:53–8.
[17] da Frota Jr ML, Braganhol E, Canedo AD, Klamt F, Apel MA, Mothes B, et al. Brazilian marine sponge *Polymastia janeirensis* induces apoptotic cell death in human U138MG glioma cell line, but not in a normal cell culture. Invest New Drugs 2009;27(1):13–20.
[18] Zanotto-Filho A, Delgado-Cañedo A, Schröder R, Becker M, Klamt F, Moreira JC. The pharmacological NFkappaB inhibitors BAY117082 and MG132 induce cell arrest and apoptosis in leukemia cells through ROS-mitochondria pathway activation. Cancer Lett 2010;288(2):192–203.
[19] Braganhol E, Zamin LL, Cañedo AD, Horn F, Tamajusuku AS, Wink MR, et al. Antiproliferative effect of quercetin in the human U138MG glioma cell line. Anticancer Drugs 2006;17(6):663–71.

[20] Zanotto-Filho A, Gelain DP, Schröder R, Souza LF, Pasquali MA, Klamt F, et al. The NFkappaB-mediated control of RS and JNK signaling in vitamin A-treated cells: duration of JNK-AP-1 pathway activation may determine cell death or proliferation. Biochem Pharmacol 2009;77:1291–301.
[21] Dhandapani KM, Mahesh VB, Brann DWJ. Curcumin suppresses growth and chemoresistance of human glioblastoma cells via AP-1 and NFkappaB transcription factors. J Neurochem 2007;102(2):522–38.
[22] Klamt F, Shacter E. Taurine chloramine, an oxidant derived from neutrophils, induces apoptosis in human B lymphoma cells through mitochondrial damage. J Biol Chem 2005;280:21346–52.
[23] Lin HJ, Su CC, Lu HF, Yang JS, Hsu SC, Ip SW, et al. Curcumin blocks migration and invasion of mouse-rat hybrid retina ganglion cells (N18) through the inhibition of MMP-2, -9, FAK, Rho A and Rock-1 gene expression. Oncol Rep 2010;23(3): 665–70.
[24] Uliasz TF, Hewett SJ. A microtiter trypan blue absorbance assay for the quantitative determination of excitotoxic neuronal injury in cell culture. J Neurosci Methods 2000;100(1–2):157–63.
[25] Takano T, Lin JHC, Arcuino G, Gao Q, Yang J, Nedergaard M. Glutamate release promotes growth of malignant gliomas. Nature Med 2001;7:1010–5.
[26] Morrone FB, Oliveira DL, Gamermann P, Stella J, Wofchuk S, Wink MR, et al. In vivo glioblastoma growth is reduced by apyrase activity in a rat glioma model. BMC Cancer 2006;6:226–36.
[27] Braganhol E, Morrone FB, Bernardi A, Huppes D, Meurer L, Edelweiss MI, et al. Selective NTPDase2 expression modulates in vivo rat glioma growth. Cancer Sci 2009;100(8):1434–42.
[28] De Oliveira MR, Moreira JC. Impaired redox state and respiratory chain enzyme activities in the cerebellum of vitamin A-treated rats. Toxicology 2008;253(1–3): 125–30.
[29] Brown RE, Law A. Morphoproteomic demonstration of constitutive nuclear factor-kappaB activation in glioblastoma multiforme with genomic correlates and therapeutic implications. Ann Clin Lab Sci 2006;36(4):421–6.
[30] Gao X, Deeb D, Jiang H, Liu Y, Dulchavsky SA, Gautam SC. Synthetic triterpenoids inhibit growth and induce apoptosis in human glioblastoma and neuroblastoma cells through inhibition of prosurvival Akt, NF-kappaB and Notch1 signaling. J Neurooncol 2007;84(2):147–57.
[31] Nakanishi C, Toi M. Nuclear factor-kappaB inhibitors as sensitizers to anticancer drugs. Nat Rev Cancer 2005;5(4):297–309.
[32] Yahanda AM, Bruner JM, Donehower LA, Morrison RS. Astrocytes derived from p53-deficient mice provide a multistep in vitro model for development of malignant gliomas. Mol. Cell Biol 1995;15:4249–59.
[33] Lowe SW, Bodis S, McClatchey A, Remington L, Ruley HE, Fisher DE, et al. p53 Status and the efficacy of cancer therapy in vivo. Science 1994;266:807–10.
[34] Lowe SW, Ruley HE, Jacks T, Housman DE. p53-Dependent apoptosis modulates the cytotoxicity of anticancer agents. Cell 1993;74:957–67.
[35] Devarajan E, Sahin AA, Chen JS, Krishnamurthy RR, Aggarwal N, Brun AM, et al. Down-regulation of caspase 3 in breast cancer: a possible mechanism for chemoresistance. Oncogene 2002;21:8843–51.
[36] Igney FH, Krammer PH. Death and anti-death: tumour resistance to apoptosis. Nat. Rev Cancer 2002;2:277–88.
[37] Jaattela M. Multiple cell death pathways as regulators of tumour initiation and progression. Oncogene 2004;23:2746–56.
[38] Ansari SA, Safak M, Del Valle L, Enam S, Amini S, Khalili K. Cell cycle regulation of NF-kappa b-binding activity in cells from human glioblastomas. Exp. Cell Res 2001;265:221–33.
[39] Bredel M, Bredel C, Juric D, Duran GE, Yu RX, Harsh GR, et al. Tumor necrosis factor-alpha-induced protein 3 as a putative regulator of nuclear factor-kappaB-mediated resistance to O6-alkylating agents in human glioblastomas. J Clin Oncol 2006;24(2):274–87.
[40] Wang H, Wang H, Zhang W, Huang HJ, Liao WS, Fuller GN. Analysis of the activation status of Akt, NFkappaB, and Stat3 in human diffuse gliomas. Lab Invest 2004;84(8):941–51.
[41] Park S, Hatanpaa KJ, Xie Y, Mickey BE, Madden CJ, Raisanen JM, et al. The receptor interacting protein 1 inhibits p53 induction through NF-kappaB activation and confers a worse prognosis in glioblastoma. Cancer Res 2009;69(7):2809–16.
[42] Sethi G, Ahn KS, Chaturvedi MM, Aggarwal BB. Epidermal growth factor (EGF) activates nuclear factor-kappaB through IkappaBalpha kinase-independent but EGF receptor-kinase dependent tyrosine 42 phosphorylation of IkappaBalpha. Oncogene 2007;26(52):7324–32.
[43] Raychaudhuri B, Han Y, Lu T, Vogelbaum MA. Aberrant constitutive activation of nuclear factor kappaB in glioblastoma multiforme drives invasive phenotype. J Neurooncol 2007;85(1):39–47.
[44] Robe PA, Bentires-Alj M, Bonif M, Rogister B, Deprez M, Haddada H, et al. In vitro and in vivo activity of the nuclear factor-kappaB inhibitor sulfasalazine in human glioblastomas. Clin Cancer Res 2004;10(16):5595–603.
[45] Sansal I, Sellers WR. The biology and clinical relevance of the PTEN tumor suppressor pathway. J Clin Oncol 2004;22(14):2954–63.
[46] Lim GP, Chu T, Yang F, Beech W, Frautschy SA, Cole GM. The curry spice curcumin reduces oxidative damage and amyloid pathology in an Alzheimer transgenic mouse. J Neurosci 2001;21:8370–7.
[47] Thiyagarajan M, Sharma SS. Neuroprotective effect of curcumin in middle cerebral artery occlusion induced focal cerebral ischemia in rats. Life Sci 2004;74:969–85.
[48] Opel D, Westhoff MA, Bender A, Braun V, Debatin KM, Fulda S. Phosphatidylinositol 3-kinase inhibition broadly sensitizes glioblastoma cells to death receptor- and drug-induced apoptosis. Cancer Res 2008;68(15):6271–80.
[49] Weaver KD, Yeyeodu S, Cusack Jr JC, Baldwin AS, Ewend MG. Potentiation of chemotherapeutic agents following antagonism of nuclear factor kappa B in human gliomas. J Neurooncol 2003;61:187–96.
[50] Stewart LA. Chemotherapy in adult high-grade glioma: a systematic review and meta-analysis of individual patient data from 12 randomised trials. Lancet 2002;359:1011–8.
[51] Nagane M, Levitzki A, Gazit A, Cavenee WK, Huang HJ. Drug resistance of human glioblastoma cells conferred by a tumor-specific mutant epidermal growth factor receptor through modulation of Bcl-XL and caspase-3-like proteases. Proc Natl Acad Sci USA 1998;95:5724–9.
[52] Cheng Q, Lee HH, Li Y, Parks TP, Cheng G. Upregulation of Bcl-x and Bfl-1 as a potential mechanism of chemoresistance, which can be overcome by NF-kappaB inhibition. Oncogene 2000;19:4936–40.
[53] Jiang Z, Zheng X, Rich KM. Down-regulation of Bcl-2 and Bcl-xL expression with bispecific antisense treatment in glioblastoma cell lines induce cell death. J Neurochem 2003;84:273–81.
[54] Anand P, Kunnumakkara AB, Newman RA, Aggarwal BB. Bioavailability of curcumin: problems and promises. Mol Pharm 2007;4(6):807–18 [Review].
[55] Shankar S, Ganapathy S, Chen Q, Srivastava RK. Curcumin sensitizes TRAIL resistant xenografts: molecular mechanisms of apoptosis, metastasis and angiogenesis. Mol Cancer 2008;7:16–29.
[56] Dujic J, Kippenberger S, Ramirez-Bosca A, Diaz-Alperi J, Bereiter-Hahn J, Kaufmann R, et al. Curcumin in combination with visible light inhibits tumor growth in a xenograft tumor model. Int J Cancer 2009;124(6):1422–8.
[57] Purkayastha S, Berliner A, Fernando SS, Ranasinghe B, Ray I, Tariq H, et al. Curcumin blocks brain tumor formation. Brain Res 2009;1266:130–8.
[58] Perry MC, Demeule M, Régina A, Moumdjian R, Béliveau R. Curcumin inhibits tumor growth and angiogenesis in glioblastoma xenografts. Mol Nutr Food Res 2010;54:1–10.
[59] Albesiano E, Han JE, Lim M. Mechanisms of local immunoresistance in glioma. Neurosurg Clin N Am 2010;21(1):17–29.

European Journal of Pharmaceutics and Biopharmaceutics 83 (2013) 156–167

Contents lists available at SciVerse ScienceDirect

European Journal of Pharmaceutics and Biopharmaceutics

journal homepage: www.elsevier.com/locate/ejpb

Research paper

Curcumin-loaded lipid-core nanocapsules as a strategy to improve pharmacological efficacy of curcumin in glioma treatment

Alfeu Zanotto-Filho [a,1], Karine Coradini [b,1], Elizandra Braganhol [c], Rafael Schröder [a], Cláudia Melo de Oliveira [d], André Simões-Pires [a], Ana Maria Oliveira Battastini [a], Adriana Raffin Pohlmann [e], Sílvia Stanisçuaski Guterres [b], Cassiano Mateus Forcelini [f], Ruy Carlos Ruver Beck [b,*], José Cláudio Fonseca Moreira [a]

[a] Departamento de Bioquímica, Universidade Federal do Rio Grande do Sul (UFRGS), Porto Alegre, Rio Grande do Sul, Brazil
[b] Programa de Pós-Graduação em Ciências Farmacêuticas, Universidade Federal do Rio Grande do Sul (UFRGS), Porto Alegre, Brazil
[c] Centro de Ciências Químicas, Farmacêuticas e de Alimentos, Universidade Federal de Pelotas (UFPel), Pelotas, Rio Grande do Sul, Brazil
[d] Faculdade de Farmácia, Universidade Federal do Rio Grande do Sul (UFRGS), Porto Alegre, Brazil
[e] Departamento de Química Orgânica, Instituto de Química, Universidade Federal do Rio Grande do Sul (UFRGS), Porto Alegre, Rio Grande do Sul, Brazil
[f] Hospital São Vicente de Paulo, Faculdade de Medicina da Universidade de Passo Fundo (UPF), Passo Fundo, Rio Grande do Sul, Brazil

ARTICLE INFO

Article history:
Received 18 July 2012
Accepted in revised form 23 October 2012
Available online 28 November 2012

Keywords:
Curcumin
Lipid-core nanocapsules
Glioma
Drug delivery
In vivo

ABSTRACT

In this study, we developed curcumin-loaded lipid-core nanocapsules (C-LNCs) in an attempt to improve the antiglioma activity of this polyphenol. C-LNC showed nanotechnological properties such as nanometric mean size (196 nm), 100% encapsulation efficiency, polydispersity index below 0.1, and negative zeta potential. The *in vitro* release assays demonstrated a controlled release of curcumin from lipid-core nanocapsules. In C6 and U251MG gliomas, C-LNC promoted a biphasic delivery of curcumin: the first peak occurred early in the treatment (1–3 h), whereas the onset of the second phase occurred after 48 h. In C6 cells, the cytotoxicity of C-LNC was comparable to non-encapsulated curcumin only after 96 h, whereas C-LNCs were more cytotoxic than non-encapsulated curcumin after 24 h of incubation in U251MG. Induction of G2/M arrest and autophagy were observed in C-LNC as well as in free-curcumin treatments. In rats bearing C6 gliomas, C-LNC (1.5 mg/kg/day, i.p.) decreased the tumor size and malignance and prolonged animal survival when compared to same dose of non-encapsulated drug. In addition, serum markers of tissue toxicity and histological parameters were not altered. Considered overall, the data suggest that the nanoencapsulation of curcumin in LNC is an important strategy to improve its pharmacological efficacy in the treatment of gliomas.

1. Introduction

Gliomas are the most common, aggressive, and difficult type of primary brain tumor to treat. Despite recent advances in chemotherapeutic strategies to treat other types of cancer, gliomas frequently resist contemporary drugs, and prognosis remains dismal [1,2]. A number of dysregulated cell signaling cascades have been described in gliomas, including the Ras/MEK/ERK, JAK/STAT3, NFkappaB, and PI3K/Akt pathways. Dysregulation of these pathways is driven by mutation, amplification, and overexpression of multiple genes such as PTEN, EGFR, PDGFR-a, p53, and mTOR [2–4]. In addition, the privileged location of these tumors limits the efficacy of classical chemotherapeutics due to restrictions imposed by the blood brain barrier (BBB) [1–3]. These characteristics together contribute to the high rates of growth and invasiveness observed in gliomas culminating in median survival of ~14 months after diagnosis [1–4]. Thus, the development of new therapeutic strategies to treat this disease is urgently required.

For decades, curcumin has been considered one of the most promising natural compounds for the treatment of diverse types of maladies including cancer and neurodegenerative diseases [5]. Previous studies by our group [6,7] and others [8–14] have demonstrated that curcumin can inhibit the growth of several glioma cell lines through a variety of mechanisms involved in cell cycle progression (induction of p21 and p53, inhibition of cyclin D1), invasiveness (blocking of secretion of MMPs), anti/proapoptotic response (decreases in bcl-2, bcl-xL, and caspases activation), autophagy and modulation of survival pathways such as JAK/STAT3, EGFR, PI3K/Akt, and NFkappaB [7–14]. Previous studies reported by our group [6,7] and by Dhandapani et al. [14] showed

* Corresponding author. Faculdade de Farmácia, Universidade Federal do Rio Grande do Sul (UFRGS), Av. Ipiranga, 2752, CEP 90610-000, Porto Alegre, RS, Brazil. Tel.: +55 51 3308 5951; fax: +55 55 3308 5090.
E-mail address: ruy.beck@ufrgs.br (R.C.R. Beck).
[1] These authors made equal contributions and are considered first co-authors.

0939-6411/$ - see front matter © 2012 Elsevier B.V. All rights reserved.
http://dx.doi.org/10.1016/j.ejpb.2012.10.019

that curcumin is selectively cytotoxic to tumor cells, but it spares normal neural cells such as astrocytes and neurons.

Despite promising *in vitro* tests, the potential of curcumin to limit glioma growth *in vivo* remains poorly described [7–9,13]. Summarizing the *in vivo* findings, we recently reported that a 10-day treatment with 50 mg/kg/day of curcumin decreased brain-implanted C6 tumors in Wistar rats [7]. Similar results were obtained in U87-implanted mice treated with 100 mg/kg/day curcumin [13] and in mice bearing tumors derived from implanted glioma-initiating cells treated with 300 mg/kg curcumin [8]. Others reported the ability of dietary curcumin (0.05%/w ad libitum) to inhibit the growth of Tu-9648-brain implants in C6B3F1 mice [9]. In human clinical trials, high doses of oral curcumin brought clear benefits in familial adenomatous polyposis (FAP), whereas its potential in colorectal, pancreatic, breast, and other cancers remains open or inconclusive due to the reduced number of patients enrolled in the studies [15–19]. In this regard, there is a consensus that the *in vivo* potential of curcumin probably remains underestimated and the development of new formulations could be useful to improve its therapeutic potential [20,21].

Much of the knowledge regarding the actions of curcumin was obtained from *in vitro* models of cell growth in variable drug concentrations, which are almost impossible to reach under *in vivo* conditions [7–13]. Particularly in cases of cancer, despite the promising results in cultured cancer cell lines at concentrations as low as 10 μM, curcumin blood levels do not reach these concentrations via dietary consumption in humans due to its poor aqueous solubility, limited mucosal absorption and first-pass metabolism, evidencing a gap between basic findings and clinical applications of this drug [22]. Results from experiments in the Caco-2 cell line have classified curcumin as a Biopharmaceutics Classification System (BCS) class IV molecule; this information allows the prediction of the rate-limiting step involved in intestinal absorption after oral administration of curcumin [23]. In addition, the susceptibility of curcumin to degrade at alkaline and neutral pH and in the presence of light has been demonstrated [24].

Several authors have designed drug delivery systems, such as solid lipid nanoparticles [25,26], phospholipid and cyclodextrin complexes [27,28] and polymeric nanoparticles, aimed at enhancing the bioavailability and therapeutic potential of curcumin [5,29]. Among the numerous benefits that nanoparticles possess, it is important to highlight the demonstrated ability of these carriers in increasing the delivery of drugs to the brain, this being a promising strategy for the treatment of diseases affecting the central nervous system [20,21,30–32]. The exact mechanism whereby nanoparticles enhance the transport of drugs across the brain–blood barrier (BBB) is unclear. Previous studies have reported that the polysorbate 80 coating is a suitable strategy for brain delivery aimed at improving the receptor-mediated endocytosis of nanoparticles at the level of the BBB [21,32]. Recently, two important studies showed an enhanced transport, increased retention, and sustained release of curcumin to the brain when this polyphenol was associated with polymeric nanoparticles [20,21].

In the present study, we tested a new type of particle developed by our group called lipid-core nanocapsules (LNCs). These particles are able to improve the stability of formulations and exert photoprotective effects [33–37]. In previous studies, LNCs have increased the biodistribution of trans-resveratrol in different tissues, including the brain [34], and promoted a significant reduction in the growth of malignant gliomas by increasing intracerebral levels of the nonesteroidal anti-inflammatory indomethacin [32]. In an attempt to improve the antiglioma potential of curcumin, we formulated curcumin-loaded lipid-core nanocapsules (C-LNCs) and evaluated their physicochemical characteristics, uptake and cytotoxicity to C6 and U251MG glioma cells *in vitro* and, mainly, the potential to inhibit the growth of brain-implanted gliomas *in vivo*. The effects of C-LNC and non-encapsulated curcumin were compared.

2. Materials and methods

2.1. Reagents

Curcumin, poly(ε-caprolactone) (PCL), and sorbitan monoestearate were obtained from Sigma–Aldrich (São Paulo, Brazil); grape seed oil was acquired from Delaware (Porto Alegre, Brazil); polysorbate 80 was purchased from Vetec (Rio de Janeiro, Brazil) and acetone from Nuclear (São Paulo, Brazil). HPLC grade acetonitrile was obtained from Tedia (São Paulo, Brazil). All chemicals and solvents were of pharmaceutical or HPLC grade and used as received. Propidium iodide, EDTA, acridine orange, trypsin, and MTT (3-(4,5-dimethyl)-2,5-diphenyl tetrazolium bromide) were supplied by Sigma–Aldrich (São Paulo, Brazil), and reagents for cell cultures were purchased from Difco (Detroit, MI, USA).

2.2. Preparation of lipid-core nanocapsules

The lipid-core nanocapsules were prepared by interfacial deposition of preformed polymer [36,37]. PCL (0.1 g), grape seed oil (165 μL), sorbitan monostearate (0.0385 g), and curcumin (0.005 g) were dissolved at 40 °C in 27 mL of acetone. The organic phase was injected, under stirring, into the aqueous phase consisting of polysorbate 80 (0.077 g) and water (54 mL). The suspension was kept under stirring for 10 min, and then, the acetone was evaporated and the final volume (10 mL) of the suspension was adjusted using reduced pressure. This formulation was called C-LNC. Blank lipid-core nanocapsules (B-LNCs) were prepared in the same way, omitting the presence of the drug. The formulations were prepared in triplicate and stored at room temperature and protected from light (amber glass flasks).

2.3. Characterization of lipid-core nanocapsules

2.3.1. Particle size analysis, polydispersity index, and zeta potential

Particle size and the polydispersity index were determined at 25 °C by photon correlation spectroscopy (Zetasizer Nano ZS®, Malvern Instruments, Malvern, UK) after previous dilution of the nanoparticles with ultrapure water. The zeta potential values were estimated on the basis of electrophoretic mobility on the same equipment at 25 °C, after dilution of the samples in a 10 mM NaCl aqueous solution. To ensure that the particle size of the formulations was submicrometric, the suspensions were also analyzed by laser diffraction (Mastersizer® 2000, Malvern Instruments, Malvern, UK). The results were expressed by the number size distribution (%) of the particles, considering the recent definition of the European Commission for nanomaterials [38].

2.3.2. Nanoparticle tracking analysis (NTA)

For visualization of the C-LNC, nanoparticle tracking analysis (NTA) experiments were carried out (NanoSight LM 10 & NTA 2.2 Analytical Software, Nanosight Ltd., Amesbury, UK). After appropriate dilution of the C-LNC in ultrapure water, the sample was introduced into the Nanosight sample chamber with a disposable syringe. The samples were measured at room temperature for 60 s with automatic detection. When the particles suspended in fluid are irradiated by a laser source, they scatter light and the image can be captured by a charge-coupled device (CCD) camera. The software is able to identify and track each individual particle, and it calculates the particle diameter from its Brownian motion [39,40].

2.3.3. Transmission electron microscopy (TEM)

Morphological analysis was conducted by transmission electron microscopy (JEM 1200 Exll, JEOL, Tokyo, Japan) operating at 120 kV (Centro de Microscopia of the Federal University of Rio Grande do Sul). For this analysis, the suspensions were diluted in ultrapure water (1:10 v/v) and placed on a specimen grid (Formvar-Carbon support films). Uranyl acetate solution (2% w/v) was used as a negatively-stained control.

2.3.4. Determination of drug content, encapsulation efficiency, and pH

Curcumin was assayed by high-performance liquid chromatography (HPLC). The system consisted of a pump, UV detector, autoinjector (Series 2000, PerkinElmer Instruments, Waltham, USA) and an RP-18 Sigma–Aldrich column (150 mm × 4.6 mm × 5 μm particle size, 110 Å pore diameter). Curcumin was eluted using a mobile phase consisting of acetonitrile: 0.1% trifluoracetic acid (50/50 v/v), (adjusted with pH 3.0 with triethylamine) at the flow rate of 0.6 mL min^{-1} [41]. The injection volume was 20 μL, and the detection wavelength used was 360 nm. The validated parameter showed linearity between 5.0 and 50.0 μg mL^{-1} ($y = 50110x - 22965$, $r = 0.9998$), inter- and intra-day variability lower than 1.5%, specificity and detection and quantification limits of 0.2 μg mL^{-1} and 0.6 μg mL^{-1}, respectively. The total drug was determined after dissolution of nanoparticles (1 mL) in 10 mL of acetonitrile. This solution was centrifuged at 4120*g* for 10 min, and 2 mL aliquots of the supernatant were collected and diluted in the mobile phase. The samples were filtered (Millipore 0.45 μm) and injected into the HPLC. Curcumin encapsulation efficiency was determined by the ultrafiltration/centrifugation technique (Ultrafree Microcon 10,000 MW, Merck Millipore, Darmstadt, Germany) at 2150*g* for 10 min. The ultrafiltrate was diluted in acetonitrile and injected into the HPLC to determine the free curcumin. Drug entrapped in the nanostructures was calculated by the difference between the total and the free drug concentrations as measured in the nanoparticles (total drug) and in the ultrafiltrate (non-entrapped drug), respectively. Encapsulation efficiency was determined by the quotient of the drug entrapped and the total drug content. The pH measurements were determined directly in the samples using a calibrated potentiometer (VB-10, Denver Instrument, Arvada, USA).

2.3.5. In vitro release of curcumin-loaded lipid-core nanocapsules

The *in vitro* release of non-encapsulated curcumin (curcumin ethanolic solution, C-ES) and that associated with LNC (C-LNC) was evaluated using the dialysis bag method. The dialysis bags (Spectra Por 7, 10 Kd, Spectrum Laboratories Rancho Dominguez, USA) containing 1 mL of the samples were suspended in 200 mL of release medium (water/polysorbate 80/ethanol (80:2:20 v/v)) at 37 °C with constant moderate stirring. The sink condition was maintained during the experiment. At predetermined time intervals, 1 mL of the external medium was withdrawn and replaced with fresh medium. The samples were diluted with mobile phase, filtered through a 0.45 μm membrane and analyzed by HPLC according to a method previously described, with slight modifications. A Shimadzu HPLC (LC-20A Prominence, Shimadzu, Japan) was used at a detection wavelength of 427 nm, and the injection volume was adjusted to 50 μL in order to allow a better detection. This HPLC method was validated according to the following characteristics: linearity ($y = 570110x - 9441.8$, $r = 1$), range (0.1–5 μg mL^{-1}), precision (repeatability and intermediate precision lower than 2%), specificity and detection and quantification limits (0.01 μg mL^{-1} and 0.05 μg mL^{-1}, respectively).

2.3.6. Stability studies

The tendency to physical instability of the formulations was studied by multiple light scattering by means of evaluation of coalescence, creaming, or flocculation (Turbiscan LAb®, Formulaction, L'Union, France). The analysis was performed with undiluted sample during 1 h (one scan every 5 min) at 25 °C. After preparation, the sample (20 mL) was directly poured into the glass cells without dilution and analyzed at 25 °C. The data acquisition was repeated every 5 min for 1 h, totaling 12 readings. The profile obtained during the analysis allows the detection of variations in particle size (based on the variation in the transmitted or backscattered light signals obtained) due to the coalescence or flocculation and sedimentation or creaming phenomena associated with particle migration [42]. In addition, the formulations containing curcumin were stored at room temperature for 3 months and the granulometric profile, particle size, polydispersity index, zeta potential, and drug loaded parameters were monitored ($n = 3$).

2.4. Cell cultures

C6 and U251MG glioma cell lines were obtained from the American Type Culture Collection (ATCC) (Rockville, Maryland, USA). The cells were grown and maintained in low-glucose Dulbecco's modified Eagle's medium (DMEM; Gibco BRL, Carlsbad, USA) containing 0.1% amphotericin B, 100 U/l gentamicin, and supplemented with 10% fetal bovine serum. Cells were kept at 37 °C in a humidified atmosphere with 5% CO_2. For *in vitro* experiments, non-encapsulated curcumin was prepared by dissolution of curcumin in absolute DMSO to give a stock concentration of 100 mM. This solution was used for dilution in the culture medium. Nanocapsule suspensions (0.5 mg/mL = 1.36 mM curcumin) did not require dilutions.

2.5. MTT assay

MTT reduction by cellular dehydrogenase was used to estimate the cell viability [6,7]. Cells were plated in 24-well plates (5×10^4/well) and then treated to reach 60–70% confluence. At the end of the incubations, the medium was changed for a drug-free medium containing 0.25 mg/mL MTT. Cells were incubated for 30 min at 37 °C. Formazan salt was then solubilized in DMSO, and the absorbance was read at 560 and 630 nm (A_{560}–A_{630}) (Spectramax M5, Molecular Devices, Sunnyvale, USA). Data were expressed as percentage compared to untreated cells.

2.6. Curcumin uptake studies

The levels of intracellular curcumin were monitored fluorimetrically by quantification of its autofluorescence. C6 and U251MG gliomas were grown in 12-well culture plates up to 70% confluence and then treated with non-encapsulated curcumin or C-LNC. At the end of the treatments, the cells were washed three times with culture medium to avoid extracellular curcumin contamination, trypsinized, and centrifuged (760*g*, 5 min). The resulting pellet was resuspended in 300 μL DMSO, sonicated, and incubated for 5 min at room temperature for extraction of curcumin. The intracellular curcumin was detected fluorimetrically (Ex 420 nm/Em 498 nm; Spectramax M5, Molecular Devices, Sunnyvale, USA). A standard plot of curcumin dissolved in DMSO (0.001–100 μM) was prepared identically to calculate the curcumin uptake by the cells. In all experiments, fluorescence values were normalized to the cell counts to minimize the bias attributed to curcumin-induced decreases in cell number, principally after long time exposure (24–96 h periods). Data were expressed as fentomols of curcumin per cell (fmol/cell). Fluorescence microphotographs also were taken to show intracellular accumulation of curcumin. In these experiments, C6 cells were washed with PBS to avoid background interference of fluorescence of extracellular curcumin/C-LNCs (500 ms exposure, 100× magnification, Nikon Eclipse TE 300) [5].

In order to assess the contribution of the endocytosis to the curcumin uptake by glioma cells, we performed curcumin uptake experiments in the presence of intracellular potassium depletion or hypertonic sucrose as described previously [43]. Intracellular potassium depletion protocol: C6 cells in 6-well culture plates were washed twice with potassium-free buffer (140 mM NaCl, 20 mM HEPES, pH 7.4, 1 mM $CaCl_2$, 1 mM $MgCl_2$, 1 mg/L glucose, pH 7.4) prior to incubation in hypotonic medium (potassium-free buffer/water (1:1 v/v) for 10 min. Following hypotonic shock, cells were washed three times with potassium-free buffer and incubated in potassium-free buffer for 30 min prior to treatment. Control cells were incubated in DMEM. Hypertonic sucrose protocol: cells were incubated for 30 min with 450 mM sucrose in serum-free DMEM. At the end of the protocols, cells were treated for an additional 6 h with C-LNC and the internalized curcumin was measured after DMSO extraction as above described. For detection of intracellular curcumin over 96 h, every 24 h the medium containing C-LNC was collected under sterile conditions, cells were exposed to sucrose or potassium depletion protocols and the same medium was re-incubated.

2.7. Flow cytometry for cell cycle distribution and autophagy

For cell cycle analysis, 24-well plated cells were trypsinized, centrifuged, and resuspended in 500 μL lysis buffer (10 mM phosphate-buffered saline, 0.1% v/v Nonidet P-40, 1.2 mg/mL spermine tetrahydrochloride, 5 μg/mL RNAse, 2.5 μg/mL propidium iodide, pH 7.4). Cells were vortexed and incubated on ice for at least 10 min for permeabilization. DNA content was determined by flow cytometry [6,7,44]. For the quantification of autophagic cells, we performed acridine orange staining followed by flow cytometry. In acridine orange-stained cells, cytoplasm and nucleolus fluoresce was bright green or dim red, whereas the acidic compartment fluoresce was bright red. The intensity of the red fluorescence is proportional to the degree of acidity. Cells were incubated with acridine orange (1 μg/mL) for 15 min, detached from the plate with trypsin–EDTA, centrifuged, and resuspended in phosphate-buffered saline. The green (FL1-H) and red (FL3-H) fluorescence from cells illuminated with blue (488 nm) excitation light was measured with a flow cytometer (BD FACSCalibur, BD Biosciences, San Jose, USA). In FACS experiments, ten thousand events were counted per sample. Data analysis was performed using the FlowJo® 7.6.5 and CellQuest® software programs.

2.8. Pre-clinical study: C6 glioma in vivo

2.8.1. Implantation

The *in vivo* model of rat glioma was carried out as previously described by Takano et al. [45] and validated in our laboratory [7,32]. Exponentially growing C6 cells were trypsinized, washed once in DMEM, spun down, and resuspended at 0.8×10^6 cells/3 μL DMEM. Cells were injected using a 5 μL Hamilton microsyringe coupled with the infusion pump (1 μL/min) at a depth of 6.0 mm into the right striatum (coordinates with regard to bregma: 0.5 mm posterior and 3.0 mm lateral) of adult male Wistar rats (8 weeks old, 220–260 g) previously anesthetized by intraperitoneal (i.p.) administration of ketamine/xylazine. The number of animals ($n = 11$ per group) required to provide 95% confidence was statistically calculated in agreement with the means and standard deviations previously reported for the *in vivo* glioma model [45]. Statistical parameters: $\mu A = 73$ mm^3; $\mu B = 27$ mm^3; SA = 13 mm^3; SB = 37 mm^3; $\alpha = 0.05$, power = $1 - \beta = 0.9$; $\beta = 0.1$; $t\alpha = 2.101$; $u\beta = 1{,}734$; $n0 = 10$. Formula: $n = ((SA)^2 + (Sb)^2)/(\mu A - \mu B)^2 \times (t\alpha + u\beta)^2$; $n = 11$ rats/group. All procedures used in the present study followed the "Principles of Laboratory Animal Care" of the National Institutes of Health (NIH) and were approved by the Ethics Committee of the Federal University of Rio Grande do Sul (Protocol number: 17823).

2.8.2. Treatments

Seven days after glioma implantation, animals were randomized and divided into groups as follows: (1) Saline (1 mL 0.9% NaCl/d); (2) B-LNC (blank lipid-core nanocapsules; 1 mL/d); (3) C-LNC1.5 (curcumin-loaded lipid-core nanocapsules; ~1 mL/d = 1.5 mg/kg/day curcumin); (4) C1.5 (~0.1 mL/d = 1.5 mg/kg/day non-encapsulated curcumin); (5) C50 (~0.1 mL/d = 50 mg/kg/day non-encapsulated curcumin). The formulations were administered i.p. for 14 consecutive days. DMSO controls were performed, and no effects were observed compared to the saline solution (data not shown) [7,32]. After 21 days (7 days for glioma implantation + 14 days for treatment), rats were decapitated. The brain, liver, kidney, and lungs were removed, sectioned and fixed with 10% paraformaldehyde. Blood samples were collected for glucose, alanine aminotransferases (ALTs), creatinine, and triglycerides quantification, which was performed in a LabMax 240 analyzer (Labtest Diagnostica, Brazil).

2.8.3. Tumor volume quantification

For the quantification of tumor volume, three hematoxylin and eosin (H&E) coronal sections (2–3 μm thick, paraffin embedded) from each animal were analyzed. Images were captured using a digital camera connected to a microscope (Nikon Eclipse TE300), and the tumor area (mm^2) was determined using Image Tool Software™. The total volume (mm^3) of the tumor was computed by the multiplication of the slice sections and by summing the segmented areas [7,32]. Animals for which a tumor mass was not detected by H&E were not used for tumor volume quantification.

2.8.4. Survival studies

For survival studies, rats received treatments from days 7 to 21 after the tumor implantation as described above ($n = 9$ per group). After this period, treatments were discontinued and animals were maintained without treatments for a maximum of 60 days. The number of survival days was monitored. Rats that displayed neurological symptoms (seizures, paresis, and awareness disturbance) were decapitated before dying. In these animals, the brains were dissected and the presence of tumors was confirmed.

2.9. Hemolysis test

To evaluate the potential safety of C-LNC for use in humans, the formulations were checked for hemolytic compatibility. In this study, 5 mL of whole blood collected from a healthy male was centrifuged at 760*g* for 10 min to obtain 2 mL red blood cells, which were collected and resuspended in 4 mL phosphate-buffered saline (PBS, pH 7.4). Different concentrations of C-LNC or B-LNC (0–120 μM) were incubated at 37 °C with 200 μL of red blood cells in eppendorf tubes to a final volume of 500 μL for 2 h at 37 °C. After this period, the extent of hemolysis was observed macroscopically, the tubes were centrifuged (760*g*, 10 min), and the supernatant was measured for optical density at 571 nm (Spectramax M5, Molecular Devices, Sunnyvale, USA). Blanks for C-LNC and B-LNC were performed by incubating nanocapsules in PBS without red blood cells, and absorbance was taken properly considering test tube values. NaCl 0.2% and sodium dodecyl sulfate (SDS 0.2%) were used as positive controls; PBS was used as a negative control. Absorbances were expressed as fold-induction.

2.10. Interaction of nanoparticles with plasma proteins

Curcumin-loaded lipid-core nanocapsules (up to 120 μM) were incubated with 700 μg of plasma proteins diluted in

phosphate-buffered saline to a final volume of 500 μL in eppendorf tubes at 37 °C. During incubation, adsorption of proteins to nanoparticle surfaces was allowed. Following 2 h of incubation, the samples were centrifuged at 15,000*g* for 15 min to obtain pellets of nanoparticles (resulting supernatants were collected). Pellets were washed with 1 mL PBS and centrifuged again. The proteins adsorbed in pelleted nanocapsules were removed by adding 60 μL electrophoresis Laemmli sample buffer (10% beta-mercaptoethanol) and heating at 95 °C for 5 min. These protein samples (25 μL) were loaded in 10% polyacrylamide gel and then underwent sodium dodecyl sulfate–polyacrylamide gel electrophoresis at 160 V for 1.5 h. The resulting gel was washed three times with distillated water and incubated with Comassie blue (50% methanol, 10% acetic acid, 0.1% Comassie blue R, q.s.p. water) for 1 h. The gel was then discolored by bleaching solution (1:3:6 acetic acid/methanol/water) for 1 h. The gel was photographed, and the resulting bands were analyzed by densitometry (ImageJ® software). Plasma incubated with PBS was considered as the negative control. Proteins were quantified by the Bradford method.

2.11. Statistical analysis

Results were expressed as mean ± standard deviation (SD). The experimental data were analyzed for statistical significance by one-way analysis of variance (ANOVA) using the software BioEstat 5.0. Post-hoc multiple comparisons were carried out using the Tukey's test. For survival rate experiments, the Chi-square test was used. For the qualitative data (Table 2 experiments), the *Z*-test for two proportions was chosen. Differences were considered significant at $p < 0.05$.

3. Results and discussion

3.1. Preparation and characterization of lipid-core nanocapsules

Lipid-core poly(ε-caprolactone) nanocapsules coated with polysorbate 80 were prepared by interfacial deposition of preformed polymer. After preparation, curcumin-loaded lipid-core nanocapsule suspensions presented a bright yellow opalescent aspect (data not shown). The physicochemical characteristics of C-LNC and B-LNC are presented in Table 1. The formulations showed particle size between 196 and 202 nm, polydispersity index (PDI) below 0.1 and negative zeta potential (mean values between −9.56 and −11.48) (Table 1). Analysis by laser diffraction confirmed the presence of particles only at the nanoscale and narrow size distribution (Fig. S1A). In addition, more than 50% of the particles were below 100 nm. This result is in agreement with the definition of nanomaterial by the European Commission which is based on the size of the particles and considers nanomaterials as systems that have 50% or more of the particles in the number size distribution between 1 and 100 nm [38]. As assessed by TEM (Fig. S1B), the morphology of C-LNC is spherical in shape and the diameters of the particles were similar to those determined by photon correlation spectroscopy (PCS). These physicochemical characteristics are consistent with other PCL-based formulations previously described in the literature [46,47]. From the NTA analysis, the average size calculated for C-LNC was 196 nm (Fig. S1C). This result is in agreement with the PCS and MET assays. NTA is an innovative technique that combines the advantages of single particle (transmission electron microscopy) and ensemble (photon correlation spectroscopy) approaches. The upper right photo in Fig. S1C shows a representative image of the C-LNC obtained by NTA. This technique allows the direct and real-time visualization of nanoparticles in liquids, and it is considered a method that is complementary to photon correlation spectroscopy in the determination of the average particle diameter [40]. Regarding the drug content and encapsulation efficiency, the formulations of C-LNC presented values which were in agreement with the theoretical value (0.50 mg mL^{-1}) and 100% of encapsulation efficiency (EE). Both formulations presented slightly acid pH (6.01–5.87) (Table 1). The results for C-LNC and B-LNC were similar, suggesting that entrapment of the curcumin does not affect the physicochemical characteristics of the nanocapsules.

The physical stability of the nanoparticles was analyzed by multiple light scattering (Fig. S2). This technique is able to rapidly detect destabilization phenomena, such as creaming, sedimentation, flocculation, and coalescence, without destruction of the sample. Since the optical transmittance of formulations was below 0.2%, the profiles of delta backscattering were analyzed (Fig. S2). In both formulations, no significant phenomena associated with physical instability were observed during the analysis (1 h). This result is in agreement with Venturini et al. who formulated very stable colloidal suspensions exclusively composed of lipid-core nanocapsules [36]. Besides, after a 3-month storage period, no difference was observed in the following parameters of the formulations containing curcumin: particle size, polydispersity index, zeta potential and drug loaded, which suggests the good stability of the suspensions (data not shown). Considered overall, the above results confirm the nanotechnological characteristics of these formulations, allowing the investigation of their antiglioma activity *in vitro* and *in vivo*.

In vitro release experiments were performed to study the release of curcumin from lipid-core nanocapsules (C-LNC) compared to non-encapsulated curcumin in ethanolic solution (C-ES). Fig. 1 shows the curves for the percentage release of curcumin from C-LNC and C-ES as a function of time (up to 72 h). The results show that curcumin release by the LNC was slower as compared with the non-encapsulated drug. At the end of 72 h, only 35% of curcumin was released by the LNC, while more than 80% was released from the non-encapsulated curcumin solution. The controlled and sustained release of curcumin from LNC indicates a

Table 1
Physicochemical characteristics of C-LNC and B-LNC after preparation.

Formulation	C-LNC	B-LNC
Zeta potential (mV)	−9.56 ± 0.66[a]	−11.48 ± 3.01[a]
Particle size (nm)	196 ± 1.40[a]	202 ± 2.65[a]
PDI	0.08 ± 0.02[a]	0.10 ± 0.02[a]
Drug content (mg mL^{-1})	0.50 ± 0.02	–
EE (%)	100 ± 0.00	–
pH	6.01 ± 0.24[a]	5.87 ± 0.08[a]

Means with the same letter are not significantly different between C-LNC and B-LNC groups ($p < 0.05$, $n = 3$, ANOVA).

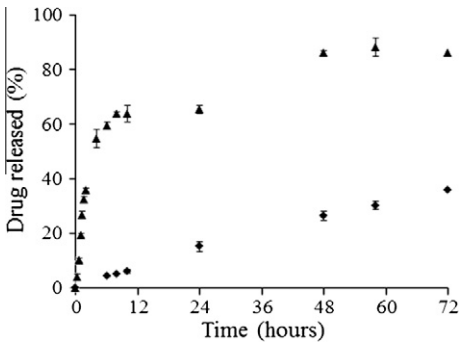

Fig. 1. Profile of curcumin release from lipid-core nanocapsules (square) and from ethanolic solution (triangle) *in vitro* using the dialysis bag method ($n = 3$).

significant drug entrapment within the nanocapsules. A faster diffusion of non-encapsulated curcumin to the external medium is expected, since it is dependent only on the diffusion of the drug through the dialysis bag [47]. The controlled release of curcumin by other kinds of nanocarriers has been described in the literature, but most studies did not involve a comparative analysis between the release profiles of curcumin incorporated in the nanosystems and its respective solution [20,21,48]. For C-LNC, the percentage of drug released during the initial hours was not expressed since the values were below the limit of quantification obtained by the HPLC method.

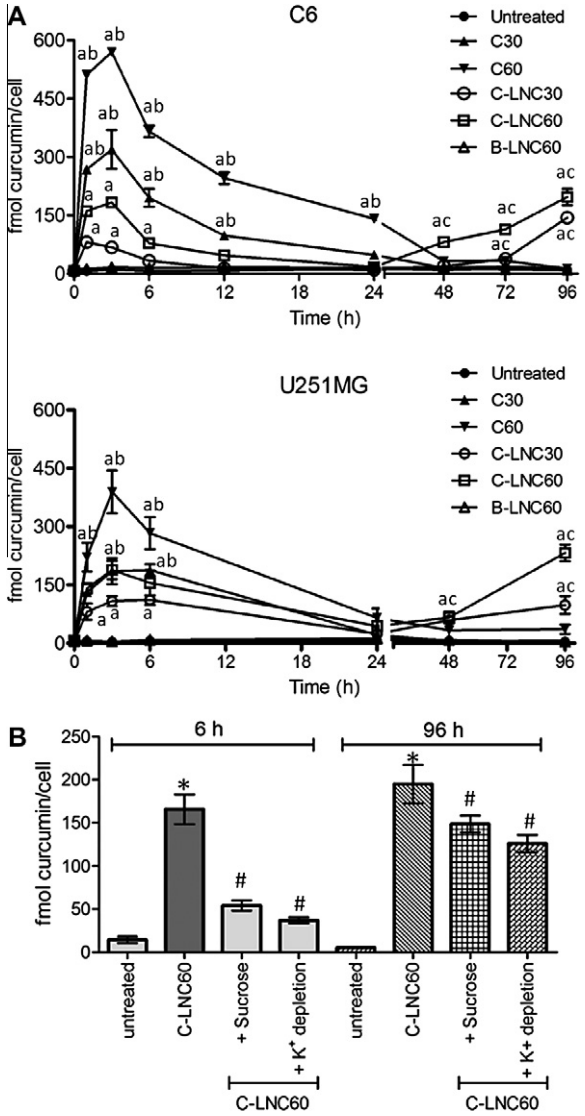

Fig. 2. Curcumin uptake by glioma cells. (A) C6 cells were treated, and intracellular curcumin was quantified from 1 to 96 h incubation. Data were expressed as fmol curcumin/cell (means ± S.D.; $n = 3$). (B) Effect of endocytosis inhibition on curcumin uptake by C6 cells. Cells were exposed to endocytosis inhibition followed by treatments with C-LNC for different times. Legends: C15, C30, and C60 (non-encapsulated curcumin at 15, 30, and 60 μM); C-LNC15, C-LNC30, C-LNC60 (curcumin-loaded lipid-core nanocapsules 15, 30, and 60 μM curcumin); B-LNC (blank/control nanocapsules). Graphic A statistics: [a] different from untreated cells at same time of incubation; [b] means are higher than C-LNC considering the same treatment time and curcumin concentration; [c] means are higher than non-encapsulated curcumin considering the same treatment time and concentration. Graphic B statistics: *different from untreated cells; # different from untreated and from C-LNC-treated cells.

3.2. Cell studies: curcumin uptake and cytotoxicity

Cellular uptake studies are useful to predict the drug delivery potential and biocompatibility of novel formulated nanocapsules. To study the kinetics of curcumin uptake in glioma cells, C6 and U251MG cells were treated with non-encapsulated curcumin (C lanes), C-LNC or B-LNC for different times and concentrations. Fig. 2A shows that non-encapsulated curcumin uptake was higher when compared to C-LNC during the first 24 h of treatment, but decreased to untreated levels at 24–48 h in both cell lines. For example, after 3 h of incubation, the intracellular content of curcumin was 320 fmol/cell in 30 μM non-encapsulated curcumin and 68 fmol/cell in 30 μM C-LNC in C6 cells (Fig. 2A). In contrast, intracellular accumulation of curcumin from the C-LNC delivery system occurred through a biphasic mechanism, with a rapid peak within 1–3 h followed by a sustained delivery observed for 48–96 h in both cell lines. Basal fluorescence values observed in untreated cells are attributed to cellular basal fluorescence in the emission wavelength.

In order to assess a possible internalization of nanocapsules by endocytosis, we performed uptake experiments in the presence of endocytosis inhibition (hypertonic sucrose and intracellular potassium depletion) (Fig. 2B). Inhibition of endocytosis almost completely inhibited the uptake of curcumin by C6 cells after 6 h. At later time points, curcumin uptake could also be attributed to the release of curcumin from nanocapsules and its subsequent uptake by the cells, since hypertonic sucrose and potassium depletion had only a minor, but significant, effect on the intracellular curcumin content. Thus, the first/rapid peak of intracellular curcumin could be attributed to internalization/endocytosis of nanocapsules by the cells and the second/later phase could be a consequence, at least in part, of gradual drug release by C-LNC, in agreement with the results obtained in the dialysis bag release experiments. Fig. 3 shows representative microphotographs obtained in the curcumin

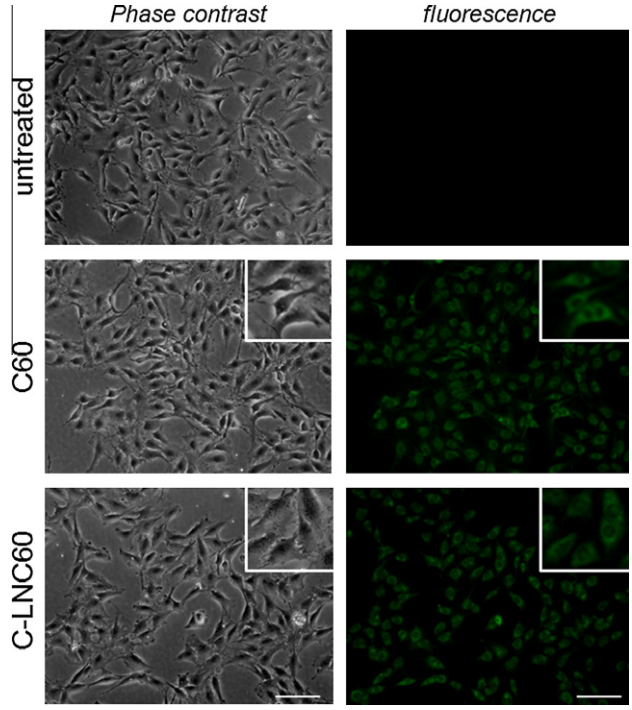

Fig. 3. Representative fluorescence microphotographs (100× magnification) showing fluorescence of intracellular curcumin in non-encapsulated curcumin (C60, 60 μM) and C-LNC (60 μM) treatments after 6 h incubation in C6 cells. (For interpretation of the references to color in this figure legend, the reader is referred to the web version of this article.)

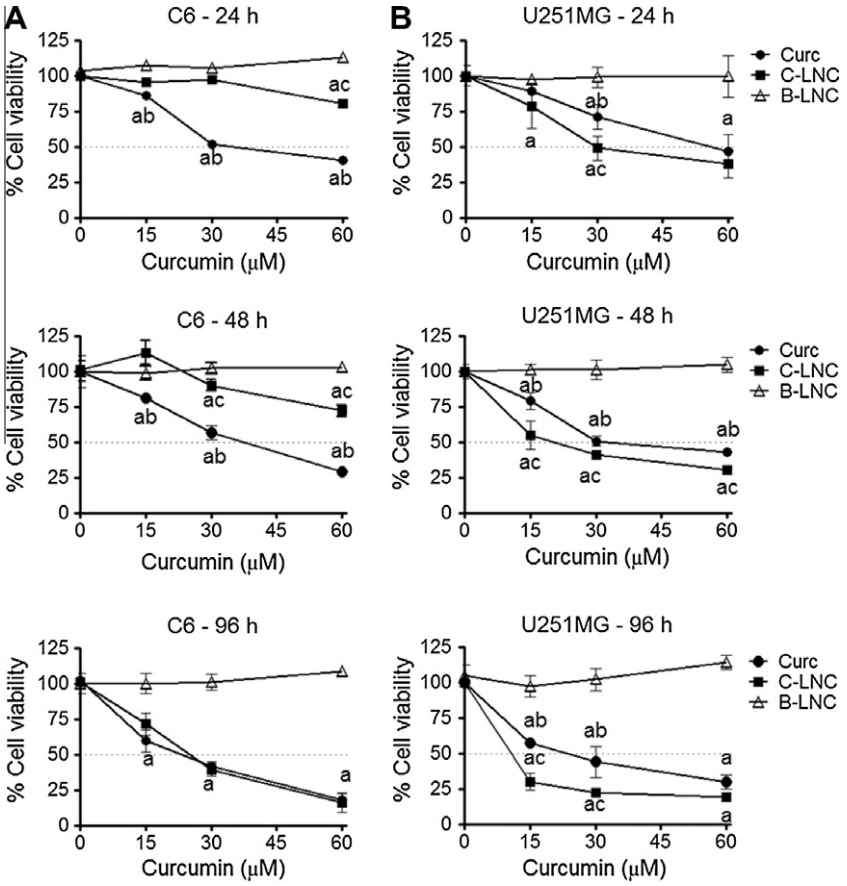

Fig. 4. Comparative cytotoxicity of curcumin in solution and C-LNC against C6 and U251MG glioma cells. Time-course effect of different concentrations of non-encapsulated curcumin and C-LNC on (A) C6 and (B) U251MG glioma cell viability at 24, 48, and 96 h. Legends: Curc (non-encapsulated curcumin); C-LNC (curcumin-loaded nanocapsules); B-LNC (blank nanocapsules). Data are expressed as means ± S.D. [a] Different from untreated cells; [b] different from C-LNC considering the same time of treatment and concentration; [c] different from non-encapsulated curcumin considering the same treatment time and concentration.

uptake experiments. As shown in the inserted figure, intracellular curcumin elicited a green cytoplasmic fluorescence accumulated in the surroundings of the C6 cells nuclei in both C-LNC and non-encapsulated curcumin-treated cells. This cytoplasmic compartmentalization profile is in agreement with previous studies [48]. It is important to emphasize that the intracellular accumulation of curcumin visualized in Fig. 3 is attributed to endocytosis of C-LNC as suggested from Fig. 2B experiments.

We performed MTT assays to estimate of the effects of curcumin and C-LNC on glioma cells viability. By comparing similar concentrations of curcumin, we observed that the non-encapsulated drug was more cytotoxic than C-LNC at the end of 24-h and 48-h treatments in C6 cells (Fig. 4A). However, cytotoxicity at later time points (96 h) was similar for the different delivery systems. Recently, Shao et al. showed that cytotoxicity of curcumin-loaded poly(ε-caprolactone) nanoparticles in C6 cells was similar to that observed in non-encapsulated curcumin for up to 48 h, whereas IC50 values were ~2-fold lower in curcumin-loaded nanoparticles treatments after 72 h incubation [48]. In contrast, we observed that C-LNC was more cytotoxic than non-encapsulated curcumin in U251MG cells, which was clearly observed for the 24-h treatment (Fig. 4B). The difference in the sensitivity of the glioma cells to different curcumin-loaded nanoparticles will be properly addressed in future studies, but differences in the genetic mutations profile, endocytic potential, membrane permeability, and multidrug resistance mechanisms are potential candidates. Lipid-core nanocapsules without curcumin (B-LNC) did not cause alterations in cell viability suggesting that the cell toxicity of C-LNC can be attributed to entrapped curcumin rather than nanoparticle components (Fig. 4A and B).

Pharmaceutical formulations do not interfere with the mechanism of action of the bioactive agent. Despite the different mechanisms of cell death induced by curcumin, the arrest in the G2/M phase of the cell cycle and induction of autophagy are two well-described mechanisms in glioma cells [7–9]. To test whether nanoencapsulation affects curcumin mechanisms, cells were treated with 30 μM curcumin in solution or C-LNC for 72 h, and cell cycle distribution and formation of acidic autophagic vacuoles were assessed by flow cytometry. As shown in Fig. 5A and B, nanoencapsulation did not affect the mechanisms whereby curcumin induces cytotoxicity in glioma cells since alterations in cell cycle distribution (G2/M arrest) and induction of autophagy were observed in both C-LNC and non-encapsulated curcumin treatments, in agreement with previous studies based on curcumin in solution [7–9].

3.3. In vivo studies: effects of C-LNC on tumor growth, animal survival, and peripheral toxicity in pre-clinical model of glioma

Curcumin has received considerable attention due to its potential clinical application in cancer. However, the potential of curcumin to treat gliomas *in vivo* remains poorly investigated, and it has been restricted to a few studies by our group and by other researchers who showed that curcumin doses as high as 50–300 mg/kg are required for efficacy *in vivo* [7–9]. In fact, drug delivery to the brain represents a challenge in the treatment of gliomas due to restrictions imposed by the blood–brain barrier (BBB). In this pursuit, many approaches have been applied in the development of drug delivery systems, for example, the use of nanoparticles. In this regard, the major biological relevance of

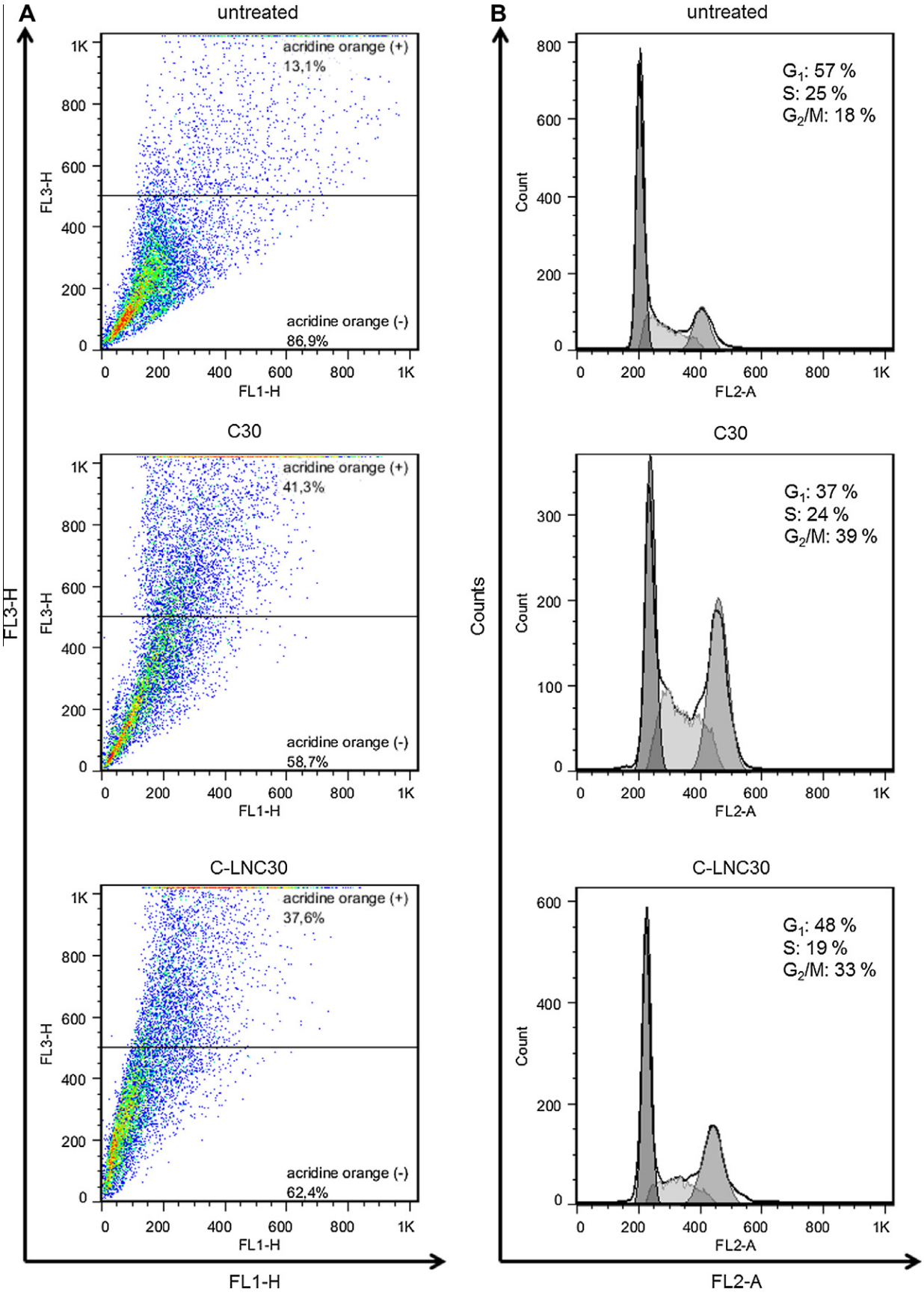

Fig. 5. Cell cycle distribution and formation of acidic vacuoles in C6 cells. (A) Cells were treated with 30 μM curcumin in solution or C-LNC for 72 h and stained with acridine orange. (B) Cell cycle distribution after 72 h treatment with curcumin or C-LNC (30 μM). Cells were analyzed by flow cytometry as described in Section 2. Graphs are representative of experiments performed in triplicate. (For interpretation of the references to color in this figure legend, the reader is referred to the web version of this article.)

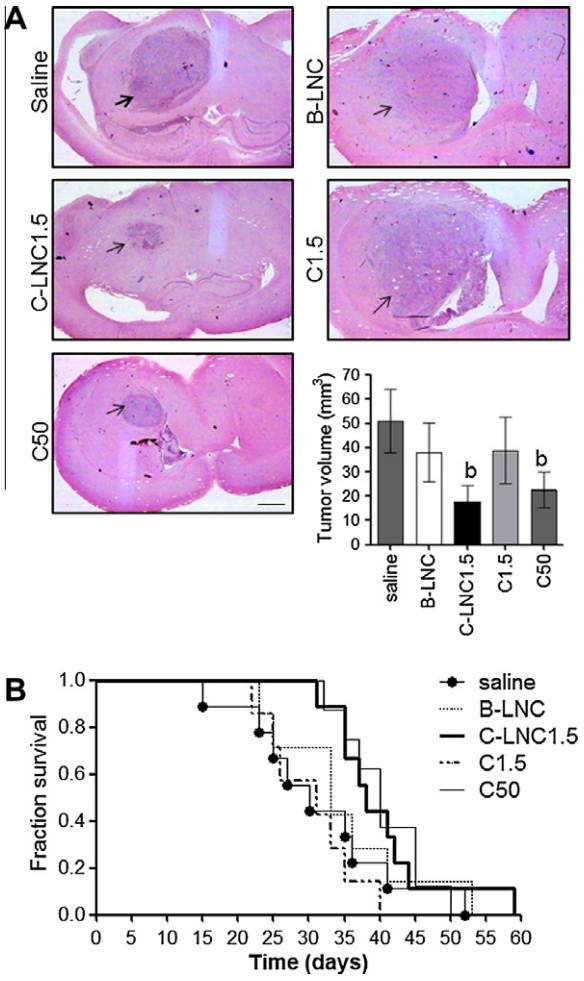

Fig. 6. Antiglioma activity of C-LNC against C6 gliomas *in vivo*. (A) Representative H&E microphotographs of C6 brain tumors (0.65× magnification; Bar: 1 mm) and tumor size quantification (means ± S.D., $n = 11$/group) in saline, C-LNC1.5, B-LNC, C1.5 and C50 treated rats. Data were analyzed by ANOVA followed by post-hoc comparisons (Tukey's test). (B) Survival rate of animals with C6-implanted gliomas. Animals were treated and observed over a total of 60 days ($n = 9$ animals per group). Data were analyzed by Chi-square test. [b]Different from control/saline, drug-unloaded lipid-core nanocapsules (B-LNC) and C1.5 groups. (For interpretation of the references to color in this figure legend, the reader is referred to the web version of this article.)

nanotechnology is based on its ability to improve the biological effect of drugs by increasing their absorption, permeability, drug circulating time, and delivery to body compartments.

Considering the pharmacokinetic limitations attributed to curcumin solubility and bioavailability/distribution, and the recently described potential of nanoparticles to enhance curcumin penetration into the CNS [20,21,49], we sought to investigate whether the curcumin-loaded lipid-core nanocapsules developed by our group could improve the pharmacological efficacy of this polyphenol against gliomas. In addition, our curcumin formulations were coated with polysorbate 80, which has been shown to increase curcumin delivery and penetration to the CNS [20,49,50].

In rats bearing C6 gliomas, we observed that 14-day treatment with a low dose of C-LNC (1.5 mg/kg/day i.p.; see C-LNC1.5 lane) significantly decreased tumor size when compared to the same dosage of non-encapsulated curcumin (C1.5 lanes), saline or B-LNC (Fig. 6A). Non-encapsulated curcumin only exerted significant effects on tumor size at a high dose of 50 mg/kg/day. C-LNC also decreased the incidence of intratumoral hemorrhages, necrosis, and lymphocytic infiltration, thus suggesting reduction of tumor aggressiveness (Table 2). Representative microphotographs of brain tumors and annotation of necrosis (N), hemorrhage (H), and microvessels (arrows) are shown in Fig. 7. Hemorrhagic areas and intratumoral necrosis were decreased in C-LNC and C50 treatments, whereas microvessel proliferation was similar among the different groups (Fig. 7). It is important to emphasize that these histopathological parameters are characteristic of human gliomas and are directly correlated with the worse prognosis [32,45].

Treatments with C-LNC also increased the survival rate (SR) of rats bearing gliomas compared to saline-treated animals (SR = 39 versus SR = 30 days, respectively), C1.5 (SR = 31 days) and B-LNC (SR = 33 days) (Fig. 6B). The antiglioma effects of non-encapsulated curcumin were only comparable to C-LNC at a high dose of 50 mg/kg/day (C50 lanes; SR = 40 days). Parallel to the improvement of antiglioma activity, C-LNC and B-LNC did not affect liver, lung, kidney and heart tissues, as assessed by H&E (Fig. S3). In addition, serum markers of tissue toxicity, such as creatinine (kidney dysfunction), ALT activity (tissue/liver unspecific marker), and metabolic parameters like glucose and triglycerides were not different among groups (Table S1).

In contrast to tumor growth models using immune-compromised animals, the C6 glioma model can be considered useful for the evaluation of the nanocapsule bioactivity, since in immunocompetent animals, the circulating time of the nanoparticles is affected, their clearance through phagocytosis and immunoglobulin-mediated opsonization being accelerated [51]. The decreases in tumor growth as well as in the malignance parameters, together with the prolonged survival observed in C-LNC treatments, suggest that the improvements in the efficacy of curcumin *in vivo* could be attributed to its nanoencapsulation in LNC. Recently, Sun et al. showed a 2.5-fold increase in the brain concentrations of curcumin and a 14-fold increase in mean residence time of curcumin after intravenous injections when this polyphenol was associated with poly(butylcyanoacrylate) nanoparticles coated with polysorbate 80 [21]. In agreement with this, previous studies by our group showed that lipid-core nanocapsules (LNCs) are able to increase

Table 2
Histopathological parameters of rats bearing C6 gliomas treated with C-LNC and non-encapsulated curcumin.

Formulation	Animals with tumors	Intratumoral hemorrhage	Intratumoral necrosis	Lymphocytic infiltration	Peritumoral edema	Peripheral pseudopalisading
Saline	11/11 (100%)	10/11 (91%)	7/11 (64%)	10/11 (91%)	9/11 (82%)	5/11 (45%)
C-LNC	8/11 (72%)	4/8 (50%)[a]	2/8 (25%)[a]	4/8 (50%)[a]	7/8 (88%)	4/8 (50%)
B-LNC	10/11 (91%)	8/10 (80%)	9/10 (90%)	9/10 (90%)	8/10 (80%)	4/10 (40%)
C1.5	10/11 (91%)	9/10 (90%)	7/10 (70%)	8/10 (80%)	7/10 (70%)	6/10 (60%)
C50	8/11 (72%)	5/8 (63%)	5/8 (63%)	4/8 (50%)[a]	6/8 (75%)	4/8 (50%)

Proportion of animals that developed a defined tumor mass as evaluated by H&E analysis. The histological variables (intratumoral necrosis, intratumoral hemorrhage, lymphocytic infiltration, peritumoral edema, peripheric pseudopalisading) were regarded as present or absent.
[a] Different from saline treated animals (*Z*-test, $p < 0.05$).

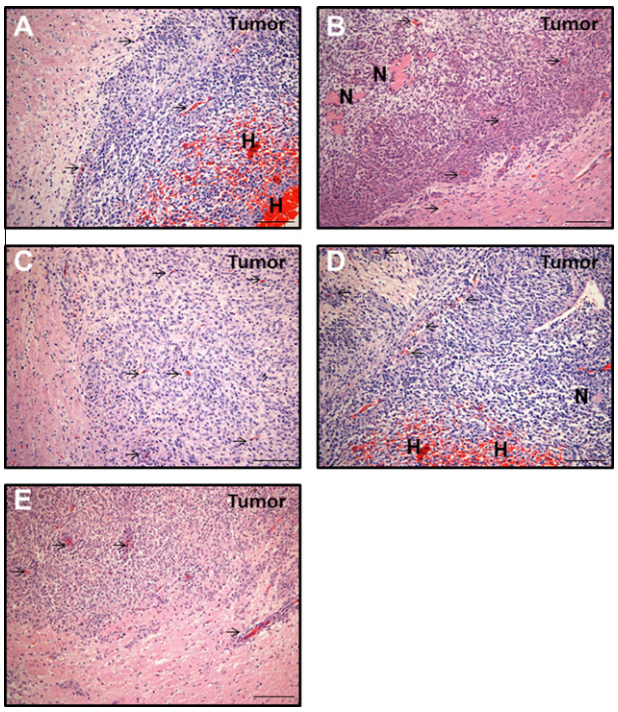

Fig. 7. Representative H&E analysis of brain tissues of saline (A), B-LNC (B), C-LNC (C), C1.5 (D), and C50 (E); 200× magnification. Legends: H: hemorrhages; N: necrosis areas; Arrows: microvessels. (For interpretation of the references to color in this figure legend, the reader is referred to the web version of this article.)

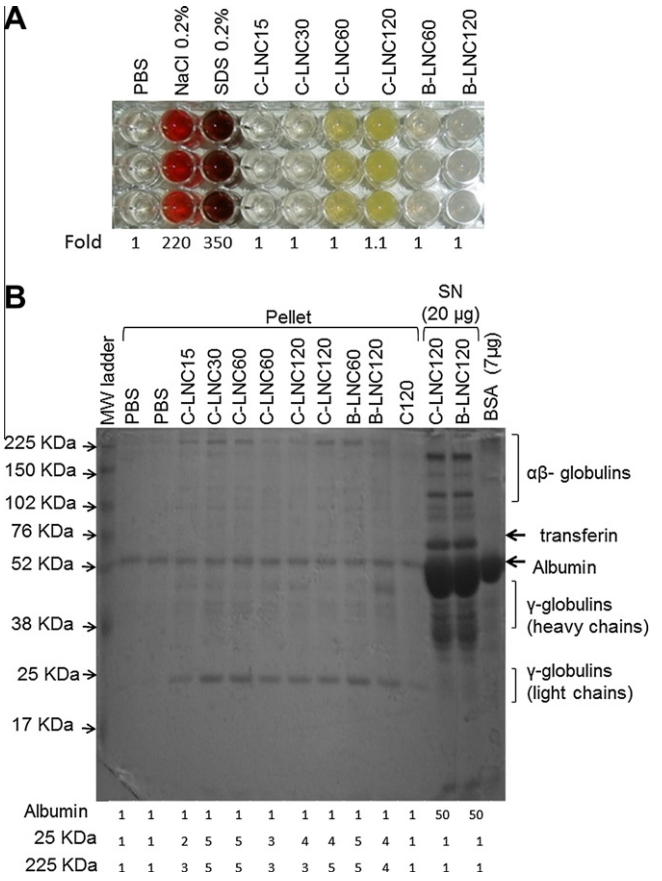

Fig. 8. Hemolysis in red blood cells and interaction with plasma proteins. A) Images of supernatants in hemolysis study. B) SDS–polyacrylamide gel electrophoresis of C-LNC incubated with human plasma. Legend: C-LNC15, C-LNC30, C-LNC60; C-LNC120 (curcumin-loaded lipid-core nanocapsules 15, 30, 60, and 120 µM curcumin, respectively); B-LNC (blank/unloaded nanocapsules); C120 (non-encapsulated curcumin 120 µM); BSA (purified bovine serum albumin); SN (20 µg): 20 µg plasma protein supernatants. (For interpretation of the references to color in this figure legend, the reader is referred to the web version of this article.)

indomethacin and resveratrol accumulation in rat brain [32,34]. Moreover, the absence of systemic toxicity, such as alterations in serum markers and tissue histology in treatments with C-LNC and B-LNC, suggests that the LNC were nontoxic in this model.

Despite the promising potential, the safety of nanocapsules is of growing concern considering that biological applications of nanoparticles could lead to unpredictable effects. To assess the *in vivo* use of lipid-core nanocapsules as carriers of curcumin, the hemolytic potential in red blood cells needs to be tested. Red blood cells incubated with C-LNC or B-LNC showed no signs of hemolysis at any concentration tested (Fig. 8A). The behavior of nanoparticle suspensions was similar to that of the negative control treatment (PBS) even at high concentrations (120 µM curcumin), suggesting a potential for their use as injectable formulations. The yellow coloration observed in some points is attributed to the color of curcumin formulations. Positive controls showed extensive hemolysis as expected.

Drug-loaded nanoparticles may have a direct interaction with tissues and cells after their administration in animals and humans. In general, serum proteins readily bind onto the surface of nanoparticles within 1 h of incubation [52]. In our experiments, we observed that lipid-core nanocapsules (C-LNC and B-LNC) weakly interacted with plasma proteins of different molecular weights (Fig. 8B). Importantly, interaction with albumin (70 kDa band), the most abundant serum/plasma protein, was not significantly increased compared to PBS incubations or non-encapsulated curcumin (C120 lanes, curcumin 120 µM). The presence of the albumin band in PBS/non-encapsulated curcumin incubated with plasma was not expected but could be attributed to precipitated or tube-adhered albumin, which was not removed by the centrifugation/washing steps. Much of the albumin content present in plasma remained in the resulting supernatants (SN lanes), a finding that supports the minimal interaction of LNC with albumin. Weak adsorption of other plasma proteins (38–225 kDa), which includes alpha and beta-globins, was observed in a dose-independent manner since the band intensity did not increase from 15 to 120 µM C-LNC (C-LNC15 to C-LNC120 lanes, Fig. 8B). Significant interaction was observed between the nanocapsules and 20–30 kDa proteins, typical range of the light chains of gamma-globulins (25 kDa). These proteins were not detected in the resulting plasma supernatants but formed a well-defined band in the case of the nanocapsule pellets, indicating interaction/adsorption. It should be noted that C-LNC120 and B-LNC120 concentrations represent a 1:10 nanocapsule/plasma ratio, thus indicating a high proportion of nanoparticles (10%) in the incubation systems which are probably unlikely to be reached after intraperitoneal or intravenous administration. It has been described that adsorption and binding to serum/plasma proteins such as albumin, IgGs, apolipoproteins, and/or opsonins can affect the biodistribution and drug release from nanoparticles [47,50–52]. The observed low binding to proteins reported herein is probably due to polysorbate 80, since its coating confers a hydrophilic surface to the particle which allows a lower interaction with proteins, and inhibited uptake of nanoparticles by the mononuclear phagocyte system triggering a prolonged circulating time [31,50,51]. On the other hand, interactions with light chains of gamma-globulins were observed and should be considered when considering the application of C-LNC *in vivo*. Further studies should be carried out to decrease the interaction of C-LNC with these proteins through polymeric modifications [52].

4. Conclusions

To the best of our knowledge, this is the first report of an *in vivo* effect of curcumin-loaded lipid-core nanocapsules in a pre-clinical model of gliomas. The comprehensive study of the physicochemical characteristics of the C-LNC confirms the nanotechnological features of this formulation. C-LNC presented efficacy at a low dose (1.5 mg/kg/day curcumin) in contrast to the high doses of non-encapsulated curcumin used to treat gliomas in animal models [7–9,14]. The results obtained suggest an improvement in the *in vivo* performance of the curcumin. Given the documented safety of curcumin in humans, data presented herein support further studies to test and improve the performance of C-LNC in limiting brain tumors.

Acknowledgements

This study was supported by the Brazilian agencies: Conselho Nacional de Desenvolvimento Científico e Tecnológico (CNPq), Coordenação de Aperfeiçoamento de Pessoal de Nível Superior (CAPES), Fundo de Incentivo à Pesquisa e Eventos (FIPE-HCPA), Fundação de Amparo à Pesquisa do Estado do Rio Grande do Sul (FAPERGS), FINEP/IBNNet (01060842-00), and INCT_if. A. Zanotto-Filho, R. Schroder, and A. Simões-Pires are recipient of CNPq doctoral fellowship. K. Coradini is recipient of CAPES doctoral fellowship.

Appendix A. Supplementary material

Supplementary data associated with this article can be found, in the online version, at http://dx.doi.org/10.1016/j.ejpb.2012.10.019.

References

[1] H. Ohgaki, P. Kleihues, Population-based studies on incidence, survival rates, and genetic alterations in astrocytic and oligodendrial gliomas, J. Neuropathol. Exp. Neurol. 64 (2005) 479–489.
[2] D. Soni, J.A. King, A.H. Kaye, C.M. Hovens, Genetics of glioblastoma multiforme: mitogenic signaling and cell cycle pathways converge, J. Clin. Neurosci. 12 (2005) 1–5.
[3] R. Roesler, A.T. Brunetto, A.L. Abujamra, C.B. de Farias, A.L. Brunetto, G. Schwartsmann, Current and emerging molecular targets in glioma, Expert Rev. Anticancer Ther. 10 (2010) 1735–1751.
[4] C. Brennan, H. Momota, D. Hambardzumyan, T. Ozawa, A. Tandon, A. Pedraza, E. Holland, Glioblastoma subclasses can be defined by activity among signal transduction pathways and associated genomic alterations, PLoS ONE 4 (2009) e7752.
[5] P. Anand, H.B. Nair, B. Sung, A.B. Kunnumakkara, V.R. Yadav, R.R. Tekmal, B.B. Aggarwal, Design of curcumin-loaded PLGA nanoparticles formulation with enhanced cellular uptake, and increased bioactivity in vitro and superior bioavailability in vivo, Biochem. Pharmacol. 79 (2010) 330–338.
[6] A. Zanotto-Filho, E. Braganhol, R. Schröder, L.H. de Souza, R.J. Dalmolin, M.A. Pasquali, D.P. Gelain, A.M. Battastini, J.C. Moreira, NFκB inhibitors induce cell death in glioblastomas, Biochem. Pharmacol. 81 (2011) 412–424.
[7] A. Zanotto-Filho, E. Braganhol, M.I. Edelweiss, G.A. Behr, R. Zanin, R. Schröder, A. Simões-Pires, A.M. Battastini, J.C. Moreira, The curry spice curcumin selectively inhibits cancer cells growth in vitro and in preclinical model of glioblastoma, J. Nutr. Biochem. 23 (2012) 591–601.
[8] W. Zhuang, L. Long, B. Zheng, W. Ji, N. Yang, Q. Zhang, Z. Liang, Curcumin promotes differentiation of glioma-initiating cells by inducing autophagy, Cancer Sci. 103 (2012) 684–690.
[9] J. Weissenberger, M. Priester, C. Bernreuther, S. Rakel, M. Glatzel, V. Seifert, D. Kögel, Dietary curcumin attenuates glioma growth in a syngeneic mouse model by inhibition of the JAK1,2/STAT3 signaling pathway, Clin. Cancer Res. 16 (2010) 5781–5795.
[10] C. Senft, M. Polacin, M. Priester, V. Seifert, D. Kögel, J. Weissenberger, The nontoxic natural compound Curcumin exerts anti-proliferative, anti-migratory, and anti-invasive properties against malignant gliomas, BMC Cancer 10 (2010) 491–499.
[11] T.Y. Huang, T.H. Tsai, C.W. Hsu, Y.C. Hsu, Curcuminoids suppress the growth and induce apoptosis through caspase-3-dependent pathways in glioblastoma multiforme (GBM) 8401 cells, J. Agric. Food Chem. 58 (2010) 10639–10645.
[12] C.C. Su, M.J. Wang, T.L. Chiu, The anti-cancer efficacy of curcumin scrutinized through core signaling pathways in glioblastoma, Int. J. Mol. Med. 26 (2010) 217–224.
[13] M.C. Perry, M. Demeule, A. Régina, R. Moumdjian, R, Béliveau, Curcumin inhibits tumor growth and angiogenesis in glioblastoma xenografts, Mol. Nutr. Food Res. 54 (2010) 1192–1201.
[14] K.M. Dhandapani, V.B. Mahesh, D.W. Brann, Curcumin suppresses growth and chemoresistance of human glioblastoma cells via AP-1 and NFkappaB transcription factors, J. Neurochem. 102 (2007) 522–538.
[15] A.S. Strimpakos, R.A. Sharma, Curcumin: preventive and therapeutic properties in laboratory studies and clinical trials, Antioxid. Redox Signal. 10 (2008) 511–545.
[16] R.E. Carroll, R.V. Benya, D.K. Turgeon, S. Vareed, M. Neuman, L. Rodriguez, M. Kakarala, P.M. Carpenter, C. McLaren, F.L. Meyskens Jr., D.E. Brenner, Phase IIa clinical trial of curcumin for the prevention of colorectal neoplasia, Cancer Prev. Res. (Phila) 4 (2011) 354–364.
[17] M. Kanai, K. Yoshimura, M. Asada, A. Imaizumi, C. Suzuki, S. Matsumoto, T. Nishimura, Y. Mori, T. Masui, Y. Kawaguchi, K. Yanagihara, S. Yazumi, T. Chiba, S. Guha, B.B. Aggarwal, A phase I/II study of gemcitabine-based chemotherapy plus curcumin for patients with gemcitabine-resistant pancreatic cancer, Cancer Chemother. Pharmacol. 68 (2011) 157–164.
[18] M. Bayet-Robert, F. Kwiatkowski, M. Leheurteur, F. Gachon, E. Planchat, C. Abrial, M.A. Mouret-reynier, X. Durando, C. Barthomeuf, P. Chollet, Phase I dose escalation trial of docetaxel plus curcumin in patients with advanced and metastatic breast cancer, Cancer Biol. Ther. 9 (2010) 8–14.
[19] C.H. Hsu, A.L. Cheng, Clinical studies with curcumin, Adv. Exp. Med. Biol. 595 (2007) 471–480.
[20] Y.M. Tsai, C.F. Chien, L.C. Lin, T.H. Tsai, Curcumin and its nano-formulation: the kinetics of tissue distribution and blood–brain barrier penetration, Int. J. Pharm. 416 (2011) 331–338.
[21] M. Sun, Y. Gao, C. Guo, F. Cao, Z. Song, Y. Xi, A. Yu, A. Li, G. Zhai, Enhancement of transport of curcumin to brain in mice by poly(*n*-butylcyanoacrylate) nanoparticle, J. Nanoparticle Res. 12 (2010) 3111–3122.
[22] P. Anand, A.B. Kunnumakkara, R.A. Newman, B.B. Aggarwal, Bioavailability of curcumin: problems and promises, Mol. Pharm. 4 (2007) 807–818.
[23] B. Wahlang, Y.B. Pawar, A.K. Bansal, Identification of permeability-related hurdles in oral delivery of curcumin using the Caco-2 cell model, Eur. J. Pharm. Biopharm. 77 (2011) 275–282.
[24] H.H. Tonnesen, M. Másson, T. Loftsson, Studies of curcumin and curcuminoids. XXVII. Cyclodextrin complexation: solubility, chemical and photochemical stability, Int. J. Pharm. 244 (2002) 127–135.
[25] V. Kakkar, S. Singh, D. Sinla, I.P. Kaur, Exploring solid lipid nanoparticles to enhance the oral bioavailability of curcumin, Mol. Nutr. Food Res. 55 (2011) 495–503.
[26] C. Puglia, G. Frasca, T. Musumeci, L. Rizza, G. Puglisi, F. Bonina, S. Chiechio, Curcumin loaded NLC induces histone hypoacetylation in the CNS after intraperitoneal administration in mice, Eur. J. Pharm. Biopharm. 81 (2012) 288–293.
[27] K. Maiti, K. Mukherjee, A. Gantait, B.P. Saha, P.K. Mukherjee, Curcumin–phospholipid complex: preparation, therapeutic evaluation and pharmacokinetic study in rats, Int. J. Pharm. 330 (2007) 155–163.
[28] V.R. Yadav, S. Prasad, R. Kannappan, J. Ravindran, M.M. Chaturvedi, L. Vaahtera, J. Parkkinen, B.B. Aggarwal, Cyclodextrin-complexed curcumin exhibits anti-inflammatory and antiproliferative activities superior to those of curcumin through higher cellular uptake, Biochem. Pharmacol. 80 (2010) 1021–1032.
[29] J. Shaikh, D.D. Ankola, V. Beniwal, D. Singh, R.M.N.V. Kumar, Nanoparticle encapsulation improves oral bioavailability of curcumin by at least 9-fold when compared to curcumin administered with piperine as absorption enhancer, Eur. J. Pharm. Sci. 37 (2009) 223–230.
[30] C. Mohanty, S.K. Sahoo, The in vitro stability and in vivo pharmacokinetics of curcumin prepared as an aqueous nanoparticulate formulation, Biomaterials 31 (2010) 6597–6611.
[31] E. Garcia-Garcia, K. Andrieux, S. Gil, P. Couvreur, Colloidal carriers and blood–brain barrier (BBB) translocation: a way to deliver drugs to the brain?, Int J. Pharm. 298 (2005) 274–292.
[32] A. Bernardi, E. Braganhol, E. Jäger, F. Figueiró, M.I. Edelweiss, A.R. Pohlmann, S.S. Guterres, A.M.O. Battastini, Indomethacin-loaded nanocapsules treatment reduces in vivo glioblastoma growth in a rat glioma model, Cancer Lett. 281 (2009) 53–63.
[33] M.C. Fontana, K. Coradini, S.S. Guterres, A.R. Pohlmann, R.C.R. Beck, Nanoencapsulation as a way to control the release and to increase the photostability of clobetasol propionate: influence of the nanostructured system, J. Biomed. Nanotechnol. 5 (2009) 254–263.
[34] R.L. Frozza, A. Bernardi, K. Paese, J.B. Hoppe, T. Silva, A.M.O. Battastini, A.R. Pohlmann, S.S. Guterres, C. Salbego, Characterization of trans-resveratrol-loaded lipid-core nanocapsules and tissue distribution studies in rats, J. Biomed. Nanotechnol. 6 (2010) 694–703.
[35] A.F. Ourique, S. Azoubel, C.V. Ferreira, C.B. Silva, M.C.L. Marchiori, A.R. Pohlmann, S.S. Guterres, R.C.R. Beck, Lipid-core nanocapsules as a nanomedicine for parenteral administration of tretinoin: development and in vitro antitumor activity on human myeloid leukaemia Cells, J. Biomed. Nanotechnol. 6 (2010) 214–223.
[36] C.G. Venturini, E. Jäger, C.P. Oliveira, A. Bernardi, A.M.O. Battastini, S.S. Guterres, A.R. Pohlmann, Formulation of lipid core nanocapsules, Colloid Surf. A 375 (2011) 200–208.
[37] E. Jäger, C.G. Venturini, F.S. Polleto, L.M. Colomé, J.P.U. Pohlmann, A. Bernardi, A.M.O. Battastini, S.S. Guterres, A.R. Pohlmann, Sustained release from lipid-core nanocapsules by varying the core viscosity and the particle surface area, J. Biomed. Nanotechnol. 5 (2009) 130–140.

[38] European Union, L 275, OJEU 54 (2011) 38–40.
[39] V. Filipe, A. Hawe, W. Jiskoot, Critical evaluation of nanoparticle Tracking Analysis (NTA) by Nanosight for the measurement of nanoparticles and protein aggregates, Pharm. Res. 27 (2010) 796–810.
[40] R.D. Boyd, S.K. Pichaimuthu, A. Cuenat, New approach to inter-technique comparisons for nanoparticle size measurements; using atomic force microscopy, nanoparticle tracking analysis and dynamic light scattering, Colloid Surf. A 387 (2011) 35–42.
[41] B.K. Jadhav, K.R. Mahadik, A.R. Paradkar, Reversed phase-HPLC method for simultaneous determination of curcumin, demethoxycurcumin and bis-demethoxycurcumin, Chromatographia 65 (2007) 483–488.
[42] O. Mengual, G. Meunier, I. Cayré, K. Puech, P. Snabre, TURBISCAN MA 2000: multiple light scattering measurement for concentrated emulsion and suspension instability analysis, Talanta 50 (1999) 445–456.
[43] L.M. Luttrell, Y. Daaka, G.J. Della Rocca, R.J. Lefkowitz, G protein-coupled receptors mediate two functionally distinct pathways of tyrosine phosphorylation in rat 1a fibroblasts. Shc phosphorylation and receptor endocytosis correlate with activation of Erk kinases, J. Biol. Chem. 272 (1997) 31648–31656.
[44] A. Zanotto-Filho, A. Delgado-Cañedo, R. Schröder, M. Becker, F. Klamt, J.C. Moreira, The pharmacological NFkappaB inhibitors BAY117082 and MG132 induce cell arrest and apoptosis in leukemia cells through ROS-mitochondria pathway activation, Cancer Lett. 288 (2010) 192–203.
[45] T. Takano, J.H.C. Lin, G. Arcuino, Q. Gao, J. Yang, M. Nedergaard, Glutamate release promotes growth of malignant gliomas, Nat. Med. 7 (2001) 1010–1015.
[46] I.C. Külkamp, B.D. Rabelo, S.J. Berlitz, M. Isoppo, M.D. Bianchin, S.R. Schaffazick, A.R. Pohlmann, S.S. Guterres, Nanoencapsulation improves the in vitro antioxidant activity of lipoic acid, J. Biomed. Nanotechnol. 7 (2011) 598–607.
[47] M.C. Fontana, K. Coradini, A.R. Pohlmann, S.S. Guterres, R.C.R. Beck, Nanocapsules prepared from amorphous polyesters: effect on the physicochemical characteristics, drug release and photostability, J. Nanosci. Nanotechnol. 10 (2010) 3091–3099.
[48] J. Shao, D. Zheng, Z. Jiang, H. Xu, Y. Hu, X. Li, X. Lu, Curcumin delivery by methoxy polyethylene glycol-poly(caprolactone) nanoparticles inhibits the growth of C6 glioma cells, Acta Biochim. Biophys. Sin. 43 (2011) 267–274.
[49] P. Kundu, C. Mohanty, S.K. Sahoo, Antiglioma activity of curcumin loaded lipid nanoparticles and its enhanced bioavailability in brain tissue for effective glioblastoma therapy, Acta Biomater. 8 (2012) 2670–2687.
[50] K.S. Soppimath, T.M. Aminabhavi, A.R. Kulkarni, W.E. Rudzinski, Biodegradable polymeric nanoparticles as drug delivery devices, J. Control. Release 70 (2001) 1–20.
[51] S.M. Moghimi, A.C. Hunter, J.C. Murray, Long circulating and target specific nanoparticles: theory to practice, Pharmacol. Rev. 53 (2001) 283–318.
[52] M.M. Yallapu, M.C. Ebeling, N. Chauhan, M. Jaggi, S.C. Chauhan, Interaction of curcumin nanoformulations with human plasma proteins and erythrocytes, Int. J. Nanomed. 6 (2011) 2779–2790.